Journal of Research of the National Bureau of Standards Vol. 47, No. 6, December 1951 Research Paper 2268

# pH of Solutions of Potassium Hydrogen *d*-Tartrate from 0° to 60°C

Roger G. Bates, Vincent E. Bower, Richard G. Miller, and Edgar R. Smith

Although it is impossible to establish a thermodynamic scale of hydrogen-ion activity, $a_H$, the NBS pH standards are assigned pH values that approach as closely as possible $-\log a_H$ in dilute buffer solutions. In order to avoid the uncertainties of the liquid junction, electromotive-force measurements of hydrogen-silver chloride cells without liquid junction were used to obtain the standard pH. To assign pH values to four standard tartrate buffer solutions in the temperature range 0° to 60° C, electromotive-force data were obtained for 30 aqueous mixtures of potassium hydrogen tartrate and sodium chloride. One of the proposed standards is a saturated solution of potassium hydrogen tartrate at 25° (pH 3.56), and the others are 0.03-, 0.02-, and 0.01-molar with respect to this salt.

Directions for the preparation and preservation of tartrate buffer standards are given.

## 1. Introduction

For several years the National Bureau of Standards has advocated the universal adoption of a standard scale of pH based upon certain standard reference buffer solutions. The materials from which three of these standards are prepared have been issued as certified pH Standard Samples for more than 6 years. These standards are aqueous solutions of potassium acid phthalate, borax (sodium tetraborate decahydrate), and aqueous mixtures of potassium dihydrogen phosphate and disodium hydrogen phosphate. The pH values assigned to them define fixed points on a modified activity scale. They correspond as closely as possible to the negative of the common logarithm of the activity of hydrogen (hydronium) ion, $-\log a_H$, in the respective solutions. It is well recognized, however, that it is impossible to achieve a thermodynamic scale of hydrogen-ion activity [1 to 5].[1]

The practical electrometric determination of pH usually rests on two measurements of the electromotive force of a galvanic cell that may be schematically represented by

$$\text{Pt; } H_2 \text{ (g, 1 atm), standard or unknown solution} \mid \text{KCl (saturated), } Hg_2Cl_2\text{; Hg.}$$

The vertical line indicates a liquid junction between the standard (or unknown) and the potassium chloride of the "bridge" solution that forms a part of the calomel electrode. In the most common forms of pH meter, a glass electrode with inner reference replaces the hydrogen electrode at the left of the above scheme. The electromotive force is first obtained with the standard solution in the cell and, secondly, with the unknown solution whose pH it is desired to obtain. These two emf values are designated $E_s$ and $E$, respectively. If the pH of the standard is called $pH_s$, we have

$$pH = pH_s + (E - E_s)\boldsymbol{F}/(2.3026RT), \qquad (1)$$

where $\boldsymbol{F}$ is the faraday, $R$ is the gas constant, and $T$ is the absolute temperature.[2]

Equation 1 is a definition of the practical pH value and of the practical scale of pH. Evidently the function of the galvanic cell outlined above is simply to compare the pH of the two different solutions, to yield a *difference* of pH. If it were not for defects in the method of comparison, the practical pH would lie on the standard pH scale. However, these defects, chief among which is the variable potential at the liquid junction, have an appreciable effect in highly acid and highly alkaline solutions [7]. In order that the practical pH values shall represent $-\log a_H$ as nearly as possible, standards with pH close to that of the highly acidic and highly alkaline unknowns are desired. The standards presently available serve successfully to calibrate pH equipment for use in the intermediate range of the pH scale, but others of high and low pH are being sought.

Potassium hydrogen tartrate is only moderately soluble in water, and its saturated solution (about 0.034 molar at 25° C) is a convenient standard with pH near 3.6 [8]. The dissociation constants of tartaric acid do not differ greatly, and accordingly solutions of the primary salt have adequate buffer capacity without the addition of tartaric acid or the secondary salt. For these reasons, potassium hydrogen tartrate was selected as the fourth independent standard of pH, although it offers only a slight extension of the range of the present standards. The assignment of standard pH values to four solutions of potassium hydrogen tartrate is described in the following sections.

## 2. Method

In order to escape the uncertainties inherent in the reduction or estimation of the liquid-junction potential, the assignment of pH values to standard buffer solutions is based on measurements of the electromotive force of galvanic cells without liquid

[1] Figures in brackets indicate the literature references at the end of this paper.

[2] Values of $2.3026RT/\boldsymbol{F}$ in absolute volts are to be found in [6].

junction. The cell with hydrogen and silver-silver-chloride electrodes has been chosen as most suitable for this purpose:

Pt; $H_2$(g, 1 atm), buffer solution, $Cl^-$, AgCl; Ag.

The electromotive force, $E$, of this cell is directly related to the standard potential, $E°$, and the activities of the hydrogen and chloride ions in the solution.[3] If the activity of each of these ions is replaced by its equivalent, $mf$, where $m$ is molality and $f$ the molal activity coefficient, we obtain an expression for the acidity function $-\log(f_H f_{Cl} m_H)$, for convenience termed pwH:

$$\text{pwH} = -\log(f_H f_{Cl} m_H) = (E - E°)F/(2.3026RT) + \log m_{Cl}. \quad (2)$$

A soluble chloride must be added to the buffer solution in order that the silver–silver-chloride electrode can be used successfully, yet the pH of the chloride-free buffer solution is desired. Accordingly, pwH was measured for three low chloride concentrations, namely 0.015 $m$, 0.01 $m$, and 0.005 $m$, and the limit, pwH°, for vanishingly small chloride concentrations obtained by extrapolation.

The standard pH, that is $pH_s$, is formally defined as $-\log f_H m_H$ and is related to pwH° by the following equation:

$$pH_s = \text{pwH}° + \log f°_{Cl}, \quad (3)$$

where $f°_{Cl}$ is the limit approached by the activity coefficient of chloride ion as the concentration of chloride in the buffer solution approaches zero. Unlike pwH, the individual ionic activity coefficient, $f°_{Cl}$, cannot be evaluated without an assumption, and consequently $pH_s$ must be defined in an arbitrary manner. The more reasonable and accurate is the estimate of $f°_{Cl}$, the closer the standard pH will approach the desired $-\log f_H m_H$.

Various assumptions have been used to compute $f°_{Cl}$ for the assignment of $pH_s$ values to the standard phthalate [11], phosphate [12], and borax [13] buffer solutions. These and other different approaches yield slightly different $pH_s$ values for solutions of ionic strengths greater than about 0.01, but all are reasonable and furnish identical pH values at high dilutions [4, 14]. The calculated activity coefficients are all consistent with the Debye-Hückel equation [15].[4]

$$-\log f°_{Cl} = A\sqrt{\mu}/(1 + Ba_i\sqrt{\mu}), \quad (4)$$

where $\mu$ is the ionic strength of the buffer solution. The several approaches differ essentially only in the means by which the value of $a_i$, the ion-size parameter, is estimated. There is little basis for choice among them. When the mean activity coefficients of strong electrolytes and the activity-coefficient terms in buffer-chloride mixtures are fitted to the Debye-Hückel equation, the value of the ion-size parameter is often found to lie between 3 and 6.[5] Hence, a choice of 4 for the calculation of $\log f°_{Cl}$ and $pH_s$ is justifiable, provided the uncertainty is recognized to be at least as large as the difference between the $pH_s$ furnished by $a_i$ values of 4 and 6. The complete equation for $pH_s$ thus becomes

$$pH_s = \text{pwH}° - A\sqrt{\mu}/(1 + Ba_i\sqrt{\mu}), \quad (5)$$

by combination of eq 3 and 4.

[3] The numerical values of the activity depend upon the standard state and the scale of concentration chosen. The NBS standard pH scale is based upon molal activities, and all activity coefficients and pH values in this paper will be referred to the molal basis. The standard potential, $E°$, is derived from the measurements of Harned and Ehlers [9] as recalculated by Hamer, Burton, and Acree [10]. Its value from 0° to 60° C in absolute volts is found in [6].

[4] Values of the constants $A$ and $B$ are tabulated in [16].

## 3. Experimental Procedures and Results

The potassium hydrogen $d$-tartrate was a composite sample of a lot of 250 lb obtained for issuance as NBS Standard Sample 188. The salt was in the form of a powder. Its aqueous solutions were strongly dextrorotatory. The assay was found to be 99.95 percent by titration with a carbonate-free sodium hydroxide solution to the endpoint of phenolphthalein. The results of other standard tests were as follows:

Chloride: No turbidity with silver nitrate after the solution had been acidified with nitric acid.
Calcium: No turbidity with ammonium oxalate in ammoniacal solution.
Insoluble in $NH_4OH$: None perceptible.
Ammonia: 0.0002 percent.
Phosphate: Less than 0.002 percent $PO_4$.[6]
Iron: Less than 0.001 percent Fe.[6]
Sulfur compounds: 0.006 percent $SO_4$.[6]
Heavy metals: 0.001 to 0.002 percent Pb.[6]

The sodium chloride was a recrystallized sample free of bromide. Both the chloride and the tartrate were ordinarily dried at 100° C before use. A good grade of distilled water was used. For the preparation of the saturated tartrate solutions, an excess of the tartrate (usually undried) was added to the solution of sodium chloride. The flask was immersed in the bath at 25° for about 2 hours and shaken occasionally. The excess salt was then removed by filtration through sintered glass. Dissolved oxygen and carbon dioxide were removed by passage of nitrogen through the solutions before the cells were filled. The apparatus, electrodes, and techniques have been fully described in earlier publications [7, 18].

The electromotive-force data were corrected in the usual way to 1-atm partial pressure of hydrogen. The corrected values are summarized in table 1. Each entry in the table represents the average potential difference for two pairs of electrodes in the same cell. In view of the decreased solubility of the tartrate at low temperatures, only the 0.01-$m$ solution was studied between 0° and 10° and only this and the 0.02-$m$ solution between 10° and 25°.

[5] A value of 5.5 was found to give the best fit of the activity-coefficient term in mixtures of sodium hydrogen tartrate, sodium tartrate, and sodium chloride [17].

[6] Analyris performed by the Inorganic Chemistry Section of the Bureau.

TABLE 1. *Electromotive-force data for hydrogen-silver-chloride cells containing aqueous mixtures of potassium hydrogen tartrate and sodium chloride*

| KH tartrate molality | NaCl molality | Electromotive force at— (° C) | | | | | | | | | | | | |
|---|---|---|---|---|---|---|---|---|---|---|---|---|---|---|
| | | 0° | 5° | 10° | 15° | 20° | 25° | 30° | 35° | 40° | 45° | 50° | 55° | 60° |
| Saturated at 25° C | 0.015 | ..... | ..... | ..... | ..... | ..... | 0.54487 | 0.54669 | 0.54846 | 0.55029 | 0.55217 | 0.55398 | 0.55582 | 0.55760 |
| | | | | | ..... | ..... | .54488 | .54670 | .54851 | .55035 | .55221 | .55406 | .55588 | .55769 |
| | | | | | ..... | ..... | .54476 | .54662 | .54830 | .55012 | .55199 | .55382 | .55554 | .55736 |
| | .010 | ..... | ..... | ..... | ..... | ..... | .54468 | .54641 | .54825 | .55008 | .55191 | .55371 | .55554 | .55736 |
| | | | | | ..... | ..... | .55533 | .55731 | .55931 | .56131 | .56333 | .56529 | .56720 | .56911 |
| | | | | | ..... | ..... | .55532 | .55747 | .55936 | .56136 | .56340 | .56545 | .56748 | .56950 |
| | | | | | ..... | ..... | .55537 | .55730 | .55928 | .56123 | .56326 | .56532 | .56729 | .56923 |
| | .005 | ..... | ..... | ..... | ..... | ..... | .55520 | .55724 | .55920 | .56103 | .56298 | .56506 | .56695 | .56912 |
| | | | | | ..... | ..... | .57340 | .57562 | .57788 | .58081 | .58243 | .58466 | .58708 | .58951 |
| | | | | | ..... | ..... | .57343 | .57571 | .57789 | .58013 | .58241 | .58469 | .58716 | .58926 |
| | | | | | ..... | ..... | .57347 | .57566 | .57795 | .58018 | .58248 | .58470 | .58694 | .58923 |
| | | | | | ..... | ..... | .57346 | .57561 | .57812 | .58032 | .58257 | .58503 | .58721 | .58962 |
| | .015 | ..... | ..... | ..... | ..... | ..... | .54503 | .54695 | .54877 | .55059 | .55245 | .55427 | .55610 | .55800 |
| | | | | | ..... | ..... | .54502 | .54689 | .54871 | .55055 | .55239 | .55422 | .55595 | .55765 |
| 0.03 | .010 | ..... | ..... | ..... | ..... | ..... | .55570 | .55768 | .55960 | .56167 | .56374 | .56573 | .56780 | .56987 |
| | | | | | ..... | ..... | .55558 | .55752 | .55955 | .56153 | .56345 | ..... | ..... | ..... |
| | | | | | ..... | ..... | .57372 | .57615 | ..... | ..... | ..... | ..... | ..... | ..... |
| | .005 | ..... | ..... | ..... | ..... | ..... | .57373 | .57609 | .57835 | .58071 | .58293 | .58518 | .58750 | .58949 |
| | | | | | ..... | ..... | .57370 | .57601 | .57825 | .58057 | .58287 | ..... | ..... | ..... |
| | .015 | ..... | ..... | 0.54035 | 0.54230 | 0.54410 | .54560 | .54786 | .54965 | .55153 | .55340 | .55536 | .55720 | .55902 |
| | | | | .54031 | .54214 | .54401 | .54588 | .54770 | .54957 | .55136 | .55313 | .55514 | .55700 | .55883 |
| 0.02 | .010 | ..... | ..... | .55052 | .55260 | .55455 | .55694 | .55854 | .56051 | .56258 | .56455 | .56665 | .56859 | .57059 |
| | .005 | ..... | ..... | .56763 | .57001 | .57226 | .57449 | .57694 | .57928 | .58160 | .58393 | .58641 | .58873 | .59115 |
| | | | | .56758 | .56986 | .57221 | .57460 | .57689 | .57925 | .58134 | .58385 | .58624 | .58853 | .59076 |
| | .015 | 0.53800 | 0.53994 | .54185 | .54375 | .54567 | .54752 | .54939 | .55119 | .55309 | .55508 | .55700 | .55873 | .56049 |
| | | | | | | | .54757 | .54948 | .55127 | .55317 | .55502 | .55698 | .55883 | .56063 |
| 0.01 | .010 | .54779 | .54986 | .55199 | .55411 | .55618 | .55799 | .56032 | .56244 | .56455 | .56671 | .56883 | .57086 | .57297 |
| | .005 | | | | | | .55824 | .56028 | .56224 | .56430 | .56630 | .56836 | .57028 | .57225 |
| | | .56452 | .56698 | .56929 | .57150 | .57406 | .57632 | .57873 | .58096 | .58335 | .58571 | .58829 | .59065 | .59303 |

## 4. Calculation of pH$_s$

The pwH was obtained from each emf value by eq 2. These values at each temperature were plotted as a function of the chloride molality, as shown in figure 1, and pwH° obtained by a straight-line extrapolation to zero concentration of chloride. The values of pwH° for the four solutions are summarized in table 2. The accuracy of pwH° is judged to be about ±0.002 unit at 25° and ±0.003 unit at the other temperatures.

TABLE 2. pwH° *for solutions of potassium hydrogen tartrate*

| | Saturated at 25° | 0.03 *m* | 0.02 *m* | 0.01 *m* |
|---|---|---|---|---|
| ° C | | | | |
| 0 | ..... | ..... | ..... | 3.757 |
| 5 | ..... | ..... | ..... | 3.738 |
| 10 | ..... | ..... | 3.688 | 3.719 |
| 15 | ..... | ..... | 3.674 | 3.703 |
| 20 | ..... | ..... | 3.663 | 3.695 |
| 25 | 3.635 | 3.641 | 3.654 | 3.685 |
| 30 | 3.629 | 3.636 | 3.650 | 3.682 |
| 35 | 3.627 | 3.632 | 3.649 | 3.679 |
| 40 | 3.626 | 3.632 | 3.646 | 3.680 |
| 45 | 3.629 | 3.637 | 3.653 | 3.684 |
| 50 | 3.633 | 3.641 | 3.660 | 3.691 |
| 55 | 3.641 | 3.649 | 3.666 | 3.697 |
| 60 | 3.651 | 3.656 | 3.675 | 3.706 |

The positions of the straight lines shown in figure 1 were determined by the method of least squares. For the other temperatures, the lines were drawn by inspection. The intercepts obtained by inspection at 25° agreed to 0.001 unit with those obtained by the method of least squares. The concentration of chloride in these mixtures was of the same order of magnitude as that of the tartrate, and the lines might be expected to display some curvature as the chloride molality decreased. Furthermore, the different solubility of the tartrate in the three chloride solutions

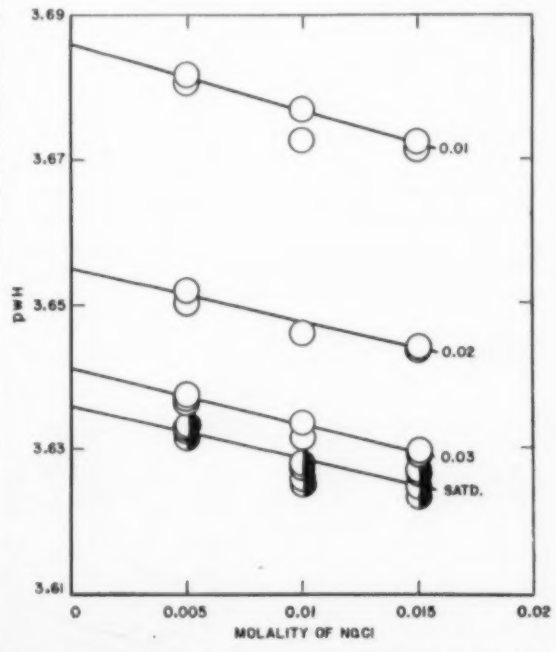


FIGURE 1. pwH *of solutions of potassium hydrogen tartrate at 25° plotted as a function of the molality of added sodium chloride.*

The molality of potassium hydrogen tartrate appears beside each line. The diameter of each circle corresponds to the estimated experimental uncertainty of 0.1 mv in the emf.

might accentuate the curvature for the saturated solution. Nevertheless, the evidence of curvature was deemed insufficient to justify abandoning the usual linear variation.

The ionic strengths, $\mu$, of the tartrate solutions without chloride are required in order to estimate $\log f'_{Cl}$ and to calculate pH from pwH°. If $m$ is the molality of potassium hydrogen tartrate (KHTar), the ionic strength is

$$\mu = m - m_{H_2Tar} + 2m_{Tar^-}. \quad (6)$$

The molalities of tartaric acid and tartrate ion can be evaluated with sufficient accuracy in the following manner [20]. From the two overlapping dissociative processes we have

$$m_{Tar^-} = m_{H_2Tar} + m_H. \quad (7)$$

As the sum of the molalities of the three tartrate species is $m$,

$$m_{H_2Tar} = 1/2(m - m_{HTar^-} - m_H), \quad (8)$$

and

$$m_{Tar^-} = 1/2(m - m_{HTar^-} + m_H). \quad (9)$$

The equilibrium among the three forms is expressed in terms of the concentration dissociation constants, $k_1$ and $k_2$, of tartaric acid by

$$\frac{k_2}{k_1} = \frac{m_{H_2Tar}\, m_{Tar^-}}{(m_{HTar^-})^2}. \quad (10)$$

If $m_H$ is so small compared with $m_{HTar^-}$ that its contribution can be neglected, we can combine eq 8 and 9 with eq 10 and solve for $m_{HTar^-}$:

$$m_{HTar^-} = m/(1 + \sqrt{4k_2/k_1}). \quad (11)$$

Combining eq 8 and 9 with eq 6 and substituting the value of $m_{HTar^-}$ from eq 11 gives the approximate expression for the ionic strength [20]:

$$\mu = m(1 + 0.5x) + 1.5m_H, \quad (12)$$

where

$$x \equiv \frac{\sqrt{4k_2/k_1}}{1 + \sqrt{4k_2/k_1}}. \quad (13)$$

The ratio of the concentration constants, $k_2/k_1$, was calculated from $K_2/K_1$, the ratio of the thermodynamic constants [17] by

$$\log (k_2/k_1) = \log (K_2/K_1) + 2A\sqrt{\mu}/(1 + 4B\sqrt{\mu}), \quad (14)$$

and the hydrogen-ion concentration was obtained with sufficient accuracy from pwH°:

$$-\log m_H = \text{pwH}° - 2A\sqrt{\mu}/(1 + 4B\sqrt{\mu}). \quad (15)$$

In this way, the ionic strengths of the 0.01-$m$, 0.02-$m$, and 0.03-$m$ solutions and that saturated at 25° were found to be 0.012, 0.024, 0.035, and 0.040, respectively. The values of $\mu$ at the other temperatures were not appreciably different from those at 25°.

The pH$_s$ at 25° was calculated by eq 5 with three values of $a_i$, namely 2, 4, and 6. The results are shown in figure 2. It is evident that the arbitrary choice of $a_i$ limits the accuracy with which the pH can be assigned to about $\pm 0.009$ unit for the saturated solution and about $\pm 0.003$ for the 0.01-$m$ solution. The pH$_s$ was calculated at the other temperatures with $a_i = 4$.

## 5. Tartrate Buffer Standards

It is apparent from figure 2 that the pH of solutions of potassium hydrogen tartrate increases by only 0.09 unit when the saturated solution is diluted to 0.01 $m$. Furthermore, it is ordinarily convenient to prepare the unsaturated solutions on a volume basis rather than on a weight basis, that is, to a definite molarity instead of a definite molality. It should be emphasized that this change does not involve an alteration of the standard state to which the numerical values of the activity are referred (compare footnote 3). Inasmuch as $d(\text{pH})/dm$ is known from the slopes of the plots shown in figure 2, only a determination of density is needed to reveal the difference of pH between 0.01-, 0.02-, and 0.03-*molal* solutions and solutions of numerically equal *molarity*. The density of the saturated solution was found with the aid of a pycnometer of 50-ml capacity to be 1.0036 g ml$^{-1}$. Thus the 0.03000-molar solution would be about 0.03005 molal, and there would be no perceptible difference between the pH of the 0.03-molar and the 0.03-molal solutions. This conclusion applies as well to the more dilute solutions. Consequently, the pH$_s$ values computed by eq 5 with $a_i = 4$ are listed in table 3 for concentrations on the molar ($M$) scale. The combined uncertainties of the pH values are estimated to be $\pm 0.012$ unit for the saturated solution and $\pm 0.006$ unit for the 0.01-$M$ solution.

TABLE 3. pH *of solutions of potassium hydrogen tartrate computed with* $a_i = 4$

| $t$ | Saturated at 25° | 0.03 $M$ | 0.02 $M$ | 0.01 $M$ |
|---|---|---|---|---|
| °C | | | | |
| 0 | ..... | ..... | ..... | 3.710 |
| 5 | ..... | ..... | ..... | 3.690 |
| 10 | ..... | ..... | 3.624 | 3.671 |
| 15 | ..... | ..... | 3.610 | 3.655 |
| 20 | ..... | ..... | 3.598 | 3.647 |
| 25 | 3.555 | 3.564 | 3.590 | 3.637 |
| 30 | 3.547 | 3.558 | 3.584 | 3.633 |
| 35 | 3.545 | 3.554 | 3.583 | 3.629 |
| 40 | 3.543 | 3.553 | 3.579 | 3.630 |
| 45 | 3.545 | 3.557 | 3.586 | 3.634 |
| 50 | 3.549 | 3.561 | 3.592 | 3.640 |
| 55 | 3.556 | 3.568 | 3.597 | 3.646 |
| 60 | 3.565 | 3.574 | 3.606 | 3.654 |

Lingane chose $3.57 \pm 0.02$ as the pH of the saturated standard [8]. For the 0.03-$M$ solution, Hitchcock and Taylor found 3.567 at 25° [21]. These

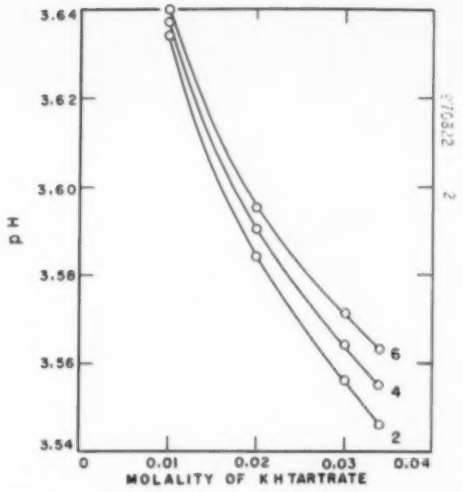


FIGURE 2. pH *of solutions of potassium hydrogen tartrate at 25° as a function of molality.*

The three curves represent pH obtained by eq 5 with $a_1$ values of 6, 4, and 2, as marked.

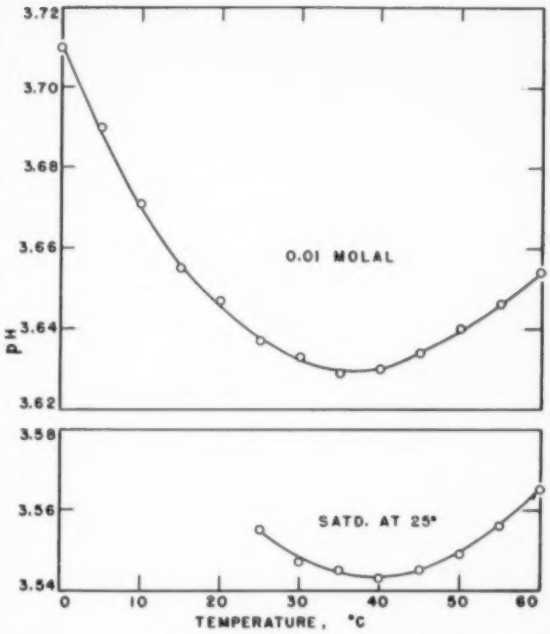


FIGURE 3. pH *of the 0.01-M and saturated solutions of potassium hydrogen tartrate as a function of temperature.*

are in good agreement with 3.555 and 3.564, respectively, the values listed in table 3.

It is important to consider the internal consistency of the scale defined by the four pH standards presently available. Ten solutions saturated with potassium hydrogen tartrate were prepared and their pH values measured by a glass-electrode pH meter calibrated with the standard phthalate and phosphate buffer solutions. The pH of each solution at 24° was found to be 3.55 or 3.56. The value obtained in an earlier study by comparison with the phosphate standard in a double hydrogen-electrode cell with liquid junction was 3.561 [7]. The $pH_s$ assigned to this saturated standard is 3.555 $\pm$0.012 at 25° (table 3).

The change of pH suffered by the tartrate standards on alteration of the temperature is primarily determined by the variation of $-\log K_1K_2$ for tartaric acid. This quantity has been shown to pass through a minimum at a temperature near 35° [17]. Consequently, the change of $pH_s$ between 25° and 60° is less than 0.03 unit, as figure 3 demonstrates. The pH of the 0.01-*M* solution is about 0.08 unit higher at 0° than at 25°.

The growth of molds in solutions of potassium hydrogen tartrate, particularly in the saturated solution, sometimes causes appreciable changes of pH within a few days after the solution is prepared [22]. It is easy to replace the saturated solution as frequently as necessary, but the solutions of lower concentration, though less susceptible to molding, are not as easily prepared. Hence, some experiments were performed to ascertain the usefulness of thymol in retarding the growth of molds. A saturated solution of potassium hydrogen tartrate to which a large crystal of thymol had been added was found to be free of mold 2 months after preparation, whereas two others without preservative molded in about 14 days. Two 0.01-*M* solutions of the tartrate salt, to one of which thymol had been added, were both free of molds 6 weeks after preparation. Thymol is only slightly soluble in aqueous solutions (about 0.006 mole dissolves in a liter of water at room temperature), and pH measurements with the glass-electrode pH meter indicated that its presence did not alter the pH of either the 0.01-*M* or the saturated buffer solution by more than 0.01 unit. Experiments with the hydrogen electrode were unsuccessful; it appeared that dissolved thymol was catalytically reduced by hydrogen at the platinum surface. Nevertheless, the usefulness of thymol in delaying the molding of tartrate solutions has been affirmed. It is suggested that a crystal of thymol, 8 to 10 mm in diameter, be added to each bottle of standard tartrate buffer.

Potassium hydrogen tartrate is not appreciably hygroscopic, and it is difficult to imagine that the salt could absorb enough moisture to alter significantly the pH of standard tartrate solutions without becoming noticeably wet. A 10-percent error in the concentration of the 0.02-*M* solution changes the pH by only 0.01 unit. Hence, it is usually unnecessary to dry the salt before it is used.

A good grade of distilled water should be used for the preparation of tartrate standards, but dissolved carbon dioxide need not be removed. The conductance of the water should not exceed $2\times10^{-6}$ $ohm^{-1}$ $cm^{-1}$ at 25°. Higher conductances may indicate the presence of small amounts of acidic or basic impurities that have a relatively large effect on the pH.

The solubility of potassium hydrogen tartrate is about 0.028 *M* at 20°, 0.034 *M* at 25°, and 0.040 *M* at 30° [19]. By reference to figure 2, it can be seen that the pH at 25° of the solution saturated at 20° does not differ by more than 0.01 unit from the pH of that saturated at 25°. The pH at 30° of the solution saturated at 30° also differs by about 0.01 unit from the pH at 30° of the solution saturated at 25°. Accordingly, the temperature at which the saturated standard is prepared need not be carefully controlled. It is suggested that the excess of the powdered salt be removed by filtration or decantation after the solution has been prepared and the solid allowed to settle. Although a crystal of thymol may successfully retard the growth of molds, these and other pH standards should probably not be considered reliable for more than 2 months after preparation.

## 6. References


[1] E. A. Guggenheim, J. Phys. Chem. **34,** 1758 (1930).
[2] D. A. MacInnes, D. Belcher, and T. Shedlovsky, J. Am. Chem. Soc. **60,** 1094 (1938).
[3] M. Kilpatrick, Jr. and M. L. Kilpatrick, J. Chem. Education **9,** 1010 (1932).
[4] R. G. Bates, Chem. Revs. **42,** 1 (1948).
[5] E. R. Smith and R. G. Bates, Compt. rend. 15th Conf., International Union of Pure and Applied Chemistry, Amsterdam, 1949, p. 118.
[6] R. G. Bates and G. D. Pinching, J. Research NBS **42,** 419 (1949) RP1982.
[7] R. G. Bates, G. D. Pinching, and E. R. Smith, J. Research NBS **45,** 418 (1950) RP2153.
[8] J. J. Lingane, Anal. Chem. **19,** 810 (1947).
[9] H. S. Harned and R. W. Ehlers, J. Am. Chem. Soc. **55,** 2179 (1933).
[10] W. J. Hamer, J. O. Burton, and S. F. Acree, J. Research NBS **24,** 269 (1940) RP1284.
[11] W. J. Hamer, G. D. Pinching, and S. F. Acree, J. Research NBS **36,** 47 (1946) RP1690.
[12] R. G. Bates and S. F. Acree, J. Research NBS **34,** 373 (1945) RP1648.
[13] G. G. Manov, N. J. DeLollis, P. W. Lindvall, and S. F. Acree, J. Research NBS **36,** 543 (1946) RP1721.
[14] R. G. Bates and E. R. Smith, J. Wash. Acad. Sci. **38,** 61 (1948).
[15] P. Debye and E. Hückel, Physik. Z. **24,** 185 (1923).
[16] G. G. Manov, R. G. Bates, W. J. Hamer, and S. F. Acree, J. Am. Chem. Soc. **65,** 1765 (1943).
[17] R. G. Bates and R. G. Canham, J. Research NBS **47,** 343 (1951) RP2260.
[18] R. G. Bates and S. F. Acree, J. Research NBS **30,** 129 (1943) RP1524.
[19] A. Seidell, Solubilities of inorganic and metal-organic compounds, 3d ed (D. Van Nostrand Co., Inc., New York, N. Y., 1940).
[20] R. G. Bates, J. Am. Chem. Soc. **70,** 1579 (1948).
[21] D. I. Hitchcock and A. C. Taylor, J. Am. Chem. Soc. **59,** 1812 (1937).
[22] R. G. Bates, Anal. Chem. **23,** 813 (1951).


WASHINGTON, June 5, 1951.

Journal of Research of the National Bureau of Standards Vol. 47, No. 6, December 1951 Research Paper 2269

# Heats of Formation of Some Barium Aluminates

R. B. Peppler and E. S. Newman

The heats of solution in HCl, 26.61 $H_2O$ of eight compounds in the system $BaO$-$Al_2O_3$-$H_2O$ were determined. From these data and data taken from the literature, the heats of formation of the compounds at 25° C were calculated.

## 1. Introduction

The hydrated barium aluminates have been studied by several investigators in order to determine their solubility relationships [1, 2, 3, 4],[1] but there are virtually no thermochemical data available on these compounds. The purpose of the present investigation is to determine the heats of formation of some of the barium aluminates and barium aluminate hydrates by measuring the heats of solution of these compounds in 2.00 *N* HCl. The following compounds were studied: $BaO.Al_2O_3$, $3BaO.Al_2O_3$, $BaO.Al_2O_3.H_2O$, $BaO.Al_2O_3.2H_2O$, $BaO.Al_2O_3.4H_2O$, $BaO.Al_2O_3.7H_2O$, $2BaO.Al_2O_3.5H_2O$, and $7BaO.6Al_2O_3.36H_2O$.

## 2. Experimental Procedure and Results

### 2.1. Preparation of the Compounds

The two anhydrous barium aluminates were obtained by igniting appropriate mixtures of $BaCO_3$ and $Al_2O_3.3H_2O$ (gibbsite) at 1,400° C to obtain $BaO.Al_2O_3$ and at 1,300° C to obtain $3BaO.Al_2O_3$. The hydrates $BaO.Al_2O_3.H_2O$ and $BaO.Al_2O_3.2H_2O$ were prepared hydrothermally; $BaO.Al_2O_3.4H_2O$ was prepared by allowing $BaO.Al_2O_3.7H_2O$ to stand in contact with an aqueous barium aluminate solution; $7BaO.6Al_2O_3.36H_2O$ and $BaO.Al_2O_3.7H_2O$ were prepared by precipitation from a supersaturated aqueous solution of $Ba(OH)_2$ and $BaO.Al_2O_3$; and $2BaO.Al_2O_3.5H_2O$ was prepared by boiling gibbsite in a $Ba(OH)_2$ solution. Full details of the preparation of these compounds have been presented elsewhere [3, 4].

The compounds were stored in glass jars for varying lengths of time prior to this investigation. The composition of each had been established by chemical analysis and petrographic examination, and it was assumed that no significant changes had occurred. The uncertainty in the composition of the compounds was estimated to be of the order of 1 percent.

### 2.2. Heat of Solution of the Compounds

The heats of solution of 2-gram samples of each compound in 640 grams of 2.00 *N* hydrochloric acid were determined in an isothermally jacketed calorimeter [5]. Solution was complete except in the cases of $BaO.Al_2O_3.H_2O$ and $BaO.Al_2O_3.2H_2O$ where about 1 and 0.1 percent, respectively, of insoluble residue remained. An analysis of these residues indicated that they were uncombined gibbsite. They were considered impurities, and the sample weights were corrected accordingly. The initial calorimeter temperature was so chosen in each case that the final temperature would be approximately 25° C, the temperature of the bath. The heat-of-solution data (see table 1) are the calculated isothermal heats of solution at 25° C. It may be noted that the heats of solution per gram of the two anhydrous compounds are higher than that of any of the hydrates, and that in the series $BaO.Al_2O_3.H_2O$, $BaO.Al_2O_3.2H_2O$, $BaO.Al_2O_3.4H_2O$, and $BaO.Al_2O_3.7H_2O$, the heat of solution decreases as the percentage of combined water in the compound increases.

TABLE 1. *Heats of solution and formation of the barium aluminates*

| Compound | Heat of solution | | Heat of formation, $\Delta H_f$, at 25° C— | |
|---|---|---|---|---|
| | cal/g | kcal/mole | From the oxides[a] | From the elements |
| | | | *kcal/mole* | *kcal/mole* |
| BaO | [b] −419.1 | [b] −64.28 | ..... | −133.4 |
| $Al_2O_3$ ($\alpha$) | [b] −588.1 | [b] −59.95 | ..... | −399.1 |
| $BaO.Al_2O_3$ | [c] −393.6±0.2 | −100.5 | −23.99 | −556.5 |
| $3BaO.Al_2O_3$ | −370.6±0.3 | −208.3 | −44.96 | −844.2 |
| $BaO.Al_2O_3.H_2O$ | −333.0±0.1 | −91.02 | −32.95 | −633.8 |
| $BaO.Al_2O_3.2H_2O$ | −300.6±0.2 | −87.57 | −36.39 | −705.5 |
| $BaO.Al_2O_3.4H_2O$ | −240.0±0.8 | −78.57 | −45.36 | −851.1 |
| $BaO.Al_2O_3.7H_2O$ | −190.4±0.2 | −72.62 | −51.29 | −1062.0 |
| $2BaO.Al_2O_3.5H_2O$ | −219.0±0.1 | −109.2 | −78.88 | −1086.6 |
| $7BaO.6Al_2O_3.36H_2O$ | −228.4±0.1 | −533.0 | −274.60 | −6092.5 |

[a] From BaO (c), $Al_2O_3$ (c, $\alpha$), and $H_2O$ (l).
[b] Calculated values.
[c] Standard deviation $= \pm\sqrt{\frac{\Sigma d^2}{N}}$.

### 2.3. Heats of Formation

The heats of formation of these barium aluminates may be calculated from their heats of solution and the heats of solution of BaO and $Al_2O_3$ in the acid used. The heats of solution of these two oxides in 2.00 *N* hydrochloric acid were calculated, because gibbsite dissolves very slowly at 25° C and BaO is difficult to prepare.

Thorvaldsen, Brown, and Peaker [6] calculated the heat of solution of $Al_2O_3$ in HCl, 200 $H_2O$. Their method is applied in the present work except that more recent data [7, 8] are used. The heat of solution of $Al_2O_3$ ($c$,$\alpha$) in HCl, 26.61[2] $H_2O$ is obtained as follows:

[1] Figures in brackets indicate the literature references at the end of this paper.

[2] In the preceding paper in this series [9], the concentration of 2.00 *N* HCl was given as HCl, 26.64 $H_2O$. This value was calculated from the data for the density of aqueous HCl at 25° C taken from the International Critical Tables. A new calculation using more precise molecular weights gives the concentration as HCl, 26.61 $H_2O$, and this new value is used through the present paper.

$$2Al(c)+6(HCl,\ 12.74H_2O)=2(AlCl_3,\ 38.21H_2O)+3H_2(g) \qquad \Delta H_1=-253.67 \text{ kcal [6]} \tag{1}$$

$$Al_2O_3(c,\alpha)=2Al(c)+3/2\ O_2(g) \qquad \Delta H_2=+399.09 \text{ kcal [7]} \tag{2}$$

$$3H_2(g)+3/2\ O_2(g)=3H_2O(l) \qquad \Delta H_3=-204.95 \text{ kcal [7]} \tag{3}$$

$$3H_2O(l)+2AlCl_3,\ 38.21\ H_2O=2(AlCl_3,\ 39.71\ H_2O) \qquad \Delta H_4=-0.24 \text{ kcal} \tag{4}$$

The sum of the above four equations gives eq 5:

$$Al_2O_3(c,\alpha)+6(HCl,\ 12.74\ H_2O)=2(AlCl_3,\ 39.71\ H_2O) \qquad \Delta H_5=-59.77 \text{ kcal} \tag{5}$$

The desired heat of solution, however, is represented by the following equation:

$$Al_2O_3(c,\alpha)+6(HCl,\ 26.61\ H_2O)=2(AlCl_3,\ 81.34\ H_2O) \qquad \Delta H_6=-59.95 \text{ kcal} \tag{6}$$

Equation 6 may be obtained by adding to eq 5 the following two equations, which represent the necessary dilutions:

$$2(AlCl_3,\ 39.71\ H_2O)=2(AlCl_3,\ 81.34\ H_2O) \qquad \Delta H_7=-2.96 \text{ kcal} \tag{7}$$

$$6(HCl,\ 26.61\ H_2O)=6(HCl,\ 12.74\ H_2O) \qquad \Delta H_8=+2.78 \text{ kcal} \tag{8}$$

The value of $\Delta H_4$ was determined by the authors to be $-0.24$ kcal; that of $\Delta H_5$ is $-59.77$ kcal, the sum of $\Delta H_1$, $\Delta H_2$, $\Delta H_3$, and $\Delta H_4$. The value of $\Delta H_7$ was found to be $-2.96$ kcal.

The heat-of-formation data for aqueous HCl [7] solutions were plotted against the square roots of their corresponding molalities, and from the resulting curve the value of $\Delta H_8$ was estimated to be $+2.78$ kcal. In each case, $\Delta H$ represents the heat effect of the equation as written.

The value of $\Delta H_6$, which is the sum of $\Delta H_5$, $\Delta H_7$ and $\Delta H_8$ was calculated to be $-59.95$ kcal.

The heat of solution of BaO in 2.00 *N* hydrochloric acid was obtained as follows:

$$BaO(c)+2(HCl,\ 26.61\ H_2O)=BaCl_2,\ 53.23\ H_2O+H_2O(l) \qquad \Delta H_9=-64.28 \text{ kcal} \tag{9}$$

$$BaCl_2,\ 53.23\ H_2O+H_2O(l)=BaCl_2,\ 54.23\ H_2O+\Delta H_{10} \tag{10}$$

The sum of these equations is

$$BaO(c)+2(HCl,\ 26.61\ H_2O)=BaCl_2,\ 54.23\ H_2O \qquad \Delta H_{11}=-64.28 \text{ kcal} \tag{11}$$

which represents the solution of BaO in an exactly equivalent amount of 2.00 *N* hydrochloric acid. The value of $\Delta H_9$ was obtained from heat-of-formation data available in the literature [7]. The value of $\Delta H_{10}$ was assumed to be negligible; consequently, the value of $\Delta H_{11}$ is the same as that of $\Delta H_9$.

When the equations describing the solutions of the compounds are subtracted from the sum of the equations describing the solution of the oxides, equations are obtained from which the heat of reaction of the constituent oxides may be deduced. The heats of formation of the compounds may be calculated from the heats of reaction of their constituent oxides, using their known heats of formation.

The calculation of the heat of formation of $BaO.Al_2O_3$ is presented in detail to illustrate the method. The three equations that represent the solution of the constituent oxides and the compound are:

$$BaO(c)+2(HCl,26.61H_2O)=BaCl_2,54.23H_2O \qquad \Delta H_{11}=-64.28 \text{ kcal} \tag{11}$$

$$Al_2O_3(c,\alpha)+6(HCl,\ 26.61H_2O)=2(AlCl_3,\ 81.34H_2O) \qquad \Delta H_6=-59.95 \text{ kcal} \tag{6}$$

$$BaCl_2,\ 2AlCl_3,\ 150.3HCl,\ 4218H_2O=BaO.Al_2O_3(c)+158.3(HCl,\ 26.61H_2O) \qquad \Delta H_{12}=+100.49 \text{ kcal} \tag{12}$$

The sum of these three equations is the following equation:

$$BaO(c)+Al_2O_3(c,\alpha)+BaCl_2,2AlCl_3,\ 150.3HCl,\ 4218\ H_2O=2(AlCl_3,\ 81.34H_2O)+BaO.Al_2O_3(c)+150.3(HCl,\ 26.61H_2O)+BaCl_2,\ 54.23H_2O \qquad \Delta H_{13}=-23.74 \text{ kcal} \tag{13}$$

It may be seen that eq 13 contains the desired equation, which is

$$BaO(c)+Al_2O_3(c,\alpha)=BaO.Al_2O_3(c) \qquad \Delta H_{14}=-23.99 \text{ kcal} \tag{14}$$

In order to obtain eq 14 from eq 13, the following two equations may be added to eq 13:

$$150.3(HCl,\ 26.61H_2O)+BaCl_2,\ 54.23H_2O=BaCl_2,\ 150.3HCl,\ 4054H_2O \qquad \Delta H_{15}=+0.072 \text{ kcal} \tag{15}$$

$$BaCl_2,\ 150.3HCl,\ 4054H_2O+2(AlCl_3,\ 81.34H_2O)=BaCl_2,\ 2AlCl_3,\ 150.3HCl,\ 4218H_2O \qquad \Delta H_{16}=+0.175 \text{ kcal} \tag{16}$$

To calculate $\Delta H_{14}$, it was necessary to determine $\Delta H_{15}$ and $\Delta H_{16}$ experimentally.

The sum of $\Delta H_{13}$, $-\Delta H_{15}$, and $-\Delta H_{16}$ is the desired value of $\Delta H_{14}$. The values of $\Delta H_6$ and $\Delta H_{11}$ have been shown to be $-59.95$ and $-64.28$ kcal, respectively. The value of $\Delta H_{12}$ was determined by the authors to be $+100.49$ kcal. The value of $\Delta H_{13}$, the sum of $\Delta H_6$, $\Delta H_{11}$, and $\Delta H_{12}$, was then calculated to be $-23.74$ kcal. To this was added the values of $\Delta H_{15}$ and $\Delta H_{16}$, determined by the authors to be $+0.072$ and $+0.175$ kcal, respectively, to obtain $-23.99$ kcal, the value of $\Delta H_{14}$.

In an exactly analogous manner, the heat of for-

mation of $3BaO.Al_2O_3$ from its constituent oxides, as represented by eq 17, may be calculated.

$$3BaO(c)+Al_2O_3(c,\alpha)=3BaO.Al_2O_3(c)$$
$$\Delta H_{17}=-44.05 \text{ kcal} \quad (17)$$

The procedure for calculating the heats of formation of the hydrates is the same, except that the water of hydration must be considered. The calculations for $BaO.Al_2O_3.H_2O$ are presented in detail to illustrate the method. The equations representing the solution in 2.00 *N* hydrochloric acid of the constituent oxides and of the compound are

$$BaO(c)+2(HCl, 26.61H_2O)=BaCl_2, 54.23H_2O$$
$$\Delta H_6=-59.95 \text{ kcal} \quad (6)$$

$$Al_2O_3(c,\alpha)+6(HCl, 26.61H_2O)=2(AlCl_3, 81.34H_2O)$$
$$\Delta H_{11}=-64.28 \text{ kcal} \quad (11)$$

$$BaCl_2, 2AlCl_3, 161.5HCl, 4517H_2O=$$
$$BaO.Al_2O_3.H_2O(c)+169.5(HCl, 26.61H_2O)$$
$$\Delta H_{18}=+91.02 \text{ kcal} \quad (18)$$

$$H_2O+BaCl_2, 2AlCl_3, 161.5HCl, 4516H_2O=$$
$$BaCl_2, 2AlCl_3, 161.5HCl, 4517H_2O+\Delta H_{19} \quad (19)$$

The sum of these four equations may be separated into the following two equations:

$$BaO(c)+Al_2O_3(c, \alpha)+H_2O(l)=BaO.Al_2O_3.H_2O(c)$$
$$\Delta H_{20}=-32.95 \text{ kcal} \quad (20)$$

and

$$BaCl_2, 2AlCl_3, 161.5HCl, 4516H_2O=BaCl_2,$$
$$54.23H_2O+2(AlCl_3, 81.34H_2O)+161.5(HCl,$$
$$26.61H_2O) \qquad \Delta H_{21}=-0.262 \text{ kcal} \quad (21)$$

where eq 20 is the desired equation and eq 21 may be broken down into components whose heat effects may be separately determined as follows:

$$161.5\ (HCl, 26.61H_2O)+BaCl_2, 54.23H_2O=BaCl_2,$$
$$161.5HCl, 4298H_2O \qquad \Delta H_{22}=+0.074 \text{ kcal} \quad (22)$$

$$BaCl_2, 161.5HCl, 4298H_2O+2(AlCl_3,$$
$$81.34H_2O)=BaCl_2, 2AlCl_3, 161.5HCl, 4516H_2O$$
$$\Delta H_{23}=+0.188 \text{ kcal} \quad (23)$$

The values of $\Delta H_6$ and $\Delta H_{11}$ have been shown to be $-59.95$ and $-64.28$ kcal, respectively, and the value of $\Delta H_{18}$ was determined experimentally to be $+91.02$ kcal. An attempt was made to determine the value of $\Delta H_{19}$ experimentally, but its magnitude was so small that it could not be measured with any degree of certainty with the available apparatus, and is therefore assumed to be zero. The sum of $\Delta H_6$, $\Delta H_{11}$, $\Delta H_{18}$, and $\Delta H_{19}$ was then calculated to be $-34.89$ kcal. The values of $\Delta H_{22}$ and $\Delta H_{23}$ were determined by the authors to be $+0.074$ and $+0.188$ kcal, respectively. Adding these to the previous sum gives a value of $-32.95$ kcal for $\Delta H_{20}$.

In an analogous manner the heats of formation from their constituent oxides of the other barium aluminate hydrates may be calculated. The corresponding reactions are:

$$BaO(c)+Al_2O_3(c,\alpha)+2H_2O(l)=BaO.Al_2O_3.2H_2O(c)$$
$$\Delta H_{24}=-36.39 \text{ kcal} \quad (24)$$

$$BaO(c)+Al_2O_3(c,\alpha)+4H_2O(l)=BaO.Al_2O_3.4H_2O(c)$$
$$\Delta H_{25}=-45.36 \text{ kcal} \quad (25)$$

$$BaO(c)+Al_2O_3(c,\alpha)+7H_2O(l)=BaO.Al_2O_3.7H_2O(c)$$
$$\Delta H_{26}=-51.29 \text{ kcal} \quad (26)$$

$$2BaO(c)+Al_2O_3(c,\alpha)+5H_2O(l)=$$
$$2BaO.Al_2O_3.5H_2O(c) \qquad \Delta H_{27}=-78.88 \text{ kcal} \quad (27)$$

$$7BaO(c)+6Al_2O_3(c,\alpha)+36H_2O(l)=$$
$$7BaO.6Al_2O_3.36H_2O(c) \qquad \Delta H_{28}=-274.60 \text{ kcal} \quad (28)$$

For each of these compounds, a group of equations was written, and appropriate dilution experiments were performed. This work required some 17 additional equations of the type already shown. These equations differed slightly from those already given because the heats of solution were all determined using 2-gram samples and a fixed amount, 640 g, of 2.00 *N* HCl. It was felt that these equations and calculations need not be shown in detail. It was found to be unnecessary to perform each dilution because of the narrow range of the heat effects. Accordingly, the values presented in table 2 were plotted and the desired heats of dilution determined by interpolation.

TABLE 2. *Heats of dilution*

| Amount of $BaCl_2$ solution | Weight of $BaCl_2$ | $+\Delta H$ | $+\Delta H$ |
|---|---|---|---|
| Varying amounts of a 17.57-percent aqueous solution of $BaCl_2$ in 610 g of 2.00 *N* HCl | | | |
| *ml* | *g* | *cal/g* | *kcal/mole* |
| 0.562 | 0.1162 | 0.517 | 0.108 |
| 5.62 | 1.1616 | .415 (avg of 4) | .086 |
| 8.09 | 1.6535 | .324 | .068 |
| 10.73 | 2.2178 | .282 (avg of 2) | .059 |
| Varying amounts of 8.34-percent aqueous $AlCl_3$ solution in 610 g of 2.00 *N* HCl and 8.18 ml of 17.57-percent $BaCl_2$ aqueous | | | |
| Amount of $AlCl_3$ solution | Weight of $AlCl_3$ | $+\Delta H$ | $+\Delta H$ |
| *ml* | *g* | *cal/g* | *kcal/mole* |
| 10.59 | 0.9491 | 1.08 (avg of 2) | 0.144 |
| 23.70 | 2.1234 | 0.66 (avg of 2) | .088 |

From the known heats of formation of the constituent oxides, the heats of formation from their constituent elements of these barium aluminates were calculated and are shown in table 1.

The authors' value of the heat of formation of $BaO.Al_2O_3$ differs widely from that of Avgustinik

and Mchedlov-Petrossian [11], who calculated their value from the pressure developed by heating an equimolar mixture of $BaSO_4$ and $Al_2O_3$. These investigators, however, did not identify the products of their reaction, and in a subsequent investigation [12] in which one of them analyzed the products formed by igniting $BaSO_4$ and $Al_2O_3$ in the appropriate stoichiometric ratio, he was unable to produce $BaO.Al_2O_3$.

Grube and Heintz [13] have calculated the heat of formation of $2BaO.Al_2O_3$ from $BaO.Al_2O_3$ and BaO to be $-2.11$ kcal/mole. The existence of $2BaO.Al_2O_3$, however, is not accepted by many investigators, and the present authors made no measurements with samples of that stoichiometric composition.

## 3. Summary

The heats of solution in 2.00 N hydrochloric acid of eight compounds in the system $BaO$-$Al_2O_3$-$H_2O$ were determined in an isothermally jacketed calorimeter. The heats of solution of two anhydrous compounds were found to be higher than those of the hydrates. In a series of hydrates that differ only in the amount of water of hydration, the heat of solution decreases as the percentage of combined water increases. The heats of formation of these barium aluminates were calculated from their heats of solution, the heats of solution of BaO and $Al_2O_3$ in the acid used, and from data available in the literature. From the data presented, the heats of hydration of several barium aluminate hydrates may be readily calculated.

---

The authors gratefully acknowledge the assistance of E. T. Carlson, who prepared the compounds studied in this investigation.

## 4. References

[1] E. Beckmann, J. prakt Chem. [2] **26,** 385 to 421, 474 to 503 (1882); **27,** 126 to 152 (1883).
[2] G. Malquori, Gazz. Chim. ital. **56,** 51 (1926).
[3] E. T. Carlson and Lansing S. Wells, J. Research NBS **41,** 103 (1948) RP1908.
[4] E. T. Carlson, T. J. Chaconas, and L. S. Wells, J. Research NBS **45,** 381 (1950) RP2149.
[5] E. S. Newman and L. S. Wells, J. Research NBS **20,** 825 (1938) RP1107.
[6] T. Thorvaldsen, W. G. Brown, and C. R. Peaker, J. Am. Chem. Soc. **52,** 3927 (1930).
[7] F. D. Rossini, Selected values of chemical thermodynamic properties, NBS C500 (1951).
[8] F. E. Young, J. Am. Chem. Soc. **66,** 777 (1944).
[9] R. B. Peppler and E. S. Newman, J. Research NBS **46,** 121 (1951) RP2183.
[10] F. D. Rossini, BS J. Research **9,** 679 (1932) RP499.
[11] A. I. Avgustinik and O. P. Mtchedlov-Petrossian, J. Applied Chem. USSR **20,** 584–90 (1947).
[12] G. M. Smirnov and O. P. Mchedlov-Petrossian, Doklvdy Akvd. Nauch. USSR **64,** 223–4 (1949).
[13] G. Grube u G. Heintz, Z. Electrochem. **41** (8) 797 (1935).

Washington, May 11, 1951.

Journal of Research of the National Bureau of Standards Vol. 47, No. 6, December 1951 Research Paper RP2270

# Thickness of Glass Electrodes

J. J. Diamond and Donald Hubbard

A nondestructive magnetic method has been developed for the measurement of the thickness of glass electrode bulbs. It involves the use of the Brenner Magne-Gage as the measuring instrument and carbonyl iron powder as the backing material. Each of the four glasses investigated was found to have a characteristic "departure thickness," ranging from 54 to 130 microns. A glass electrode whose minimum thickness was equal to or less than this departure thickness was found to give the full 59 millivolts per pH unit electrode response. Bulbs of increasingly greater thickness showed increasing departures from this theoretical response. The departure thicknesses of the glasses investigated were found to be a function of their hygroscopicities.

## 1. Introduction

The effect of the thickness of the membrane of a glass electrode on its electrode function is of interest in connection with a continuing study of the glass electrode [10, 12, 13, 16].[1] Kratz [18] made the statement that the theoretical variation of potential with pH can be obtained only with thin-walled membranes. Kahler and DeEds [17] found that there was roughly a linear relationship between the "average electrical thickness" of an electrode and the difference, in millivolts per pH unit, between its electrode response and that of a hydrogen electrode. This difference approached zero as the membrane thickness approached zero. Dole [7], however, quotes von Steiger [20] to the effect that glass electrode potential is completely independent of the thickness of the glass. The present study has been made in order to clarify the matter.

MacInnes and Dole [19] determined the thickness of their thin membranes by weighing a measured area of uniform thickness, this uniformity being determined by the use of interference colors. Knowing the glass density, they calculated their films to be about 1$\mu$ thick. Von Steiger [20] measured the thickness of his Cremer-Haber electrodes [5, 9] by bringing a glowing glass rod up to a selected distance from the glass surface. By observing the reflection against a black background, he observed interference fringes and then calculated thicknesses. Yoshimura [22], in his study of the effect of thickness on asymmetry potential, assumed the thicknesses of his electrodes were in the order of their electrical resistances and had no direct knowledge of the thicknesses involved. Kahler and DeEds [17] measured the thicknesses of their electrodes by using a microscope with a calibrated fine focus adjustment to focus on the two surfaces of the membrane. The difference in setting, corrected for the refractive index of the glass, gave the thickness.

For the purpose of this study, a nondestructive, magnetic method for the measurement of the glass membrane thickness has been developed. It involves the use of the Magne-Gage [2] [1], developed by Brenner [2, 3], for the measurement of electroplated coatings on metals, and is also used for measurements on paint, porcelain enamel, plastic, and other films or coatings that are or can be backed by iron or steel plates.

The adaptation made by us is the use of carbonyl iron powder as the backing material and the use of a corresponding direct calibration procedure.

## 2. Experimental Work

### 2.1. Method of Measuring Thickness

The operation of the Magne-Gage is based on the decrease in magnetic attraction resulting from the interposition of a nonmagnetic material between a magnet and a magnetic material. The apparatus, shown in figure 1, consists of a lever arm that is connected to a coiled spring, which is in turn connected to a dial and knob. Suspended from the end of the lever arm is one of several interchangeable permanent bar magnets of different weights and pole strengths. Two of the magnets available have been found to cover the range of thicknesses of interest in this study.

In use, the steel-backed specimen is placed in position under the magnet, and the knob is rotated counterclockwise until the presser arm, which is slip-mounted on the assembly, brings the rounded tip of the magnet into contact with the surface of the specimen. The counterclockwise rotation is continued until the built-in stop is reached, or until a trial or previous experience indicates that the tension on the spring has been released sufficiently so that the magnet will remain in contact with the specimen when the knob is rotated clockwise, taking the presser arm off the lever arm and magnet. The knob is then rotated clockwise, increasing the tension on the spring until the force is sufficient to pull the magnet away from the specimen surface. The dial reading at this point is a function of the thickness of the nonmagnetic material. When the instrument is properly calibrated with material of known thickness, the dial reading can be converted to a thickness reading.

A Cremer-Haber type glass electrode is typically a thin glass bulb about 10 to 20 mm in diameter blown on one end of a glass tube a few millimeters in diameter. Since it is impossible to use a steel plate as a backing material, for a thickness measurement on an

[1] Figures in brackets indicate the literature references at the end of this paper.
[2] Manufactured by the American Instrument Co., Silver Spring, Md.

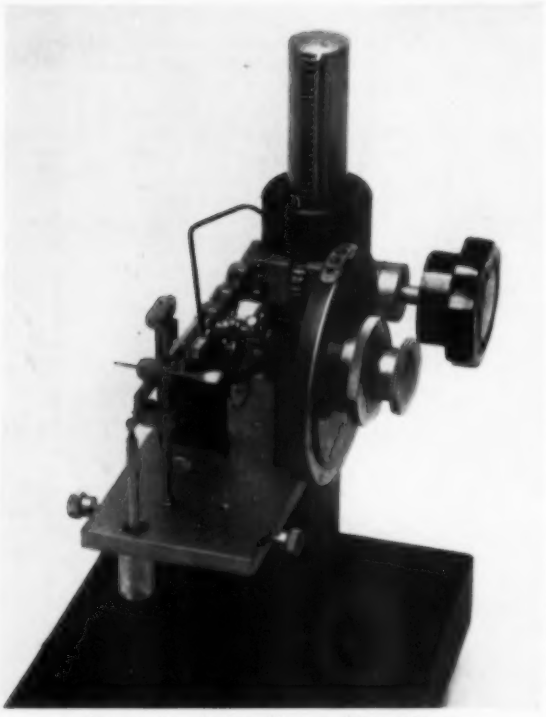

FIGURE 1. *Aminco-Brenner Magne-Gage.*
An instrument for the measurement of film thickness.

object of this shape, carbonyl iron powder is used instead. The powder is placed in the clean, dry electrode by a standard procedure, and its open end is stoppered. After adjusting the magnet to the appropriate height by means of the rack and pinion, the bulb is placed in contact with the plastic guard around the magnet, and the measurement is made. Contact with the guard serves to steady the specimen during measurement, and, if maintained during multiple measurements made to obtain a precise value for the dial reading, will insure that the readings are being made on the same spot. This is important, as all such glass bulbs are quite nonuniform in thickness. One additional precaution must be observed in handling the instrument when making measurements on powder-backed, thin membranes. It is easy for the magnet tip to dent soft or thin metal or to puncture a thin glass membrane unless contact is made gently and no pressure is exerted on the specimen by further counterclockwise rotation of the instrument knob. But in the usual case, the spring tension must be decreased to insure that the magnet will remain in contact with the specimen when the presser arm is lifted. This is accomplished before contact is made and without removing the specimen from contact with the guard, by rotating the knob counterclockwise, while using the thumb to prevent the presser arm from also rotating.

When used for the measurement of steel-backed

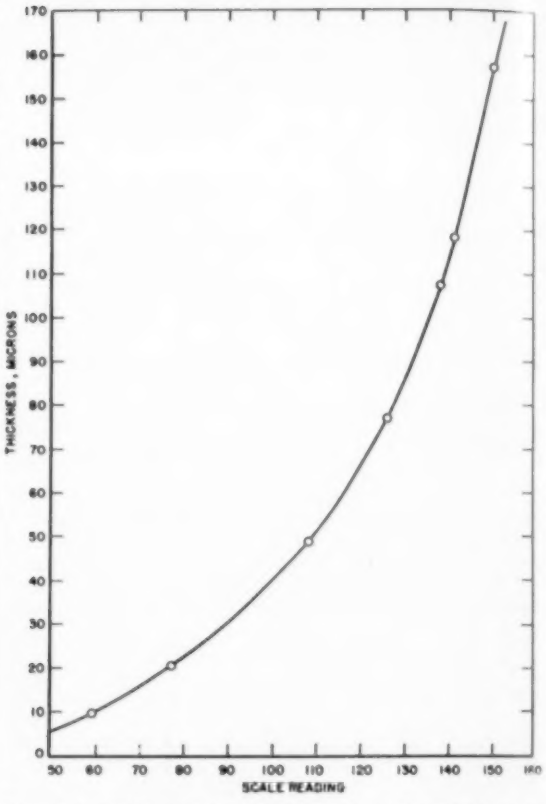


FIGURE 2. *Calibration curve showing scale reading as a function of thickness for magnet 2 of the Magne-Gage.*
Carbonyl iron powder L (20 $\mu$ average particle size), vibration-packed to equilibrium, used as backing material.

films or coatings, the Magne-Gage is calibrated against thickness standards supplied by the manufacturer. These standards are squares of steel electroplated with known thicknesses of a nonmagnetic metal. The resulting calibration curves are useless for interpreting dial readings obtained with powder-backed samples. We use instead thickness standards made by cementing aluminium or platinum foils of known and uniform thickness [3] over the open ends of glass tubes of about 9-mm diameter. These simulated electrodes are filled with carbonyl iron and measured in the same manner as the electrodes. The calibration curves resulting for magnets 2 and 3 are shown in figures 2 and 3.

In his work on the thickness of electroplated metals, Brenner [2, 3] found that the geometry of the specimen may have an appreciable effect on the scale reading obtained. In order to prove that no serious errors are introduced by the difference in shape between the Cremer-Haber electrode and the straight-tube standards, the following experiment was performed. A thick-walled bulb 15.5 mm in outside

[3] Foil-thickness measurements made by A. G. Strang.

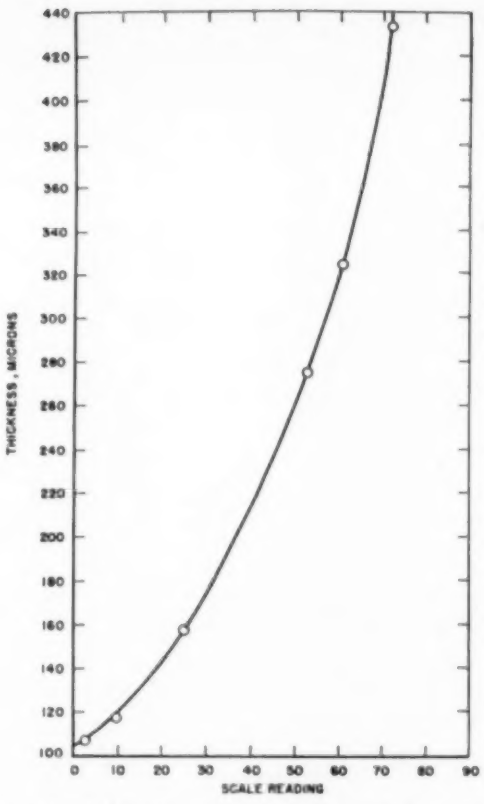


FIGURE 3. *Calibration curve showing scale reading as a function of thickness for magnet 3 of the Magne-Gage.*

Carbonyl iron powder L (20 $\mu$ average particle size), vibration-packed to equilibrium, used as backing material.

diameter was blown at the end of a piece of 6-mm tubing. A second similar electrode was prepared with a 19.0-mm bulb. The ends of the bulbs were ground off to leave holes about 2 to 3 mm in diameter. Pieces of aluminum foil 118 $\mu$ in thickness were then cemented over these holes. These simulated electrodes were filled with powder, the foil thicknesses measured with the Magne-Gage, and the readings compared with that obtained from the 118-$\mu$ straight-tube standard. Scale readings of 141, 141, and 142 were obtained, the higher reading for the 15.5-mm bulb. This is of the order of the experimental errors involved.

From the very nature of a powder, it seemed likely that the dial reading obtained on the Magne-Gage would depend on the degree of compacting of the powder, as well as on its particle size. Experiments were accordingly made on four of the five sizes available.[4] They were performed on the 118-$\mu$ straight-tube thickness standard and essentially duplicated on a typical glass electrode. The powder

[4] Available from Antara Division, General Aniline and Film Corp.

TABLE 1. *Magne-Gage scale reading as affected by vibration time and partial size*

| Vibration time | Iron powder grade | | | |
|---|---|---|---|---|
| | SF (3 $\mu$) | TH (5 $\mu$) | E (8 $\mu$) | L (20 $\mu$) |
| 118 $\mu$ straight-tube thickness standard Average scale reading (magnet 3) | | | | |
| *min* | | | | |
| 0.5 | ..... | ..... | ..... | 11.5 |
| 1 | 30 | 21.5 | 15 | 10.5 |
| 1.5 | ..... | ..... | ..... | 10 |
| 2 | 28 | 20.5 | 14 | 10 |
| 2.5 | ..... | ..... | ..... | 10 |
| 3 | 27 | 20 | 13.5 | ..... |
| 4 | 26.5 | 19.5 | 13.5 | ..... |
| 5 | ..... | 19.5 | 13.5 | ..... |
| 6 | 26 | 19.5 | ..... | ..... |
| 8 | 25.5 | ..... | ..... | ..... |
| 10 | 26 | ..... | ..... | ..... |
| Typical Cremer-Haber type glass electrode Average scale reading (magnet 2) | | | | |
| 1 | ..... | ..... | 127 | 120.3 |
| 2 | 138.5 | ..... | 125.5 | 120.2 |
| 3 | ..... | ..... | 125 | ..... |
| 4 | 136 | ..... | 125 | ..... |
| 6 | 135 | ..... | ..... | ..... |
| 8 | 134.5 | ..... | ..... | ..... |
| 10 | 134.5 | ..... | ..... | ..... |

was packed by holding the filled electrode in the normal bulb-down position and running a mechanical vibrator up and down the outside of the glass tube. In these experiments, a Sargent Ideal electric marker, set for a fairly high vibration amplitude, was used. Preliminary experiments indicated that vibration time required to reach equilibrium and Magne-Gage scale reading at equilibrium both depended on the energy of vibration. No quantitative data were obtained on this point, but it must be emphasized that the method and energy of vibration selected must be the same during measurement as during standardization.

From the data summarized in table 1, several facts are evident. For each of the four grades of carbonyl iron powder tried, vibration will result in packing to an equilibrium condition. The time needed to reach equilibrium decreases with increasing particle size. Figure 4, from the data for the straight-tube standard in table 1, illustrates this tendency. In addition, the scale readings at equilibrium decrease numerically with increasing particle size, as illustrated in figure 5. As can be seen from the calibration curves shown in figures 2 and 3, the sensitivity of measurement, as microns per scale division, decreases with increasing scale reading. Partially to keep this sensitivity as high as possible for any given thickness, but mainly to take advantage of the saving in vibration time involved, we selected 20-$\mu$ iron powder (grade L) as standard. Measurements were made after vibrating for 1.5 minutes.

The data, table 2, indicate the precision possible. Measurements were made on two electrodes, using magnet 2, filling with iron powder L, and vibrating for 1.5 minutes. After every reading, the electrode was held bulb up, still stoppered, vibrated for about 30 seconds until the powder separated from the

TABLE 2. *Multiple measurements of the thickness of two glass electrode bulbs*

| | Scale readings | |
|---|---|---|
| | Electrode 1 | Electrode 2 |
| | 121.2 | 131.0 |
| | 120.1 | 131.0 |
| | 120.1 | 130.7 |
| | 120.1 | 130.9 |
| | 120.1 | 130.2 |
| | 120.0 | 131.0 |
| | 120.2 | 131.0 |
| | 120.1 | 130.9 |
| | 121.0 | 131.0 |
| | 120.5 | 131.1 |
| | 120.2 | |
| | 121.0 | |
| $\bar{X}$—Average | 120.4 | 130.9 |
| $S$—Standard deviation, $\sqrt{\Sigma D^2/N-1}$ | 0.43 | 0.26 |
| $S/\sqrt{N}$—Standard error of mean, $S/\sqrt{N}$ | .12 | .08 |
| Limits for true average (statistical probability=0.99) | ±.12 | ±.09 |

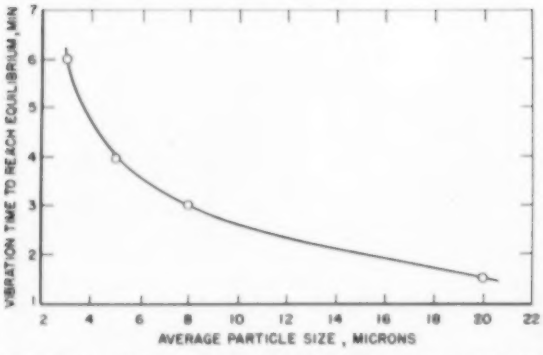


FIGURE 4. *Duration of vibration required to reach equilibrium state of packing, as a function of average particle size of the carbonyl iron powders.*

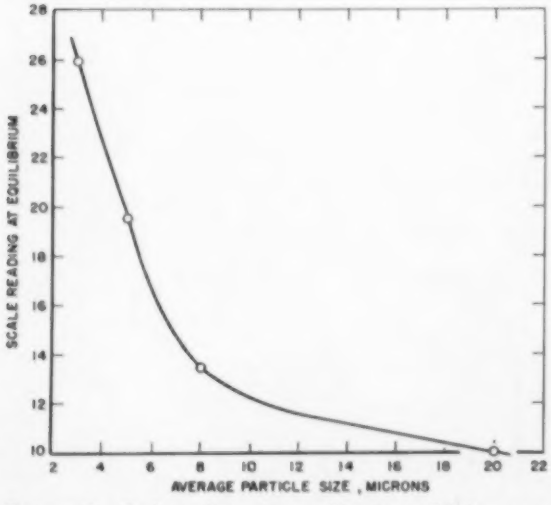


FIGURE 5. *Scale reading after packing to equilibrium as a function of average particle size of the carbonyl iron powders.*

electrode tip and then held bulb down and repacked for 1.5 minutes before the next reading was taken.

With ordinary care, scale readings can easily be reproduced to within one unit. From an examination of the calibration curves shown in figures 2 and 3, it can be seen that one scale unit amounts to about 2 to 3 percent of the thickness measured, for thicknesses down to about 30 $\mu$. For thinner membranes, this percentage increases somewhat, but measurement to 1 $\mu$ is easily obtained.

### 2.2. Measurement of Electrode Response

Each electrode was prepared for voltage response measurement by soaking in distilled water overnight or longer. It was then filled with mercury [21], into which the measurement lead was dipped. A Beckman model G pH meter was used to measure the differences in potential developed in a series of Britton universal buffer solutions [4] between the experimental electrode and a well-conditioned commercial glass electrode (Beckman 1190) serving as a reference electrode. The difference between the measured potentials for the buffer solutions of pH 4 and 8, divided by four, gave the departure of the electrode from the theoretical, in millivolts per pH unit. This departure subtracted from the theoretical 59 mv per pH unit, gave the electrode response of the experimental electrode.

## 3. Results

### 3.1. Thickness Profile of a Glass Electrode

It is obvious from the nature of the glass blowing process that a bulb blown at the end of a glass tube will be nonuniform in thickness. Many measure-

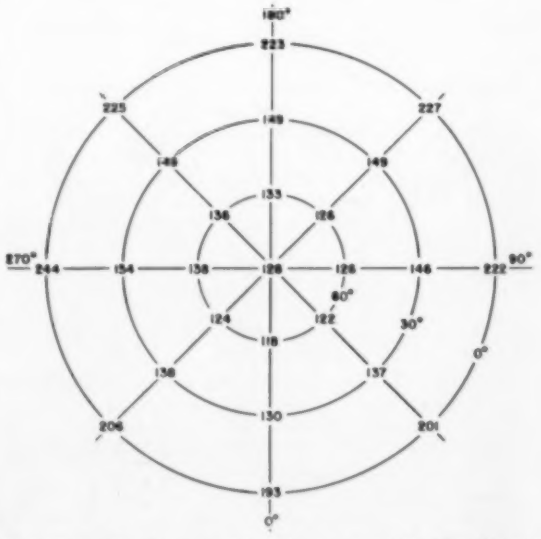


FIGURE 6. *Thickness profile of a commercial glass electrode*

Azimuthal equidistant projection, with bulb tip taken as central point. Thicknesses in microns.

ments of the thickness of glass electrode bulbs, using the powder-backed magnetic method, have shown that only in very unusual cases will the thin spot be where it might be expected, at the tip of the bulb in line with the axis of the tube. Almost invariably, it is 15 to 30 degrees off this spot.

In order to fully illustrate the range of thickness in a glass electrode bulb, a typical commercial electrode (Beckman 1190) was emptied, cleaned and dried, and its thickness profile taken by means of measurements at 25 points on the lower half of the bulb. For presentation of the data, the bulb was treated as a geographic globe with the tip as a pole, and thickness measurements were taken along the circles of latitude and longitude. The great circle passing through the thin spot of the electrode was selected as the prime meridian. The data are plotted in figure 6 on an azimuthal equidistant projection [6] of the bulb, where the tip is taken as the central point.

### 3.2. Electrode Response versus Thickness

The dependence of electrode response on bulb thickness was investigated for four different glasses, two of which were purported to be identical. They are (1) 9-mm, thin-walled Corning 015 glass electrode tubing, recently purchased for this investigation, (2) Corning 015 glass slab purchased about 20 years ago, (3) Kimble soft glass tubing, and (4) glass A, a single length of 9-mm, thick-walled tubing included in the shipment of Corning 015 tubing, but differing from it in appearance and in all properties investigated.

The electrode bulbs were blown on tubes of the same glass for all except the Corning 015 slab glass. Bulbs of that glass were blown on the thin-walled 015 tubing, the only available glass tubing from which it would not crack away on cooling.

The electrode responses obtained for bulbs of various thicknesses of the four glasses are shown in figure 7. The thickness given is that of the thin spot of the glass bulb. The area of this thin spot is estimated to vary from perhaps 2 to 10 $mm^2$, and would in any case be no smaller than the 0.75 $mm^2$ which MacInnes and Dole found to be large enough to give full electrode response with their thin-membrane electrodes [19].

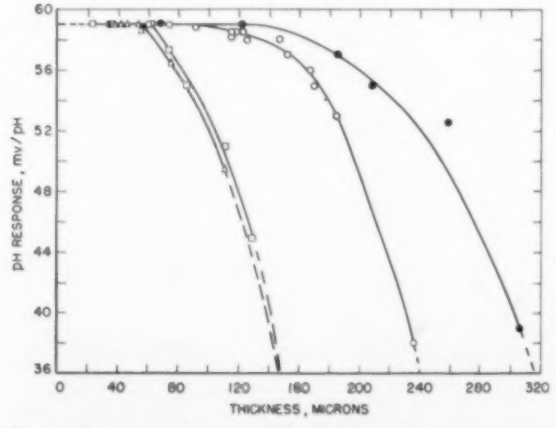


FIGURE 7. *Electrode response as a function of the thickness of the thinnest part of the electrode bulb, for four glasses.*

●, Corning 015 glass tubing; ○, Corning 015 glass slab; □, Kimble soft glass tubing; △, glass A.

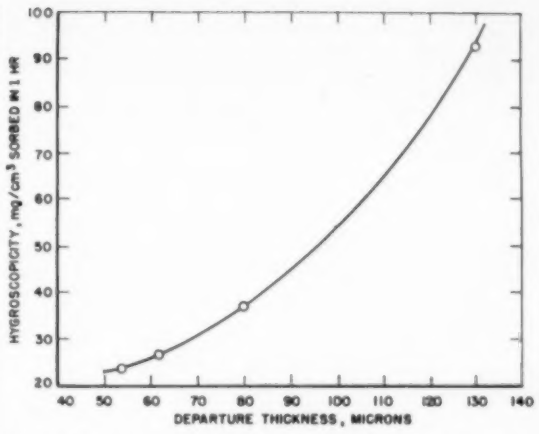


FIGURE 8. *"Departure thickness" of four glasses as a function of their hygroscopicities*

The data show that, for each of the four glasses investigated, relatively thin bulbs give the full theoretical 59 mv/pH electrode response. For each glass there is a characteristic "departure thickness", the maximum thickness that will permit full theoretical response. Beyond this point, increasingly thick bulbs show increasing voltage departures, as well as increasing difficulties and uncertainties of voltage measurement. From the data it is also evident why the two batches of Corning 015 glass were considered as different glasses. This bears out the earlier findings of others [8] that this glass may be somewhat variable in composition.

When the hygroscopicities of the four glasses were compared by the method of Hubbard [11, 16], it was found that the higher the hygroscopicity of the glass, the greater was its departure thickness. This is shown in figure 8, and is consistent with previous findings that it is impossible to get full electrode response with glasses of very low hygroscopicity [14, 15]. It is also of interest to note that the logarithm of the hygroscopicity appears to be a linear function of the departure thickness.

## 4. Conclusions and Summary

1. A magnetic method, employing iron powder, has been developed for the simple, rapid, and accurate determination of the thickness of glass electrode bulbs. The procedure has the additional advantage of not destroying the specimen. The method as given could be used with equal facility for thickness measurements on odd-shaped envelopes made of any nonmagnetic material.

2. A Cremer-Haber electrode bulb is nonuniform in thickness and has a thin spot that is usually 15 to 30 degrees from the tip of the bulb. The tip is usually not, therefore, the weakest spot on the bulb, as has been supposed.

3. Thin glass electrodes made of any of the glasses investigated will give full theoretical electrode response.

4. For each glass investigated there is a characteristic departure thickness. A glass electrode whose minimum thickness is equal to or less than this departure thickness will give full theoretical electrode response, whereas a thicker one will not.

5. For the glasses investigated, the departure thickness is a function of the hygroscopicity. Those of greater hygroscopicity will therefore permit the manufacture of electrodes of thicker and hence more rugged construction.

## 5. References


[1] American Instrument Co., Bulletin 2150, Aminco-Brenner Magne-Gages.
[2] A. Brenner, J. Research NBS **18,** 565 (1937) RP994.
[3] A. Brenner, J. Research NBS **20,** 357 (1938) RP1081.
[4] H. T. S. Britton, Hydrogen ions, 2d ed., Table 57 (c), p. 225 (D. Van Nostrand and Co., Inc., New York, N. Y., 1932).
[5] M. Cremer, Z. Biol. **47,** 562 (1906).
[6] C. H. Deetz and O. S. Adams, Elements of map projection, 5th ed., p. 43, Special Publication No. 68, Coast and Geodetic Survey, U. S. Department of Commerce (1944).
[7] M. Dole, The glass electrode, p. 28 (John Wiley and Sons, Inc., New York, N. Y., 1941).
[8] M. Dole, The glass electrode, p. 68 (John Wiley and Sons, Inc., New York, N. Y., 1941).
[9] F. Haber and Z. Klemensiewicz, Z. Physik. Chem. **67,** 385 (1909).
[10] D. Hubbard, E. H. Hamilton, and A. N. Finn, J. Research NBS **22,** 339 (1939) RP1187.
[11] D. Hubard, J. Research NBS **36,** 365 (1946) RP1706.
[12] D. Hubbard and G. F. Rynders, J. Research NBS **39,** 561 (1947) RP1848.
[13] D. Hubbard and G. F. Rynders, J. Research NBS **40,** 105 (1948) RP1859.
[14] D. Hubbard, G. W. Cleek, and G. F. Rynders, J. Research NBS **44,** 247 (1950) RP2076.
[15] D. Hubbard, M. H. Black, and G. F. Rynders, J. Research NBS **44,** 430 (1950) RP2154.
[16] D. Hubbard, M. H. Black, S. F. Holley, and G. F. Rynders, J. Research NBS **46,** 168 (1951) RP2189.
[17] H. Kahler and F. DeEds, J. Am. Chem. Soc. **53,** 2998 (1931).
[18] L. Kratz, Z. Elektrochem. **46,** 405 (1940).
[19] D. A. MacInnes and M. Dole, Ind. Eng. Chem., Anal. Ed. **1,** 57 (1929).
[20] A. L. von Steiger, Z. Elektrochem. **30,** 259 (1924).
[21] M. R. Thompson, BS J. Research **9,** 833 (1932) RP511.
[22] H. Yoshimura, Bull. Chem. Soc. Japan **12,** 443 (1937).


WASHINGTON, May 18, 1951.

Journal of Research of the National Bureau of Standards Vol. 47, No. 6, December 1951 Research Paper 2271

# Some Characteristics of Stedman Packing in the Distillation of Hydrogen and Its Isotopes

Abraham Fookson, Philip Pomerantz, and Simon Rothberg

Apparatus was designed and constructed in which some characteristics of Stedman packing in the distillation of hydrogen isotopes were measured. The average still hold-up and the hold-up at various boil-up rates were measured using both hydrogen and deuterium as still charge. Mixtures of hydrogen–hydrogen deuteride of known composition were distilled at boil-up rates of 454 milliliters per hour and 1,190 milliliters per hour, respectively. From the distillation data the height equivalent to a theoretical plate was calculated and found to be 1.0 inch for the 12-inch packing used in these experiments.

## 1. Introduction

This investigation was undertaken to determine some of the characteristics of Stedman [7] [1] packing of value in engineering calculations relating to the distillation of hydrogen isotopes. Specifically, the still hold-up at various boil-up rates and the efficiency of the packing in fractionating hydrogen–hydrogen-deuteride mixtures were studied, and the flood point determined. To obtain these data, measurements were made with a Stedman still that was designed for use at very low temperatures.

## 2. Apparatus and Material

The apparatus, similar to that described previously [1], is shown assembled in figure 1. It consisted of a still, A, with a 25- by 300-mm stainless-steel Stedman-packed section and a graduated pot of 50-ml capacity, shown in detail in figure 2. A cylinder, integral with the still, surrounded the condenser and served as a reservoir for the liquid hydrogen coolant. The vacuum jacket of this cylinderical portion was continuous with that of the still itself. The still was surrounded by a dewar (not shown) filled with liquid nitrogen and was connected to a manometer, B, enabling the pressure in the still to be read. When stopcock C was closed the still could be operated under total reflux conditions, when C was open, admission of charge or withdrawal of distillate was possible. A regular valve, D, operated by solenoid E, permitted control of the rate of distillation. This regulator consisted of a length of small diameter drill rod fixed to an iron core. The drill rod fit loosely into a glass capillary, the length of the rod in the capillary being controllable by the solenoid, the annular space through which the gas had to pass was thereby variable.

The regulator valve led to a graduated Toepler pump, F, of 500-ml capacity, and to a bypass, G. The latter was used when charging or evacuating the still. The top of the Toepler pump was connected to a manometer. The readings on manometers B and H indicated the pressure differential across the regulator, D. A length of pressure rubber tubing, J, led from the Toepler pump to a mercury reservoir. Raising or lowering of this reservoir permitted adjustment of the mercury level in the Toepler pump and consequently of the pressure within it. This, together with the regulator valve setting, constituted the method of distillation rate control used in this work.

The Toepler pump led to a manifold to which were affixed the bulbs for receiving samples (about 20 ml each), and the calibrated 5,000-ml flasks [2] used for storing hydrogen deuteride and collecting distillate. The manifold was in turn connected to a mercury diffusion pump. A line (not shown in fig. 1) between the Toepler pump and the diffusion pump bypassed the manifold, enabling the evacuation of the system whether or not bulbs were affixed to the manifold.

The hydrogen gas (99.97% $H_2$) used in this work was identical with that used in the preparation of liquid hydrogen at the Bureau. It was prepared at the low temperature laboratory of the Bureau by

[1] Figures in brackets indicate the literature references at the end of this paper.

[2] These receivers were calibrated with the assistance and equipment of the Volumetric Glassware Section of the Bureau.

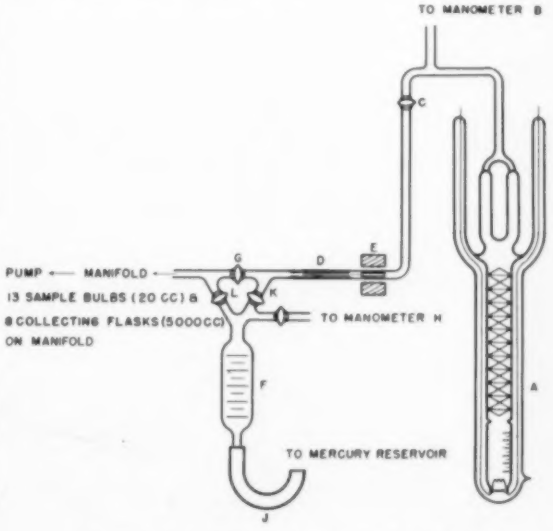


FIGURE 1. *Assembly of distillation apparatus.*

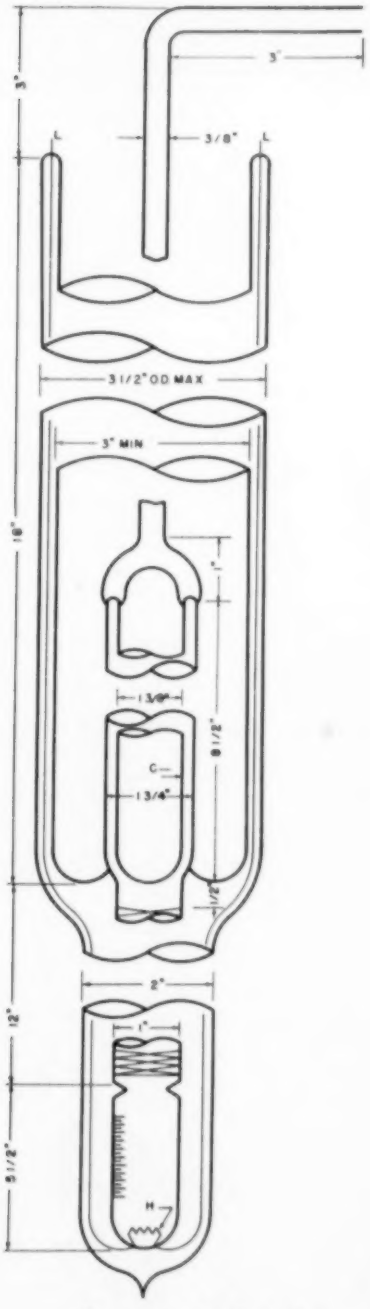


FIGURE 2. *Detail of still.*

C, Condenser; H, heater, No. 34 Constantan. Heater leads to go through No. 18 Kovar wire through glass rectifying section to be 1-in. by 1-in. Stedman packing. L, Heater leads, No. 20 copper wire.

the electrolysis of potassium hydroxide solution and pumped into a steel cylinder of convenient size.

The hydrogen deuteride was prepared by the method of Wender, Friedel, and Orchin [2], involving the reaction at 0° C between lithium aluminum hydride and deuterium oxide. For this work, about 50 liters of hydrogen deuteride was prepared, consisting of about 98.5 percent of HD, 1 percent of $H_2$, and 0.5 percent of $D_2$.[3] This material was used without purification, allowance being made for the hydrogen content when mixtures to be distilled were prepared.

## 3. Technique

### 3.1. Hold-up Measurements

The apparatus was cooled by filling the appropriate Dewars with liquid hydrogen and nitrogen. A quantity of hydrogen or deuterium, about 50 ml liquid as measured in the still-pot, was then introduced into the still as gas, and permitted to liquefy, stopcock C (fig. 1) was closed, and the exact volume noted. Current was then passed through the heater, and the volume in the still-pot and the pressure in the still were noted when equilibrium had been established. The difference between the initial volume and the equilibrium volume was taken as the hold-up corresponding to the boil-up rate as calculated from the heat input. This was repeated for various values of the current.

The results of these experiments had to be corrected for three factors. 1. There existed a heat leak into the still from the exterior, whose magnitude was estimated. 2. The initial volume as measured by means of the graduations on the still-pot was less than the amount of material actually in the still, since an unknown amount was present wetting the column (static hold-up). 3. At each boil-up rate, the volume as read on the still-pot graduations at equilibrium did not take into account the volume of the bubbles in the liquid.

### 3.2. Heat Leak and Static Hold-up

The magnitude of the heat leak was computed from the results of two subsequent experiments. The first experiment was performed by charging hydrogen into the still and reducing the pressure by means of the vacuum pump so that the liquid would boil at a temperature below that of the condenser. The vacuum pump was isolated from the system by closing stopcocks G and L, and hydrogen gas was withdrawn with the Toepler pump at such a rate that the still pressure remained constant. The time rate of withdrawal of gas was observed, and from the known heat of vaporization of hydrogen, the heat leak was calculated. This method will be referred to as the "withdrawal method" in later discussion.

The second method employed for estimating the heat leak consisted of introducing into the still a

[3] All analyses of gas mixtures reported in this work were made by the Mass Spectrometry Laboratory of the NBS.

quantity of hydrogen, reducing the pressure to a measured low value, and observing the time necessary for the pressure to rise to its normal equilibrium value. From the known heat capacity of the still contents (the still itself having negligible heat capacity at 20° K), the heat necessary to produce this pressure rise was calculated. This method will be referred to as to the "time method".

The second factor, that of the "zero" point volume, or "static" hold-up, was computed by introducing a measured quantity of hydrogen deuteride into the empty still and observing the volume of liquid that appeared in the pot. The difference in volume represented the material that wet the packing plus the amount of reflux occasioned by the heat leak into the pot.

The third factor, the augmentation in liquid volume in the pot because of the gas bubbles, could not be corrected, and volumes had to be estimated at the higher boil-up rates.

### 3.3. Distillation

The distillations conducted in this work were carried out with the apparatus shown in figure 1. After the appropriate vessels were cooled with liquid nitrogen and liquid hydrogen, a charge of hydrogen deuteride was admitted to the still from the storage flasks on the manifold. The Toepler pump was used to withdraw the hydrogen deuteride from the flasks after the equilibrium pressure of about 450 mm had been reached. From the initial and final pressures in the flasks, and their volumes, the quantity of hydrogen deuteride in the still was calculated. The volume in the still-pot was then noted, and hydrogen gas was introduced from a tank until the volume was increased to a predetermined amount. The assumption was made here that the hold-up in the column (calculated volume of hydrogen deuteride introduced minus volume measured in still-pot) would remain approximately unchanged, and hence the increase in volume represented hydrogen introduced.

Current was then passed through the still heater to provide a predetermined boil-up rate, while stopcock C was closed. The pressure as read on manometer B was noted from time to time, and when this was constant, distillation was started. Stopcock C was opened, regulator D was adjusted, and the Toepler pump allowed to fill up, by continuously lowering the mercury reservoir, at such a rate as to correspond to a predetermined reflux ratio. Each time the Toepler pump was full (500 ml), stopcock K was closed and L opened, thereby discharging the contents to either the vacuum pump, a sample bulb, or a collecting flask. Samples were collected at intervals suitably spaced during the distillation, so as to give a representative curve when the composition of distillate was plotted against amount distilled as measured by volumes in the Toepler pump and pressures read on manometer H (fig. 1). All gas volumes were corrected to 0° C and 760-mm pressure. Analyses on the several samples were determined with the mass spectrograph.

The still pressure was noted during the course of the distillation, and when it had fallen to a constant value it was presumed that the material in the still was then pure hydrogen deuteride. This pressure corresponded to the condensation temperature of hydrogen deuteride at the boil-up rate used in the experiment. Since it was a function of the rate of heat input to the still, it was not the same from run to run.

## 4. Results

### 4.1. Hold-up Measurements

The data obtained in the first experiment relating boil-up rate with hold-up, using hydrogen as still charge, are given in table 1. The temperature, $T$, in the still was calculated from the observed pressure, $P$, by means of the following equation [3]

$$\mathrm{Log}_{10} P(n-\mathrm{H}_2) = 4.66687 - \frac{49.956}{T} + 0.020537\,T. \quad (1)$$

From this temperature, the molar heat of vaporization, $L_v$, was computed, using the following equation [3]

$$L_v(n-\mathrm{H}_2) = 219.7 - 0.27(T-16.6)^2. \quad (2)$$

The molar volume of the liquid, $V_m$ (ml/mole), at the appropriate temperature was obtained by use of the following equation [8]

$$V(n-\mathrm{H}_2) = 24.747 - 0.08005\,T + 0.012716\,T^2. \quad (3)$$

From the values of $L_v$ (cal/mole), $V_m$ (ml/mole), the heater current, $I$, (amp), and the heater resistance of 46 ohms, the boil-up rate of the liquid, $B$, (ml/hr) was calculated using the equation (derived from the definitions of the quantities concerned).

$$B = \frac{I^2 V_m}{L_v} \times 3.96 \times 10^4. \quad (4)$$

The constant factor $3.9 \times 10^4$ includes the heater resistance value and the necessary conversion factors.

Flooding was first observed, using $n$-deuterium as

TABLE 1. *Hold-up measurements with hydrogen*

| $I$ | Barometer pressure | Absolute pressure in still | Equilibrium temperature | $L_v$ | $V_m$ | Boil-up rate | Volume in still | Hold-up [a] ($\Delta V$) |
|---|---|---|---|---|---|---|---|---|
| *ma* | *mm* | *mm* | *°K* | *cal/mole* | *ml/mole* | *ml/hr* | *ml* | *ml* |
| 0 | 753.4 | 771.4 | 20.45 | 215.7 | 28.43 | ..... | 46.0 | 5.7 |
| 80 | 753.4 | 791.9 | 20.52 | 215.5 | 28.47 | 33.5 | 44.0 | 7.7 |
| 150 | 753.4 | 810.4 | 20.62 | 215.3 | 28.52 | 118 | 41.5 | 10.2 |
| 200 | 752.9 | 873.9 | 20.89 | 214.7 | 28.66 | 211 | 40.0 | 11.7 |
| 250 | 752.9 | 931.9 | 21.11 | 214.2 | 28.77 | 333 | 38.5 | 13.2 |
| 310 | 752.9 | 1015.9 | 21.42 | 213.4 | 28.93 | 516 | 37.5 | 14.2 |
| 370 | 752.6 | 1106.6 | 21.74 | 212.6 | 29.18 | 744 | 36.5 | 15.2 |
| 420 | 752.6 | 1183.6 | 21.98 | 211.9 | 29.22 | 965 | 35.5 | 16.2 |
| 490 | 752.6 | 1358.6 | 22.52 | 210.2 | 29.80 | 1347 | 34.5 | 17.2 |
| 540 | 752.4 | 1496.4 | 22.93 | 208.9 | 30.35 | 1679 | 33.0 | 18.7 |

[a] Corrected by adding 5.7 ml (average of experiments 1 to 3, table 3) to observed results.

TABLE 2. *Hold-up measurements with deuterium*

| $I$ | Absolute pressure in still | Equilibrium temperature | $L_v$[a] | $V_m$[b] | Boil-up rate | Volume in still | Hold-up[c] ($\Delta V$) | Remarks |
|---|---|---|---|---|---|---|---|---|
| *ma* | *mm* | *°K* | *cal/mole* | *ml/mole* | *ml/hr* | *ml* | *ml* | |
| 0 | 266 | 20.49 | 300.8 | 23.68 | 0 | 46.8 | 5.7 | Static hold-up. |
| 303 | 410 | 21.68 | 298.1 | 24.07 | 293 | 38.8 | 13.7 | |
| 502 | 583 | 22.73 | 294.8 | 24.45 | 827 | 38.0 | 14.5 | |
| 612 | 764 | 23.59 | 291.7 | 24.79 | 1,260 | 37.0 | 15.5 | |
| 697 | 933 | 24.26 | 289.4 | 25.06 | 1,660 | 37.0 | 15.5 | |
| 748 | 1,090 | 24.81 | 287.6 | 25.30 | 1,948 | 37.0 | 15.5 | |
| 817 | 1,311 | 25.48 | 285.5 | 25.59 | 2,368 | 36.0 | 16.5 | |
| 855 | 1,439 | 25.83 | 283.7 | 25.75 | 2,626 | 31 to 33 | 19.5 to 21.5 | |
| 905 | 1,618 | 26.29 | 282.0 | 25.96 | 2,984 | ..... | ..... | |
| 960 | 1,866 | 26.85 | 279.8 | 26.24 | 3,420 | 21 | 31.5 | |
| 1,000 | 1,990 | 27.11 | 278.7 | 26.37 | 3,745 estimated | 15 | 37.5 | Flooding. |
| [d] >1,000 (estimated 15 ma) | 2,014 | 27.16 | 278.5 | 26.39 | 3,864 | ..... | ..... | Do. |

[a] Calculated by adding 85.2 cal/mole (difference between $n$-$D_2$ and $n$-$H_2$ at 19.70° K) to corresponding value of $n$-$H_2$.

[b] $V_m$ (ml/mole) = $22.965 - 0.2460\,T + 0.0137\,T^2$.

[c] Corrected by adding 5.7 ml (average of experiments 1 to 3, table 3) to observed results.

[d] Off scale.

still charge, at a boil-up rate of 3,745 ml/hr, at which rate the pressure in the still was 1,990 mm Hg. This corresponded to a vapor velocity of 0.26 ft/sec. In a previous experiment using hydrogen as still charge, the column could not be induced to flood within the limits of the apparatus. The controlling factor here was the manometer, B (fig. 1), whose upper limit was about 2,000 mm Hg.

In the case of deuterium, as the boil-up rate increased from the lower values, the level of liquid at the edges of the plates was substantially constant, increasing from approximately 1 mm at 2,626 ml/hr to about 3 mm at 3,420 ml/hr. But as the flood point was neared the amount of liquid continued to increase in the top third of the column. Shortly, on the top plate, liquid completely covered the cone and continued to increase until a column of liquid started to enter the condenser. This boil-up rate was designated as the flood point.

The calculation of the boil-up rates when deuterium was used in the hold-up measurements are not as accurate as were those when hydrogen was used. This is a consequence of the fact that there does not exist a reported heat of vaporization-temperature relationship for deuterium as there does for hydrogen. Hence, the deuterium analogues of eq 2 and 3 could not be employed. An approximation was obtained for the heats of vaporization of deuterium at various temperatures ($L_v$, table 2) by drawing a curve through the single reported value, 302.3 cal/mole at 19.70° K, parallel to the corresponding curve for hydrogen as derived from eq 2. The error in this approximation was not estimated.

The hold-up at, and in the neighborhood of, the flood point, was exceedingly difficult to measure by the technique employed here. This was due to the inability of accurately determining the volume of liquid in the pot because of the violence of the boiling. An attempt was made to eliminate this difficulty by momentarily switching off the heater current and immediately reading the volume. However, this method proved unfeasible, because before the gas bubbles ceased rising the liquid volume was changing rapidly due to the return of reflux from the column. The difficulty in accurately reading the volume under the circumstance described was undoubtedly the major factor in accounting for the discrepancy in the values for the hold-up when hydrogen (table 1) and the deuterium (table 2) were used. However, in both cases, the order of magnitude is believed to be correct.

TABLE 3. *Static hold-up measurements*

| Experiment | Material introduced into still | | | Volume observed in pot | Static hold-up |
|---|---|---|---|---|---|
| | HD | $H_2$ | Total | | |
| | *ml* | *ml* | *ml* | *ml* | *ml* |
| 1 | 16.2 | 0.3 | 16.5 | 11.0 | 5.5 |
| 2 | 26.5 | .5 | 27.0 | 21.2 | 5.8 |
| 3 | 16.6 | .3 | 16.9 | 11.0 | 5.9 |
| 4 | 31.9 | 1.2 | 33.1 | 26.2 | 6.9 |

The results of the "static" hold-up determinations are shown in table 3. In these experiments hydrogen deuteride was used. The results were used to correct the observed values of the hold-up in both the hydrogen and the deuterium experiments. The figures for the hold-up in tables 1 and 2 are the corrected values.

In computing the correction due to the static hold-up, experiment 4 of table 3 was rejected as being evidently in error. The much higher percentage of hydrogen present in the charge (5%, as opposed to 1.5% in the other three cases) would tend to give high results, since, through fractionation, this material would be localized in the column. The average of the first three experiments was therefore taken as the correction to be applied in tables 1 and 2.

## 4.2. Heat-Leak Measurements

### a. Calculation from Still Dimensions

At an atmospheric pressure of 753 mm, the pressure inside the still was 771 mm, with no current

flowing in the heater coil. This pressure differential corresponded to a temperature differential of 0.073°, from eq 1. Since the condenser wall thickness, $L$, was 0.075 cm, and its area, $A$, was 493 cm$^2$, the rate at which heat was entering and leaving the system to maintain a steady state was obtained from the equation

$$\frac{dQ}{dt} = -KA\frac{dT}{dL} \tag{5}$$

Using a value[4] for $K$ of $3\times10^{-4}$ cal cm$^{-1}$ sec$^{-1}$ deg$^{-1}$, this rate was 0.144 cal/sec, or from eq 4, equivalent to a boil-up rate of 70 ml/hr.

This value is undoubtedly too high, since the figure used for the effective area of the condensing surface is excessive. This was indicated by the fact that the pressure in the still was not dependent upon the level of liquid hydrogen coolant in the condenser over a wide range of levels, when there was no heat input. In addition, the condensing gas-condenser wall and condenser wall-coolant liquid temperature differentials were not taken into account. These differentials may exceed that across the condenser wall itself, though the latter is the one employed in the $dT/dL$ term in the eq 5.

#### b. Time Method

The "time method", described above, yielded values of 2.5 and 2.0 ml/hr, for the boil-up rate equivalent to the heat leak as the results of two experiments (table 5). Though these values possess the merit of consistency, objections can be raised to the experimental method used. The assumption implicit in the method is that when the pressure was reduced, the entire body of liquid in the still was in thermal equilibrium. This was probably not realized in practice, since cooling through evaporation would occur at the surface of the liquid, and the remainder would have to be cooled by convection. Moreover, thermal equilibrium would most likely be absent throughout the entire experiment, as the pressure rose, since the convection would be slow. In addition, the amount of material in the column, and its thermal state, was not known. Because of these considerations, the validity of the time method for measuring the heat leak is open to question.

#### c. Withdrawal Method

In the opinion of the authors, the best method for measuring the heat leak is the "withdrawal method", in which the rate at which liquid is vaporized at constant pressure as a consequence of the heat leak was measured. The results are given in table 4. In this case, the question of thermal equilibrium did not arise, since the entire process occurred at constant temperature. Also, the quantity of material in the still was of no consequence, since the heat leak was probably independent of the height of liquid in the still pot.

[4] This value was obtained by applying eq 5 to the known operating conditions and dimensions of the still used in previous work [1].

TABLE 4. *Heat-leak measurements by withdrawal method*

| Experiment | Absolute P in still | Gas collected at STP | Time | Heat leak | Corresponding boil-up rate |
|---|---|---|---|---|---|
| | *mm* | *ml* | *min* | *cal/hr* | *ml/hr* |
| 1 | 443 | 244 | 1.54 | 93.6 | 12.1 |
| 2 | 507 | 213 | 1.13 | 95.5 | 12.3 |
| 3 | 371 | 202 | 2.09 | 59.6 | 7.7 |
| 4 | 443 | 217 | 1.91 | 65.4 | 8.4 |

The inconsistencies found in the values in table 4 can probably be explained by taking into account two experimental factors. First, the Toepler pump was an inaccurate flowmeter. It was operated manually, the mercury level being lowered at such a rate that the still pressure remained constant; this was quite difficult to accomplish at a uniform rate. Second, the condition of thermal equilibrium was undoubtedly disturbed each time the pressure was reduced or permitted to increase, for the reasons pointed out in the discussion of the time method. However, the values were sufficiently close together to safely assert that the heat leak was equivalent to a boil-up rate of about 10 ml/hr. This was shown to be at least qualitatively true by the fact that the vigor of the boiling in the first hold-up measurement at 33.5 ml/hr (table 1) was very much greater than that at zero current input. At any rate, it is certain that whichever of the above heat leak measurements is nearest the truth, it is a factor of little consequence at the higher boil-up rates.

### 4.3. Distillation Measurements

Two distillations were carried out at boil-up rates of 465 ml/hr and 1,190 ml/hr. The results of these are listed in tables 6 and 7, and are shown in figures in figures 3 and 4, respectively. Because of difficulty in manual control of the level in the Toepler pump and the continuous adjustment of the take-off regulator, constant reflux ratios were difficult to maintain though the order of magnitude was the same in both cases.

As can be seen from figures 3 and 4, the efficiency of

TABLE 5. *Heat-leak measurements by time method*

| Experiment | Absolute $P$ in still | | Temperature | | Time | Volume in still | | $\Delta V$ | Heat leak | |
|---|---|---|---|---|---|---|---|---|---|---|
| | Initial | Final | Initial | Final | | Initial | Final | | | |
| | *mm* | *mm* | *°K* | *°K* | *sec* | *ml* | *ml* | | *cal/hr* | *ml/hr* |
| 1 | 283 | 772 | 17.71 | 20.45 | 27 | 25.0 | 25.3 | −0.3 | 19.0 | 2.5 |
| 2 | 276 | 768 | 17.40 | 20.43 | 33 | 21.5 | 20.0 | +1.5 | 15.2 | 2.0 |

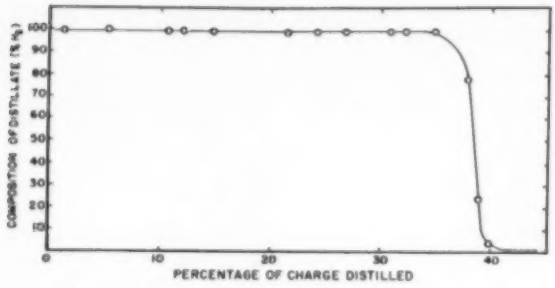


FIGURE 3. *Distillation curve at lower boil-up rate.*

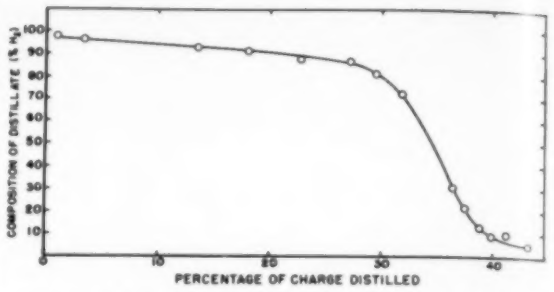


FIGURE 4. *Distillation curve at higher boil-up rate.*

TABLE 6. *Distillation of* $H_2$-HD *mixture*

Charge: 1.03 moles HD = 68.2 mole %
0.48 moles $H_2$ = 31.8 mole %
Heater resistance: 46 ohms
Current input: 318 ma

| Still pressure | Amount distilled (STP) | | Composition | | Reflux ratio | Fraction |
|---|---|---|---|---|---|---|
| | | | $H_2$ | HD | | |
| *mm abs* | *ml* | % | | | | |
| 1,025 | 453 | 1.34 | 99.7 | 0.3 | 110 | 1 |
| 1,020 | 1,812 | 5.36 | 99.8 | .2 | 21 | 2 |
| 1,016 | 3,624 | 10.71 | 99.7 | .3 | 55 | 3 |
| 1,005 | 4,077 | 12.05 | 99.7 | .3 | 62 | 4 |
| 998 | 4,983 | 14.73 | 99.6 | .4 | 55 | 5 |
| 984 | 6,344 | 18.76 | 99.4 | .6 | 62 | 6 |
| 967 | 7,250 | 21.43 | 99.2 | .8 | 69 | 7 |
| 950 | 8,156 | 24.11 | 99.3 | .7 | 62 | 8 |
| 920 | 9,062 | 26.79 | 99.3 | .7 | 83 | 9 |
| 842 | 10,421 | 30.81 | 99.4 | .6 | 83 | 10 |
| 807 | 10,874 | 32.15 | 99.4 | .6 | 69 | 11 |
| 743 | 11,770 | 34.80 | 99.5 | .5 | 93 | 12 |
| 606 | 12,819 | 37.90 | 77.2 | 22.8 | 68 | 13 |
| 600 | 13,166 | 38.93 | 23.7 | 71.3 | 93 | 14 |
| 600 | 13,513 | 39.95 | 3.5 | 96.5 | 100 | 15 |
| 602 | 13,856 | 40.97 | .8 | 99.2 | 85 | 16 |

TABLE 7. *Distillation of* $H_2$-HD *mixture*

Charge: 1.24 moles HD = 70.0 mole %
0.53 moles $H_2$ = 30.0 mole %
Heater resistance: 46 ohms
Current input: 505 ma
*Tr* = <0.1%

| Still pressure | Amount distilled (STP) | | Composition of distillate | | | Reflux ratio | Fraction |
|---|---|---|---|---|---|---|---|
| | | | $H_2$ | HD | $D_2$ | | |
| *mm apr* | *ml* | % | | | | | |
| ---- | 448 | 1.1 | 99.0 | 1.0 | ---- | 81 | 1 |
| 1,322 | 1,344 | 3.4 | 97.8 | 2.2 | ---- | 77 | 2 |
| (a) | (a) | (a) | ---- | ---- | ---- | ---- | 3 |
| 1,290 | 5,376 | 13.5 | 93.1 | 6.9 | ---- | 85 | 4 |
| 1,230 | 7,168 | 18.1 | 92.0 | 8.0 | ---- | 63 | 5 |
| 1,150 | 8,980 | 22.6 | 88.0 | 12.0 | ---- | 76 | 6 |
| 1,112 | 9,876 | 24.9 | (b) | (b) | (b) | 65 | 7 |
| 1,060 | 10,772 | 27.1 | 87.2 | 12.8 | ---- | 69 | 8 |
| 998 | 11,668 | 29.4 | 81.6 | 18.4 | ---- | 85 | 9 |
| 950 | 12,564 | 31.7 | 72.0 | 28.0 | Tr | 57 | 10 |
| 880 | 14,417 | 36.3 | 30.7 | 69.2 | Tr | (c) | 11 |
| 856 | 14,865 | 37.4 | 21.7 | 78.3 | Tr | 79 | 12 |
| 839 | 15,322 | 38.6 | 12.7 | 87.2 | 0.1 | 66 | 13 |
| 830 | 15,770 | 39.8 | 9.1 | 90.8 | .1 | 111 | 14 |
| 841 | 16,218 | 41.1 | 9.6 | 90.3 | .1 | 870 | d 15 |
| ---- | 17,114 | 43.1 | 4.9 | 95.0 | .1 | 65 | 16 |
| 843 | 18,110 | 45.7 | 4.4 | 95.5 | .1 | 119 | 17 |
| 845 | 18,558 | 46.8 | 3.2 | 96.8 | .1 | 55 | 18 |

[a] Contaminated sample not analyzed.
[b] Not taken.
[c] Failed to note time on sample, therefore no reflux ratio obtained.
[d] Taken after 21 minutes total reflux.

separation is greater at the lower boil-up rate. At the lower boil-up rate, the shape of the curve shows that the efficiency of the column was above the minimum number of plates necessary for separation. Since the reflux ratio was not absolutely constant, the fact that the points fall on a smooth curve shows that the still efficiency is not dependent upon reflux ratio at this boil-up rate.

At the higher boil-up rate, the efficiency of separation is lower. In figure 4 it is seen that the points do not fall on a smooth curve, probably because of the dependence of separation upon reflux ratio. Thus, at a value of 41.1 percent distilled the reflux ratio rose to 870 to 1 because of a time interval spent in charging sample bulbs; the fractionation of this sample was thus improved noticeably by the refluxing.

### 4.4. Estimation of Column Efficiency

In usual distillation practice, the efficiency of a column is obtained by analyzing simultaneously withdrawn samples from the pot and the head, and computing by analytical or graphical methods the number of theoretical plates required to effect the observed difference in composition [4]. This technique was not applied here because of the experimental difficulties involved in withdrawing a representative sample from the pot. Instead, the distillation data were used to calculate the efficiency of the Stedman column employed in this work. The calculation presented here is that of George Webb [6], of Hydrocarbons Research, Inc. In brief, the method involves computing the composition of the pot liquid at any chosen point in the distillation by making use of the known composition of the material already distilled, together with inferences concerning the composition of the column hold-up. The latter is assumed to vary logarithmically from the pot composition to the head composition. From the knowledge of the analysis of the material in the pot and that of the head at the chosen point in the distillation, the efficiency of the still can be calculated by conventional methods.

Thus, consider the case, in the second distillation (table 7 and figure 4), at the point where 8,000 ml (STP) have already been distilled. The charge initially was 1.77 moles (39,700 ml STP), and the hold-up was 16 ml liquid, or 12,700 ml STP. Then

Bottoms = 39,700 − 8,000 − 12,700 = 19,000 ml STP

Top composition (from an enlargement of the appropriate portion of fig. 4) = 89.3 percent of $H_2 = y$.

Distillate composition (average of composition from zero to 8,000 ml distilled) = 94.7 percent of $H_2$. If $x$ is the mole fraction of hydrogen in the pot liquid,

$$19{,}000x + 12{,}700\frac{(0.893-x)}{\ln\frac{0.893}{x}} + (0.947)(8{,}000) = (0.30)(39{,}700),$$

from which

$$x = 0.042.$$

The average value of the relative volatility, $\alpha$, for H-HD mixtures of the composition dealt with here is 1.45 [6]. For a partial condenser, under total reflux conditions, the number of theoretical plates, $n$, is given by [5].

$$\left.\begin{aligned} n+2 &= \frac{\operatorname{Log}\left(\frac{y}{1-y}\right)_{\text{top}}\left(\frac{1-x}{x}\right)_{\text{bottom}}}{\log d_{av}} \\ &= \frac{\log\left(\frac{0.893}{0.107}\right)\left(\frac{0.958}{0.042}\right)}{\log 1.46} \\ &= 13.8 \end{aligned}\right\} \quad (6)$$

or

$n = 11.8$ for the packing used in this work.

$$\text{HETP} = \frac{12}{11.8} = 1.0 \text{ in.}$$

Since the reflux in this experiment was not total, the efficiency of the column is undoubtedly higher than that indicated in the above calculation. Calculations made for amounts of distillate other than the 8,000 ml employed in the above example also gave about 1 in. for the HETP. In view of the simplifying assumptions made in these calculations, it is felt that no valid conclusions can be drawn concerning the relation between the HETP and the other variables of the experiment.

## 5. References


[1] A. Fookson, P. Pomerantz, and E. H. Rich, J. Research NBS **47,** 31 (1951) RP2224.

[2] E. Wender, R. A. Friedel, and J. J. Orchin, J. Am. Chem. Soc. **71,** 1140 (1949).

[3] H. W. Woolley, R. B. Scott, and F. G. Brickwedde, J. Research NBS **41,** 379 (1948) RP1932.

[4] Clark Robinson and Edwin R. Gilliland, Elements of fractional distillation, 4th ed., p. 118ff and 174ff (McGraw-Hill Book Co., Inc., New York, N. Y., 1950).

[5] Clark Robinson and Edwin R. Gilliland, 4th ed., p. 175 (McGraw-Hill Book Co., Inc., New York, N. Y., 1950).

[6] G. B. Webb, private communication.

[7] D. F. Stedman, Cana. J. Res. **15B,** 383 (1937); U. S. Patent 2047444 (July 14, 1936).

[8] R. B. Scott and F. G. Brickwedde, J. Research NBS **19,** 237 (1937) RP1023.



Washington, July 26, 1951.

Journal of Research of the National Bureau of Standards Vol. 47, No. 6, December 1951 Research Paper 2273

# Use of Radiation From Incandescent Particles as an Indication of Flame Temperature[1]

Earle K. Plyler and Curtis J. Humphreys

This study was undertaken to determine if the radiation from incandescent carbon particles could be utilized in the measurement of the temperature of flames. This is a preliminary investigation of the measurement of flame temperatures by using the intensities in the ultraviolet continuum at two wavelengths chosen in regions comparatively free from molecular bands and comparing these energies with the continuous emission at the same wavelengths of a calibrated tungsten ribbon lamp containing a quartz window. Fuel-rich oxyacetylene flames were used because they contain the desired incandescent particles. The ratios of intensities in the chosen spectral regions were determined photographically and photoelectrically. Interpretation of the observed ratio for a given flame, in terms of temperature has been made, and flame temperatures from 1,900° to 2,400° C have been determined.

## 1. Introduction

The temperature of a flame is something extremely difficult to define. This should become evident when it is pointed out that the energy liberated in the combustion process appears in many forms and that at a given instant a state of equilibrium can hardly be expected to be realized. Thus, the molecules formed as products of combustion will have varying amounts of translational, vibrational, or rotational energy, each form of energy leading to a corresponding temperature. A detailed discussion of flame temperatures and of several methods of measuring them is to be found in a book by Gaydon [1].[2] The apparent temperature of a flame will necessarily depend on the method of measurement chosen, because in general the method will utilize a physical process corresponding to a characteristic temperature. Several methods for the measurement of flame temperatures have been devised or proposed. For flame temperatures below 1,700° C the problem is relatively simple because high melting-point temperature detectors can be inserted directly into the flame. For higher temperatures some method utilizing radiant energy must be employed. Some of the methods are line reversal, generally by using sodium vapor, and determinations based on intensity ratios among the components of the emission bands. The last-named method leads to what may be called the rotational temperature.

The present study is concerned with a special class of flames, namely, opaque or semiopaque flames. The appearance of such a flame depends on the abundance of incandescent particles in the flame, which may be either carbon particles originating in the combustion process or solid particles of some other material purposely introduced. For practical purposes the radiant energy emitted by a cloud of glowing particles may be regarded as having properties similar to those of the spectral continuum from the surface of an incandescent body at the same temperature. The essential difference is that the over-all intensity, or total radiant flux, will depend on the number of particles present and will always be less than that from the surface of a solid or liquid at the same temperature.

The spectral distribution of energy from a hot body emitting continuously is a function of temperature. If the emitter is a black body, this temperature dependence may be expressed by any of a number of well-known formulas [2], the Planck distribution law being the most precise. The form of this distribution curve, in which energies are plotted as ordinates and wavelengths as abscissas, is somewhat similar to a probability curve. At any given temperature there is a maximum of energy emission corresponding to some wavelength. The maximum of emission shifts to shorter wavelengths for higher temperatures according to the well-known Wien displacement law, $\lambda T = K$, where $\lambda$ is the wavelength of maximum emission and $T$ the absolute temperature. It is obvious that if the wavelength position of the emission maximum could be located precisely, the corresponding absolute temperature would be determined. Unfortunately, the precise location of the emission maximum is beset with several experimental difficulties, not the least of which is that it is broad and not too well defined. Another method of temperature measurement is to establish the form of the energy distribution curve. This may be accomplished by determining the relative values of energy emitted at a number of wavelengths. When visible light is employed, this is the procedure used in determining what is called the color temperature [2, p. 23 and 382]. The method depends on the comparison of intensities of different portions of the continuous spectrum, as isolated by color filters. Its application to flame-temperature determinations is discussed by Gaydon [1, p. 175]. The temperature measured is that of the glowing particles in the flame, which may not be completely in equilibrium with the flame gases. Emission characteristics of molecules excited in the combustion process is a possible source of error, which can be avoided by

[1] A partial report of this work was given at the New York meeting of the Optical Society of America (March 1949). J. Opt. Soc. Am. 39, 639 (1949).

[2] Figures in brackets indicate the literature references at the end of this paper.

using filters that transmit only in wavelength regions free of these characteristic spectra.

The representation of spectral energy distribution from continuous emitters by a precise formula is ordinarily restricted to black bodies. Corrections, depending on variations in emissivity, necessary to interpreting spectral distributions encountered in actual glowing bodies in terms of temperature, present no great difficulty.

For this study of flame temperatures, the ultraviolet region was selected because: (1) there is no appreciable radiation from surrounding objects that have temperatures below 1,600° C, (2) the energy emitted increases more rapidly with temperature than it does in the infrared, and (3) the difference between true and brightness temperature is less than in the infrared [2, p. 380].

Although the procedures for measuring color temperatures are well known, very little work has been reported previously on the measurement of flame temperatures by establishment of the energy distribution in the ultraviolet.

## 2. Experimental Procedure

Oxyacetylene flames were selected for use in these experiments, a choice based on the availability of equipment for producing and controling such flames and the fact that rich mixtures of oxygen and acetylene burn with an opaque flame owing to the large amounts of carbon liberated, a condition favoring this method. The essential units of a commercial welding outfit, consisting of a torch with a number 4 welding tip, regulators for the respective gases, and gas cylinders, were used to produce the flames. Both the volume of the flame and the relative amounts of the two gases are controllable by manipulation of the valves in the mixing unit of the torch and finding the appropriate settings of the needle valves in the regulators. Rotameters were used in the later stages of the work in order to measure the rates of flow of the gases. The appearance of the flame varies greatly with the mixture ratio. When pure acetylene is burned it is yellow and sooty. With small amounts of oxygen it is a brilliant white. As the oxygen flow is increased the white appearance thins out, and the base of the flame becomes blue in color. Further additions of oxygen are accompanied by a complete disappearance of the white color, the flame becoming blue and essentially transparent throughout.

A ribbon-filament lamp was used as the reference temperature standard. These lamps have a heavy-duty bipost base, a silica window attached to a side arm by a graded seal, and a maximum current rating of about 40 amperes. A calibration of the lamp used was furnished by the Bureau's pyrometry laboratory. This consisted of values of filament current corresponding to brightness temperatures at 100-deg intervals from 1,900° to 2,400° C. Following the usual pyrometric practice these brightness temperatures were measured at a wave length of 0.65 $\mu$. The uncertainty of the calibration at 2,400° C was estimated at 7 deg C. The highest temperature included in the series of calibrated points represents the highest safe operating temperature of the lamp. Oxyacetylene flames giving temperatures between these limits are essentially opaque, since they occur for mixtures relatively rich in fuel.

The practical application of the method of measuring temperatures herein described requires the development of a simple portable radiometric device. The basic component around which the device was actually built was an RCA 935 phototube. Since the temperature evaluation depends on the determination of the form of the spectral energy curve, it is desirable to obtain readings at three wavelengths. Readings at two wavelengths separated by an interval of a few hundred Angstroms are, however, sufficient to establish the slope of the curve over the interval, and provide the basis for a temperature calibration.

In order to isolate two selected wavelength regions, two narrow-band-pass filters were prepared for use with the phototube. Each consisted of a combination of an interference filter with a glass filter. The interference filter, which is essentially a Fabry-Perot interferometer with a fixed separation, has a narrow transmission band at a specified wavelength. There are, however, secondary maxima at longer and shorter wavelengths. These may be eliminated by combining the interference filters with a glass filter, which isolates the region in which the principal maximum of the interference filter occurs. The following combinations were adopted: interference filter having a transmission maximum at 3541 A, with a Corning glass filter, code number 9863; interference filter, transmission maximum 4140 A, with a Schott filter designated BG28. These filters were selected after examination of flame spectrograms showed that the spectrum was sensibly free of characteristic molecular bands at the wavelengths coincident with the transmission maxima of the filters. The measurements were thus confined to the continuous emission originating in the glowing particles in the flame.

A small housing was constructed to serve as a light shield and permit placing the filters against a window opening in front of the cell cathodes. The remaining components of the metering device consisted of a balanced d-c amplifier described in an earlier publication [3] and a galvonometer and resistance network to vary the sensitivity.

The performance and reproducibility of readings of the phototube meter were tested by a series of exposures to the ribbon-filament lamp. Readings were taken with each filter combination in place for each temperature setting between 1,900° and 2,400° C. The results of this test are displayed in figure 1. Two of the curves are plots of deflections corresponding to photocell readings for the different temperatures for the respective filters. The third curve represents the ratio of deflections at each wavelength for the two filters. The variation of this ratio with temperature provides the basis for a calibration of the meter for temperature readings. The data represented in figure 1 are for one set of observations rather than for

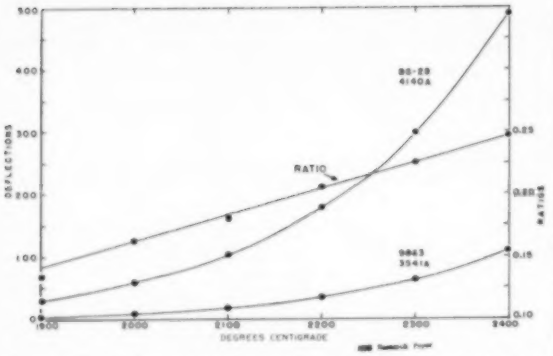


FIGURE 1. *Filter readings for different temperatures and ratios of filter readings plotted against temperatures of ribbon filament tungsten lamp.*

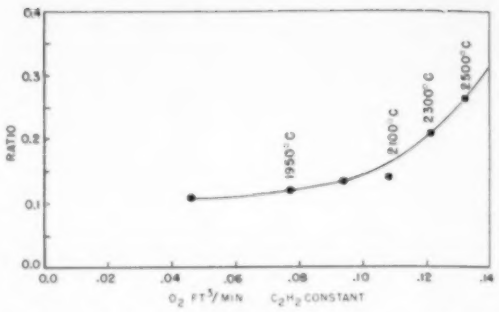


FIGURE 2. *Ratios of filter readings compared with oxygen consumption.*

Temperature equivalents noted.

an average of several. It is to be noted that the curves are extremely regular. The rapid increase in deflections with temperature, shown by the curves representing filter readings, indicates that radiant energy in the ultraviolet provides a sensitive scale of temperature. If one had been measuring temperatures lower than 1,900°C, it would have been advantageous to select two wavelengths in the visible or infrared in order to have more radiant energy available.

A series of observations were made on the flame using the same filters as were employed for the tungsten ribbon lamp. The flame was changed by using a constant amount of $C_2H_2$ and varying the $O_2$ content of the mixture. In figure 2 are shown the ratios of the radiant energy emitted through the filter at 3541 A to that emitted at 4140 A for different amounts of oxygen. All the observed ratios fall on a smooth curve except for the fourth determination. Occasionally the flame becomes unsteady and some variation in the ratio results. The conditions for the reproducibility of the flame will be discussed later. When the temperatures for the six points in figure 2 are determined from the calibration curve of figure 1, it is found that they start at about 1,850°C for the first point and reach a value of 2,500°C for the sixth point.

In order to have another method of measuring the ratios of emitted energies at 3541 and 4140 A, the spectrographic method was employed. At the time of measuring the radiant energy with the photocell, exposures were made of the flame spectra by the use of a Hilger E2 spectrograph. On evaluation of the plates it was found that the temperature of the second point of figure 2 was 1,950°C, the third close to 2,000°, the fourth 2,100°, the fifth, 2,300°, and the sixth somewhat above 2,400°.

The method of evaluation of flame temperature by the spectrograms is illustrated in figure 3 which shows a set of spectra of the flame and the filament with comparison spectra of the mercury arc. The lines, reading from the left, at 2537, 2804, 3132, 3650, and 4358 A are from an Hg arc and are used for the wave-

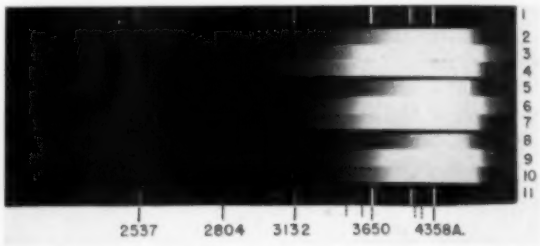


FIGURE 3. *Spectrogram showing three flame spectra compared with filament exposures at 2,400°, 2,100°, and 1,900° C.*

Exposures 1 and 11—mercury arc, five lines identified by wavelengths. Regions transmitted by the two filters designated by dotted lines. Exposures 2 and 4—continuous spectrum of ribbon filament, $T=2,400°$ C, exposures 1 and 4 sec. Exposure 3—brilliant opaque acetylene flame, exposure 3 minutes. Exposures 5 and 7—ribbon filament, $T=2,100$, exposures 3 and 12 sec. Exposure 6—bright opaque flame, exposure 4 minutes. Exposures 8 and 10—ribbon filament, $T=1,900$, exposures 5 and 18 sec. Exposure 9—yellowish opaque flame, exposure 4 minutes.

length determination of regions in the flame spectra. The spectra are displayed in groups of three. The flame spectrum under selected operating conditions is at the center of each group and is flanked on either side by filament exposures at the same temperature but with different length of exposure. The three flame spectra were produced under three different operating conditions, and are compared with filament exposures at 2,400, 2,100, and 1,900°C, respectively, reading from top to bottom on the plate. The filament exposures adjacent to each flame spectrum are in the ratio of 1 to 4. The highest filament temperature is clearly higher than the highest flame temperature recorded on the plate. For the lowest temperature the match is fairly close. The match is good for the intermediate temperature when the longest filament exposure is compared. With some experience it is possible to obtain much better matches than shown on the plate. Only the continuous portions of the flame spectra are considered in making these comparisons.

The matching of intensities was carried out by visual examination only, this being considered satisfactory in view of the limited objectives of the investigation. An alternate method that certainly would

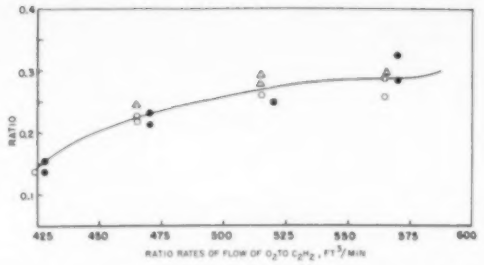


FIGURE 4. *Composite curve, filter ratios versus ratios of fuel consumption with rotameters controlling flow of both gases.*

Three types of symbols refer to three observations.

be more precise because it is entirely objective would be to determine the plate densities with a densitometer for both the flame and filament temperatures and consider the criterion of equal temperatures to be a constant ratio of the intensities between two wavelengths for the flame and for the lamp. However, this process of matching exposures on photographic plates by a spectroscopic method, which is tedious and detailed if carried out precisely, is not required for temperature measurements, but was used as a check on the photocell method.

The radiation from the part of the flame that was 2 in. above the tip of the torch, was focused on the photocell so that the results from separate trials could be compared. Figure 4 shows a plot of the ratios of the energies for different fuel mixtures as a function of the fuel mixture. The composite curve is intended to be the closest possible representation of the observations taken on several different days, each point in the graph corresponding to an observation. The same symbol is used to distinguish observations on a given day. The spread of the points at any one fuel ratio is produced largely by imperfect duplication of the fuel mixture for the separate determinations. A small change in the fuel ratio would change the ratio of energies by several percent. A smooth curve drawn through these points would give an arbitrary scale of temperature. This curve would also make it possible to operate the flame under the same condition at different times.

The temperatures estimated on the basis of the observed ratios and the calibration curve of figure 1 are in terms of the brightness temperatures of the filament of the tungsten lamp. The true temperature of the filament as calculated from the Wien equation in degrees Kelvin corresponding to 2,400° C brightness temperature is about 2,900° K. If an emissivity of 0.7 is assumed for the particles in the ultraviolet they would have a true temperature of 2,830° K when the brightness temperature of the filament is matched, and with the emissivity of 0.8 the true temperature would be 2,810° K. With almost equal fuel ratios the OH spectrum of the oxyacetylene flame has been recently measured [4]. It was found that the OH vibrational and rotational temperatures corresponded to 2,600° K with possible error being up to 200°. These results indicate that the temperature determined by the solid particles is in satisfactory agreement with the OH temperature determination. Also, the spectrum of $C_2$ emitted by an oxyacetylene flame has been observed by the use of a grating spectrometer in the near infrared [5]. The temperature deduced from the rotational spectra was of the order of 2,700° K. This value is in good agreement with results obtained on the emission of radiant energy by solid particles as found in the present work.

## 3. Discussion of Results and Evaluation of Corrections

Up to this point in the description of these experiments no discussion has been introduced regarding the limitations on temperature matching at different wavelengths when nonblack bodies are being compared. It is apparent that a change of emissivity with wavelength will change the form of the spectral energy distribution curve and thus prevent coincidence of curves from different sources, except for very limited ranges. The change of emissivity with wavelength usually proceeds at a very slow rate so that mismatch from this cause is slight over the range of wavelengths used in these experiments. It is to be noted also that, if one is comparing different radiators each with constant but different emissivities or if one is comparing one such radiator with a black body where the emissivity is always unity, it is still impossible to get an exact energy match at two wavelengths. This is a consequence of the following equation based on the Wien distribution formula,

$$\frac{1}{T}-\frac{1}{S_\lambda}=\frac{\lambda \log \epsilon_\lambda}{C_2 \log e}, \qquad (1)$$

where $T$ is the true temperature, $S_\lambda$ is the brightness temperature at wavelength $\lambda$, $C_2$ the radiation constant, and $\epsilon_\lambda$ the spectral emissivity. A conversion by means of this equation of the calibrated values of brightness temperature of the ribbon-filament lamp, at 0.6650 $\mu$, to the corresponding values of 0.4140 and 0.3541 $\mu$, based on accepted values of emissivity of tungsten has been made. The procedure is to calculate the true temperatures corresponding to the calibrated values of brightness temperature, then taking these true temperatures as the initial data, substitute in the equation to obtain the brightness temperatures at the wavelengths of the respective filter transmissions. The following typical example is selected to illustrate the mismatch at these wavelengths. Given a true temperature of 2,713° C, the brightness temperature of the filament is 2,520° C at $\lambda$=0.4140 $\mu$ and 2,547° C for $\lambda$=0.3541 $\mu$, when $\epsilon_\lambda$=0.45. The consequence of this is that, in comparing the intensity of the lamp with that of a black body, if the energies correspond at 0.4140 $\mu$, the energy would be greater for the lamp at 0.3541 $\mu$ and make it appear brighter by 27 deg C. This difference is less than the experimental error when observations are made on the

flame. It can be shown from eq 1 that the difference between the true and the brightness temperatures decreases in the ultraviolet region as compared with the visible spectrum. When the emissivity increases, the difference between the true and the brightness temperatures becomes less. While the emissivity of carbon particles is not well known at high temperatures, W. E. Forsythe [2, p. 380] gives the following values for the emissivity of carbon: $\epsilon_\lambda$ ($\lambda = 0.465\ \mu$), at $T = 1{,}200°$K, is 0.86, and, at $T = 2{,}200°$K, is 0.79.

Calculations have been made on the temperature of the particles on the basis of $\epsilon_\lambda$ being equal to 0.7 and 0.8. When the brightness temperature is 2,547° C the true temperatures at a wavelength of 0.354 $\mu$ are 2,618° and 2,591° C for emissivities of 0.7 and 0.8, respectively. If the emissivity of the particles were 0.45 instead of 0.7 at 0.354$\mu$, the true temperature would be 95 deg higher for the same brightness temperature. Until more accurate values of emissivity are known there will probably be an uncertainty in the estimates of temperature of about 100 deg C. This is of the same order of magnitude as the errors introduced by the observed ratios of intensities.

Flame temperatures determined by this method are in essential agreement with temperatures deduced from spectroscopic observations of flames produced under similar conditions.

## 4. References


[1] A. G. Gaydon, Spectroscopy and combustion theory (Chapman & Hall, London, 1948).

[2] W. E. Forsythe, Measurement of radiant energy, chapter 1 (McGraw-Hill Book Co., Inc., New York, N. Y., 1937).

[3] W. W. Coblentz and R. Stair, A portable ultraviolet intensity meter, consisting of a balanced amplifier, photoelectric cell, and microammeter, BS J. Research **12,** 231 (1934) RP647.

[4] W. S. Benedict, E. K. Plyler, and C. J. Humphreys, Vibration-rotation lines of OH in flame spectra, Bul. Am. Phys. Soc. **26,** 50 (1951).

[5] W. S. Benedict and Earle K. Plyler, Bands of $C_2$ and CN in infrared flame spectra, Bul. Am. Phys. Soc. **26,** 54 (1951).



Washington, August 29, 1950.

Journal of Research of the National Bureau of Standards Vol. 47, No. 6, December 1951 Research Paper 2273

# Electron-Optical Bench

L. Marton, M. M. Morgan, D. C. Schubert, J. R. Shah, and J. A. Simpson

A versatile electron-optical bench has been constructed for the extensive study of electron-optical elements. Three carriages for magnetic lenses and four holders for apertures, objectives, and meshes are arranged appropriately in the vacuum chamber, while provision is made for external positioning with 3 degrees of freedom for each element. The design and experimental technique are discussed in detail. A set of measurements of the focal length of a magnetic lens is presented to illustrate the practical employment of the bench and to indicate the limits of accuracy that can be attained.

## 1. Introduction

For the extensive study of the properties of electron-optical elements, an electron-optical bench has been constructed. This bench provides for the control of the positions of such elements from outside the vacuum system and quantitative measurement of the image formed on a fluorescent screen.

Very few attempts have been made to design an electron-optical bench. Among the very few electron optical benches, which have been built in the past, is the instrument designed by Reisner and Picard.[1] A minor feature of that bench was the provision for visual observation of the parts inside the vacuum chamber.

Inasmuch as all measurements required during the operation of an electron-optical bench can be made externally, the ability to see the optical system need not be considered particularly useful. For simplicity of construction and protection against X-rays the NBS electron-optical bench was made with an all-metal cylindrical vacuum chamber. It was designed to satisfy the following requirements: 1. The bench should accommodate three carriages for lenses with maximum diameter of 7 in. and four holders for apertures, test objects, and meshes (used for the electron-optical shadow method).[2]

2. A movement of 10 in. along the axis of the bench and ½ in. radially should be possible for each component of the system without breaking the vacuum.

## 2. Description of Apparatus

### 2.1. Vacuum Chamber

A rolled-steel cylinder of 15-in. inner diameter, ¼-in. wall and 39-in. length is part of the vacuum chamber used to house the electron-optical system. The end plate supporting the gun is permanently fixed to the cylinder with bolts, the vacuum seal being provided by a rubber gasket. A dural plate, A, figure 1, on wheels serves as a bed on which the electron-optical system is mounted. The specimen and aperture mounts, B, and lens carriages, C, slide in a groove along the bed. The bed may be rolled into or out of the chamber. One end of the bed is attached to the face plate by means of a flexible hinge, which does not encounter the strain that might result if a rigid joint were used.

The face plate seals against the end of the tube by a neoprene gasket compressed by atmospheric pressure. The fluorescent screen is coated on a glass plate (5⅞ in. in diameter and ⅞-in. thick) in the face plate. Motion of the elements is controlled by means of connecting shafts passing through "Wilson seals," E, in the face plate.

### 2.2. Lens Carriages

The radial adjustment of each lens is obtained by properly combining controlled vertical and horizontal motions of the lens carriage. For vertical adjustment a double-threaded worm, A, figure 2, attached to a connecting shaft, B, engages a gear, C, the shaft of which rotates in the bottom dural plate, D. A screw pinned to the worm gear turns in the top plate, E, thus moving it vertically when the worm is rotated. The top plate is constrained in its motion by sliding on four pins, F, attached to the lower plate. Horizontal adjustment is similarly achieved by a worm and gear arrangement sliding the plate, G, over plate, E, the motion being constrained by a tongue in groove. Since the vertical position of the worm, H, changes, two universal joints are inserted in its connecting shaft. The axial position of the carriage is controlled by pushing or pulling the connecting shafts through the Wilson seals.

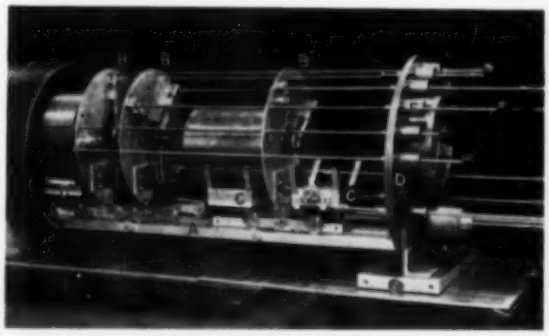

FIGURE 1. *Vacuum chamber of electron-optical bench open for changing elements.*

[1] J. H. Reisner and R. G. Picard, Rev. Sci. Instr. **19,** 556 (1948).
[2] L. Marton and S. H. Lachenbruch, J. Applied Phys. **20,** 1171 (1949); J. Research NBS **43,** 409 (1949).

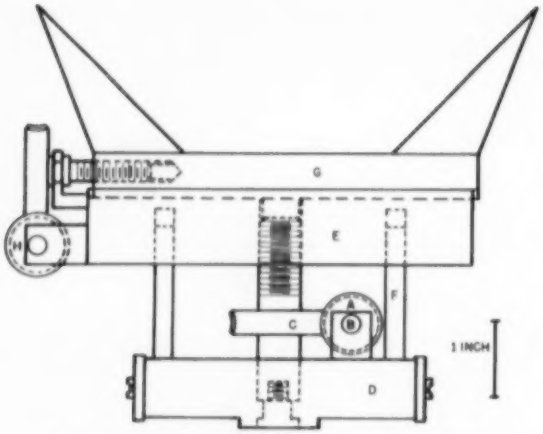


FIGURE 2. *Lens carriage for electron-optical bench.*

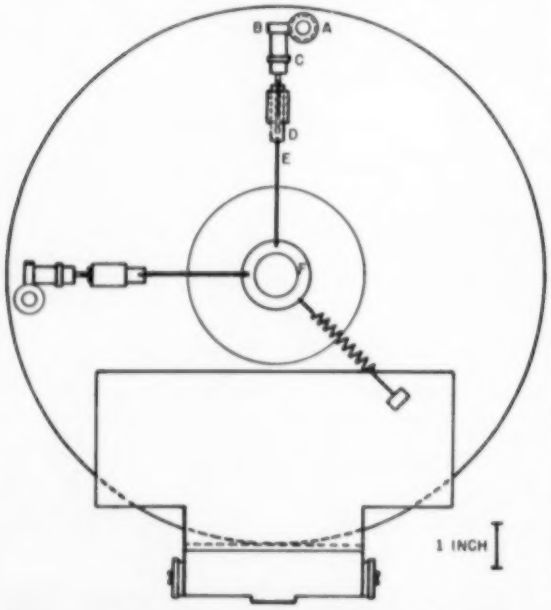


FIGURE 3. *Specimen and aperture mount for electron-optical bench.*

### 2.3. Specimen, Mesh, and Aperture Mounts

If one is to achieve a smooth motion of specimens or test objects with a minimum of jerkiness, the drive must be made as nearly frictionless as possible. Pursuant to this requirement, the radial motion in the present arrangement is constrained by elastic deformation of phosphor bronze strips instead of sliding surfaces. A similar arrangement for positioning an electron microscope stage, which reduced friction to an even greater degree, was described in an earlier paper.[3]

[3] *L. Marton, J. Applied Phys.* **16,** 131, 1945.

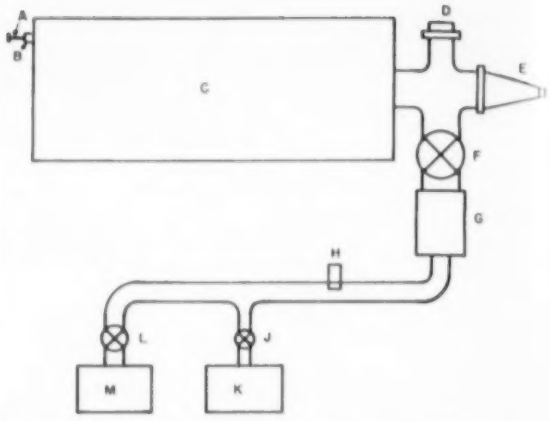


FIGURE 4. *Vacuum system for electron-optical bench.*

A, Air bleeder; B, Wilson seal; C, vacuum chamber; D, ionization gage; E, electron gun; F, 4-in. main valve; G, 4-in. diffusion pump; H, thermocouple gage; J, 1-in. 3-way valve; K, duo-seal pump; L, 2-in. valve; M, Kinney pump.

Radial adjustment of the specimen, mesh, or aperture holders is provided by a pair of worm and gear mechanisms at right angles to each other. A worm, A, figure 3, attached at the end of a connecting shaft engages a gear, B, rotating in a collar, C, fixed to the mount. A screw, pinned at the end of the worm gear shaft, turns in a sleeve, D, which is attached by means of a flexible phosphor-bronze strip, E, to the ring, F, into which an appropriate specimen, mesh, or aperture holder is screwed. In this way the ring is moved along the axis of the worm gear, B,. The elastic deformation of the phosphor-bronze connection, because of its orientation, provides a simple solution of the mechanical linkage problem of moving the ring, without the use of friction devices, in a plane perpendicular to the axis of the bench while maintaining rigidity in the axial direction. Because of the arrangement of the Wilson seals, the connecting shafts had to be attached to the circular plate forming the body of the mount near its top, thus leading to somewhat jerky axial motion. This jerkiness was reduced by using a long, heavily weighted wheel base for the mount.

### 2.4. Vacuum System

A schematic diagram of the vacuum system is shown in figure 4. The lens currents are led through the vacuum wall by metal-glass seals in the face plate; and the conductors are insulated by ceramic beads, which produce less outgassing difficulties than would result if rubber or plastic insulation were used. This is realized by means of a large fore-vacuum pump and a 4-in. oil diffusion pump. This large pump brings the pressure down from the atmospheric to about 10 microns of mercury in 5 minutes. However, as this pump causes considerable vibrations, it is turned off after initial pumping and the quieter small fore-vacuum pump is used during final adjustments and measurements. The normal operat-

ing pressure is about $3\times10^{-2}$ micron of mercury, measured by an ion gauge near the gun.

The special three-way valve near the small capacity pump is constructed to bleed air into the vacuum system at a controlled rate, as well as to insert the small capacity pump into or isolate it from the system.

### 2.5. Electrical System

A conventional 100-kilovolt X-ray power supply unit, consisting of a voltage doubler circuit with two 50-kilovolt rectifier tubes, is used as the high-voltage supply. Stabilization is provided by two 0.1-micro-farad condensers in parallel with the circuit. The voltage is measured by the current passing through a 1,000-megohm bleeder resistance connected across the high-voltage supply. The normal range of operation is from 20 to 70 kilovolts. The filament is heated by a high-frequency power supply. The lens current power supplies are a modification of those described in an earlier paper (see footnote 3) and give up to 500 milliamperes with a stability of better than 1 part in 10,000.

The lenses available for use in the bench were originally designed for use with the coils out in the atmosphere rather than in a vacuum chamber; consequently they were poorly suited to operation within the bench, and the coils released large quantities of gas to the vacuum system. An extremely rapid pumping system was needed to maintain a working vacuum under such unfavorale conditions.

### 2.6. Optical System

A great portion of the use of an electron-optical bench is in the empirical approach to the development of electron-optical lens systems. In such work the result of one measurement often determines what conditions should be used for the next measurement. Hence the direct method of measuring the image is preferred as quicker, simpler, and cheaper than the photographic method of recording results. A low-power traveling telescope reading 0.001-in. with a total travel of 2¾-in. was specially built for measurement of the image on the fluorescent screen. Since the bench was designed for use with magnetic lenses with their attendant rotation of the image, the measuring telescope is mounted on a turntable, which can be moved either horizontally or vertically a distance of 3 in. in such a way that its center of rotation may be concentric with that of the image. In this way all measurements are radial. Variable intensity side illumination of the reticule reduces the difficulty in seeing the cross hair when the intensity of the pattern on the screen is low.

Zinc cadmium silicate was used for the fluorescent screen. To make the screen conducting, it was aluminized, using the technique suggested by Bachman.[4]

A 100-kv electron gun, identical to the one described in an earlier publication (see footnote 3), is the source of electrons, the grid bias being obtained from a potentiometer connected across three 45-volt batteries in series.

### 2.7. Measurements

Sample measurements taken on the electron-optical bench are presented graphically (fig. 5) for the purpose of illustrating its use. These measurements of focal length were taken with the condenser lens, a mesh object, and the objective lens in the system. The objective lens has 10,000 turns. A symmetrical cold-rolled steel pole piece of 0.081-in. bore diameter and 0.060-in. gap width fits into the ⅝-in. inner diameter of the iron enclosure of the lens. Diffuse illumination of the object, obtained by applying a thin Formvar film and a thin conducting aluminum coating on the source side of the mesh was used to make focusing critical. The image distance was held constant throughout the measurements; for a particular accelerating voltage the object position was adjusted to give approximate focus for different objective currents, the final focus being made by a small adjustment of the current. The focal length was computed by the equation $f=q/(M+1)$, where $q$ is the image distance and $M$ is the magnification.

With the assumption that the curves drawn are approximately as good fits as would be obtained by

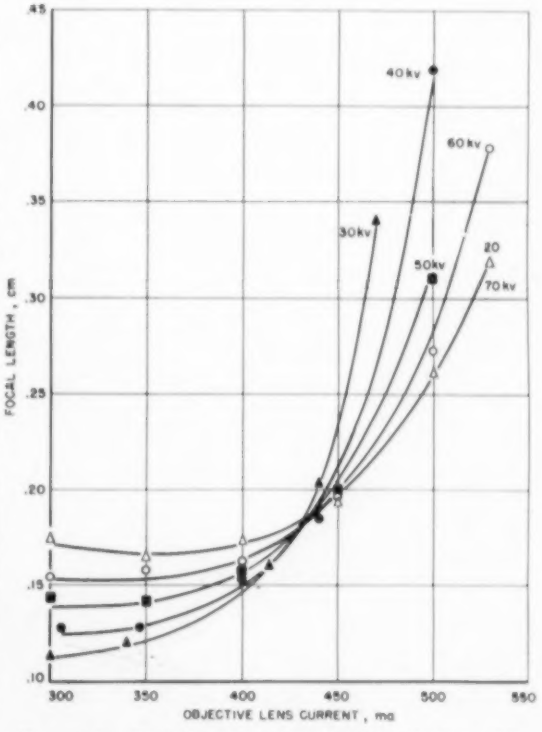


FIGURE 5. *Variation of focal length of objective lens with lens current for different accelerating voltages.*

[4] C. H. Bachman, Techniques in experimental electronics, p. 235 (John Wiley & Sons, Inc., New York, N. Y., 1948).

applying the least-squares method to a "known" function, the *rms* error in the focal length is found to be less than $\pm 0.001$ cm. From the graph the maximum error seems about $\pm 0.01$ cm. The major limitation on accuracy seems to be the difficulty in setting the cross hair on a point of the mesh image. Improvement of the cross-hair design and development of greater skill in setting may reduce the error from this source to less than 1 percent from a present value as high as 2.5 percent. Another limitation is in the precision with which the image can be focused. With the objective lens and pole piece previously described, a change of lens current of the order of $\pm 3$ ma, over the range of currents used, is required to produce a detectable change in definition from best focus, that is, the image appears to be in perfect focus over a range of about 6 ma. The center of this range can be located within about $\pm 2$ ma. It is believed that this cannot be much improved without elaborate additions to the equipment. Errors due to small inaccuracies in alinement and to hysteresis are believed to be negligible compared to these two limiting factors; no particular care was taken to eliminate hysteresis errors in these preliminary measurements.

The electron-optical bench is quite versatile because of the ease with which elements may be added and removed, and because three-dimensional movement of all elements is possible from outside the vacuum wall. It can be used for almost any electron-optical measurement and can be adapted for use in electron-optical field mapping and as an electron microscope.

---

Practically all the construction work was done by August B. Dauses, whose collaboration is gratefully acknowledged. Two Grant-in-Aids, one from Sigma Xi Research Fund and one from the American Philosophical Society, are gratefully acknowledged by J. R. Shah. These enabled Mr. Shah to extend a stay in the United States by several months and thus contribute to the completion of this project.

WASHINGTON, April 16, 1951.

Journal of Research of the National Bureau of Standards Vol. 47, No. 6, December 1951 Research Paper 2274

# Random Determinants[1]

R. Fortet

Determinants whose elements involve random variables are discussed and expressions derived for the first and second moments. Applications are made to $n$-dimensional geometry, especially, to finding limiting probabilities for the event: "a given point lies above a random hyperplane", under fairly general hypotheses. The random variable $A_n h - B$ is considered, where $A_n$ and $B$ are certain minors of the determinantal equation of the random hyperplane, and $h$ is a coordinate of the given point.

An asymptotic expression for $E\{A_n^2\}$ is obtained, and it is shown that $E\{B^2\}$ is of the order of $(1/n)\ E\{A_n^2\}$.

## 1.

In this section real random variables $X_{ij}$ depending on two indices $i$ and $j$ and having the following properties are considered:

Let $A_1, A_2, \ldots, A_k$ be $k$ random variables chosen from the $X_{ij}$'s. Then we make the assumptions that

(a) for any $i$ and $j$, for any $k$, and for any choice of the $A_l$'s, the conditional mathematical expectation

$$E(X_{ij}|A_1, \ldots, A_k)=0,$$

if $X_{ij}$ is not one of the $A_l$'s.

(b) For any $i$, $j$, for any $k$, and for any choice of the $A_l$'s, the conditional second order moment

$$E(X_{ij}^2|A_1, \ldots, A_k)=\sigma_i^2,$$

(where $\sigma_i$ is a constant that depends only on $i$) provided $X_{ij}$ is not one of the $A_l$'s.

Consider the following random determinant:

$$\Delta_n=\begin{vmatrix} X_{11} & X_{12} \ldots X_{1n} \\ X_{21} & X_{22} \ldots X_{2n} \\ \cdot & \\ \cdot & \\ \cdot & \\ X_{n1} \quad \ldots & X_{nn} \end{vmatrix}$$

We have the

*Lemma:* $E(\Delta_n)=0$ *and* $E(\Delta_n^2)=n!\prod_{i=1}^{n}\sigma_i^2$.

*Proof.* Let $A_{ij}$ be the cofactor of $X_{ij}$ in $\Delta_n$; we can write

$$\Delta_n=\sum_j A_{1j}X_{1j}$$

$$E(\Delta_n)=\sum_j E\{A_{1j}E(X_{1j}|A_{1j})\}.$$

From (a), $E(X_{1j}|A_{1j})=0$; hence

$$E(\Delta_n)=0.$$

Also

$$\Delta_n^2=\sum_j A_{1j}^2X_{1j}^2+\sum_{j\neq k}A_{1j}A_{1k}X_{1j}X_{1k}.$$

Now

$$E\{\sum_{j\neq k}A_{1j}A_{1k}X_{1j}X_{1k}\}=\sum_{j\neq k}E\{A_{1j}A_{1k}X_{1j}E(X_{1k}|A_{1j},A_{1k},X_{1j})\}$$

From (a) $E(X_{1k}|A_{1j},A_{1k},X_{1j})=0$; hence

$$E\{\Delta_n^2\}=\sum_j E\{A_{1j}^2X_{1j}^2\}=\sum_j E\{A_{1j}^2E(X_{1j}^2|A_{1j})\},$$

and from (b) this reduces to

$$E\{\Delta_n^2\}=\sigma_1^2\sum_j E(A_{1j}^2). \tag{1}$$

Now $A_{1j}$ is a $\Delta_{n-1}$, which depends only on those $X_{ij}$ with $i\neq 1$. If we assume that the formula

$$E\{\Delta_n^2\}=n!\sum_{i=1}^{n}\sigma_i^2 \tag{2}$$

is true for $n=1, 2, \ldots, r$, (1) shows that (2) is also valid for $n=r+1$; on the other hand (2) obviously holds for $n=1$. Thus (2) is established by induction, and the proof of the lemma is complete.

$$d_n=\begin{vmatrix} x_{11} & x_{12} \ldots & x_{1n} \\ x_{21} & \ldots & x_{2n} \\ \cdot & \\ \cdot & \\ \cdot & \\ x_{n1} \quad \ldots & x_{nn} \end{vmatrix}.$$

Nonrandom real numbers $x_{ij}$ and the determinant are now considered.

Suppressing the $k$ rows $i_1, i_2, \ldots, i_k$ in $d_n$, a rectangular matrix is obtained with $(n-k)$ rows; $T[i_1,i_2, \ldots, i_k;d_n]$ is called the sum of the squares of all determinants of $(n-k)$th order deduced from this matrix.

[1] The preparation of this paper was sponsored (in part) by the Office of the Air Comptroller, USAF.

Let $D_n$ be the following random determinant:

$$D_n=\begin{vmatrix} x_{11}+X_{11} & x_{12}+X_{12} & \cdots & x_{1n}+X_{1n} \\ x_{21}+X_{21} & \cdot & \cdots & \\ \cdot & & & \\ \cdot & & & \\ x_{n1}+X_{n1} & x_{n2}+X_{n2} & \cdots & x_{nn}+X_{nn} \end{vmatrix}$$

$D_n$ can be written as a sum of elementary determinants, the elements of which are either $x_{ij}$ or $X_{ij}$ but never $x_{ij}+X_{ij}$. One of these elementary determinants is $d_n$; all the other elementary determinants are random determinants. Let $S$ be one of these random determinants: $S$ consists of $k$ rows of $X_{ij}$'s ($k \geq 1$) and $(n-k)$ rows of $x_{ij}$'s. For instance, suppose that the first row of $S$ consists of the $X_{1j}$; $S$ is a linear homogeneous form in the $X_{1j}$'s, the coefficients of which are independent of the $X_{1j}$'s. Thus according to (a) $E(S)=0$; consequently $E(D_n)=d_n$.

Let $i_1, i_2, \ldots, i_k$ be the $k$ rows of $S$ consisting of some $X_{ij}$'s, that is, row $i_1$ consists of the $X_{i_1 j}$, row $i_2$ of the $X_{i_2 j}$, etc. Employing the Laplace development of $S$ in terms of these $k$ rows $i_1, i_2, \ldots, i_k$, we can write $S$ in the form:

$$S=\Sigma^*\Delta_k(j_1 j_2, \ldots, j_k)B(j_1 j_2, \ldots, j_k),$$

where $\Delta_k(j_1 j_2, \ldots, j_k)$ is a determinant of the preceding $\Delta$ type, the elements of which are those $X_{ij}$ with $i \in i_1, i_2, \ldots, i_k$, $j \in j_1, \ldots, j_k$; $B(j_1 j_2, \ldots, j_k)$ is the algebraic complement of $\Delta_k(j_1 j_2, \ldots, j_k)$; and the summation $\Sigma^*$ is extended over all combinations $(j_1 j_2, \ldots, j_k)$ of order $k$ taken from the $n$ integers $1, 2, \ldots, n$. For two different combinations we have:

$$E\{\Delta_k(j_1 j_2, \ldots, j_k)\cdot\Delta_k(j_1' j_2', \ldots, j_k')\}=0, \quad (3)$$

since there is at least one $j_\alpha$, $j_1$ say, which is not a $j_\beta'$, so that the product $\Delta_k(j_1, \ldots, j_k)\cdot\Delta_k(j_1', \ldots, j_k')$ is a homogeneous linear form in $X_{i_1 j_1}$, $X_{i_2 j_1}, \ldots, X_{i_k j_1}$, and (3) follows from (a). Consequently

$$E(S^2)=\Sigma^* B^2(j_1, \ldots, j_k)E\{\Delta_k^2(j_1, \ldots, j_k)\},$$

and by the lemma,

$$E(S^2)=\sum{}^*(B^2(j_1, \ldots, j_k)\cdot k!\prod_{\alpha=1}^{k}\sigma_{i_\alpha}^2)$$
$$=k!\prod_{\alpha=1}^{k}\sigma_{i_\alpha}^2[\Sigma^* B^2(j_1, \ldots, j_k)].$$

But obviously,

$$\Sigma^* B^2(j_1, \ldots, j_k)=T(i_1, i_2, \ldots, i_k; d_n).$$

Hence we have

$$E(S^2)=T(i_1, i_2, \ldots, i_k; d_n)k!\prod_{\alpha=1}^{k}\sigma_{i_\alpha}^2.$$

Consider the product of two different elementary determinants $S_1$ and $S_2$. There is at least one row consisting of some $X_{ij}$ that appear in $S_1$ and not in $S_2$, or in $S_2$ and not in $S_1$. For example, suppose the first row in $S_1$, consisting of the $X_{1j}$'s, does not appear in $S_2$; then the product $S_1 S_2$ is a linear homogeneous form in the $X_{1j}$'s, the coefficients of which are independent of the $X_{1j}$'s. Consequently by (a), $E(S_1 S_2)=0$ and $E(D_n^2)$ reduces to the sum of the squares of all the elementary determinants. This gives us the following:

*Theorem* 1: *Under assumptions* (a) *and* (b),

$$E(D_n)=d_n \quad (4)$$

$$E(D_n^2)=\sum_{k=0}^{n}k!(\sum{}^* T(i_1, i_2, \ldots, i_k; d_n)\prod_{\alpha=1}^{k}\sigma_{i_\alpha}^2). \quad (5)$$

In (5) the summation $\Sigma^*$ is extended over all combinations $(i_1, i_2, \ldots, i_k)$ of order $k$ of the integers $1, 2, \ldots, n$; for convenience we put

$$T(1,2, \ldots, n; d_n)=1.$$

An interesting feature of formulas (4) and (5) is that these formulas do not depend on the probability laws of the $X_{ij}$'s. This fact remains valid even if the $\sigma_i$'s depend on $j$, but (5) becomes more complicated; on the other hand it is possible to compute the higher moments of $D_n$ by using similar reasoning and suitable assumptions. However, the formulas seem quite complicated. It also appears difficult to obtain the probability law of $D_n$, even under such hypotheses as that the $X_{ij}$ are normally distributed.

Of course if $\sigma_1=\sigma_2=\cdots=\sigma_n=\sigma$, where $\sigma$ is a constant independent of $i$, (5) reduces to:

$$E(D_n^2)=\sum_{k=0}^{n}T_k(d_n)k!\sigma^{2k}, \quad (5a)$$

where

$$T_k(d_n)=\Sigma^* T(i_1, \ldots, i_k; d_n).$$

From (5) certain interesting results may be deduced, which are perhaps already known. These results are connected with the geometrical interpretation of the coefficients of (5). Let $E_n$ be an $n$-dimensional Euclidean space, with orthogonal coordinates. The $n$ numbers $x_{i1}, x_{i2}, \ldots, x_{in}$ may be regarded as the coordinates of a point $P_i$ in $E_n$, and $x_{i1}+X_{i1}, x_{i2}+X_{i2}, \ldots, x_{in}+X_{in}$ can be considered as the coordinates of a random point $M_n$ in $E_n$. That $d_n$ is invariant under orthogonal transformations is well known. If $(0, P_1 P_2 \ldots P_n)$ is the volume in $E_n$ of the parallelepiped formed by the vectors $\overrightarrow{0P_1}$, $\overrightarrow{0P_2}$, $\ldots$, $\overrightarrow{0P_n}$ we have:

$$d_n=\pm(0, P_1 P_2 \ldots P_n).$$

An analogous interpretation holds for $D_n$ and $(0, M_1 M_2 \ldots M_n)$; hence $E(D_n^2)$ is invariant under an orthogonal transformation. If the $X_{ij}$'s are normally distributed, this property also persists. The

$\sigma_i$ remain unaltered also. We conclude that the coefficients $T(i_1, \ldots, i_k; d_n)$ are invariant.

$T(i_1, \ldots, i_k; d_n)$ depends only on $P_{i_1}, \ldots, P_{i_k}$; consider the set of points $P'_{i_1}, P'_{i_2}, \ldots, P'_{i_k}$ defined as follows:

$$\overrightarrow{0P'_{i_1}}=\overrightarrow{0P_{i_1}}$$

$$\overrightarrow{0P'_{i_2}}=\overrightarrow{0P_{i_2}}+\lambda_{21}\overrightarrow{0P_{i_1}}$$

$$\overrightarrow{0P'_{i_k}}=\overrightarrow{0P_{i_k}}+\lambda_{k1}\overrightarrow{0P_{i_1}}+\ \ldots\ +\lambda_{k,\,k-1}\overrightarrow{0P_{i_{k-1}}},$$

where the $\lambda_{ij}$ are such that the vectors $\overrightarrow{0P'_{i_1}}, \overrightarrow{0P'_{i_2}}, \ldots, \overrightarrow{0P'_{i_k}}$ are mutually orthogonal. From a classical property of determinants we can replace $P_{i_1}, \ldots, P_{i_k}$ by $P'_{i_1}, \ldots, P'_{i_k}$ without altering $T(i_1, \ldots, i_k; d_n)$. The invariance of $T(i_1, \ldots, i_k; d_n)$ under orthogonal transformations implies that the vectors $\overrightarrow{0P'_\alpha}$ ($\alpha=1, \ldots, k$) can be taken as coordinate axes. Then it becomes obvious that

$$T(i_1, \ldots, i_k; d_n)=(0, P'_{i_1} \ldots P'_{i_k})^2,$$

the volume $(0, P'_{i_1} \ldots P'_{i_k})$ being considered as a volume in a $k$-dimensional subspace of $E_n$; but it is also obvious that

$$(0, P'_{i_1} \ldots P'_{i_k})^2=(0, P_{i_1} P_{i_2} \ldots P_{i_k})^2,$$

and we have established:

*Theorem 2:*

$$T(i_1, \ldots, i_k; d_n)=(0, P_{i_1} \ldots P_{i_k})^2, \tag{6}$$

*and consequently,*

$$T_k(d_n)=\sum{}^*(0, P_{i_1} \ldots P_{i_k})^2. \tag{7}$$

On the other hand, considering $P_1, \ldots, P_n$ as fixed points in $E_n$, and $\Omega$ as a moving point, $(\Omega, P_{i_1} \ldots P_{i_k})^2$ and $\Sigma^*\ (\Omega, P_{i_1} \ldots P_{i_k})^2$ are given by (6) or (7) under a simple change of the origin of coordinates. If one puts

$$(\Omega, P_{i_1} \ldots P_{i_k})^2=C \tag{8}$$

and

$$\Sigma^*(\Omega, P_{i_1} \ldots P_{i_k})^2=C^*, \tag{9}$$

where $C$ and $C^*$ are any positive constants, then eq (8) and (9) define quadrics $Q(i_1, \ldots, i_k; C)$ and $Q_k(C^*)$, respectively, of ellipsoidal type. Thus it follows from (5) that the relation

$$E\{(\Omega, M_1 \ldots M_n)^2\}=\epsilon, \tag{10}$$

where $\epsilon$ is some positive constant, also defines a quadric $Q(\epsilon)$ (which is in general an ellipsoid).

2.

In Euclidean $n$-space with the coordinates defined as above consider $n$ fixed points $P_1, P_2, \ldots, P_n$, and a fixed point $S$ on the axis $0x_n$ with coordinates $(0, 0, \ldots, 0, h)$. Let $M_1, M_2, \ldots, M_n$ be $n$ random points, and consider the random plane $\Pi$, (i. e., an $(n-1)$-dimensional linear variety) defined by $(M_1, M_2, \ldots, M_n)$. The equation of $\Pi$ has the following determinantal form

$$U=\begin{vmatrix} x_1 & x_2 & \ldots & x_{n-1} & x_n & 1 \\ x_{11}+X_{11} & x_{12}+X_{12} & \ldots & x_{1,n-1}+X_{1,n-1} & X_{1n} & 1 \\ \cdot & & & \cdot & \cdot & \cdot \\ \cdot & & & \cdot & \cdot & \cdot \\ \cdot & & & \cdot & \cdot & \cdot \\ x_{n1}+X_{n1} & \cdot & \cdot & x_{n,n-1}+X_{n,n-1} & X_{nn} & 1 \end{vmatrix}=0$$

Developing this determinant in terms of the elements of the first row and their cofactors, one obtains

$$U=\sum_{j=1}^{n} A_j x_j - B=0. \tag{11}$$

For convenience we set

$$Y_{ij}=x_{ij}+X_{ij} \qquad (i=1, 2, \ldots, n;\ j=1, 2, \ldots, n-1).$$

Let $M'_i$ be the point $(Y_{i1}, \ldots Y_{i,n-1}, 0)$ and $V$ the linear variety of $n-2$ dimensions defined by

$$x_n=0, \qquad U=0, \tag{12}$$

and let $H_i$ be the orthogonal projection of $M_i$ or $M'_i$ on $V$. An elementary computation shows that, in absolute value,

$$\frac{\overline{M'_i M_i}}{\overline{H_i M'_i}}=\frac{|X_{in}|}{\overline{H_i M'_i}}=\frac{\sqrt{\sum_{j=1}^{n-1} A_j^2}}{|A_n|} \tag{13}$$

We now suppose that:

(A) the distance between $P_i$ and $P_j$ is equal to 1, for any $i$ and $j$. In this case the $n$ points $P_i$ form a regular polyhedron in the variety $x_n=0$; this polyhedron admits $\binom{n}{k}$ linear varieties $V_{ij}$ as varieties of symmetry, $V_{ij}$ being defined as that $(n-2)$-dimensional variety formed by the points in $x_n=0$ which are equidistant from $P_i$ and $P_j$ $(i \neq j)$. Now suppose that $V$ is a moving $(n-2)$-dimensional variety, and consider the quantity

$$s=\max_i \text{ (distance from } V \text{ to } P_i).$$

$s$ attains its minimum value when $V$ is a $V_{ij}$, in which case $s=\frac{1}{2}$. Consequently in all cases there is at least one point $P_i$ such that the distance from $V$ to $P_i$ is at least $\frac{1}{2}$.

Now suppose that $n$ tends to $+\infty$ with condition (A) always holding; we make the following assumptions:

(B) $\lim_{n\to\infty} Pr\left\{\text{Max } |X_{in}|<\epsilon\right\}=1$ for any $\epsilon>0$;

(C) there exists a positive number $a<\frac{1}{2}$ and independent of $n$ such that:

$$\lim_{n\to\infty} Pr\left\{\text{Max}_i \sum_{j=1}^{n} X_{ij}^2<a^2\right\}=1.$$

If for instance the distance from $P_i$ to $V$ is a maximum when $i=1$, then except in cases of small probability:

$$\overline{H_1M_1}>\frac{1}{2}-a,$$

and

$$|X_{1n}|<\epsilon.$$

Thus we have:

*Theorem 3: Under hypotheses* (A), (B), *and* (C),

$$\lim_{n\to\infty} Pr\left\{\frac{\sqrt{\sum_1^{n-1} A_j^2}}{|A_n|}>0\right\}=0.$$

*Remark:* Assumptions (B) and (C) are not particularly restrictive. They are satisfied, for instance if the $X_{ij}$'s are independent and normally distributed with

$$E(X_{ij}^2)=\frac{\rho^2}{n}, \tag{14}$$

$\rho$ being $<\frac{1}{2}$ and independent of $i, j, n$; also when the $M_i$ are independently distributed with uniform probability density over the interior of the sphere of center $P_i$ and radius $\rho<\frac{1}{2}$.

Denote the center of gravity of $P_1, \ldots, P_n$ by $G$, with coordinates $(\xi_1, \ldots, \xi_n)$ given by

$$\xi_j=\frac{1}{n}\sum_{i=1}^{n} x_{ij}, \qquad (j=1, 2, \ldots, n), \tag{15}$$

$\xi_n=0$. Let $K$ be the center of gravity of $M_1, \ldots, M_n$ with coordinates $\xi_j+Z_j$ $(j=1,2, \ldots, n)$. Put

$$Z_j=\frac{1}{n}\sum_{i=1}^{n} X_{ij}. \tag{16}$$

We make the following assumptions:

(D) the distance $\overline{OG}$ remains bounded as $n\to+\infty$;

(E) the $X_{ij}$ satisfy assumptions (a) and (b) of section 1, with

$$\sigma_i\leq\frac{\rho}{\sqrt{n}},$$

where $\rho^2$ is a constant independent of $i$ and $n$. The algebraic distance $L$ from $G$ to $\Pi$ is equal to:

$$L=\frac{\sum_{j=1}^{n-1} A_j\xi_j-B}{\sqrt{\sum_{j=1}^{n} A_j^2}}. \tag{17}$$

$K$ belongs to $\Pi$, so that

$$|L|\leq\overline{GK}.$$

But the coordinates of the vector $\overrightarrow{GK}$ are the $Z_j$'s defined by (16). From (E) it then follows that

$$E(\overline{GK}^2)\leq\frac{\rho^2}{n}.$$

Hence $\overline{GK}$ and *a fortiori* $L$ tend toward zero in probability. Write (17) as

$$\frac{\sum_{j=1}^{n-1} A_j\xi_j-B}{\sqrt{\sum_{j=1}^{n} A_j^2}}=-\frac{B}{A_n}\cdot\frac{A_n}{|A_n|\sqrt{1+\frac{\sum_1^{n-1} A_j^2}{|A_n|^2}}}+\frac{\sum_{j=1}^{n-1} A_j\xi_j}{|A_n|\sqrt{1+\frac{\sum_1^{n-1} A_j^2}{|A_n|^2}}}.$$

We have by the Schwartz inequality

$$\left|\sum_{j=1}^{n-1} A_j\xi_j\right|\leq\sqrt{\sum_{j=1}^{n-1} A_j^2}\cdot\sqrt{\sum_{j=1}^{n-1}\xi_j^2},$$

so that

$$\frac{\left|\sum_{j=1}^{n-1} A_j\xi_j\right|}{|A_n|\sqrt{1+\frac{\sum_1^{n-1} A_j^2}{|A_n|^2}}}\leq\sqrt{\sum_{j=1}^{n-1}\xi_j^2}\,\frac{\sqrt{\frac{\sum_1^{n-1} A_j^2}{|A_n|}}}{\sqrt{1+\frac{\sum_1^{n-1} A_j^2}{|A_n|^2}}}.$$

Now $\sqrt{\sum_{j=1}^{n-1}\xi_j^2}$ is bounded and $\sqrt{\sum_1^{n-1} A_j^2}\Big/|A_n|$ tends to zero in probability. Therefore under the assumptions (A)–(E) we have:

*Lemma: As* $n\to\infty$, $|B/A_n|$ *tends to zero in probability.*

The algebraic distance from $S$ to $\Pi$ is

$$\Delta=\frac{hA_n-B}{\sqrt{\sum_{j=1}^{n}A_j^2}}=\frac{hA_n-B}{|A_n|\sqrt{1+\frac{\sum_{1}^{n-1}A_j^2}{|A_n|^2}}}$$

$$=\left(h\frac{A_n}{|A_n|}-\frac{B}{|A_n|}\right)\frac{1}{\sqrt{1+\frac{\sum_{1}^{n-1}A_j^2}{|A_n|^2}}}. \qquad (18)$$

Suppose that $h>0$; then $S$ is above $\Pi$ if $\Delta A_n>0$, or what is the same thing, $(hA_n^2-BA_n)>0$. We may write this last expression as

$$h-\frac{B}{A_n}>0.$$

Thus according to the above lemma (and under the same hypotheses, viz., assumption (A)-(E)):

*Theorem 4. If $h>0$, the probability that $S$ is above $\Pi$ tends to 1 when $n\to+\infty$; if $h<0$, this probability tends to zero.*

The case $h=0$ is not clear-cut. But if, for instance, the $M_i$'s are independent with the same continuous probability law which is symmetric about the plane $x_n=0$, then clearly $Pr\{S>\pi\}=\frac{1}{2}$.

3.

Keeping the notations of section 2, we assume that $\overline{P_iP_j}=1$ for any $i$, $j$ and that the $X_{ij}$'s satisfy conditions (a) and (b) of section 1 with $\sigma_1=\ldots=\sigma_n=\rho/\sqrt{n}$ where $\rho$ is a constant independent of $i$ and $n$. The other assumptions, (B), (C), and (D) of section 2, will not be required. We wish to obtain some information about the random variable:

$$H=A_nh-B. \qquad (19)$$

Theorem 1 implies immediately that

$$E(H)=V_nh, \qquad (20)$$

where $V_n$ is the determinant

$$V_n=\begin{vmatrix} x_{11} & x_{12}\ldots x_{1,n-1} & 1\\ x_{21} & x_{22}\ldots x_{2,n-1} & 1\\ \cdot & \cdot & \cdot\\ \cdot & \cdot & \cdot\\ \cdot & \cdot & \cdot\\ x_{n1} & x_{n2}\ldots x_{n,n-1} & 1 \end{vmatrix}.$$

$V_n$, as we have seen, is given by

$$V_n=\pm(P_1,P_2P_3\ldots P_n).$$

That is to say (cf. formula (33) of the Appendix)

$$V_n=\pm\sqrt{\frac{n}{2^{n-1}}}. \qquad (21)$$

Let $w_n$ be the determinant

$$\begin{vmatrix} x_{11} & x_{12}\ldots x_{1,n-1} & 0\\ x_{21} & \ldots x_{2,n-1} & 0\\ \cdot & \cdot & \cdot\\ \cdot & \cdot & \cdot\\ \cdot & \cdot & \cdot\\ x_{n1} & \ldots x_{n,n-1} & 0 \end{vmatrix}.$$

For $E(H^2)$ we have at once:

$$E(H^2)=h^2E(A_n^2)+E(B^2). \qquad (22)$$

Since $B$ is a determinant of the form $D_n$ (section 1) formula (5*a*) gives the result that

$$E(B^2)=\sum_{k=1}^{n}T_k(w_n)k!\frac{\rho^{2k}}{n^k}. \qquad (23)$$

$A_n$ is not exactly of type $D_n$, but in entirely similar fashion we find

$$E(A_n^2)=\sum_{k=0}^{n-1}T_k'(V_n)k!\frac{\rho^{2k}}{n^k}. \qquad (24)$$

$T_k'(V_n)$ is the sum of the minors of order $(n-k)$ of $V_n$ obtained without suppressing the last column of $V_n$. For instance

$$T_k'(i_1,\ldots,i_k;V_n)=(P_{j_1},P_{j_2}P_{j_3}\ldots P_{j_{n-k}})^2,$$

where $j_1,j_2,\ldots,j_{n-k}$ run through all the numbers $1,2,\ldots,n$ except $i_1,i_2,\ldots,i_{n-k}$. Hence

$$T_k'(i_1,\ldots,i_k;V_n)=V_{n-k}^2=\frac{n-k}{2^{n-k-2}}, \qquad (25)$$

and

$$T_k'(V_n)=\binom{n}{k}(n-k)2^{-n+k+1}. \qquad (26)$$

Substituting this expression into (24) one finds

$$E(A_n^2)=\sum_{k=0}^{n-1}\binom{n}{k}(n-k)2^{-n+k+1}\cdot k!\frac{\rho^{2k}}{n^k}$$

$$=\frac{n}{2^{n-1}}\sum_{k=0}^{n-1}\frac{(n-1)\ldots(n-k)}{n^k}(2\rho^2)^k. \qquad (27)$$

If we suppose that $2\rho^2<1$, (27) yields immediately:

$$E(A_n^2)\sim\frac{1}{1-2\rho^2}\cdot\frac{n}{2^{n-1}}, \qquad (27a)$$

as $n\to\infty$.

$B$ is of the form $D_n$; we know that $Q_k(C^*)$ is a quadric, and it must have as planes of symmetry the $\binom{n}{2}$ planes of symmetry $V_{ij}$ of the polyhedron

$(P_1, P_2, \ldots, P_n)$. Consequently the center of $Q_k(C^*)$ is $G$, and $Q_k(C^*)$ is a sphere since $\binom{n}{2} > n$, and we can write:

$$T_k(w_n)=\lambda_k(n)\overline{OG}^2+T_k^*(w_n), \tag{28}$$

where $T_k^*(w_n)$ is the value of $T_k(w_n)$ when $\overline{OG}=0$. On the other hand

$$T_k(i_1, \ldots, i_k; w_n)=(O, P_{j_1}P_{j_2}\ldots P_{j_{n-k}}),$$

where $j_1, j_2, \ldots, j_{n-k}$ are all the numbers $1, 2, \ldots, n$ except $i_1, i_2, \ldots, i_k$. If $O=G$, we find (cf. appendix, formula (36)):

$$T^*(i_1, \ldots, i_j; w_n)=\frac{k}{n2^{n-k}}$$

and

$$T_k^*(w_n)=\binom{n}{k}\frac{k}{n2^{n-k}}.$$

Hence

$$\sum_{k=1}^{n}T_k^*(w_n)k!\frac{\rho^{2k}}{n^k}=\frac{1}{n2^n}\sum_{k=1}^{n}k\frac{n(n-1)\ldots(n-k+1)}{n^k}(2\rho^2)^k. \tag{29}$$

If $2\rho^2<1$, (29) becomes asymptotically

$$\sum_{k=1}^{n}T_k^*(w_n)k!\frac{\rho^{2k}}{n^k}\sim\frac{1}{n2^n}\cdot\frac{1\rho^2}{(1-2\rho^2)^2}. \tag{29a}$$

We can now compute the value $T_k^{**}(w_n)$ of $T_k(w_n)$ for $P_n=O$ (cf. appendix, formula (38)). Writing

$$T_k^{**}(w_n)=\lambda_k(n)\overline{GP}_n^2+T_k^*(w_n),$$

we have an equation which determines $\lambda_k(n)$; we find

$$\lambda_k(n)=\frac{n(n-2)(n-3)\ldots(n-k)}{(k-1)!2^{n-k-1}}$$

and

$$\sum_{k=1}^{n}\lambda_k(n)k!\frac{\rho^{2k}}{n^k}=\frac{1}{2^{n-1}}\sum_{k=1}^{n}\frac{n(n-2)(n-2)\ldots(n-k)}{n^k}k(2\rho^2)^k. \tag{30}$$

Asymptotically this expression becomes, for $2\rho^2<1$,

$$\sum_{k=1}^{n}\lambda_k(n)k!\frac{\rho^{2k}}{n^k}\sim\frac{1}{2^{n-1}}\frac{2\rho^2}{(1-2\rho^2)^2}. \tag{30a}$$

We verify that $E(B^2)$ is of the order of $(1/n)E(A_n^2)$, which agrees with the lemma of section 2. In the particular case when $G=O$, $E(B^2)$ is of the order of $(1/n^2)\,E(A_n^2)$.

## Appendix

Given $n$ points $P_1, \ldots, P_n$ in an $(n-1)$-dimensional Euclidean space $E_{n-1}$ such that $\overline{P_iP_j}=1$ for any $i$ and $j$ $(i\neq j)$ (that is, these points are the vertices of a regular polyhedron $P_n$) we wish to find an expression for the volume $(1/n!)\,|V_n|$ of $P_n$ in $E_{n-1}$. Let $G_i$ be the center of gravity of the points $P_1, P_2, \ldots, P_i$; $h_n$ the distance between $G_{n-1}$ and $P_n$; and $d_n$ the distance between $G_n$ and any $P_i$. We have

$$|V_n|=h_n|V_{n-1}|$$

$$(n-1)\ \overrightarrow{G_nG_{n-1}}+\overrightarrow{G_nP_n}=0. \tag{31}$$

$G_{n-1}$, $G_n$, $P_n$ are on the same "straight line" (one-dimensional linear variety); and $P_1G_{n-1}P_n$ is a right triangle; hence:

$$1=\overline{P_1P_n}^2=\overline{P_1G_{n-1}}^2+\overline{G_{n-1}P_n}^2.$$

It follows that

$$d_n=\frac{n-1}{n}h_n$$

$$h_n^2=1-\left(\frac{n-2}{n-1}\right)^2h_{n-1}^2. \tag{32}$$

Clearly $h_2$ is known; the recurrence equation (32) can be solved for $h_n$:

$$h_n=\frac{1}{\sqrt{2}}\sqrt{\frac{n}{n-1}}.$$

It follows by recurrence from (31), $|V_2|$ being equal to $\sqrt{3}/2$, that:

$$|V_n|=\sqrt{\frac{n}{2^{n-1}}}, \tag{33}$$

On the other hand,

$$d_n=\frac{1}{\sqrt{2}}\sqrt{\frac{n-1}{n}}, \tag{34}$$

and

$$\overline{G_nG_{n-1}}^2=\frac{1}{2(n-1)n}=\frac{1}{2}\left(\frac{1}{n-1}-\frac{1}{n}\right). \tag{35}$$

We now compute the volume $(G_n, P_1P_2\ldots P_{n-k})$. If $L_{nk}$ is the orthogonal projection of $G_n$ on the linear variety $(P_1P_2\ldots P_{n-k})$, we have:

$$(G_n, P_1P_2\ldots P_{n-k})^2=\overline{G_nL_{nk}}^2|V_{n-k}|^2.$$

But $L_{nk}=G_{n-k}$, so that

$$\overline{G_nL_{nk}}^2=\overline{G_nG_{n-1}}^2+\overline{G_{n-1}G_{n-2}}^2+\ \ldots\ +\overline{G_{n-k+1}G_{n-k}}^2.$$

As in (35),

$$\overline{G_nL_{nk}}^2=\frac{1}{2}\left(\frac{1}{n-k}-\frac{1}{n}\right)=\frac{k}{2n(n-k)},$$

and so

$$(G_n, P_1\ldots P_{n-k})^2=\frac{k}{n2^{n-k}}. \tag{36}$$

We can also compute $(P_n, P_1P_2\ldots P_{n-k})$:

$$(P_n, P_1P_2\ldots P_{n-k})^2=\overline{P_nL_{nk}}^2|V_{n-k}|^2$$

$$\overline{P_nL_{nk}}^2=\overline{P_nG_{n-1}}^2+\overline{G_{n-1}G_{n-2}}^2+\ \ldots\ +\overline{G_{n-k+1}G_{n-k}}^2$$

$$=\frac{1}{2}\left(1+\frac{1}{n-k}\right).$$

Therefore

$$(P_n, P_1\ldots P_{n-k})^2=\frac{(n-k+1)}{2^{n-k}}. \tag{37}$$

From (37) it follows that

$$T_k^{**}(w_n)=\binom{n-1}{k-1}\frac{n-k+1}{2^{n-k}}, \tag{38}$$

Los Angeles, January 11, 1951.

Journal of Research of the National Bureau of Standards Vol. 47, No. 6, December 1951 Research Paper 2275

# Solutions of $Ax = \lambda Bx$[1]

M. R. Hestenes[2] and W. Karush[3]

The problem is to determine characteristic numbers and vectors for the problem $Ax=\lambda Bx$, where $A$, $B$ are $n\times n$ Hermitian matrices. A generalized gradient $\eta$ is defined. From a first approximation $x_0$, a second approximation $x_1=x_0+\alpha\eta$ is determined. Successive approximations, with appropriate alphas, converge to a solution.

## 1. Introduction

Let $A$, $B$, be Hermitian matrices of order $n$ with $B$ positive definite. Then the characteristic vectors of the equation

$$Ax=\lambda Bx \tag{1}$$

are the critical points of the "Rayleigh quotient"

$$\mu(x)=\frac{(x, Ax)}{(x, Bx)}, \qquad x\neq 0, \tag{2}$$

and the corresponding values of the quotient are the characteristic values $\lambda$. In particular the minimum (maximum) of $\mu$ is the least (greatest) characteristic value of (1). Our purpose is to discuss a method of finding the solutions of (1) that is based upon this observation and that avoids a transformation of the problem.

The method is an iterative one that may be described briefly as follows.[4] With each non-null vector $x$ we associate a vector $\eta(x)$ that is in a certain sense the gradient of $\mu$ at $x$. We then pass from one approximation $x$ to the next $x'$ by means of the formula

$$x'=x-\alpha\eta, \qquad \alpha>0,$$

where the scalar $\alpha$ may depend upon $x$. The gradient used here is determined by the equation

$$G\eta=Ax-\mu(x)Bx, \tag{3}$$

where $G$ is an arbitrary positive definite Hermitian matrix. In computational practice $G$ would be selected so that its inverse $G^{-1}$ is known (e. g., $G=I$, the identity matrix). In section 4 it will be shown that this method is convergent if the scalars $\alpha(x)$ are appropriately chosen, and in section 6 two feasible schemes for this choice will be described. In general, convergence is established only to some, possibly intermediate, characteristic value (and vector). Under special hypotheses this will be the least characteristic value (see section 5).

The method has several computational advantages. It avoids a transformation of problem (1).[5] It minimizes round-off errors by beginning each step with a new initial vector. The calculations at each stage of the iteration are simple and identical in form with those of the preceding one. The method is thereby particularly suited to high-speed automatic computing machines. However, it appears to converge too slowly to be of use for hand calculation.

When one or more characteristic vectors are known the method may be modified so as to yield a new characteristic vector (see section 7). This is achieved by appropriately altering eq. 3 for the gradient.

For arbitrary complex matrices $A$, $B$ it is of interest to know when the problem

$$Cx=\lambda Dx \tag{4}$$

may be transformed to one of type (1). Several characterizations[6] are given in section 8, some of which are of computational value.

## 2. Preliminary Results

In this section we shall state some definitions and assemble some well-known facts on matrices. No proofs will be given.

By a vector we understand an $n$-tuple $x=(a_1, a_2, \ldots, a_n)$ of complex numbers. We deal with the space of such vectors over the scalar field of complex numbers. We let

$$(x,y)=a_1\overline{b}_1+a_2\overline{b}_2+\ldots+a_n\overline{b}_n,\ y=(b_1, b_2, \ldots, b_n),$$

where $\overline{c}$ denotes the complex conjugate of the scalar $c$. Thus $(x,y)=\overline{(y,x)}$. The length of $x$ is $[x]=(x,x)^{\frac{1}{2}}$. If $C$ is an arbitrary matrix then

$$(x,Cy)=(C^*x,y)$$

where $Cy$ has the usual meaning, and $C^*$ is the conjugate transpose of $C$. A matrix $H$ is Hermitian if and only if

$$H^*=H.$$

In this case $(x,I_1x)$ is a real number. We shall say

[1] The preparation of this paper was sponsored (in part) by the Office of Naval Research.

[2] Univ. of California at Los Angeles and NBS at Los Angeles.
[3] Univ. of Chicago and NBS at Los Angeles.

[4] It is an extension of one used by the authors in the case that $A$ is real symmetric and $B$ is the identity matrix. See for example, A method of gradients for the calculation of the characteristic roots and vectors of a real symmetric matrix, J. Research NBS **47**, 45 (1951) RP2227.

[5] Such a transformation may, for example, involve finding the inverse of $A$ or $B$. A more feasible scheme computationally is to write $B=LL^*$ with $L$ triangular ($L^*$=conjugate transpose of $L$). The latter method is discussed on p. 159 to 160 of Fox, Huskey, and Wilkinson, Notes on the solution of algebraic linear simultaneous equations, Quart. J. Mech. and Applied Math. p. 147 to 173 (1948).

[6] These results are closely related to some of H. Wielandt, Zur Abgrenzung der selbstadjungierten Eigenwertaufgaben. I. Raume endlicher Dimension, Math. Nachrichten **2**, No. 6, 328 (1949).

that two vectors $x$ and $y$ are $H$-orthogonal in case

$$(x,Hy)=(y,Hx)=0.$$

Two sets of vectors are $H$-orthogonal in case each vector of one set is $H$-orthogonal to each vector of the other. By orthogonality is meant $I$-orthoganality, with $I$ the identity matrix.

A matrix $G$ is positive definite in case it is Hermitian and

$$(x,Gx)>0 \qquad \text{whenever } x\neq 0.$$

Let $G$ be positive definite. There exist positive numbers $m(G)$ and $M(G)$ such that

$$m(G)|x|^2\leq(x,Gx)\leq M(G)|x|^2. \tag{5}$$

Also, we have the inequality

$$|(x,Gy)|^2\leq(x,Gx)(y,Gy). \tag{6}$$

the equality holding if and only if $x$ and $y$ are linearly dependent. Further, the matrix $G^{-1}$ is positive definite, and there exists a positive definite matrix $G_1$ such that $G=G_1^2$.

We turn now to problem (4), where $C$ and $D$ are arbitrary matrices. The number $\lambda'$ is a characteristic number (root, value) of (5) in case there is a non-null vector $y'$ such that

$$Cy'=\lambda' Dy'.$$

We allow the characteristic value $\lambda'=\infty$; in this case $Dy'=0$. We say that $y'$ is a characteristic vector belonging to $\lambda'$. For a problem of type (1), where $A$ is Hermitian and $B$ is positive definite, every characteristic value is finite and real. Let

$$\lambda_1<\lambda_2<\ldots<\lambda_k$$

be the $k$ distinct real characteristic roots of (1), and let $\boldsymbol{L}_j=\boldsymbol{L}(\lambda_j)$ be the characteristic manifold belonging to $\lambda_j$, that is, linear subspace spanned by the characteristic vectors belonging to $\lambda_j$. Then any two subspaces belonging to distinct $\lambda$'s are $B$- and $A$-orthogonal, and have only the null vectors in common. Further, every vector $z$ has a unique decomposition of the form

$$z=z_1+z_2+\ldots z_k, \qquad z_j\epsilon\boldsymbol{L}_j.$$

For problem (1) the important extremum principle is

$$\lambda_j=\min_{x\neq 0}\mu(x), \qquad x\ B\text{-orthogonal to } \boldsymbol{L}_1,\ldots,\boldsymbol{L}_{j-1},$$

$$\lambda_j=\max_{x\neq 0}\mu(x), \qquad x\ B\text{-orthogonal to } \boldsymbol{L}_k,\ldots,\boldsymbol{L}_{j+1}.$$

In particular,

$$\lambda_1\leq\mu(x)\leq\lambda_k, \qquad x\neq 0.$$

## 3. The Gradient

The direction for which the directional derivative of the function, $\mu$ given by (2), is a maximum will now be calculated. This optimal direction will be determined relative to the inner product $(x,Gy)$ corresponding to an arbitrary, fixed positive definite matrix $G$. The generality of an arbitrary inner product has computational significance as well as theoretical interest; in practice it is limited to matrices $G$ whose inverses are known. The iteration method and convergence theorems that are to follow later depend only upon the final formula that will be obtained for the maximizing direction, not upon the derivation of the formula; the derivation is intended to suggest the motivation for the method.

For fixed vectors $x\neq 0$ and $\delta x\neq 0$, consider the function $\mu(x+\epsilon\delta x)$ for real $\epsilon$. By a simple calculation we find that at $\epsilon=0$,

$$\frac{d\mu}{d\epsilon}=\frac{2\boldsymbol{R}\{\delta x,\xi)\}}{(x,Bx)},$$

where

$$\xi=\xi(x)=Ax-\mu(x)\ Bx, \qquad x\neq 0, \tag{7}$$

and $\boldsymbol{R}\{c\}$ denotes the real part of $c$. We therefore seek that vector $\delta x$ for which

$$\boldsymbol{R}\{(\delta x,\xi)\}=\max, \qquad (\delta x,G\delta x)=1. \tag{8}$$

$\eta$ is defined by the equation

$$G\eta=\xi=Ax-\mu\ Bx. \tag{9}$$

Then, using (6),

$$\begin{aligned}\boldsymbol{R}\{(\delta x,\xi)\}=\boldsymbol{R}\{(\delta x,G\eta)\}&\leq|(\delta x,G\eta)|\\&\leq(\delta x,G\delta x)^{\frac{1}{2}}\ (\eta,G\eta)^{\frac{1}{2}}=(\eta,G\eta)^{\frac{1}{2}}.\end{aligned}$$

It is an easy matter to verify that $\delta x=\eta/(\eta,G\eta)^{\frac{1}{2}}$ is the unique normalized vector for which equality holds between the first and last terms above. Hence this vector is the desired solution of (8). Introducing a change in normalization for convenience, $\eta$ is termed the gradient of $\mu$ (with respect to $G$).

We shall have occasion to use the gradient relative to a side condition

$$(\delta x,z)=0, \qquad z \text{ fixed}. \tag{10}$$

Here we wish to solve (8) relative to (10). $\zeta$ is defined by the equation

$$G\zeta=\xi+hz=G\eta+hz$$

where $h$ is determined so that $(\zeta,z)=0$. Thus

$$h=-\frac{(\eta,z)}{(G^{-1}z,z)}. \tag{12}$$

Then, in light of (10), $(\delta x,\xi)=(\delta x,G\zeta)$. As before, it follows that the maximizing vector is proportional to $\zeta$, and this vector is chosen to be the gradient.

More generally, with several independent side

conditions

$$(\delta x, z_1)=0,\ (\delta x, z_2)=0,\ \ldots$$

is as the gradient the vector $\zeta$ is obtained, where

$$G\zeta=\xi+h_1z_1+h_2z_2+\ \ldots, \tag{13}$$

with the $h$'s determined so that $\zeta$ is orthogonal to each of the $z$'s.
Thus the $h$'s are the solutions of

$$\begin{aligned} h_1(G^{-1}z_1,z_1)+h_2(G^{-1}z_2,z_1)+\ \ldots &=-(\eta,z_1)\\ h_1(G^{-1}z_1,z_2)+h_2(G^{-1}z_2,z_2)+\ \ldots &=-(\eta,z_2) \end{aligned} \tag{14}$$

$$\ldots\ldots\ldots\ldots\ldots\ldots$$

in which the determinant of the $h$'s is nonzero, by the positive definiteness of $G^{-1}$ and the independence of the $z$'s.

The change in $\mu$ when we pass from a vector $x\neq 0$ to the vector $x-\alpha\eta$, will now be computed where $\alpha$ is some real number and $\eta(x)$ is given by (9). Assume that $x$ is not characteristic, i. e. $\eta\neq 0$. Direct calculation leads to

$$\mu(x)-\mu(x-\alpha\eta)=\frac{(\eta,G\eta)}{(x,Bx)}f(x,\alpha),\qquad x\neq 0,\ \eta\neq 0, \tag{15}$$

where

$$f(x,\alpha)=\frac{\alpha(2-ps\alpha)}{1-2q\alpha+r\alpha^2} \tag{16}$$

with

$$p=\frac{(\eta,B\eta)}{(\eta,G\eta)},\ q=\frac{\boldsymbol{R}\{(x,B\eta)\}}{(x,Bx)},\ r=\frac{(\eta,B\eta)}{(x,Bx)},\ s=\mu(\eta)-\mu(x).$$

Our iteration procedure takes the following form. An initial vector $x_0$ is given. Then the sequence $\{x_i\}$ is determined by

$$x_{i+1}=x_i-\alpha_i\,\eta_i,\qquad \eta_i=\eta(x_i), \tag{17}$$

where the real number $\alpha_i$ is to be specified at each step. In order to be sure that (17) determines a well-defined sequence we must verify that $x_i\neq 0$ for every $i$. To this end suppose that for a given $j$, $x_j\neq 0$; notice that from (9)

$$(x_j,G\eta_j)=(Gx_j,\ \eta_j)=0.$$

Hence by (17)

$$(x_{j+1},Gx_{j+1})=(x_j,Gx_j)+\alpha_j^2(\eta_j,G\eta_j)>0, \tag{18}$$

since $G$ is positive definite. Hence $x_{j+1}\neq 0$. Since $x_0\neq 0$, the sequence is well defined.

From (15) we have

$$\mu(x_i)-\mu(x_{i+1})=\frac{(\eta_i,G\eta_i)}{(x_i,Bx_i)}f_i(\alpha_i),\qquad f_i(\alpha)=f(x_i,\alpha), \tag{19}$$

this equation holding whenever $\eta_i\neq 0$.

## 4. General Convergence Theorems

In this section and the next will be established convergence theorems under a certain general assumption on the real sequence $\{\alpha_i\}$. In the section following these two we shall describe two effective ways of meeting these conditions. For the present, we assume that the sequence has the property that there exist real positive constants $b_2$ and $c$ such that

$$0\neq\alpha_i\leq b_2,\ \text{and}\ 0<c\leq f_i(\alpha_i)\ \text{whenever}\ \eta_i\neq 0. \tag{20}$$

To simplify our discussion we wish to dispose of the trivial case in which $\eta_j=0$ for some first index $j$. In this instance $x_j$ is a characteristic vector belonging to the characteristic value $\mu_j$, and $x_i=x_j$, $i\neq j$. The results to be given in this, and the next, section are now immediately verifiable. Hence we shall proceed on the basis that

$$\eta_i\neq 0,\qquad i=0,\ 1,\ 2,\ \ldots.$$

In particular (19) holds for every $i$.

*Theorem* 1. *Suppose that the sequence* $[\alpha_i]$ *satisfies* (20). *Then* $\mu_i=\mu(x_i)$ *is a decreasing sequence that converges to a characteristic value* $\lambda$ *of* (1). *Also* $\lim_{i\to\infty}(x_i,\ Gx_i)=d>0$; *in particular the lengths* $|x_i|$ *are bounded and bounded away from zero. Every accumulation point of* $[x_i]$ *is a characteristic vector in* $\boldsymbol{L}(\lambda)$.

To make the proof, we notice first that by (19) and (20) that the sequence $\{\mu_i\}$ is decreasing, since $B$ and $G$ are positive definite. Since this sequence is bounded from below by the minimum characteristic value $\lambda_1$, it follows that it has a limit, call it $\mu'$. By (5), (19), (20) there is a positive constant $e$ such that

$$t_i\leq e(\mu(x_i)-\mu(x_{i+1})),\qquad t_i=\frac{(\eta_i,G\eta_i)}{(x_i,Gx_i)}>0.$$

Hence $t_i\to 0$; in fact

$$\sum_{i=0}^{\infty}t_i<\infty. \tag{21}$$

From (18) we derive

$$(x_{i+1},Gx_{i+1})=(x_0,Gx_0)\prod_{j=0}^{i}(1+\alpha_i^2t_j).$$

It is well known that the product on the right converges if $\sum_0^\infty\alpha_i^2t_j$ does. The latter condition holds by (20) and (21). This establishes the existence of the limit $d$ and the asserted property of $|x_i|$.

It now follows that $\eta_i\to 0$ and hence, by (9),

$$Ax_i-\mu_iBx_i\to 0. \tag{22}$$

Let $y'$ be any limit point of $\{x_i\}$; there exists at least one. Then $y'$ is a non-null vector which, by (22), satisfies

$$Ay'-\mu'By'=0.$$

Thus $\mu'$ is a characteristic value and $y'$ belongs to $\boldsymbol{L}(\mu')$. This completes the proof.

*Theorem* 2. *Let* (20) *hold. If the sequence* $\{x_i\}$ *has an isolated accumulation point* $y$, *then* $\{x_i\}$ *converges to* $y$. *Consequently if the characteristic root* $\lambda$ *of the preceding theorem is simple* (i. e., *dim* $\boldsymbol{L}(\lambda)=1$), *then* $\{x_i\}$ *converges to a characteristic vector.*

Let $y$ be an isolated accumulation point and let $\boldsymbol{P}$ be the set of remaining accumulation points. Let $\boldsymbol{S}_1$ and $\boldsymbol{S}_2$ be open sets with disjoint closures with $y$ in $\boldsymbol{S}_1$ and $\boldsymbol{P}$ in $\boldsymbol{S}_2$. There is an $i'$ such that for $i\geq i'$ $x_i$ lies in the union of the two open sets. Let $d'>0$ be the greatest lower bound of $|u-v|$ for $u$ in $\boldsymbol{S}_1$, $v$ in $\boldsymbol{S}_2$. Since $\eta_i\to 0$ by the preceding proof, we may, by (20) and (17), choose an $i''\geq i'$ such that $|x_{i+1}-x_i|<\frac{1}{2}d'$ for $i\geq i''$. Hence if $x_i$ is in $\boldsymbol{S}_1$, $i\geq i''$, then $x_{i+1}$ is in $\boldsymbol{S}_1$. It follows that for some $j$, $x_i$ is in $\boldsymbol{S}_1$ for all $i\geq j$. Thus $\boldsymbol{P}$ is null. This establishes the first conclusion of the theorem.

Let $\lambda$ be a simple root. From Theorem 1 every accumulation point $y$ must satisfy $(y, Gy)=d$. There are exactly two vectors in $\boldsymbol{L}(\lambda)$ which satisfy this condition. By the first part of the theorem $\{x_i\}$ must converge to one of them. This completes the proof.

*Theorem* 3. *Let* (20) *hold, and let* $\lambda$ *be the characteristic value of Theorem* 1. *Then there is a sequence of vectors* $\{y_i\}$ *in* $\boldsymbol{L}(\lambda)$ *such that*

$$\lim_{i\to\infty}(x_i-y_i)=0.$$

For the proof we utilize the decomposition

$$x_i=y_i+z_i,\ y_i \text{ in } \boldsymbol{L}(\lambda) \text{ and } z_i \text{ } B\text{-orthogonal to } \boldsymbol{L}(\lambda).$$

Now suppose $z_i$ does not converge to zero. Then some subsequence $\{z_i'\}$ converges to $z\neq 0$. The corresponding subsequence $\{x_i'\}$ has a further subsequence $\{x_i''\}$ which converges to $y$ in $\boldsymbol{L}(\lambda)$, by Theorem 1. By the above decomposition, the corresponding subsequence $\{y_i''\}$ converges, necessarily to a vector $y''$ in $\boldsymbol{L}(\lambda)$. Hence,

$$z=\lim_{i\to\infty}(x_i''-y_i'')=y-y''.$$

Thus $z$ is both in $\boldsymbol{L}(\lambda)$ and $B$-orthogonal to this subspace. Hence $z=0$. This contradiction completes the proof.

It is worthy of notice that insofar as the iteration described in this paper is to be used as a practicable numerical method for finding some characteristic vector of (1), then the conclusion of the preceding theorem is as effective as the assertion that the sequence $\{x_i\}$ actually converges. For the theorem asserts that the sequence will come, and remain, within an arbitrarily small distance of some characteristic vector, this vector possibly varying with $x_1$.

## 5. Convergence to the Least Characteristic Vector

Because our iteration method is a gradient procedure which decreases $\mu(x)$, it is to be expected that under appropriate hypotheses on the problem (1) and the matrix $G$ the sequence $\mu_i$ will converge to $\lambda_1$, the minimum characteristic value. We shall show under a rather strong assumption that such convergence will take place, and further, that the sequence $\{x_i\}$ will converge, whether or not $\lambda_1$ is simple.

In passing, we remark that although for definiteness the iteration so as to produce a decreasing sequence $\mu_i$ has been formulated a slight modification in (20) produces an increasing sequence; the change is

$$0\leq -\alpha_i<b_2 \text{ and } f_i(\alpha_i)\leq c<0.$$

The results of the previous section hold in this case, and under the forthcoming additional hypothesis of this section, convergence will take place to $\lambda_k$, the the greatest characteristic value, and to a corresponding characteristic vector.

*Lemma* 1. *Suppose that*

$$AG^{-1}B=BG^{-1}A. \tag{23}$$

*Then problem* (1) *and the problem*

$$Gx=\nu Bx \tag{24}$$

*have a common complete set of characteristic vectors* $y_1, y_2, \ldots, y_n$ *with* $(y_p, By_q)=\delta_{pq}=$*Kronecker delta.*

To prove this $B=H^2$ is written with $H$ positive definite and Hermitian. Then (1) and (24), respectively, are equivalent to $H^{-1}AH^{-1}z=\lambda z$ and $H^{-1}GH^{-1}z=\nu z$ where $z=Hx$. It is easily verified that the condition (23) is equivalent to the commutativity of the Hermitian matrices $H^{-1}AH^{-1}$ and $H^{-1}GH^{-1}$. It follows by standard theory that these matrices are simultaneously reducible to diagonal form by a unitary transformation; hence they share a complete ortho-normal set of characteristic vectors $z_1, z_2, \ldots, z_n$. The desired vectors $y_p$ are now given by $z_p=Hy_p$.

*Theorem* 4. *Assume that* (20) *and* (23) *hold. For a given initial vector* $x_0$, *let* $m$ *be the smallest integer* $j$ $(j=1, 2, \ldots, k)$ *for which* $x_0$ *is not* $B$*-orthogonal to the characteristic manifold* $\boldsymbol{L}_j$. *Then*

$$\lim_{i\to\infty}\mu_i=\lambda_m, \qquad \lim_{i\to\infty}x_i=y\neq 0 \text{ with } y \text{ in } \boldsymbol{L}_m.$$

We employ the basis of Lemma 1 to write

$$x_0=a_{01}\,y_1+a_{02}\,y_2+\ \ldots\ +a_{0n}\,y_n.$$

It is assumed that the basis has been ordered so that the first $r_1$ vectors span $\boldsymbol{L}_1$, the next $r_2-r_1$ vectors span $\boldsymbol{L}_2$, etc. (We take $r_0=0$.) By multiplying each vector of the basis by $\pm 1$ we may assume that

$$a_{0p}\geq 0, \qquad p=1, 2, \ldots, n.$$

Let

$$\tau_1\leq\tau_2\leq\ \ldots\ \leq\tau_n$$

be the characteristic numbers of (1) corresponding

to the successive vectors of the basis. Thus $\tau_1 = \ldots = \tau_{r_1} = \lambda_1$, $\tau_{r_1+1} = \ldots = \tau_{r_2} = \lambda_2$, etc. Furthermore let $\nu_p$ be the characteristic number of (24) corresponding to $y_p$. Thus

$$\nu_p = (y_p,\ Gy_p) > 0$$

and

$$G^{-1}By_p = \nu_p^{-1} y_p, \qquad p = 1, 2, \ldots, n.$$

Using (17), (9), (1) and the preceding equality it is found that

$$x_i = a_{i1}y_1 + a_{i2}y_2 + \ldots$$

with

$$a_{i+1,p} = a_{ip}\{1 + \alpha_i \nu_p^{-1}(\mu_i - \tau_p)\}. \tag{25}$$

Also

$$a_{ip} = (y_p, Bx_i). \tag{26}$$

Since $x_0$ is by hypothesis $B$-orthogonal to each of the subspaces $\boldsymbol{L}_1, \ldots, \boldsymbol{L}_{m-1}$, we have $a_{0q} = 0$ for $q = 1, 2, \ldots, r_{m-1}$. By (25), $a_{iq} = 0$ for every $i$. Hence every $x_i$ is $B$-orthogonal to the same subspaces and by the extremum principle of section 2 we have

$$\mu_i \geq \lambda_m.$$

Now for each $q = r_{m-1}+1, \ldots, r_m$ consider the sequence $\{a_{iq}\}$. For $i = 0$, $a_{0q} \geq 0$, with the strict inequality holding for at least one value of $q$. From (25) it follows that the sequence is nonnegative and nondecreasing, since the term in braces is not less than 1 for the present range of $q$ by (20), $\nu_p > 0$, and the last displayed inequality. The sequence is also bounded, since $|x_i|$ is, by Theorem 1. Thus

$$\lim_{i\to\infty} a_{iq} = c_q \geq 0, \qquad q = r_{m-1}+1, \ldots, r_m, \tag{27}$$

with at least one limit positive.

Let $y'$ be an arbitrary accumulation point of $\{x_i\}$ (there is at least one). Let $\{x_{i_s}\}$ be a subsequence converging to $y'$. By Theorem 1, $y'$ is a characteristic vector of (1). In addition it must belong to $\boldsymbol{L}_m$, for otherwise

$$a'_{i_q} = (y_q, Bx'_i) \to (y_q, By') = 0,$$

contrary to (27). It now follows that $a'_{ip} \to 0$ for $p$ outside the range of $q$, as in (27). Thus

$$y' = \lim_{i\to\infty} x'_i = \sum_{r_{m-1}+1}^{r_m} c_q y_q \neq 0 \text{ in } \boldsymbol{L}_m.$$

Since $y'$ was an arbitrary limit point we have the desired convergence of $x_i$ to a vector $y$ in $\boldsymbol{L}_m$. Finally,

$$\lim_{i\to\infty} \mu_i = \lim_{i\to\infty} \frac{(x_i, Ax_i)}{(x_i, Bx_i)} = \frac{(y, Ay)}{(y, By)} = \lambda_m.$$

*Corollary. The condition* (23) *is satisfied if* (1) $G = B$, *or* (2) $G = I$ *and* $AB = BA$.

This is easily verified. The case $G = B = I$ with $A$ real symmetric was studied in greater detail in the paper by the present authors referred to earlier.

## 6. Construction of the Sequence $\{\alpha_i\}$

We shall describe two methods of constructing this sequence so that condition (20) is satisfied.

*Lemma* 2. *Let the real number* $b_2$ *satisfy*

$$0 < b_2 < \frac{2}{\lambda_k - \lambda_1} \cdot \frac{m(G)}{M(B)}, \tag{28}$$

*where* $\lambda_k - \lambda_1$ *is the spread of the characteristic values of* (1) *and the other quantities are defined by* (5). *Then there is a constant* $c_1 > 0$ *such that for every* $x \neq 0$ *with* $\eta \neq 0$ *we have*

$$f(x, \alpha) \geq c_1 \alpha \quad \text{for} \quad -b_2 \leq \alpha \leq b_2.$$

Let $x$ and $\alpha$ satisfy the required conditions. Assume further that $\alpha \neq 0$. Then we may write (16) in the form

$$\frac{f(x,\alpha)}{\alpha} = \frac{(2 - ps\alpha)}{(x - \alpha\eta, B(x - \alpha\eta))/(x, Bx)}. \tag{29}$$

Now

$$|ps\alpha| \leq \frac{M(B)}{m(G)}(\lambda_k - \lambda_1)b_2 \equiv b_3 < 2,$$

where we have used (5) and the extremum property of $\lambda_1$ and $\lambda_k$. Thus the numerator on the right side of (29) exceeds the positive number $(2 - b_3)$. Our proof will be complete if we can show that the corresponding (positive) denominator is bounded uniformly in $x$ and $\alpha$. By (5) it is sufficient to show $|\eta|/|x|$ is bounded. But this is an immediate consequence of (9).

As a consequence of Lemma 2 we have the following result.

*Theorem* 5. *Let the sequence* $\{\alpha_i\}$ *of real numbers be such that*

$$0 < b_1 \leq \alpha_i \leq b_2 \tag{30}$$

*for constants* $b_1$, $b_2$ *with the latter as in* (28). *Then this sequence satisfies condition* (20).

Our second method of prescribing $\alpha = \alpha(x)$ stems from the idea of maximizing $f(\alpha) = f(x, \alpha)$ as a function of $\alpha$, hence choosing $\alpha$ as a zero of $f'(\alpha)$. A simple calculation leads to

$$f'(\alpha) = 2\frac{(pqs - r)\alpha^2 - ps\alpha + 1}{(1 - 2q\alpha + r\alpha^2)^2}, \qquad x \neq 0, \eta \neq 0. \tag{31}$$

A function $\alpha(x)$ is now defined as follows. Choose an arbitrary fixed positive constant $b_4$. Let

$$\alpha(x) = \begin{cases} \text{first zero of } f'(\alpha) \text{ on } 0 \leq \alpha \leq b_4, \\ b_4, \text{ if no such zero exists.} \end{cases} \qquad (x \neq 0, \eta \neq 0).$$

This function is computationally simple; its con-

struction involves only the solution of a quadratic equation and a comparison of numbers.

*Theorem* 6. *For a given constant $b_4>0$ and a given initial vector $x_0\neq 0$ determine the sequence $\{\alpha_i\}$ by means of the iteration formula* (17) *and the equation*

$$\alpha_i=\begin{cases}\alpha(x_i) \text{ if } \eta_i\neq 0,\\ b_4 \quad \text{if } \eta_i=0,\end{cases}$$

*where $\alpha(x)$ is given by* (32). *Then this sequence satisfies condition* (20).

For the proof several properties of the function (32) are established. The coefficients of the quadratic expression in the numerator in (31) are uniformly bounded in $x$. This is a consequence of (9) and (5). It follows that its zeros are uniformly bounded away from 0. Hence, there is a number $b_3>0$ such that

$$b_3\leq\alpha(x)\leq b_4.$$

Thus the first condition of (20) is fulfilled. Now $f(\alpha)$ is a non-decreasing function on $0\leq\alpha\leq\alpha(x)$; for, by $f'(0)=2$ and (32) its derivative is non-negative on this interval. Select $b_2<b_3$ so that (28) holds. Then

$$f(\alpha(x))\geq f(b_2)\geq c_1 b_2$$

uniformly in $x$. From this we see that the second condition of (20) also holds. The proof is complete.

## 7. Obtaining Further Characteristic Vectors.

Suppose that a characteristic vector $y'$ with characteristic value $\lambda'$ is known. We propose to show how the preceding iteration scheme may be modified so as to secure a new, independent characteristic vector. The procedure will be to start with an initial vector $z_0$ which is $B$-orthogonal to $y'$ and maintain this orthogonality at each step of the iteration.

Thus, let

$$z=By' \tag{33}$$

and suppose we have a vector $x\neq 0$ such that $(x, z)=0$. We wish our next approximation $x-\alpha\zeta$ to be orthogonal to $z$, i. e., we require

$$(\zeta, z)=0. \tag{34}$$

In order to select the direction $\zeta$ in an optimal manner, according to section 3, it is chosen proportional to the solution of (8) with the side condition (10), $z$ as in (33). We thereby determine $\zeta$ by (11) and (12). Notice that by (11),

$$(\zeta, G\zeta)=(\zeta, \xi), \qquad (x, G\zeta)=0 \tag{35}$$

using (34) and (7). Now suppose $\zeta=\zeta(x)\neq 0$. Then a straightforward calculation using the first equation of (35) shows that equations (15) and (16) are valid with $\eta$ everywhere replaced by $\zeta$.

The iteration formula (17) is now replaced by

$$x_{i+1}=x_i-\alpha_i\zeta_i \tag{36}$$

with the corresponding formula (18) valid by the second equation of (35). Our present sequence however has the additional property

$$(x_i, By')=0. \tag{37}$$

An examination of section 4 shows that with one necessary verification, to be remarked on soon, the three theorems of that section remain valid. We may now add, however, that the characteristic accumulation vectors $y$ in Theorem 1 and 2 are $B$-orthogonal to $y'$, and that the vectors $y_i$ of Theorem 3 have the same property. The required verification is to establish the equivalence of $\zeta(x)=0$ with $\eta(x)=0$ and $\zeta_i\to 0$ with $\eta_i\to 0$. Here, of course, $\eta$ is given by (11). We shall prove only the second equivalence; this will suggest the proof of the first. That $\zeta_i\to 0$ when $\eta_i\to 0$ is immediate from (9), (11) and (12). Suppose $\zeta_i\to 0$. We note first that $(\xi_i, y')=0$; this follows from (7), (37) and the fact that $y'$ is characteristic. Hence by (11)

$$(G\zeta_i, y')=h_i(By', y'),$$

where $h_i$ of (12) has the obvious meaning. Hence $h_i\to 0$. It follows by (11) that $\xi_i\to 0$ and hence $\eta_i\to 0$, as desired.

The constructions of section 6 remain valid under the present iteration (36). It is only necessary to verify the uniform boundedness of $|\zeta|/|x|$, $x\neq 0$, $\zeta\neq 0$. This is an immediate consequence of (11), (12) and (9).

To maintain the validity of Theorem 4 of section 5 in the present context it is not necessary to modify the iteration procedure from (17) to (36). The earlier method is adequate. For, by (25), we see that if the initial vector $x_0$ is $B$-orthogonal to $y'$, so is each vector $x_i$, and hence the limit vector $y$.

If several characteristic vectors $y'$, $y''$, . . . with characteristic values $\lambda'$, $\lambda''$, . . . are known then the iteration (36) is to be used with $\zeta$ determined by (13) and (14), where $z_1=By'$, $z_2=By''$, . . . . The resulting sequence $\{x_i\}$ will be $B$-orthogonal to the known characteristic vectors and hence all limit vectors will have this property. It may be easily verified that the preceding remarks concerning the validity of the results of the previous sections remain in force.

The iteration $x-\alpha\zeta$ determined by (13) and (14) is theoretically equivalent to the following procedure. First form the vector $x'=x-\alpha\eta\equiv x-\alpha G^{-1}\xi$, and then determine $k_1, k_2, \ldots$ so that

$$x''=x'+k_1G^{-1}z_1+k_2G^{-1}z_2+\ \ldots \tag{38}$$

is $B$-orthogonal to $y', y'', \ldots$. It is easy to verify that $x''=x-\alpha\zeta$. However the procedure just described has the computational advantage that the vector $x_i$ formed at each stage is accurately $B$-orthogonal to the known characteristic vectors. In

the alternative procedure (36), $B$-orthogonality of $x_i$ may be gradually lost through round-off errors (although this may be remedied by the additional work of occasional $B$-orthogonalization).

It would also be extremely convenient for the determination of the $k'$s in (38) (or the $h$'s in (13)) to have $(G^{-1}z_j,z_m)=0$ for $j\neq m$. This may be achieved by successively orthogonalizing as additional characteristic vectors are accumulated. Suppose $y''$ has been calculated with $y'$ known. Then with $z_1=By'$, define $z_2$ by

$$z_2=By''+lz_1$$

with $l$ chosen so that $(z_2,G^{-1}z_1)=0$. Then the $G^{-1}$-orthogonal set $(z_1,z_2)$ may be used in (38) (or (13)). Suppose now that a third independent characteristic vector $y'''$ is calculated. Put

$$z_3=By'''+l_1z_1+l_2z_2$$

with $l_1$, $l_2$, chosen so that $(z^3,G^{-1}z_1)=(z_3,G^{-1}z_2)=0$; this determination is simplified by the $G^{-1}$-orthogonality of $(z_1,z_2)$. The new $G^{-1}$-orthogonal set $(z_1,z_2,\ z_3)$ may now be used in (38). The extension to more vectors is clear.

## 8. Problems Equivalent to (1)

We leave now the calculation of characteristic vectors and values and raise the question of when a general problem of the type

$$Cx=\lambda Dx, \text{ with } |C-\lambda D|\not\equiv 0 \text{ in } \lambda, \tag{39}$$

is equivalent to one of type (1), that is, one with $A$ Hermitian and $B$ positive definite. For the moment we impose no additional conditions on the complex matrices $C$ and $D$. Clearly (39) has at most $n$ characteristic roots (including the possible real value $\lambda=\infty$), where $n$ is the order of the matrices.

Consider a second problem

$$Rz=\lambda Sx. \tag{40}$$

By asserting that problems (39) and (40) are equivalent we mean that there is a nonsingular matrix $K$ and one-to-one correspondence between the distinct characteristic values of (39) and those of (40) with the following property: if $\lambda'$ of (39) corresponds to $\lambda''$ of (40), then $y'$ is a characteristic vector of (39) belonging to $\lambda'$ if and only if $y''=Ky'$ is a characteristic vector of (40) belonging to $\lambda''$. If $b$ is a number such that $|C-bD|\neq 0$, then (39) is equivalent to $(C-bD)x=(\lambda-b)Dx$, and hence to

$$Ex=\nu Fx, \text{ with } E=D, F=C-bD, \nu=\frac{1}{\lambda-b}, \quad |F|\not\equiv 0. \tag{41}$$

Notice that $\nu=\infty$ is not a characteristic value of (41).

*Lemma 2. Let $\lambda_j$, $j=1,\ 2,\ \ldots,\ k$, be the distinct characteristic values of* (39) *and let $\boldsymbol{H}$ be the space spanned by the spaces $\boldsymbol{L}_j=\boldsymbol{L}(\lambda_j)$. Then*

$$\sum_{j=1}^{k}\dim \boldsymbol{L}(\lambda_j)=\dim \boldsymbol{H}.$$

It is sufficient to make the proof for the equivalent problem (41), where $\nu_j=1/(\lambda_j-b)$ and $\boldsymbol{L}_j=\boldsymbol{L}(\nu_j)$. It may be assumed that the characteristic values so ordered that if $\nu=0$ is a characteristic value, then $\nu_1=0$. Let $\boldsymbol{H}_j$ be the space spanned by $\boldsymbol{L}_1, \boldsymbol{L}_2, \ldots, \boldsymbol{L}_j$. Any two spaces $\boldsymbol{L}_j$ have only the null vector in common. It follows that the statement

$$\sum_{l=1}^{j}\dim \boldsymbol{L}_l=\dim \boldsymbol{H}_j \tag{42}$$

is valid for $j=2$. Assume that (42) holds for $j=m<k$; we shall show that it is then valid for $j=m+1$. If (42) were false for $j=m+1$, then there would exist a vector $y_{m+1}\not\equiv 0$ of $\boldsymbol{L}_{m+1}$ such that

$$y_{m+1}=y_1+y_2+\ \ldots\ +y_m, \qquad y_l\epsilon\boldsymbol{L}_l, \quad l=1,2,\ \ldots,\ m,$$

with not all the terms on the right null. From $Ey_l=\nu_lFy_l$ is obtained

$$Ey_{m+1}=F(\nu_1y_1+\ \ldots\ +\nu_my_m).$$

But $Ey_{m+1}=\nu_{m+1}Fy_{m+1}$. Since $|F|\not\equiv 0$,

$$\nu_{m+1}y_{m+1}=\nu_1y_1+\ \ldots\ +\nu_my_m,$$

so that

$$\left(\frac{\nu_1}{\nu_{m+1}}-1\right)y_1+\ \ldots\ +\left(\frac{\nu_m}{\nu_{m+1}}-1\right)y_m=0,$$

since $\nu_{m+1}\not\equiv 0$. But (42) holds for $j=m$. Hence each term on the left above must vanish. At least one $y_l$, say $y_l'$, is not null. Then $\nu_{m+1}=\nu_l'$, $l'\leq m$. This contradiction completes the proof.

From the lemma it is clear that the condition

$$\sum_{j=1}^{k}\dim \boldsymbol{L}_j=n \tag{43}$$

for (39) is equivalent to the assertion that every vector may be written uniquely, apart from order of terms, as a sum of characteristic vectors belonging to distinct characteristic values.

Our main theorem is the following.

*Theorem 8. For a problem* (39) *each of the following conditions implies the other.*

I. *Problem* (39) *is equivalent to one of type* (1).

II. *The characteristic values of* (39) *are real and* (43) *holds.*

III. *There exists a positive definite matrix $P$ such that $CPD^*$ is Hermitian.*

That II follows from I is a consequence of the well-known fact that for problem (1) condition II is valid. To show that II implies III we construct the

nonsingular matrix $Y$ whose columns are the $n$ linearly independent (by Lemma 2) characteristic vectors of (41). Thus $EY=FY\Lambda$, where $\Lambda$ is a real diagonal matrix comprising the characteristic roots of (41). Hence $\Lambda=Y^{-1}F^{-1}EY$ is Hermitian, that is

$$Y^{-1}F^{-1}EY=Y^*E^*F^{*-1}Y^{*-1}.$$

Hence

$$EPF^*=FPE^*, \qquad P=YY^*. \tag{44}$$

From the definition of $E$ and $F$ in (41) is obtained

$$DPC^*=CPD^* \tag{45}$$

as desired.

Finally, to show that III implies I we observe first that (45) implies (44). Problem (41) is equivalent to

$$EPF^*z=\nu FPF^*z, \qquad x=PF^*z,$$

which is of type (1). This completes the proof.

*Corollary. The following condition may be added to those of Theorem* 8.

IV. *There exists a positive definite matrix $P$ such that $C^*PD$ is Hermitian.*

For the proof we need only observe that II holds for (39) if and only if it holds for

$$C^*x=\lambda D^*x,$$

and then apply III to this problem.

If our theory is limited to real vectors over the field of real numbers, then the following specializations occur. The matrices $A$ and $B$ are to be taken real symmetric and the matrices $C$ and $D$ are to be taken real. The matrix $P$ of III and IV is real symmetric and the condition of reality in II is superfluous.

If the matrix $P$ of III or IV is known then the transformation of (39) to (1) involves only matrix multiplications and hence is computationally feasible. For example, in case of III with $|D|\neq 0$ we write

$$CPD^*z=\lambda DPD^*z, \qquad x=PD^*z.$$

From the solutions $z$ of this problem we obtain the solutions $x$ of (39) by a direct matrix transformation. If $|C|\neq 0$, we write

$$DPC^*z=\nu CPC^*z, \qquad \lambda=\frac{1}{\nu}, \qquad x=PC^*z.$$

In the case of IV with, say $|D|\neq 0$, we write

$$D^*PCx=\lambda D^*PDx$$

which is of type (1) with solutions exactly those of (39). In the case of either III or IV with $|C|=|D|=0$, we first transform to (41) and then apply the preceding technique indicated for $|D|\neq 0$.

Los Angeles, September 11, 1950.

Journal of Research of the National Bureau of Standards Vol. 47, No. 6, December 1951 Research Paper RP2276

# Proposed Revision of the Conventional Method of Wave-Filter Design

Paul J. Selgin

A modification of the conventional "classical" method of electrical filter design is proposed. The change consists of the use of new parameters, "frequency numbers", which permit the design to be made from specification of peak and cut-off attenuation rather than idealized cut-off frequency, as in the conventional method.

The method is extended to cover the dissipative, as well as the nondissipative, or lossless case. Suitable design curves and tabulations are included.

## 1. Introduction

The so-called conventional method of wave-filter design is not as powerful nor as flexible as more recent methods, based on the "lattice" form of filter section [1];[1] nevertheless, it still has usefulness because of its relative simplicity, and is, in fact, used by practically all designers of equipment to whom the solution of a filter problem is an occasional necessity rather than a constant challenge.

Because simplicity is the main virtue of the conventional approach, one is led to ask whether the ultimate of simplicity and effectiveness has been reached in this particular domain, or otherwise. Upon examining the question, one finds that the conventional method, since its inception (Zobel's first paper on the subject [2] was published in 1923) has remained essentially unchanged, the attention of network specialists having been diverted, by the work of Cauer [3] and Bode [4], to other methods of synthesis.

The chief purpose of this paper is to make the conventional image method better suited to the solution of practical filter problems, having regard to the form in which the design data must be formulated. In practice the cut-off frequency as such is not given, but minimum and maximum attenuations are given together with the respective frequency ranges (see fig. 7). The present design method is geared to this formulation of the problem and does not require assumptions regarding the cut-off frequency value. Also, the method permits the minimizing of reflection losses at the critical frequencies by removing the arbitrary assumption that the "nominal" filter impedance must coincide with the load impedance.

The method is further refined by suitably selecting the parameters that determine the values to be used in the elements of each filter section. In the classical method the cut-off frequency is one such parameter, the cut-off attenuation another. In the present approach a single function of frequency, the "frequency number," is used throughout, and values of this function corresponding to the cut-off and peak-attenuation frequencies are used as the design parameters.

[1] Figures in brackets indicate the literature references at the end of this paper.

## 2. Basic Structures

Space does not permit a full treatment of all filter types in this article. We will, therefore, limit the discussion to the three most frequently used types: high-pass, low-pass, and symmetrical band-pass.

The basic "$L$" structure, or "half section," for these three classes is shown in figure 1, in two equivalent configurations, suitable for the formation of "$T$" section and "$\pi$" sections, respectively. The so-called "$T$-connected" configuration will be given particular attention in the discussion. For each class is given, along with the two alternative configurations, the "frequency number" that is, the function of frequency that should be used, instead of the frequency itself, in all computations concerning the filter.

## 3. Dependence of the Transfer Constant on the Arms Ratio

The ratio $Z_s/Z_p$ between the series arm and shunt arm impedances of the $L$ half section determines the attenuation and phase shift characteristics of the *image-terminated* $T$ or $\pi$ section obtained by joining two such half sections. (Conventional filter theory is predicated on the existence of image-termination or "image match" [5] between the various sections and to the remainder of the system.) The complex number $\alpha+j\beta$, where $\alpha$ is the attenuation in nepers, $\beta$ the phase shift in radians, is, in general, the transfer constant $\theta$ of an image-connected 4-pole. According to this definition, $\theta$ may be shown to equal the complex ratio of output to input voltage (output to input current) of the 4-pole [5, p. 30].

In the following, $\theta$ will always be associated to a complete $T$ or $\pi$ section (it makes no difference which), while $Z_s$ and $Z_p$ will be the values for the component half-sections.

The relationship between $Z_s/Z_p$ and $\theta$ is the following:

$$\frac{Z_s}{Z_p}=\sinh^2\frac{\theta}{2}, \tag{1}$$

or, expressing $e^\theta$:

$$e^\theta=\frac{\sqrt{1+\frac{Z_s}{Z_p}}+\sqrt{\frac{Z_s}{Z_p}}}{\sqrt{1+\frac{Z_s}{Z_p}}-\sqrt{\frac{Z_s}{Z_p}}}. \tag{2}$$

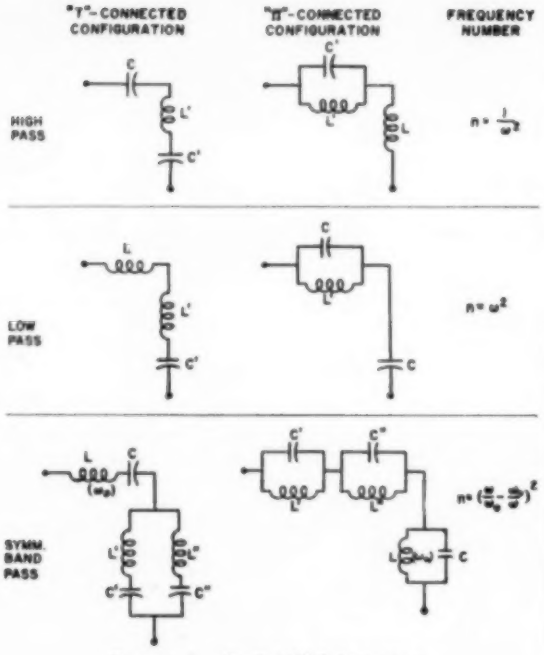


FIGURE 1. *Basic "L" half-sections.*

These expressions and the corresponding families of curves will be found in any standard textbook on filters [6].[2]

The dependence of $\alpha$ and $\beta$ on $Z_s/Z_p$, for $Z_s$ and $Z_p$ purely reactive, may be summarized in the diagram of figure 2, which is schematic and not suitable for purposes of evaluation.

## 4. Arms Ratio Expressions

From what has been said it is apparent that the arms ratio $Z_s/Z_p$ determines the transmission characteristics of the filter section. At the moment we are interested only in the dissipation-less case; however, since ultimately dissipation will have to be considered, it is convenient (in spite of the added algebraic difficulty) to derive at the outset the arms ratio

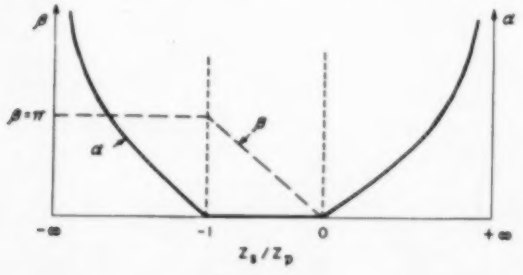


FIGURE 2.

[2] A set of curves of constant $U$ and $V$ (real and imaginary parts of $Z_s/Z_p$ in the $\alpha, \beta$ plane), is given on figure 8.

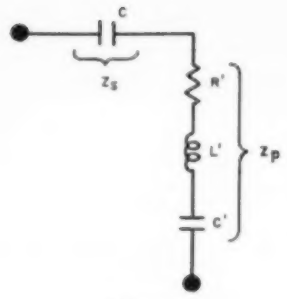


FIGURE 3.

for the case of dissipative structures, differing from those of figure 1 in that the pure inductances are replaced by physical coils of given dissipation factor $d=R/\omega L$, approximately constant over the operating range. The three classes of figure 1 will be considered in turn.

### 4.1. High-pass

Consider the first form (for $T$ connection). The equivalent circuit, allowing for dissipation in the coil, is shown in figure 3. The arms ratio is:

$$\frac{Z_s}{Z_p}=\frac{1}{jC\omega\left(R'+j\omega L'+\frac{1}{j\omega C'}\right)}$$

$$=\frac{-1}{CL'\omega^2\left(1-jd-\frac{1}{L'C'\omega^2}\right)}. \tag{3}$$

At this point we discard $\omega$ as the variable denoting frequency and use instead the *frequency number* appropriate for this class of filters, that is (fig. 1) the variable:

$$n=\frac{1}{\omega^2}. \tag{4}$$

Equation 3 can be rewritten in terms of $n$ by noting that for zero dissipation, the infinite attenuation frequency is given by

$$n=n_\infty=\frac{1}{\omega_\infty^2}=L'C' \tag{5}$$

and the lower cut-off frequency ($Z_s/Z_p=-1$ or $n=n_c$) by

$$\frac{n_c}{L'C\left(1-\frac{n_c}{n_\infty}\right)}=1. \tag{6}$$

These relations allow (3) to be written as

$$\frac{Z_s}{Z_p}=\left(\frac{n}{n_\infty}-\frac{n}{n_c}\right)\frac{1-\frac{n}{n_\infty}+jd}{\left(1-\frac{n}{n_\infty}\right)^2+d^2}. \tag{7}$$

Since the dissipation factor $d$ (reciprocal of the coil $Q$) is always a small number, it is permissible to neglect $d^2$ in the above, provided we do not attempt to use the resulting expressions in the immediate neighborhood of the frequency of peak attenuation, in which case the denominator of (7) becomes infinite if $d^2$ is neglected. This is not a serious limitation to the design of dissipative filters, since the peak values of attenuation are never critical, being far in excess of design limits.

With this simplification, (7) goes into the form:

$$\frac{Z_s}{Z_p}=\frac{\frac{n}{n_\infty}-\frac{n}{n_c}}{1-\frac{n}{n_\infty}}\left(1+jd\,\frac{1}{1-\frac{n}{n_\infty}}\right). \tag{8}$$

The same expression goes for the second alternative form of high-pass filter section, which is in dual relationship to the first (7).

### 4.2. Low-Pass

Again consider the $T$ connected form (fig. 1). The equivalent circuit for dissipative coils appears in figure 4.

The arms ratio is:

$$\frac{Z_s}{Z_p}=\frac{j\omega L(1-jd)}{j\omega L'\left(1-jd-\frac{1}{L'C'\omega^2}\right)}. \tag{9}$$

Discarding $\omega$ in favor of the frequency number $n$, as before, we let:

$$n=\omega^2 \tag{10}$$

Again, in the dissipation-less case we have

$$n_\infty=\omega_\infty^2=\frac{1}{L'C'} \tag{11}$$

and at cut-off:

$$-1=\frac{L}{L'}\,\frac{1}{1-\frac{n_\infty}{n_c}} \tag{12}$$

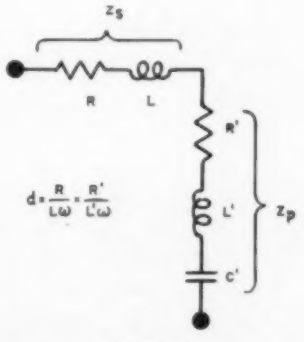


FIGURE 4.

so that (9) becomes

$$\frac{Z_s}{Z_p}=\left(\frac{n_\infty}{n_c}-1\right)\frac{1-\frac{n_\infty}{n}+d^2+jd\,\frac{n_\infty}{n}}{\left(1-\frac{n_\infty}{n}\right)^2+d^2} \tag{13}$$

As in the high-pass case, we may neglect $d^2$ with the understanding that the resulting expressions will not be accurate in the neighborhood of the peak attenuation frequency. Hence:

$$\frac{z_s}{z_p}=\frac{\frac{n}{n_\infty}-\frac{n}{n_c}}{1-\frac{n}{n_\infty}}\left(1-jd\,\frac{1}{1-\frac{n}{n_\infty}}\right) \tag{14}$$

The dual low-pass form, for $\pi$ connection, yields the same value for $Z_s/Z_p$.

### 4.3. Symmetrical Band-Pass

The impedance of a series resonant arm,

$$Z=R+j\omega L+\frac{1}{j\omega c}$$

may conveniently be written

$$Z=r(d+jW) \tag{15}$$

where

$$\left.\begin{aligned} r&=\sqrt{\frac{L}{C}}\\ d&=R\sqrt{\frac{C}{L}}\\ W&=\frac{\omega}{\omega_0}-\frac{\omega_0}{\omega}\\ \omega_0&=\frac{1}{\sqrt{LC}}\end{aligned}\right\} \tag{16}$$

Using this expression for the series combinations of the band-pass structure (fig. 5), its arms ratio takes the form:

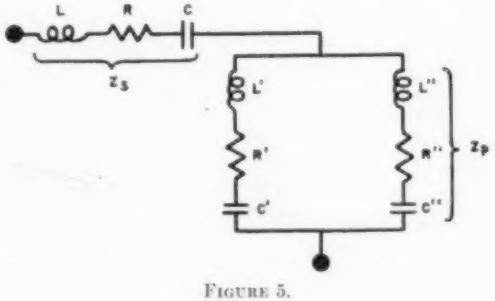


FIGURE 5.

$$\frac{Z_s}{Z_p}=r(d+jW)\left[\frac{1}{r'(d'+jW')}+\frac{1}{r''(d''+jW'')}\right] \quad (17)$$

Design requirements inherent to the band-pass filter impose a definite relationship upon the coefficients. This is best understood by examing the behavior of the function $Z_s/Z_p$ with frequency in the nondissipative case.

In the dissipation-less case,

$$\frac{Z_s}{Z_p}=0 \text{ when } W=0, \text{ at } \omega=\omega_0=\frac{1}{\sqrt{LC}}$$

and

$$\frac{Z_s}{Z_p}=\infty \text{ when } W' \text{ or } W''=0, \text{ at } \omega_\infty'=\frac{1}{\sqrt{L'C'}} \text{ or } \omega_\infty''=\frac{1}{\sqrt{L''C''}}, \text{ respectively.}$$

In general, the band-pass structure yields two pass-bands. To make these contiguous, we must meet the "condition of congruence" [8] that $rW$ and $1/r'W'+1/r''W''$ vanish at a common frequency. Since $W=0$ at $\omega=\omega_0$ we need

$$\frac{1}{r'\left(\frac{\omega_0}{\omega_\infty'}-\frac{\omega_\infty'}{\omega_0}\right)}+\frac{1}{r''\left(\frac{\omega_0}{\omega_\infty''}-\frac{\omega_\infty''}{\omega_0}\right)}=0. \quad (18)$$

If the filter is to have a symmetrical pass characteristic (on a logarithmic frequency scale),

$$\frac{\omega_0}{\omega_\infty'}=\frac{\omega_\infty''}{\omega_0}, \quad (19)$$

leading directly to

$$r'=r''. \quad (20)$$

If we add the condition that each series resonant arm has the same dissipation factor $d$, (17) simplifies to

$$\frac{z_s}{z_p}=\frac{r}{r'}(d+jW)\left[\frac{1}{d+jW'}+\frac{1}{d+jW''}\right]. \quad (21)$$

As before, the denominator is to be rationalized and $d^2$ neglected, yielding

$$\frac{z_s}{z_p}=\frac{r}{r'}\frac{W(W'+W'')}{W'W''}\left\{1+jd\left[\frac{W'^2+W''^2}{W'W''(W'+W'')}-\frac{1}{W}\right]\right\}. \quad (22)$$

We now define the frequency number for the symmetrical band-pass case as

$$n=\left(\frac{\omega}{\omega_0}-\frac{\omega_0}{\omega}\right)^2=W^2 \quad (23)$$

for a generic value of frequency; hence the value:

$$n_\infty=\left(\frac{\omega_\infty'}{\omega_0}-\frac{\omega_0}{\omega_\infty'}\right)^2=\left(\frac{\omega_\infty''}{\omega_0}-\frac{\omega_0}{\omega_\infty''}\right) \quad (24)$$

for either frequency of peak attenuation, by (19), and the value:

$$n_c=\left(\frac{\omega_c'}{\omega_0}-\frac{\omega_0}{\omega_c'}\right)^2=\left(\frac{\omega_c''}{\omega_0}-\frac{\omega_0}{\omega_c''}\right)^2 \quad (25)$$

for either cut-off frequency (again because of symmetry).

Equation 22 may now be rewritten in terms of the above values of $n$ in place of $W$, $W'$, $W''$. By using the identities:

$$\left.\begin{aligned} &W=\sqrt{n}\\ &W'+W''=\sqrt{n}\sqrt{n_\infty+4}\\ &W'W''=n-n_\infty\\ &W'^2+W''^2=nn_\infty+2(n+n_\infty)\end{aligned}\right\} \quad (26)$$

we find:

$$\frac{Z_s}{Z_p}=\frac{r}{r'}\frac{n\sqrt{n_\infty+4}}{n-n_\infty}\left\{1+j\frac{d}{\sqrt{n}}\left[\frac{nn_\infty+2(n+n_\infty)}{(n-n_\infty)\sqrt{n_\infty+4}}-1\right]\right\} \quad (27)$$

We have not yet imposed the condition that $Z_s/Z_p$ must equal $-1$ (for $d=0$) at the cut-off frequencies, corresponding to $n=n_c$. There is no ambiguity on this point, because the other possible value that $Z_s/Z_p$ might take at the cut-off frequencies, which is zero, actually occurs at the midband frequency, $\omega_0$, the cut-off frequency common to two pass-bands, which merge into one by virtue of the "congruence" condition.

The cut-off relation is

$$-1=\frac{r}{r'}\frac{n_c\sqrt{n_\infty+4}}{n_c-n_\infty}, \quad (28)$$

and the arms ratio becomes:

$$\frac{Z_s}{Z_p}=\frac{\frac{n}{n_\infty}-\frac{n}{n_c}}{1-\frac{n}{n_\infty}}\left\{1+\frac{jd}{\sqrt{n}}\left[\frac{nn_\infty+2(n+n_\infty)}{(n-n_\infty)\sqrt{n_\infty+4}}-1\right]\right\} \quad (29)$$

## 5. Determination of the Section Numbers and of the Cut-Off Frequency

The real part of the ratio $Z_s/Z_p$ is independent of $d$ and is given by the same expression for all three cases (8), (14), (29):

$$Re\left(\frac{Z_s}{Z_p}\right)=\left(\frac{Z_s}{Z_p}\right)_{d=0}=\frac{X_s}{X_p}=\frac{\frac{n}{n_\infty}-\frac{n}{n_c}}{1-\frac{n}{n_\infty}}, \quad (30)$$

where $n$ is the "frequency number" appropriate to each case in turn.

We may now substitute this value in eq 2 and thereby obtain expressions suitable for the construction of universal sets of curves of attenuation and phase shift, valid for all the filter sections shown in figure 1. To avoid imaginary arguments, three distinct cases (corresponding to the three ranges of fig. 2) will be considered:

(1):

$$\alpha=0, \beta\neq 0, 0>\frac{X_s}{X_p}>-1, \qquad n<n_c<n_\infty$$

(transmitted frequency range)

$$\beta=2\sin^{-1}\sqrt{-\frac{X_s}{X_p}}=2\sin^{-1}\sqrt{\frac{\frac{n_c}{n_\infty}-1}{\frac{n_c}{n}-\frac{n_c}{n_\infty}}}. \quad (31)$$

(2):

$$\alpha\neq 0, \beta=0, \frac{X_s}{X_p}<0, n_c<n_\infty<n\rightarrow$$

$$\alpha=2\sinh^{-1}\sqrt{\frac{X_s}{X_p}}=2\sinh^{-1}\sqrt{\frac{1-\frac{n_c}{n_\infty}}{\frac{n_c}{n}-\frac{n_c}{n_\infty}}}. \quad (32)$$

(3):

$$\alpha\neq 0, \beta=\pm\pi\frac{X_s}{X_p}<-1, n_c<n<n_\infty$$

$$\alpha=2\cosh^{-1}\sqrt{\frac{X_s}{X_p}}=2\cosh^{-1}\sqrt{\frac{1-\frac{n_c}{n_\infty}}{\frac{n_c}{n}-\frac{n_c}{n_\infty}}}. \quad (33)$$

Note that in all cases $n_\infty>n_c$. The value of $\alpha$ or $\beta$ is seen to depend on two ratios, $n_c/n$ and $n_c/n_\infty$. For a given ratio $n_c/n_\infty$, $\alpha$ or $\beta$ may be plotted against $n_c/n$. These plots may be used to *select* values of the ratio $n_c/n_\infty$, which we will call the *section number* and designate by $N$:

$$N=\frac{n_c}{n_\infty}. \quad (34)$$

If more than one section is used in a filter, a different value of $N$ will generally be used for each section. As a rule there will be one section having $N=0$ (the "prototype" of the literature) and one section having $0.6<N<0.7$: the latter is usually divided into two half sections which serve as *terminations* for the filter.

Another purpose of the attenuation plots (fig. 6) is the determination of the *cut-off frequency* (or frequencies). This is generally treated as a known requirement of the filter, but actually it is not. What is required of a filter may be summarized in figure 7, which is drawn for the high-pass case. Two frequencies and two values of attenuation are assigned: the *pass band* is assigned by a "boundary" value of frequency, $f_a$, and a value of *permissible attenuation*, $a$; the attenuation band, by a boundary frequency $f_b$ and a *required attenuation*, $A$. The theoretical cut-off frequency generally lies somewhere between the two boundaries. To determine its exact location, the section number for the entire filter must be tentatively established. Suppose for example a three-section high-pass filter were to be based on the requirements of figure 7. Let us tentatively make:

$N=0$ for section 1

$N=0.5$ for section 2

$N=0.7$ for section 3

Adding the attenuations plotted on figure 6 for the above values of $N$ over a range of values of $n_c/n$, we find that the over-all attenuation goes through the value 55 *db* (the value of $A_1$ required attenuation) when $n_c/n$ has the value 0.74. We may

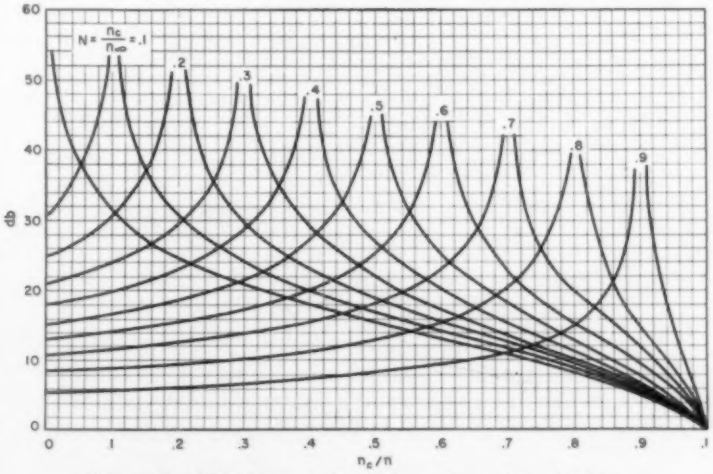


FIGURE 6. *Plot of $\alpha$ against $n_c/n$ for various values of $n_c/n_\infty$.*

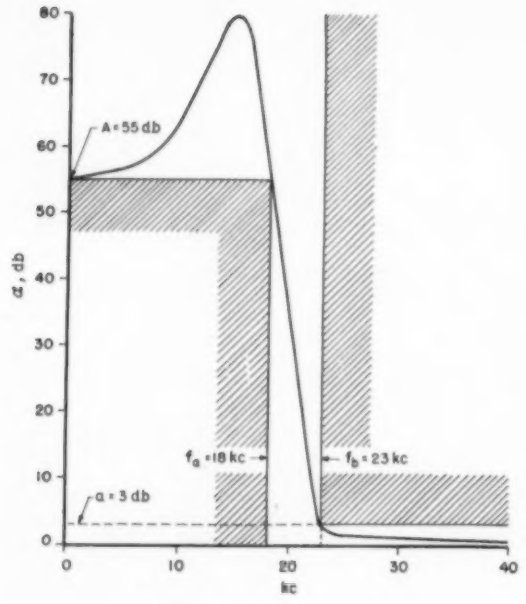


FIGURE 7.

therefore impose the condition $n=n_a$ for $n_c/n=0.74$, thus causing the attenuation to be exactly equal to $A$ at the "boundary frequency" $f_a$ (fig. 7). Hence we write:

$$\frac{n_c}{n_a}=0.74, \tag{36}$$

from which recalling the equivalence $n=1/\omega^2$ for high-pass filters:

$$f_c=f_a\frac{1}{\sqrt{0.74}}=20.9\,kc;\ n_c=\frac{1}{(2\pi f_c)^2}=5.8\times10^{-6} \tag{37}$$

The selection of the section number may be based on several criteria. If the problem is given in the terms of figure 7, the designer will attempt to secure the necessary minimum attenuation $A$ (in the example 55 *db*) with the least number of sections. Charts that permit the automatic selection of the optimum section number, and give at the same time the value $n_c/n_a$, for filters of three sections or less, have been published by the writer [7] on the basis of this criterion.

Another possible consideration affecting the selection of the section number is the phase-shift over the transmitted band. It may be desirable to have the phase shift vary as linearly as possible with the frequency, to eliminate phase distortion. Generally speaking, a certain amount of "cut and try" is unavoidable when designing a filter by the conventional method. The labor involved may be minimized, however, by a favorable choice of parameters, which justifies the present treatment.

## 6. Determination of the Maximum Permissible Dissipation Factor

Given the values of $N=n_c/n_\infty$ for the different sections, we may now determine for each value of $n$ (that is, for each frequency), $Z_s/Z_p$ in the *dissipative* case ($d\neq0$) using one of the three equations (8), (14) and (29) (fig. 10 may conveniently be used in place of eq. 29). From the values of $Z_s/Z_p$, using eq 2 or an appropriate chart (fig. 8), the true values of $\alpha$ and $\beta$, may be obtained.

It is not necessary, as a rule, to obtain these values for more than one or two values of frequency. A check on the attenuation at the edge of the transmitted band (frequency $f_b$, fig. 7) is usually sufficient, since this is the critical value: the attenuation due to losses is always less toward the center of the passband (in the case of figure 7, toward infinite frequency) than at the edges.

As an illustration, let us determine the maximum

TABLE 1. *Sample computation of dissipation factor*

$$\left.\begin{aligned}&\text{High-pass filter (fig. 7): } n_b/n_a=(f_a/f_b)^2=0.612\\ &n_c/n_a=0.74\ \text{(eq 36)}\\ &n_b/n_c=n_b/n_a\cdot n_a/n_c=\frac{0.612}{0.74}=0.828\end{aligned}\right\} \tag{38}$$

| | Section 1 | Section 2 | Section 3 | Over-all |
|---|---|---|---|---|
| Section number $N=n_c/n_\infty-2$ | 0 | 0.5 | 0.7 | |
| Ratio $n_b/n_\infty=\frac{n_c}{n_\infty}\cdot\frac{n_b}{n_c}=0.828N$ | 0 | 0.414 | 0.58 | |
| Real part of $\frac{Z_s}{Z_p}$ for $n=n_b$: $U=\frac{n_b/n_\infty-n_b/n_c}{1-n_b/n_\infty}$ (eq 8) | −0.828 | −0.705 | −0.59 | |
| Assuming $d=0.01$ | | | | |
| Imaginary part of $\frac{Z_s}{Z_p}$ for $n=n_b$: $V=-d\frac{U}{1-n_b/n_\infty}$ (eq 8) | 0.00828 | 0.012 | 0.01405 | |
| Attenuation $\alpha$, db: (from chart, fig. 8) | 0.2 | 0.25 | 0.25 | 0.7 |
| Phase shift $\beta$, degrees (from chart, fig. 8) | 131 | 114 | 96 | 341 |
| Assuming $d=0.02$ | | | | |
| $V$ | 0.01656 | 0.024 | 0.0281 | |
| $\alpha$ | 0.32 | 0.46 | 0.48 | 1.26 |
| $\beta$ | 131 | 114 | 95.5 | 340.5 |
| Assuming $d=0.05$ | | | | |
| $V$ | 0.0414 | 0.06 | 0.0702 | |
| $\alpha$ | 0.96 | 1.15 | 1.20 | 3.31 |
| $\beta$ | 130 | 113.5 | 95 | 339.5 |

The over-all attenuation values thus obtained for several values of $d$ may now be plotted to find, by interpolation, the value of $d$ consistent with the maximum required attenuation at $f_b$ (3 db). This is carried out in figure 9, giving as a result $d=0.046$ as the maximum allowable dissipation factor, corresponding to a "$Q$" of about 22.

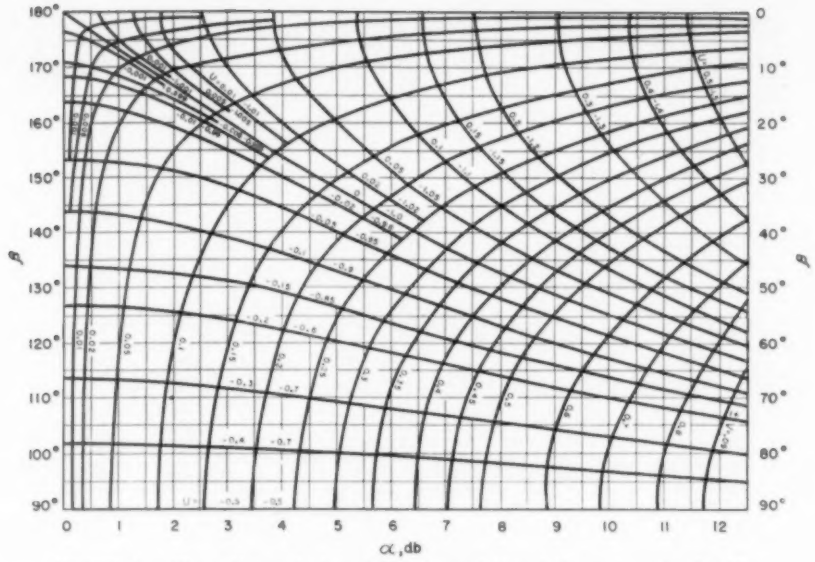


FIGURE 8. *Attenuation and phaseshift in term of U and V, components of* $Z_s/Z_p$.
NOTE.—For $U>-0.5$, $0<\beta<90°$; for $U<0.5$, $90°<\beta<180°$.

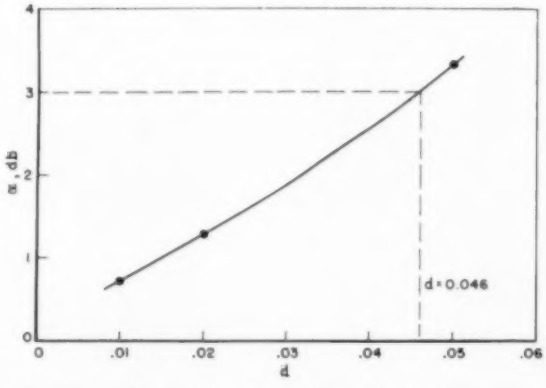


FIGURE 9. *Interpolation for maximum dissipation factor.*

allowable dissipation (minimum $Q$) for the filter of figure 7, using the values of $N$ already selected.

Equation 8 is used to find $Z_s/Z_p$ (hence $\alpha$ and $\beta$) for each of the three sections of the filter, at the boundary frequency $f_b$ (fig. 7) and assuming for $d$ (dissipation factor) a series of arbitrary values. Then by interpolation (fig. 9) one may arrive at a value of $d$ just low enough to secure the desired maximum attenuation $\alpha$ (fig. 7) at $f_b$. The transition from $Z_s/Z_p$, as computed from eq 8, to $\alpha$ and $\beta$, is best accomplished by means of charts, such as that of figure 8. In this chart, as in table 1, the notation $Z_s/Z_p=U+jV$ is used. The computation may be conveniently carried out in tabular form, as shown in table 1.

## Midseries and Midshunt Impedances

Having determined the frequency numbers $n_c$ (for the filter) and $n_m$ (for each filter section) as well as the maximum allowable dissipation factor, the designer still has the problem of "image matching" the filter sections to each other and to the terminations between which the filter is to be inserted. We must, therefore, reexamine the basic filter structures of figure 1 from the standpoint of their image impedances.

In this discussion the $L$ structure, or half-section, has been taken as the basic constituent of the filter. Such a structure has two distinct image impedances: that is, those impedance values which, connected to the input and output of the $L$ network, match, or simulate over the entire frequency range, the input and output impedances of the network, respectively (fig. 11). In filter terminology, the image impedance on the side of the series arm (to the left of fig. 11) is called "mid-series impedance", $Z_{0s}$; the other image impedance is the "mid-shunt impedance", $Z_{0p}$. The essential difference between the two types of $L$ structures shown in figure 1 under the headings "for connection in $T$" and "for connection in $\pi$", is this: In the first type, the *midseries* impedance is independent of the resonant frequency of the $L$-$C$ arm, so that, if such $L$ structures are connected together into $T$ sections, these can be designed to match one another at all frequencies in spite of having different peak attenuation frequencies.

On the other hand, the second type of $L$ structure has midshunt impedance independent of the $L$-$C$ arm resonance, and must therefore be paired off into $\pi$ sections before assembling into a matching filter.

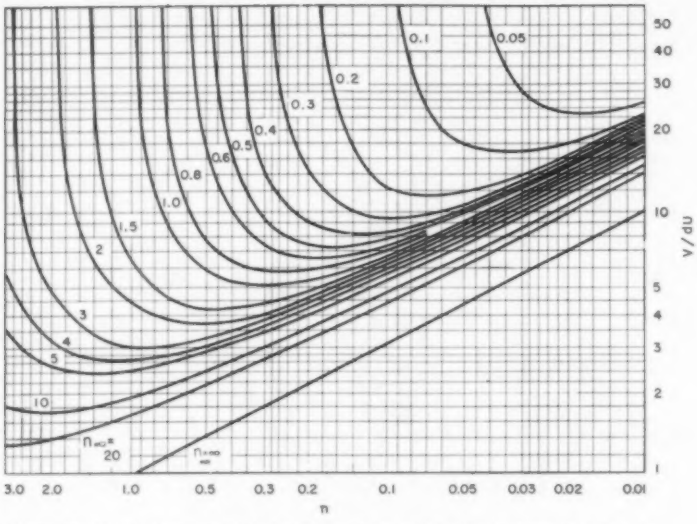


FIGURE 10. *Values of V (imaginary part of $Z_s/Z_p$) in term of n and $n_\infty$.*
To obtain $V$ multiply ordinates by $d$ (dissipation factor) and by $U$ (real part of $Z_s/Z_p$). See eq 45.

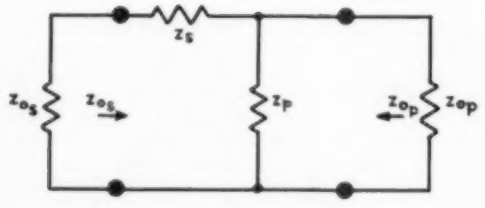


FIGURE 11.

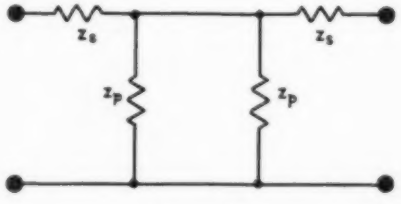


FIGURE 12.

To avoid confusion, let us limit our discussion to the first, or T-connected, type of $L$ structure. The midseries impedance of these will now be obtained, for the nondissipative case.

The midseries impedance is the characteristic impedance of the $T$ (fig. 12). Accordingly, if $Z_{0c}$ and $Z_{sc}$ are the open and shortcircuited impedances of the $T$, respectively, we have for the mid-series impedance:

$$Z_{0s}=\sqrt{Z_{0c}Z_{sc}}$$

$$=\sqrt{\left(Z_s+\frac{Z_p}{2}\right)\left(Z_s+\frac{1}{2}\frac{Z_sZ_p}{Z_s+\frac{Z_p}{2}}\right)}$$

$$=Z_s\sqrt{1+\frac{Z_p}{Z_s}} \tag{39}$$

We have already obtained an expression for the arms ratio in the nondissipative case, for all three classes of filters:

$$\frac{Z_s}{Z_p}=\frac{\frac{n}{n_\infty}-\frac{n}{n_c}}{1-\frac{n}{n_\infty}}. \tag{30}$$

We may now substitute this expression into 39, obtaining:

$$Z_{0s}=Z_s\sqrt{\frac{\frac{n_c}{n}-1}{\frac{n_c}{n_\infty}-1}}. \tag{40}$$

We must now differentiate between high-, low- and band-pass filters. For the basic *high-pass* structure, we have (fig. 3 and eq 4):

$$Z_s=-\frac{j}{\omega C}=-j\frac{\sqrt{n}}{C}, \tag{41}$$

and also (eq 6)

$$\frac{n_c}{n_\infty}-1=-\frac{n_c}{CL'}, \tag{42}$$

hence combining

$$Z_{0s}=-j\sqrt{\frac{L'}{C}}\cdot\sqrt{\frac{n}{n_c}-1}. \tag{43}$$

Let us now define:

$$(\textit{high-pass}) \qquad R_0=\sqrt{\frac{L'}{C}}, \tag{44}$$

and write the mid-series impedance in the form:

$$Z_{0s}=-jR_0\sqrt{\frac{n}{n_c}-1}. \tag{45}$$

A plot of $Z_{0s}$ against the frequency number $n$ is shown diagrammatically in figure 13. For $n<n_c$ (transmitted band) the radical must be assigned the positive imaginary value to fit the physical facts: then the midseries impedance is a positive real, with maximum value $R_0$ for $n=0$, which corresponds in all cases to the zero phase-shift or "midband" frequency. Hence $R_0=\sqrt{L'/C}$ is the *midband impedance*.

It will be noted that $Z_{0s}$ does not depend upon $n_\infty$, hence is not affected by the peak attenuation frequency. High-pass sections differing in the location of the attenuation peak may therefore be image "matched" to one another within the same filter, provided they share the same values of $n_c$ (cut-off frequency number) and $R_0$. The above plot applies to all three classes of filters except for the sign of the imaginary part; eq 45 also applies, except that $R_0$ has different values in terms of the circuit elements. For *low-pass filters* (see fig. 4 and eq 40):

$$Z_{0s}=j\omega L\sqrt{\frac{\frac{n_c}{n}-1}{\frac{n_c}{n_\infty}-1}}, \tag{46}$$

which can be written

$$Z_{0s}=j\sqrt{\frac{L}{C'}}\sqrt{\frac{n}{n_c}-1}, \tag{47}$$

which, if we let

$$\sqrt{\frac{L}{C'}}=R_0 \tag{48}$$

becomes

$$Z_{0s}=jR_0\sqrt{\frac{n}{n_c}-1}. \tag{49}$$

In this case also the midseries impedance becomes a positive real in the range $n<n_c$, provided we assign a negative imaginary value to the radical. Outside this frequency range the impedance is a positive reactance, whose dependence on $n$ is the same as in the case of high-pass filters, except for sign (fig. 13).

Finally, for *symmetrical band-pase filters* (fig. 5, eq 40)

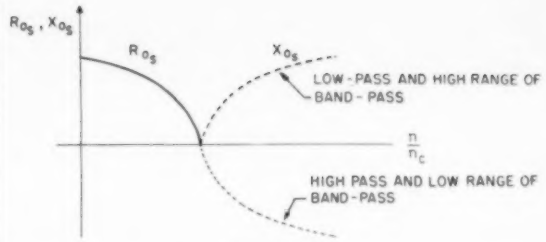


FIGURE 13.

$$Z_{0s}=\pm jr\sqrt{n}\sqrt{\frac{n_c/n-1}{n_c/n_\infty-1}}$$
$$=\pm jr\frac{\sqrt{n/n_c-1}}{\sqrt{1/n_c-1/n_\infty}}. \tag{50}$$

The midseries impedance will have the same form as in the high-pass and low-pass cases, provided

$$r=R_0\sqrt{\frac{1}{n_c}-\frac{1}{n_\infty}}, \tag{51}$$

in which case:

$$Z_{0s}=\pm jR_0\sqrt{\frac{n}{n_c}-1}.$$

$R_0$, as before, is the *midband impedance*. The midseries impedance follows the plot of figure 13 for $n>n_c$; the sign of $\sqrt{n}$ in eq 49 is positive if the frequency is above the transmitted band ($Z_{0s}$ inductive), and negative if below.

In conclusion, we have found that in all three cases (high, low, and band-pass) the midseries impedance is the same function of the frequency number; in each case it is, therefore, invariant throughout the filter, whatever the location of the attenuation peaks in the individual sections. This permits the filter to be image-connected throughout; which is the assumption upon which the entire "conventional" filter theory is predicated. Of course, this is only true provided $R_0$, the midband impedance, and $n_c$, the cut-off frequency number, are constant throughout the filter. This is ensured by determining these two parameters first and selecting element values so that eq 44, 48 and 51, for high, low and band-pass filters, respectively, are satisfied.

We have discussed the determination of $n_c$ but not that of $R_0$. This is based on the terminating impedance of the filter. Always assuming that the "$T$-connected" type of structure is used, and therefore, that the midseries impedance is invariant from section to section, we could put together the filter (a three-section filter, for example) as indicated in figure 14. Each $L$ half-section is shown separate: in practice, adjoining arms are "lumped" together.

This arrangement would offer to the outside terminations the same impedance (the midseries impedance) that recurs at each internal junction. If the terminations are equal resistances, which we

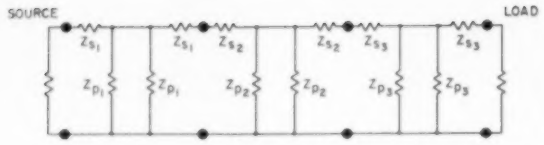


FIGURE 14.

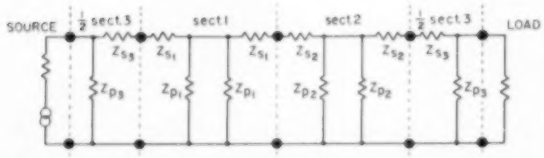


FIGURE 15.

assume to be the case, considerable "mismatching" would result, as indicated by the plot of figure 13; the midseries impedance plot is actually an arc of circle within the transmitted range when frequency, rather than $n$, is taken as the abscissa.

## 8. Terminating Half-sections

A significant improvement may result if we connect the filter as shown in figure 15. One of the sections, suitably selected, is "split" into its component half-sections and these are used to "terminate" the filter. The filter now presents to its terminations (source and load) not the midseries, but the *midshunt* impedance of the terminating section.

The frequency dependence of the *midshunt* impedance must now be examined. This will show how the terminating section should be selected and how the parameter $R_0$, equal to the midband value of both the midshunt and the midseries impedances, should be assigned with reference to the outside terminations.

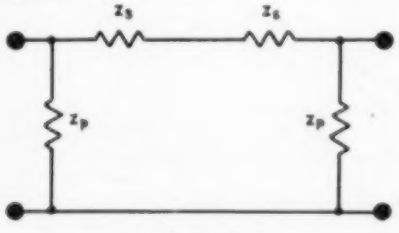


FIGURE 16.

The midshunt impedance $Z_{0p}$ is the characteristic impedance of the $\pi$ section of figure 16. We have, therefore:

$$Z_{0p}=\sqrt{Z_{0c}Z_{sc}}$$

$$=\frac{Z_p}{\sqrt{1+\frac{Z_p}{Z_s}}}=\frac{Z_pZ_s}{Z_{0s}}=\frac{Z_p}{Z_s}\left(\frac{Z_s}{Z_{0s}}\right)^2Z_{0s} \qquad (52)$$

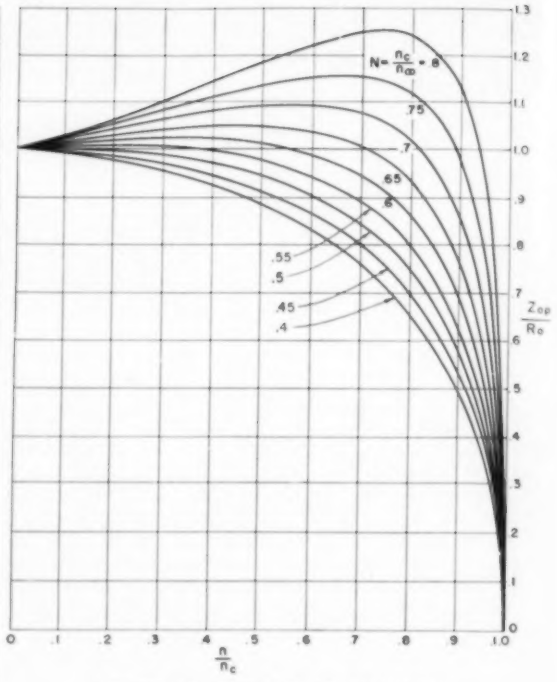


FIGURE 17. *Plots of $Z_{0p}/R_0$ against $n/n_c$.*

Using eq 30, 45, and 52, we may write:

$$Z_{0p}=\pm jR_0\frac{1-\frac{n}{n_\infty}}{\sqrt{\frac{n}{n_c}-1}}. \qquad (53)$$

The midshunt impedance, like the midseries, is real in the transmission range ($n<n_c$) and takes the value $R_0$ at midband ($n=0$). Its frequency-dependence, however, may vary from section to section according to the value of $n_\infty$. Plots of $Z_{0p}$ against $n/n_c$ in the transmitted band are given in figure 17. These show that for $N=n_c/n_\infty=0.7$, or thereabouts, $Z_{0p}$ is substantially constant over a large part of the transmitted band. This is the value of $N$ that should be used in designing the terminating section.

## 9. Determination of $R_0$

The use of properly designed terminating sections reduces, but does not eliminate, reflection losses due to mismatching at the terminations [1, p. 352ff]. These losses can be evaluated, but if the designer merely has to meet some such requirement as that shown in figure 7, this is not necessary. If the filter is designed to match its terminations exactly at $f=f_b$, at this frequency there will be no added loss due to mismatching. Above and below this frequency there may be some added loss, but attenua-

tion falls off toward midband more rapidly than would be required to offset the increasing reflection loss.

The high-pass filter previously chosen as example, and based upon the requirements of figure 7, includes a section for which $N=0.7$ (section 3). Choosing this as the terminating section, we go to the plots of figure 17. The abscissa corresponding to $f=f_b$ is (eq 38, table 1):

$$\frac{n_b}{n_c}=0.828.$$

Hence, in order to avoid mismatching, we must have, if $R_T$ is the terminating resistance:

$$Z_{0s}=R_T,$$

at the point where the curve for $N=0.7$ crosses the abscissa $n/n_c=0.828$.

But at this point:

$$\frac{Z_{0s}}{R_0}=0.985,$$

hence, we must make:

$$R_0=\frac{R_T}{0.985}=1.015\,R_T.$$

The difference between the optimum value of $R_0$ and that of $R_T$ is generally small, so that $R_0$ is often taken equal to $R_T$. But this simplification is not always permissible if accuracy is desired.

## 10. Computation of Filter Elements

From the design parameters $n_c$ and $R_0$, common to all the sections of a filter, and $N=n_c/n_\infty$, varying from section to section, plus, in the case of symmetrical band-pass filters, the midband angular frequency $\omega_0$, all the filter element values may be obtained by straightforward computation. Table 2 gives the expressions for all element values of the three "basic" structures of the "$T$-connected" type, in terms of the parameters used throughout this discussion, and with reference to equations appearing elsewhere in the discussion. Because of the dual relationship between "$T$-connected" "$\pi$-connected" filters, it is easy to obtain the equivalent $\pi$-connected expressions: as always in a dual circuit relationship, capacitance is replaced by inductance, resistance by conductance, series by parallel, and vice-versa [1, p. 246ff].

The so-called "prototype" sections are considered here as limiting cases of the "basic" section, for $N=0$. In high- and low-pass sections, the element values are obtained in this limiting case by simply making $N=0$ in the expressions for the basic section. One of the elements drops out, as indicated by the fact that the capacitor $C''$ in the high-pass section becomes infinite and the inductor $L'$ in the low-pass section goes to zero. In the band-pass case, it is not convenient to let $N$ go to zero, as indeterminate expressions will result. Separate expressions for the prototype elements, which can be obtained quite simply by going back to basic considerations, are given.

Finally, it should be noted that the series arms of adjoining sections are combined into a single arm of the assembled filter. Thus, the series inductances add in the low-pass case and the series capacitances go together according to the usual rules in the high-pass case. In band-pass filters, it is convenient to add together values of $r=\sqrt{L/C}$ for adjoining sections. This will give the value of $r$ for the "combined" series arm. As for the resonant frequency, this is the same for all series arms, hence also for their combinations.

## 11. Conclusion

*Comparison with conventional method.* The principal difference between the method outlined here and the "classical" method lies in the choice of the design parameters for the simply derived filter section. In the classical method these are: $f_c$, cut-off frequency, and $m$ derivation factor. In the modified method they are: $n_c$, value of the frequency number at cut-off, and $n_\infty$, value of the frequency number at the frequency of peak attenuation. Why is this an advantage? Because the frequency number is that particular variable that permits the use of a single function, or a single family of curves, to express the attenuation and phase-shift characteristics of all filter sections (low, high, and band-pass) over the frequency spectrum. With the aid of these universal curves or the corresponding functions it is simple to relate the design parameters, as used in the present method, with performance. If any other set of parameters is used, an intermediate step is required.

When using the classical method the designer is required to choose values of $f_c$ and $m$ based upon his general knowledge of filter characteristics. When the problem is an academic one $f_c$ is usually given, but this is not the case in practice, the requirements of the filter being summarized in some form similar to figure 7. After $f_c$ and $m$ have been selected, formulas are given for obtaining $f_\infty$, the peak attenuation frequency; on the basis of this and $f_c$ the filter performance can be checked, to see whether or not the choice of $f_c$ and $m$ was correct in the first place. With the present method the choice of parameters and the verification of performance are one and the same. The parameters are selected by means of the universal charts, which show attenuation and phase-shift at the various frequencies.

An additional improvement made possible by the present method is the computation of "minimum $Q$." The new parameters greatly simplify the analysis of dissipative filter sections. Formulas given in classical texts for the dissipative value of $Z_s/Z_p$ in the band-pass case, for example, are much more complicated than eq 29 and do not permit the drawing of a single family of curves as in figure 10.

TABLE 2. *Computation of element values*

### High-pass

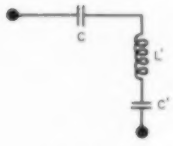


GIVEN:

$$R_0,\ n_c,\ N=\frac{n_c}{n_\infty}$$

From eq 7, 11, 60:

$$C=\frac{1}{R_0}\sqrt{\frac{n_c}{1-N}}$$

$$L'=CR_0^2=R_0\sqrt{\frac{n_c}{1-N}}$$

$$C'=\frac{n_c}{NL'}=\frac{\sqrt{n_c(1-N)}}{NR_0}$$

"*T*" SECTION:

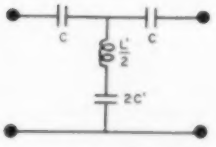


### Low-pass

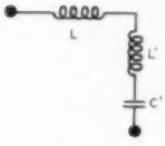


GIVEN:

$$R_0,\ n_c,\ N=\frac{n_c}{n_\infty}$$

From eq 15, 17, 64:

$$L=R_0\sqrt{\frac{1-N}{n_c}}$$

$$C'=\frac{L}{R_0^2}=\frac{1}{R_0}\sqrt{\frac{1-N}{n_c}}$$

$$L'=\frac{N}{C'n_c}=\frac{R_0N}{\sqrt{n_c(1-N)}}$$

"*T*" SECTION:

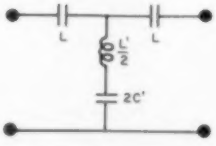


### Symmetrical band-pass

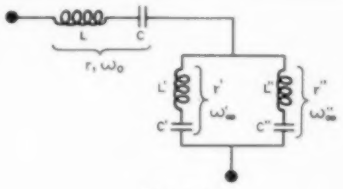


GIVEN:

$$R_0,\ n_c,\ N=\frac{n_c}{n_\infty},\ \omega_0=\frac{1}{\sqrt{LC}}$$

SERIES ARM: from eq 67:

$$r=\sqrt{\frac{L}{C}}R_0\sqrt{\frac{1-N}{n_c}}$$

$$\omega_0=\frac{1}{\sqrt{LC}}=\text{midband ang. freq. (given)}$$

Compute

$$L=\frac{\Sigma r}{\omega_0},\ C=\frac{1}{\Sigma r\omega'}$$

after adding $r$ values of adjoining arms

SHUNT ARM: from eq 44:

$$r'=r''=r\frac{n_c\sqrt{n_\infty+4}}{n_\infty-n_c}=R_0\sqrt{N\frac{1+4N/n_c}{1-N}}$$

from eq 37:

$$\omega'_\infty=\frac{1}{2}\omega_0\sqrt{\frac{n_c}{N}}\left\{\sqrt{1+4\frac{N}{n_c}}-1\right\}$$

$$\omega''_\infty=\frac{1}{2}\omega_0\sqrt{\frac{n_c}{N}}\left\{\sqrt{1+4\frac{N}{n_c}}+1\right\}$$

hence:

$$L'=\frac{r'}{\omega'_\infty}\qquad C'=\frac{1}{r'\omega'_\infty}$$

$$L''=\frac{r''}{\omega''_\infty}\qquad C''=\frac{1}{r''\omega''_\infty}$$

"*T*" SECTION:

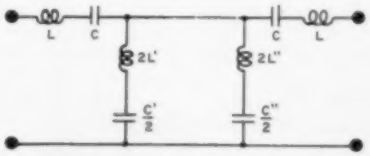


### "PROTOTYPE" BAND-PASS ($N=0$)

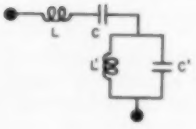


$$r=\sqrt{\frac{L}{C}}=\frac{R_0}{\sqrt{n_c}}$$

$$\omega_0=\frac{1}{\sqrt{LC}}\ \text{(given)}$$

$$L'=\frac{R_0\sqrt{n_c}}{\omega_0}$$

$$C'=\frac{1}{R_0\omega_0\sqrt{n_c}}$$

## 12. References


[1] E. A. Guillemin, Communication networks, Vol. **II**, p. 378ff (John Wiley & Sons, Inc., New York, N. Y., 1948).

[2] O. J. Zobel, Theory and design of uniform and composite electric wave filters, Bell System Tech. J. (Jan. 1923).

[3] W. Cauer, New theory and design of wave filters, Phys. (April 1932).

[4] H. W. Bode, A general theory of electric wave filters, J. Math. & Phys. (Nov. 1934).

[5] P. J. Selgin, Electrical transmission in steady state, p. 47ff (McGraw-Hill Book Co., Inc., New York, N. Y., 1946).

[6] T. E. Shea, Transmission networks and wave filters (D. Van Nostrand & Co., Inc., New York, N. Y., 1948).

[7] P. J. Selgin, Multi-section filter design procedure, Communications (July 1945).


WASHINGTON, February 7, 1950.

Journal of Research of the National Bureau of Standards Vol. 47, No. 6, December 1951 Research Paper 2277

# On the Derivation and Accuracy of Certain Formulas for Sample Sizes and Operating Characteristics of Nonsequential Sampling Procedures[1]

Uttam Chand[2]

Formulas are given that are needed for the computation of number of observations and operating characteristics of single sample acceptance sampling procedures based on tests of statistical hypotheses. Some of the same results may be obtained by reference to existing tables and curves located in widely scattered places. The hypotheses considered concern the means and standard deviations of certain populations (that is, binomial, Poisson, normal) where the test is made against a one-sided alternative. The comparison of two means or two variances as well as the test of a single mean or variance is discussed. The accuracy of the formulas is considered, and where approximations are involved, the results are compared with existing tables.

This paper develops and considers the question of the accuracy of certain formulas needed for the number of observations and operating characteristics of single-sample acceptance-sampling procedures based on statistical tests of hypotheses. For purposes of completeness the paper also contains formulas that are already known.

## 1. Introduction

It is now common knowledge among users of modern statistical tools that the characteristics of a sampling plan must be specified in terms of the risks of rejecting good material (Type I error: producer's risk) and accepting poor material (Type II error: consumer's risk). The problem of determining a sample size for a given probability of Type I error, which will minimize the probability of Type II error, has been considered by several authors, in particular [1 to 4].[3] This problem belongs to the category of that broad class of problems in the field of planned experimentation in which one is asked to provide adequate replication to detect treatment differences with desired amount of protection against taking wrong decisions. If for a certain sample size it is impossible to reduce simultaneously to small proportions the risks of two kinds it will be helpful to know this in advance.

Answers to most of the questions raised in this paper can be obtained from the existing published tables and curves. The effectiveness of these formulas in relation to assumptions and approximations that have been made in their derivation also has a theoretical interest. We shall restrict ourselves to the consideration of certain parametric hypotheses concerning means and standard deviations of certain populations, mainly against one-sided alternatives.

## 2. Preliminaries and Notation

In the ensuing sections $H_1$ denotes the null hypothesis, $H_2$ any one of a set of alternative hypotheses, $\alpha$ the probability of rejecting the null hypothesis $H_1$ when true, and $\beta$ the probability of accepting $H_1$ when some alternative hypothesis, $H_2$, is true. In connection with the hypotheses concerning the means of certain populations in which the standard deviations are functionally related to the means and consequently unspecified, the reader will at once recognize that the acceptance-rejection criterion $A$ used for a statistic $T$ is not the best in the sense of the likelihood ratio test [5]. This difficulty, however, can be avoided by transformation of the original variables and has been indicated in the appropriate sections. In connection with the two-sample problem the formulas assume equal sample sizes. These formulas can obviously be extended to cases in which it is desired to take unequal sample sizes of $N_1$ and $N_2$ that are assumed in advance to be functionally related.

## 3. A General Formula Concerning Sample Size and Region of Rejection

Let $x=x(N)$ be a normally distributed variable with mean $\mu_1$ and standard deviation (sd) $\sigma_1=f(\mu_1)F(N)$ under $H_1$ and with mean $\mu_2$ and sd $\sigma_2=f(\mu_2)F(N)$ under $H_2(\mu_2>\mu_1)$, where $F(N)$ is a certain function of the sample size $N$ and is independent of $\sigma$. We assume $x>A$ as the critical region and obtain

$$\frac{1}{\sqrt{2\pi}}\int_{K_\alpha}^{\infty} e^{-t^2/2}dt=\alpha$$

and

$$\frac{1}{\sqrt{2\pi}}\int_{K_{1-\beta}}^{\infty} e^{-t^2/2}dt=1-\beta,$$

where $K_\epsilon$ is the standardized normal deviate exceeded with probability $\epsilon$ and actually

$$\frac{A-\mu_1}{f(\mu_2)F(N)}=K_\alpha \tag{1}$$

$$\frac{A-\mu_2}{f(\mu_2)F(N)}=K_{1-\beta}=-K_\beta \tag{2}$$

Solving (1) and (2) for $F(N)$ and $A$ we obtain

[1] Revision of a paper written during the summer of 1947 when the author was a guest worker at the National Bureau of Standards. The manuscript was actually revised while the author was teaching at Boston University.

[2] Present address, c/o P. V. Sukhatme, Indian Council of Agricultural Research, New Delhi, India.

[3] Figures in brackets indicate the literature references at the end of this paper.

$$F(N)=\frac{\mu_2-\mu_1}{K_\alpha f(\mu_1)+K_\beta f(\mu_2)} \tag{3}$$

$$A=\frac{K_\alpha \mu_2 f(\mu_1)+K_\beta \mu_1 f(\mu_2)}{K_\alpha f(\mu_1)+K_\beta f(\mu_2)}, \tag{4}$$

which may also be written as

$$1=\frac{\mu_2-\mu_1}{K_\alpha \sigma_1+K_\beta \sigma_2} \tag{5}$$

$$A=\frac{K_\alpha \mu_2 \sigma_1+K_\beta \mu_1 \sigma_2}{K_\alpha \sigma_1+K_\beta \sigma_2}, \tag{6}$$

for later convenience in certain simplifications. We note in passing that in particular cases of application $f(\mu)$ will either be a function of $\mu$ (cf. binomial and Poisson), or it will not depend on $\mu$, in which case it will be a certain function of the population sd $\sigma$ (cf. normal) or a pure number (cf. transformed binomial and Poisson).

## 4. Tests Relating to the Parameter of the Binomial Distribution

### 4.1. Single Binomial

Consider a random sample of $N$ items drawn from an infinite population in which a proportion $P$ of the items possesses a definite attribute $B$ and let $p$ be the fraction of the items possessing $B$ in the sample. Then $E(p)=P$ and $\sigma(p)=\sqrt{P(1-P)}/\sqrt{N}$. Our hypotheses are $H_1{:}P=P_1$ and $H_2{:}P=P_2(P_2>P_1)$. Using the normal approximation for the binomial variable $p$, (3) and (4) imply

$$N\cong\left(\frac{K_\beta\sqrt{P_2(1-P_2)}+K_\alpha\sqrt{P_1(1-P_1)}}{P_2-P_1}\right)^2 \tag{7}$$

$$A\cong\frac{K_\beta P_1\sqrt{P_2(1-P_2)}+K_\alpha P_2\sqrt{P_1(1-P_1)}}{K_\alpha\sqrt{P_1(1-P_1)}+K_\beta\sqrt{P_2(1-P_2)}} \tag{8}$$

While (7) determines directly the sample size that will (approximately) guarantee a specified $\alpha$ and $\beta$, this may also be looked upon as providing the values of the probability of accepting $H_1$ for different values of $P$ for given $N$ and $\alpha$. For example (7) yields

$$K_\beta\cong\frac{\sqrt{N}(P_2-P_1)-K_\alpha\sqrt{P_1(1-P_1)}}{\sqrt{P_2(1-P_2)}}. \tag{9}$$

The inverse sine transformation $\theta=2\sin^{-1}\sqrt{p}$ where $\theta$ is measured in radians [16] avoids the difficulty of the dependence of the standard deviation of of $p$ on unknown $P$, since $\theta$ is approximately normally distributed about $2\sin^{-1}\sqrt{P}$ with sd $\sigma(\theta)\cong\sqrt{(1/N)}$. In terms of the transformed quantities we obtain

$$N\cong\frac{1}{4}\left(\frac{K_\alpha+K_\beta}{\sin^{-1}\sqrt{P_2}-\sin^{-1}\sqrt{P_1}}\right)^2 \tag{10}$$

$$A\cong 2\left(\frac{K_\beta\sin^{-1}\sqrt{P_1}+K_\alpha\sin^{-1}\sqrt{P_2}}{K_\alpha+K_\beta}\right) \tag{11}$$

$$K_\beta\cong 2\sqrt{N}\,(\sin^{-1}\sqrt{P_2}-\sin^{-1}\sqrt{P_1})-K_\alpha. \tag{12}$$

We have derived (7) and (10) to illustrate the use of the results given in section 3. The comparison of the two formulas raises questions of quite a complicated nature. We have so far not found any convenient yardstick with which to compare their accuracy. In the light of the fact that the critical region $\theta>A$ (11) has certain theoretical advantages against $p>A$ (8) there is the temptation to recommend (10). As the following example will indicate ($\alpha=.05$, $P_1=0.1$ and $P_2=0.2$) the recommendation has nothing to do with the relative magnitude of the values of $N$ given by (7) and (10).

| $\beta=$ | 0. 20 | 0. 10 | 0. 05 | 0. 01 |
|---|---|---|---|---|
| (7) | 68. 9 | 101. 2 | 132. 6 | 202. 8 |
| (10) | 76. 8 | 106. 3 | 134. 4 | 195. 8 |

### 4.2. Comparison of Two Binomials

Consider two binomial processes with $P$ and $P^*$ as the values of true proportions and let $p$ and $p^*$ be the observed proportions in a sample of $N$ from each process. We have here $H_1{:}P^*-P=0$ and $H_2{:}P^*-P>0$. The test function $X=p^*-p$ under $H_1$ has an unspecified variance $V(X)=2[\hat{P}(1-\hat{P})]/N$, where $\hat{P}$ is the common (unspecified) value of $P$ and $P^*$ under $H_1$. Under $H_2$ we have $V(X)=P(1-P)/N+[P^*(1-P^*)]/N$, where $P^*-P=\xi>0$ say, with the value of $\xi$ specified but not the values of $P^*$ and $P$. We are then faced with the problem of comparing two means having unspecified and unequal variances under $H_1$ and $H_2$.

The only satisfactory solution to the problem of the comparison of two binomial means—see [4, chapter 7]—is usually given in terms of the transformed variables (section 4.1). Under the inverse sine transformation $\sin^{-1}\sqrt{p^*}-\sin^{-1}\sqrt{p}$ is approximately normally distributed (except when $N$ is very small or the $P$'s are close to 0 or 1) with mean $\sin^{-1}\sqrt{P^*}-\sin^{-1}\sqrt{P}$ and variance $(1/2N)$. We now use results of section 3 and obtain

$$N\cong\frac{1}{2}\left(\frac{K_\alpha+K_\beta}{\sin^{-1}\sqrt{P^*}-\sin^{-1}\sqrt{P}}\right)^2. \tag{13}$$

$$A\cong\frac{K_\alpha}{\sqrt{2N}} \tag{14}$$

$$K_\beta\cong\sqrt{2N}\,(\sin^{-1}\sqrt{P^*}-\sin^{-1}\sqrt{P})-K_\alpha. \tag{15}$$

## 5. Tests Relating to the Parameter of the Poisson Distribution

### 5.1. Single Poisson

Let $\bar{x}$ denote the mean of a random sample of size $N$ from a Poisson population with parameter $m$. Let $H_1{:}m=m_1$ and $H_2{:}m=m_2$ $(m_2>m_1)$. To apply

the results of Section 3 we assume normality for $\bar{x}$ with mean $m$ and variance $m/N$ and obtain

$$N \simeq \left( \frac{\sqrt{m_1}K_\alpha + \sqrt{m_2}K_\beta}{m_2 - m_1} \right)^2 \tag{16}$$

$$A \simeq \frac{m_2\sqrt{m_1}K_\alpha + m_1\sqrt{m_2}K_\beta}{\sqrt{m_1}K_\alpha + \sqrt{m_2}K_\beta} \tag{17}$$

$$K_\beta \simeq \frac{(m_2 - m_1)\sqrt{N} - \sqrt{m_1}K_\alpha}{\sqrt{m_2}} \tag{18}$$

We notice that under both $H_1$ and $H_2$ the variance of $\bar{x}$ is known given $N$ but differs for $H_1$ and $H_2$. If we make use of the well known square-root transformation [17], the variance of the transformed variate is approximately independent of the unknown mean and is approximately equal to $1/4N$. We now obtain

$$N \simeq \frac{1}{4}\left( \frac{K_\alpha + K_\beta}{\sqrt{m_2} - \sqrt{m_1}} \right)^2 \tag{19}$$

$$A \simeq \frac{K_\alpha\sqrt{m_2} + K_\beta\sqrt{m_1}}{K_\alpha + K_\beta} \tag{20}$$

and

$$K_\beta \simeq 2\sqrt{N}(\sqrt{m_2} - \sqrt{m_1}) - K_\alpha. \tag{21}$$

For example for $m_1 = 3.0$, $m_2 = 4.0$, $\alpha = .05$, $\beta = .10$, formulas (16) and (19) yield $N = 29.3$ and $N = 29.8$, respectively. This is just an illustration; otherwise remarks made in connection with the single binomial in the last paragraph of section 4.1 apply here as well.

### 5.2. Comparison of Two Poissons

Let $M$ and $M^*$ be the parameters of two Poisson populations. Let $H_1: M = M^*$ and $H_2: M < M^*$, e.g. $\sqrt{M^*} - \sqrt{M} = \eta > 0$. Consider two independent random samples of size $N$ drawn one from each of the two populations. Let $\bar{x}$ and $\bar{x}^*$ be the corresponding sample means. We may regard the quantity $\sqrt{\bar{x}^*} - \sqrt{\bar{x}}$ as approximately normally distributed with mean $m = \sqrt{M^*} - \sqrt{M}$ and variance $1/2N$ and consequently obtain

$$N = \frac{1}{2}\left( \frac{K_\alpha + K_\beta}{\sqrt{M^*} - \sqrt{M}} \right)^2 \tag{22}$$

$$A \simeq \frac{K_\alpha}{\sqrt{2N}} \tag{23}$$

and

$$K_\beta \simeq \sqrt{2N}(\sqrt{M^*} - \sqrt{M}) - K_\alpha. \tag{24}$$

## 6. Tests Concerning the Mean of the Normal Population

### 6.1. Single Mean Test ($\sigma$ known)

Let $\bar{x}$ denote the mean of a random sample of $N$ observations from a normal population $(\mu, \sigma^2)$. We shall assume that $\sigma$ is known from past experience. Our hypotheses are $H_1: \mu = \mu_1$ and $H_2: \mu = \mu_2$ $(\mu_2 > \mu_1)$. Set $\mu_2 - \mu_1 = \Delta\sigma$. The test function $\bar{x}$ is normally distributed with mean $\mu$ and sd $\sigma/\sqrt{N}$. Using results of Section 3 we obtain

$$N = \left( \frac{K_\alpha + K_\beta}{\Delta} \right)^2 \tag{25}$$

$$A = \frac{K_\alpha\mu_2 + K_\beta\mu_1}{K_\alpha + K_\beta} \tag{26}$$

and

$$K_\beta = \Delta\sqrt{N} - K_\alpha. \tag{27}$$

### 6.2. Comparison of Two Normal Means ($\sigma$'s known)

Let $\bar{x}_1$, $\bar{x}_2$ be the sample means of two independent random samples of equal size $N$ drawn one from each of the two normal populations $\pi_1(\mu_1, \sigma_1^2)$, $\pi_2(\mu_2, \sigma_2^2)$ respectively. We assume both $\sigma_1^2$ and $\sigma_2^2$ to be known from past experience. Our hypotheses are $H_1: \mu_1 = \mu_2$ and $H_2: \mu_1 < \mu_2$. The test function $\bar{x}_2 - \bar{x}_1$ is normally distributed $[(\mu_2 - \mu_1), (\sigma_1^2 + \sigma_2^2)/N]$ and, therefore, we obtain

$$N = \left( \frac{K_\alpha + K_\beta}{d} \right)^2 \tag{28}$$

$$A = \frac{K_\alpha(\mu_2 - \mu_1)}{K_\alpha + K_\beta} \tag{29}$$

and

$$K_\beta = \sqrt{N}d - K_\alpha \tag{30}$$

where

$$d = \frac{\mu_2 - \mu_1}{\sqrt{\sigma_1^2 + \sigma_2^2}}.$$

If $\sigma_1^2 = \sigma_2^2 = \sigma^2$ we obtain

$$N = 2\left( \frac{K_\alpha + K_\beta}{\Delta} \right)^2 \tag{31}$$

$$A = \frac{K_\alpha(\mu_2 - \mu_1)}{K_\alpha + K_\beta} \tag{32}$$

and

$$K_\beta = \Delta\sqrt{\frac{N}{2}} - K_\alpha. \tag{33}$$

### 6.3. Single Mean Test ($\sigma$ unknown)

For notation see section 6.1. In this case the well known Student's statistic $t = \sqrt{N}(\bar{x} - \mu_1)/s$ where $s^2$ is the unbiased estimate of $\sigma^2$, is used to accept or reject $H_1$. Tables for determining the sample size for detecting a given value of $\Delta$ with preassigned $\alpha$ and $\beta$ are given in [1] and operating characteristic curves for the same are given in [2]. To obtain a convenient formula for the sample size we proceed as follows:

Consider $P\{t \geq k\} = P\{[(\bar{x} - \mu) - (ks/\sqrt{N})] > 0\}$ where $k$ is a certain constant. The quantity $Z = (\bar{x} - \mu_1) - (ks/\sqrt{N})$ consists of two parts: $(\bar{x} - \mu_1)$ is normally distributed $(0, \sigma^2/N)$ under $H_1$, and

$(\mu_2-\mu_1,\ \sigma^2/N)$ under $H_2$; and for fixed $N$, $ks/\sqrt{N}$ is a constant multiple of $s$ where $s$ is approximately normally distributed $(C_1\sigma,\ C_2\sigma/\sqrt{2(N-1)})$ and $C_1$ and $C_2$ are certain constants less than 1.[4] It will be assumed for the purpose of this discussion that both $C_1$ and $C_2$ are equal to unity. The dual nature of these assumed approximations to the distribution of $s$ should be noted. Therefore,

$$E(Z|H_1)=Z_1=-\frac{k}{\sqrt{N}}\,\sigma$$

$$E(Z|H_2)=Z_2=(\mu_2-\mu_1)-\frac{k}{\sqrt{N}}\,\sigma$$

$$V(Z)=\frac{\sigma^2}{N}+\frac{k^2}{N}\,\frac{\sigma^2}{2(N-1)}.$$

For $Z>A$ as the critical region we obtain (see section 3)

$$\frac{A-\left(-k\frac{\sigma}{\sqrt{N}}\right)}{\frac{\sigma}{\sqrt{N}}\sqrt{1+\frac{k^2}{2(N-1)}}}=K_\alpha$$

$$\frac{A-\left(\mu_2-\mu_1-\frac{k}{\sqrt{N}}\,\sigma\right)}{\frac{\sigma}{\sqrt{N}}\sqrt{1+\frac{k^2}{2(N-1)}}}=-K_\beta$$

Eliminating $A$ from the above two equations we get

$$\frac{\Delta}{K_\alpha+K_\beta}=\frac{1}{\sqrt{N}}\sqrt{1+\frac{k^2}{2(N-1)}} \tag{34}$$

where $\Delta$ has been previously defined (section 6.1). This is a quadratic in $N$ and could be solved for $N$ if $k$ were known. We now determine $k$ from the consideration that $A$ is to be independent of $\sigma$. After simplification we obtain

$$A=\sigma\left(\frac{\Delta K_\alpha}{K_\alpha+K_\beta}-\frac{k}{\sqrt{N}}\right)$$

The right-hand side will be independent of $\sigma$ if and only if the quantity in parentheses vanishes.

[4] The general expressions for $C_1$ and $C_2$ are:

$$C_1=\frac{\sqrt{\frac{2}{N-1}}\,\Gamma\left(\frac{N}{2}\right)}{\Gamma\left(\frac{N-1}{2}\right)},\qquad C_2=\sqrt{2(N-1)(1-C_1^2)}.$$

For small values of $N$, $C_1$, and $C_2$ take the following values:

| $N$ | $C_1$ | $C_2$ |
|---|---|---|
| 2 | 0.798 | 0.852 |
| 3 | .886 | .927 |
| 4 | .921 | .954 |
| 5 | .940 | .965 |
| 10 | .973 | .985 |
| 25 | .990 | .995 |

Therefore,

$$k=\frac{K_\alpha\Delta\sqrt{N}}{K_\alpha+K_\beta} \tag{35}$$

whence $A=0$ and is not only independent of $\sigma$ but actually takes the originally intended value in the inequality $P(Z>0)$. Substituting this value of $k$ in (34) we finally obtain

$$N=\frac{b+\sqrt{b^2-4a}}{2a} \tag{36}$$

where $$a=\left(\frac{\Delta}{K_\alpha+K_\beta}\right)^2$$

and $$b=\left(1+a\left(1+\frac{K_\alpha^2}{2}\right)\right)$$

Similarly

$$K_\beta=-K_\alpha+\frac{\Delta}{\sqrt{N-1}}\left(N^2-N\left(1+\frac{K_\alpha^2}{2}\right)\right)^{1/2} \tag{37}$$

If we replace $N-1$ by $N$, the above two formulas reduce to somewhat simpler expressions of the form

$$N=\left(\frac{1}{a}+\frac{1}{2}K_\alpha^2\right)+1 \tag{36a}$$

$$K_\beta=-K_\alpha+\Delta\left(N-\frac{K_\alpha^2}{2}\right)^{1/2}. \tag{37a}$$

For any given $\Delta$, $\alpha$, and $\beta$, values of $N$ from (36) are compared with the Neyman-Tokarska[5] Tables [1] are given in table 1. These values will be found to be approximately the same.

As pointed out in the previous paragraph (34) was obtained under the assumption that $k$ is unknown. The classical procedure employs $k=t_\alpha\ (n)$ where $n=N-1$.[5] Therefore if the probability points of $t$ are not available, (35) furnishes an approximation to such points $t_\alpha$. We have considered the accuracy of such $k$ points in relation to $t_\alpha$ in terms of $P[t>x]=\alpha(x)$. Values of $t_\alpha$, $k$, $\alpha(t_\alpha)$, and $\alpha(k)$ are given in tables 2a and 2b for different $N$'s and for different $\alpha$ and $\beta$. Strictly speaking $\alpha(t_\alpha)\equiv\alpha$, but when $t_\alpha$ to only three decimals is used, $\alpha(t_\alpha)$ may differ slightly from $\alpha$ as shown in tables 2a and 2b.

We notice that $k$ values are in general conservative $t_\alpha$ estimators and that the values of $\alpha(k)$ are consistently greater than the corresponding value of $\alpha(t_\alpha)$. In this sense a user of our formulas is likely to declare slightly too many significant results. The danger, if it can be so called, is not very great, but it is still there.

The question is asked: is it possible to eliminate this "danger" and still utilize formula (36) for $N$? It should be noticed that we can not utilize the available percentage points of $t$ in the derivation of (36). However, (34) can still be solved for $N$ as-

[5] Neyman-Tokarska's $\rho$ is equal to our $\Delta\sqrt{N}$. Since the standard table of probability points of $t$, [18] table 4, gives the *two-tail* probability points of $t$, our $t_\alpha(n)$ corresponds to the entry given there for $2\alpha$ and $n$ degrees of freedom.

TABLE 1. *Comparisons among different methods for obtaining necessary sample sizes*

[Single sample one-sided mean test]

| $\Delta$ | $N-T$ [a] | (36) | (38) | (25) | $N-T$ | (36) | (38) | (25) | $N-T$ | (36) | (38) | (25) |
|---|---|---|---|---|---|---|---|---|---|---|---|---|
| | $\alpha=.05$ | | | | | | | | | | | |
| | $\beta=.20$ | | | | $\beta=.10$ | | | | $\beta=.05$ | | | |
| 2 | 3 | 3 | 4 | 2 | 4 | 4 | 4 | 2 | 5 | 4 | 4 | 3 |
| 1 | 8 | 8 | 8 | 6 | 10 | 10 | 10 | 9 | 12 | 12 | 12 | 11 |
| .5 | 26 | 26 | 26 | 25 | 36 | 36 | 36 | 34 | 45 | 45 | 45 | 43 |
| .25 | 100 | 100 | 100 | 99 | 139 | 138 | 138 | 137 | 175 | 175 | 175 | 173 |
| .125 | 398 | 397 | 397 | 396 | 550 | 550 | 550 | 548 | 694 | 694 | 694 | 693 |
| | $\alpha=.01$ | | | | | | | | | | | |
| $\Delta$ | $\beta=.10$ | | | | $\beta=.05$ | | | | $\beta=.01$ | | | |
| 2 | 6 | 6 | 7 | 3 | 7 | 7 | 7 | 4 | 8 | 8 | 9 | 5 |
| 1 | 16 | 16 | 16 | 13 | 19 | 19 | 19 | 16 | 24 | 24 | 25 | 22 |
| .5 | 55 | 55 | 55 | 52 | 66 | 66 | 66 | 63 | 80 | 80 | 80 | 87 |
| .25 | 211 | 211 | 211 | 208 | 255 | 255 | 255 | 252 | 349 | 349 | 349 | 346 |
| .125 | 837 | 836 | 836 | 833 | 1012 | 1012 | 1012 | 1009 | 1388 | 1388 | 1388 | 1388 |

[a] "$N-T$" refers to values obtained either directly or by interpolation from Neyman and Tokarska Tables [1]. Values under "(25)" are for $\sigma$ known and are included here for purposes of comparison with the other three for $\sigma$ unknown. For a relation between the comparison of sample sizes for $\sigma$ known and unknown see section 6.5.

TABLE 2a.[a] *Comparison of the accuracy of the different percentage points of t and k values for the same* $\Delta$

| | Neyman and Tokarska | | | This paper | | |
|---|---|---|---|---|---|---|
| | $N$ | $t_\alpha$ | $\alpha(t_\alpha)$ | $N$ | $k$ | $\alpha(k)$ |
| | $\alpha=.05$ | | | | | |
| $\beta=.50$ | 3 | 2.920 | 0.05000 | 3 | 3.338 | 0.04958 |
| | 4 | 2.353 | .05000 | 4 | 2.110 | .06270 |
| | 12 | 1.796 | .05003 | 12 | 1.753 | .05370 |
| $\beta=.20$ | 3 | 2.920 | .05000 | 3 | 2.458 | .06659 |
| | 8 | 1.895 | .04996 | 8 | 1.840 | .05412 |
| | 26 | 1.708 | .05012 | 26 | 1.691 | .05163 |
| $\beta=.10$ | 4 | 2.353 | .05000 | 4 | 2.235 | .05575 |
| | 10 | 1.833 | .04999 | 10 | 1.783 | .05414 |
| $\beta=.05$ | 5 | 2.132 | .04995 | 4 | 2.110 | .06270 |
| | 12 | 1.796 | .05003 | 12 | 1.753 | .05370 |
| $\beta=.01$ | 6 | 2.015 | .05003 | 6 | 1.959 | .05370 |
| | 17 | 1.746 | .04995 | 17 | 1.718 | .05250 |

[a] Values of $P(t>k)=\alpha(k)$ and $P(t>t_\alpha)=\alpha$ $(t_\alpha)$ for $N\leq 21$ were obtained by interpolation in "Student's" Table I [6] and for $22\leq N\leq 31$ by interpolation in Table XXV of [7].

TABLE 2b.[a] *Comparison of the accuracy of the different percentage points of t and k values for the same* $\Delta$

| | Neyman and Tokarska | | | This paper | | |
|---|---|---|---|---|---|---|
| | $N$ | $t_\alpha$ | $\alpha(t_\alpha)$ | $N$ | $k$ | $\alpha(k)$ |
| | $\alpha=.01$ | | | | | |
| $\beta=.50$ | 4 | 4.541 | 0.00997 | 5 | 4.371 | 0.00594 |
| | 8 | 2.998 | .01003 | 8 | 2.912 | .01130 |
| | 24 | 2.500 | .01250 | 24 | 2.473 | .01322 |
| $\beta=.20$ | 5 | 3.747 | .01000 | 6 | 3.531 | .00833 |
| | 13 | 2.681 | .01002 | 13 | 2.644 | .01070 |
| $\beta=.10$ | 6 | 3.365 | .00996 | 6 | 3.277 | .01099 |
| | 16 | 2.602 | .00996 | 16 | 2.571 | .01064 |
| $\beta=.05$ | 7 | 3.143 | .01003 | 7 | 3.120 | .01033 |
| | 19 | 2.552 | .00974 | 19 | 2.528 | .01043 |
| $\beta=.01$ | 8 | 2.998 | .01003 | 8 | 2.912 | .01130 |
| | 24 | 2.500 | .01250 | 24 | 2.473 | .01322 |

[a] Values of $P(t>k)=\alpha(k)$ and $P(t>t_\alpha)=\alpha$ $(t_\alpha)$ for $N\leq 21$ were obtained by interpolation in "Student's" Table I [6] and for $22\leq N\leq 31$ by interpolation in Table XXV of [7].

suming $k$ to be known, say equal to $t_\alpha(n)$, resulting in

$$N=\frac{(a+1)+\sqrt{(a-1)^2+2at_\alpha^2(n)}}{2a} \tag{38}$$

Values of $N$ from (38) corresponding to different $t_\alpha(n)$, $\Delta$, $\alpha$ and $\beta$ are also given in table 1. Since the values of $N$ as given by (36), (38) and the Neyman-Tokarska Tables are approximately the same, it is recommended that (38) be used in conjunction with the $t$-tables. This will save the labor of calculating $k$ values.

Since any symmetric two-sided test may be regarded as a combination of two one-sided tests, values of $N$ and $k$ may be obtained from the corresponding single-tailed formulas by substituting $K_\alpha/2$ for $K_\alpha$ and $t_\alpha/2$ for $t_\alpha$, in which case the "$\beta$" deduced from the resulting value of $K_\beta$ will over-estimate the true value of $\beta$, the probability of accepting $H_1$ when $\mu_2-\mu_1=\Delta\sigma$, by the amount $1-\beta'$ where $\beta'$ is given by (37) or (37a) with the term in $\Delta$ taken with a negative sign. Values of $N$ obtained from [8] and [9] and from the formulas (36) and (38) of this paper are given in table 3. The corresponding two-tailed values of $t$ and $k$ are also given in table 3.

### 6.4. Comparison of Two Means: (common $\sigma$ unknown)

For notation refer to section 6.2. Consider two samples of equal size $N$. Our hypotheses are $H_1$: $\mu_1=\mu_2$; $H_2$: $\mu_1<\mu_2$. Let $s^2$ denote the unbiased estimate of the common variance $\sigma^2$. The statistic $t=\frac{\bar{x}_2-\bar{x}_1}{s\sqrt{\frac{2}{N}}}$ which under $H_1$ has "Student's" $t$-distribu-

TABLE 3.[a] *Comparisons among different methods for obtaining necessary sample sizes*

[Two-sided single mean test: $\sigma$ unknown]

| $\Delta$ | $\beta=.30$ | | | | | $\beta=.20$ | | | | |
|---|---|---|---|---|---|---|---|---|---|---|
| | Tabulated | (36) | (38) | $t_\alpha/2$ | $k$ | Tabulated | (36) | (38) | $t_\alpha/2$ | $k$ |
| $\alpha=.05$ | | | | | | | | | | |
| 2 | 4 | 4 | 4 | 3.182 | 3.190 | 4 | 4 | 5 | 3.182 | 2.949 |
| 1 | 8 | 8 | 8 | 2.365 | 2.280 | 10 | 10 | 10 | 2.262 | 2.210 |
| .5 | 27 | 27 | 27 | 2.036 | 2.038 | 33 | 33 | 33 | 2.037 | 2.021 |
| .25 | 101 | 101 | 101 | 1.982 | 1.979 | 128 | 128 | 128 | 1.977 | 1.975 |
| .125 | 397 | 397 | 397 | 1.966 | 1.965 | 504 | 504 | 504 | 1.964 | 1.964 |
| $\alpha=.01$ | | | | | | | | | | |
| 2 | 6 | 6 | 6 | 4.032 | 4.184 | 6 | 7 | 7 | 4.032 | 3.933 |
| 1 | 13 | 13 | 13 | 3.055 | 3.019 | 15 | 15 | 15 | 2.977 | 2.941 |
| .5 | 42 | 42 | 42 | 2.701 | 2.687 | 50 | 50 | 50 | 2.680 | 2.668 |
| .25 | 157 | 157 | 157 | 2.607 | 2.604 | 190 | 190 | 190 | 2.601 | 2.599 |
| .125 | 618 | 618 | 618 | 2.584 | 2.583 | 751 | 751 | 751 | 2.583 | 2.582 |

[a] "Tabulated" values were obtained from [8] and [9] and $t_\alpha/2$ indicates the two-tailed $\alpha$ value of $t$. See footnote 5.

tion with $2(N-1)$ d.o.f. is used to accept or reject $H_1$. Consider $P\left(t \geq k_1\right) = P\left(\bar{x}_2 - \bar{x}_1 - k_1\sqrt{\frac{2}{N}}\, s > 0\right)$ where we assume $k_1$ to be a certain unknown constant. Let

$$Z = (\bar{x}_2 - \bar{x}_1) - k_1\sqrt{\frac{2}{N}}\, s.$$

We assume that $s$ is approximately normally distributed with mean $\sigma$ and sd, $\sigma/\sqrt{4(N-1)}$. Therefore $Z$ is approximately normally distributed with

$$E(Z|H_1) = -k_1\sqrt{\frac{2}{N}}\,\sigma$$

$$E(Z|H_2) = \mu_2 - \mu_1 - k_1\sqrt{\frac{2}{N}}\,\sigma$$

$$\sigma(Z) = \sigma\sqrt{\frac{2}{N} + \frac{k_1^2}{2N(N-1)}}$$

where $\sigma(Z)$ denotes the standard deviation of $Z$. Proceeding as in section 3.3 we obtain

$$\frac{\Delta}{K_\alpha + K_\beta} = \sqrt{\frac{2}{N} + \frac{k_1^2}{2N(N-1)}} \tag{39}$$

and

$$A = \frac{K_\alpha \sigma \Delta}{K_\alpha + K_\beta} - \sigma\sqrt{\frac{2}{N}}\, k_1. \tag{40}$$

If we assume $k_1 = t_\alpha(n)$ where $t_\alpha$ is the *one-sided* $\alpha$-point of $t$ for $n=2\ (N-1)$ d.o.f the equation (39) yields

$$N = \frac{a + 2 + \sqrt{(a-2)^2 + 2at_\alpha^2(n)}}{2a} \tag{41}$$

where $a$ has been defined in section 6.3. The reason for such an illogical assumption about the knowledge of $t_\alpha(n)$ before actually $N$ is determined has been indicated in the previous section. If $k_1$ is unknown we determine $k_1$ from the consideration that $A$ is to be independent of $\sigma$. The relation (40) yields

$$k_1 = \sqrt{\frac{N}{2}} \cdot \frac{K_\alpha \Delta}{K_\alpha + K_\beta}. \tag{42}$$

We substitute this value of $k_1$ in (39) and obtain

$$N = \frac{b_1 + \sqrt{b_1^2 - 8a}}{2a} \tag{43}$$

where $a$ has been previously defined (section 6.3) and

$$b_1 = 2 + a\left(1 + \frac{K_\alpha^2}{4}\right).$$

For determining the operating characteristic we similarly obtain

$$K_\beta = -K_\alpha + \Delta\left[\frac{N}{2}\left(1 - \frac{K_\alpha^2}{4(N-1)}\right)\right]^{1/2}. \tag{44}$$

We give in table 4 values of $N$ as obtained from (43) and Tables of Neyman [6] and Tokarska [1]. While (42) provides approximate values of the per-

TABLE 4. *Comparisons among different methods for obtaining necessary sample sizes $N$* [a]

[Two means one-sided test; common $\sigma$ unknown: $\Delta=2$]

| | $\alpha=.05$ | | $\alpha=.01$ | |
|---|---|---|---|---|
| | Neyman-Tokarska | (43) | Neyman-Tokarska | (43) |
| $\beta=.50$ | 2 | 2 | 4 | 4 |
| $\beta=.20$ | 4 | 4 | 6 | 7 |
| $\beta=.10$ | 5 | 5 | 8 | 8 |
| $\beta=.05$ | 6 | 6 | 9 | 9 |
| $\beta=.01$ | 8 | 9 | 12 | 12 |

[a] $N$ is the size of one of the two equal samples.

[b] For this particular case $\rho$ as defined in [1] is equal to $\Delta\sqrt{\frac{N}{2}}$.

centage points of $t$ for $2(N-1)$ d.o.f, the formula (43) may be used advantageously by utilizing the available percentage points of $t$ as acceptance-rejection criteria. Formulas obtained here for single-tailed comparisons can also be used for a two-tailed test by substituting appropriate two-tailed values of the quantities involved. If the two populations have unequal variances and their ratio is known we still can construct a test function similar to $t$ and use the above formulas. (For the structure of the test function see [10].)

### 6.5. Comparison of Sample Sizes for Known and Unknown $\sigma$

It need hardly be emphasized that in situations in which large sample sizes are required, the normal test (sections 6.1 and 6.2) and $t$-test (sections 6.3 and 6.4) will both yield approximately the same $N$ (see for example table 1). To determine the relations between the two, let $N_m$ be the number of observations required when $\sigma$ is known and $N_t$ the corresponding number when $\sigma$ is not known. After some simplification the following asymptotic relations between $N_m$ and $N_t$ are obtained. For the single-mean test, (25) and (36a) yield

$$N_t \sim N_m\left(1+\frac{K_\alpha^2}{2N_m}\right)+1 \tag{45}$$

and for the two-means test, (31) and (43) yield

$$N_t \sim N_m\left(1+\frac{K_\alpha^2}{4N_m}\right)+1. \tag{46}$$

## 7. Tests Concerning Variances of Normal Populations

Tests relating to population variances fall into two well defined categories. In one case we assume that the variability of a certain product is known and it is desired to find out whether a new product is more variable than this. In the other case we are asked to choose between two products on the basis of their variability which is unknown. We discuss these situations in the following sections.

### 7.1 Single Variance Test

Consider a random sample of size $N$ $(=n+1)$ from a normal population $(m, \sigma^2)$. Let $s^2$ be the unbiased sample estimate of $\sigma^2$. Our hypotheses are $H_1$: $\sigma^2=\sigma_0^2$ and $H_2$: $\sigma^2=\lambda\sigma_0^2(\lambda>1)$. For a given level of significance $\alpha$, if $\chi^2=ns^2/\sigma_0^2>\chi_\alpha^2$, we reject $H_1$ and conclude that $\sigma^2>\sigma_0^2$.

Let $\lambda(\alpha,\beta,n)$[7] denote the value of $\sigma^2/\sigma_0^2$ for which the probability of the decision $\sigma^2=\sigma_0^2$ equals $\beta$ when the test is conducted at the $\alpha$ level of significance with $n$ d.o.f. It can be shown [2], [4] that the probability error of the second kind is exactly $\beta$ if $\lambda(\alpha,\beta,n)=\chi_\alpha^2(n)/\chi_{1-\beta}^2(n)$. If we are testing $H_1$: $\sigma^2=\sigma_0^2$ against $H_2$: $\sigma^2=\lambda\sigma_0^2$ $(\lambda<1)$ we have $\lambda(\alpha,\beta,n)=\chi_{1-\alpha}^2/\chi_\beta^2$.

[7] Our $\lambda(\alpha,\beta,n)$ is equivalent to $\rho(\alpha,\beta,n)$ of [4].

Curves for the operating characteristics of such testing procedures are given in [2] and [4]. Eisenhart [4] has also given extensive tables for $\lambda(\alpha,\beta,n)$.

The problem of determining a direct relation between large $n$ and any given set of values of $\lambda$, $\alpha$, $\beta$ was first considered by Wallis [1, footnote of p. 278]. Assuming normality of $s$ (see section 6.3) and applying the results of Section 3 we obtain

$$n=\frac{1}{2}\left(\frac{K_\alpha+K_\beta\sqrt{\lambda}}{\sqrt{\lambda}-1}\right)^2 \tag{47}$$

$$A=\frac{\sqrt{\lambda}\sigma_0(K_\alpha+K_\beta)}{K_\alpha+\sqrt{\lambda}K_\beta} \tag{48}$$

$$\lambda(\alpha,\beta,n)=\left(\frac{K_\alpha+\sqrt{2n}}{\sqrt{2n}-K_\beta}\right)^2 \tag{49}$$

To compare the accuracy of this formula with the Tables [4] consider the following situation: if a decision $\sigma=\sigma_0$ is a serious error from the practical viewpoint when $\sigma=1.500\,\sigma_0$ and it is desired to keep the risk of such an error below .05 when the test is conducted at the 5-percent level of significance, how many d.o.f. will be needed for $s^2$? The formula (47) gives $n=33.8$ and from [4] we find that 34 d.o.f. are needed. Table 5 presents the calculated values of $n$ from (47) and table 6 presents the calculated values of $\lambda$ from (49). For a comparative discussion on the use of these formulas in relation to others see next section.

### 7.2. An Alternative Formula for the Single Variance Test Based on the Distribution of Log $s$[8]

As pointed out by Bartlett and Kendall [11] the distribution of $\log s^2$ depends on $\sigma^2$ only through the term $\sigma^2$ in its expected value. Consequently the choice of the critical region based on the distribution of $\log s$ in place of $s$ has obvious advantages. In this section we explore the possibility of using some formulas based on the distribution of $\log s$.

The cumulant function $K(t)$ of $\log s$ is given [11] by

$$K(t)=\frac{it}{2}\left(\log\sigma^2-\log\frac{n}{2}\right)+\log\Gamma\left(\frac{n+it}{2}\right)-\log\Gamma\left(\frac{n}{2}\right)$$

which yields the following expressions for the first two cumulants

$$\kappa_1=\frac{1}{2}\left(\log\sigma^2-\log\frac{n}{2}\right)+\frac{1}{2}\Psi\left(\frac{n}{2}\right)$$

$$\kappa_2=\frac{1}{4}\Psi'\left(\frac{n}{2}\right),$$

where $\Psi(x)=\frac{d}{dx}\log\Gamma(x)$. The results of Section 3

[8] All logarithms are to the base $e$.

applied to $\log s$ yields

$$\kappa_2(n)=\left(\frac{\log\frac{\sigma}{\sigma_0}}{K_\alpha+K_\beta}\right)^2 \tag{50}$$

$$A=\frac{K_\beta\log\sigma_0+K_\alpha\log\sqrt{\lambda}\,\sigma_0}{K_\alpha+K_\beta}+\frac{1}{2}\left(\Psi\left(\frac{n}{2}\right)-\log\frac{n}{2}\right) \tag{51}$$

$$\lambda(\alpha,\beta,n)=e^{2\sqrt{\kappa_2(n)}(K_\alpha+K_\beta)}. \tag{52}$$

These formulas assume no other approximation except that of normality and in that sense may be regarded as exact relative to (47), which assumes dual type of approximation for the distribution of $s$ (see section 6.3). While the accuracy of (50) and (52) does not depend upon the accuracy with which we estimate $\kappa_1$, it does depend upon the complicated expression $\Psi'\left(\frac{n}{2}\right)$. For a given $\alpha$, $\beta$, and $\lambda$ the only way in which we can utilize (50) for finding the necessary sample size is to approximate the asymptotic expansion of $\Psi'\left(\frac{n}{2}\right)$ [12].

As a first approximation if we set $\kappa_2\cong 1/[2(n-1)]$ we obtain

$$n=1+2\left(\frac{K_\alpha+K_\beta}{\log\lambda}\right)^2 \tag{53}$$

$$\log\lambda=\sqrt{\frac{2}{n-1}}\,(K_\alpha+K_\beta). \tag{54}$$

In tables 5a and 5b values of $n$ from [4], and values calculated from (47) and (53) for different values of $\alpha$, $\beta$, and $\lambda$ are compared. In table 6 we give values of $\lambda(\alpha, \beta, n)$ to reemphasize the nature of approximations based on the distribution of $s$ and $\log s$. In this connection for the application of (52) values of $\kappa_2(n)$ were taken from [11].

It appears that for the customary values of the probabilities of errors of the two kinds $\alpha=\beta=.05$ and $\alpha=\beta=.01$, formulas (47) and (53) provide very good approximations to $n$ for small sample sizes. If the percentage points of the $\chi^2$-distribution are available, (47) is preferable because it is easier to compute $n$ from (47) than from (53). Even for such a small value as $n=5$, (47) errs on the safe side in this sense that it gives (at least for $\alpha=\beta$) a sample size which will be always sufficient to detect this difference. The formula (53) also shares this property with (47). In the absence of the percentage points of the $\chi^2$-distribution it perhaps ought to be emphasized that on comparison of the critical regions for $s$ and $\log s$ (cf. (48) and (51)) there is not much basis for choice. The choice of the critical region based on the distribution of $\log s$ has certain theoretical advantages, but the computation of the critical region is somewhat more complicated since it involves the approximation of $\Psi(n/2)$.

The effectiveness of formulas (47) and (53) varies when $\alpha$ and $\beta$ are not equal. It appears (see table 5 and table 6) that for $\beta>\alpha$ it is safer to use (53) because it is always likely to err on the safe side in the sense of the previous paragraph. However, if $\beta<\alpha$ it appears that it is safer to use (47) because (53) is likely to give a value of $n$, which will actually be less than the necessary sample size.

TABLE 5a. *Comparison of the sample sizes ($n=N-1$) for the single variance test*

| $\alpha=.05$ | | | | | | |
|---|---|---|---|---|---|---|
| $\lambda$ | $\beta=.05$ | | | $\beta=.10$ | | |
| | (47) | (53) | Tabulated | (47) | (53) | Tabulated |
| 2 | 46.0 | 46.1 | 46.4 | 34.9 | 36.7 | 36.0 |
| 2.5 | 26.7 | 26.8 | 26.6 | 20.0 | 21.4 | 20.5 |
| 3 | 18.8 | 18.9 | 18.8 | 13.9 | 15.2 | 14.5 |
| 3.5 | 14.7 | 14.8 | 14.6 | 10.8 | 11.9 | 11.1 |

TABLE 5b. *Comparison of the sample sizes ($n=N-1$) for the single variance test*

| $\alpha=.01$ | | | | | | |
|---|---|---|---|---|---|---|
| $\lambda$ | $\beta=.01$ | | | $\beta=.05$ | | |
| | (47) | (53) | Tabulated | (47) | (53) | Tabulated |
| 2 | 91.9 | 91.1 | 91.4 | 63.1 | 66.6 | 64.3 |
| 2.5 | 53.4 | 52.6 | 53.1 | 35.9 | 38.6 | 37.2 |
| 3 | 37.7 | 36.9 | 37.6 | 25.0 | 27.1 | 25.6 |
| 3.5 | 29.4 | 28.6 | 28.7 | 19.3 | 21.1 | 19.8 |

## 7.3. Comparison of Two Population Variances

Let $\sigma_1^2$ and $\sigma_2^2$ denote the variances of the two normal populations and let $s_1^2$ and $s_2^2$ be their inde-

TABLE 6. *Comparison of the tabulated and calculated values of $\lambda$ ($\alpha$, $\beta$, $n$)*

| $\alpha=.05$ | | | | | | | | | | | | |
|---|---|---|---|---|---|---|---|---|---|---|---|---|
| $n$ | $\beta=.25$ | | | | $\beta=.05$ | | | | $\beta=.01$ | | | |
| | (49) | (52) | (54) | Tabulated | (49) | (52) | (54) | Tabulated | (49) | (52) | (54) | Tabulated |
| 5 | 3.734 | 5.073 | 5.155 | 4.139 | 10.037 | 10.01 | 10.239 | 9.664 | 33.065 | 16.14 | 16.577 | 19.972 |
| 10 | 2.595 | 2.977 | 2.984 | 2.717 | 4.681 | 4.700 | 4.715 | 4.646 | 8.126 | 6.476 | 6.501 | 7.156 |
| 15 | 2.199 | 2.401 | 2.403 | 2.265 | 3.454 | 3.463 | 3.468 | 3.442 | 5.109 | 4.479 | 4.487 | 4.780 |
| 20 | 1.990 | 2.122 | 2.122 | 2.033 | 2.900 | 2.906 | 2.907 | 2.895 | 3.973 | 3.625 | 3.627 | 3.802 |

pendent sample estimates based on $n_1$ and $n_2$ d.o.f. respectively. Our hypotheses are $H_1$: $\sigma_1^2=\sigma_2^2$ and $H_2$: $\sigma_1^2>\sigma_2^2$. The statistic $F=s_1^2/s_2^2$ is used to accept or reject $H_1$. For a given level of significance $\alpha$, if $F\leq F_\alpha$ we accept $H_1$ and accept $H_2$ when $F>F_\alpha$. Let $\phi$ denote the true value of $\sigma_1^2/\sigma_2^2$. It has been shown in [2] and [4] that the probability of an error of the second kind will be exactly $\beta$ if

$$\phi(\alpha,\beta,n_1,n_2)=\frac{F_\alpha(n_1,n_2)}{F_{1-\beta}(n_1,n_2)}=F_\alpha(n_1,n_2)F_\beta(n_2,n_1). \quad (55)$$

The operating characteristics ($\phi$, $\beta$) for one-sided alternatives have been given in [2] and [4]. We shall develop here certain approximate formulas for $\phi$ in terms of $\alpha$, $\beta$, $n_1$, and $n_2$.

By taking one-half the logarithm of (55) we obtain

$$\frac{1}{2}\log\phi=z_\alpha(n_1,n_2)+z_\beta(n_2,n_1) \quad (56)$$

where $z_\alpha$ denotes the $\alpha$-probability point of Fisher's $z$-distribution. For purposes of approximation, (56) has decided advantage over (55) in that it enables us to make better use of the Cornish-Fisher approximation [13] since the $z$-distribution approaches normality relatively faster than the $F$-distribution. We shall employ the following approximations [14] for the cumulants of $z$:

(i) $\kappa_1=\frac{1}{2}\left(\frac{1}{n_2}-\frac{1}{n_1}\right)$

(ii) $\kappa_2=\frac{1}{2}\left(\frac{1}{n_i}+\frac{1}{n_2}\right)$

(iii) $\kappa_s=\frac{(s-2)!}{2}\left(\frac{1}{(n_2-1)^{s-1}}+\frac{(-1)^s}{(n_1-1)^{s-1}}\right)(s>1).$

Let $z_1$ and $z_2$ denote the mathematical expectation of $z$ under $H_1$ and $H_2$, respectively. Consequently we have

$$z_1\cong\frac{1}{2}\left(\frac{1}{n_2}-\frac{1}{n_1}\right)$$

$$z_2\cong\frac{1}{2}\left(\frac{1}{n_2}-\frac{1}{n_1}\right)+\frac{1}{2}\log\phi$$

$$V(z)\simeq\frac{1}{2}\left(\frac{1}{n_1}+\frac{1}{n_2}\right)$$

By applying the results of section 3 to $z$, it is found that

$$2\left(\frac{1}{n_1}+\frac{1}{n_2}\right)=\left(\frac{\log\phi}{K_\alpha+K_\beta}\right)^2, \quad (57)$$

which may be rewritten as

$$\log\phi=\frac{2(K_\alpha+K_\beta)}{\sqrt{h}}, \quad (58)$$

where $h=\frac{2n_1n_2}{n_1+n_2}$. By using $\kappa_2=\left(\frac{1}{n_2-1}+\frac{1}{n_1-1}\right)$ there results

$$2\left(\frac{1}{n_1-1}+\frac{1}{n_2-1}\right)=\left(\frac{\log\phi}{K_\alpha+K_\beta}\right)^2 \quad (59)$$

Directly applying to (56) the Cornish-Fisher approximation [13] for the percentage points of the $z$-distribution in conjunction with Cochran's $\lambda$-corrections [15], we obtain (58) and the following two expressions for $\log\phi$:

$$\log\phi=2\left(\frac{K_\alpha}{\sqrt{h-\lambda_\alpha}}+\frac{K_\beta}{\sqrt{h-\lambda_\beta}}\right) \quad (60)$$

$$\log\phi=2\left(\frac{K_\alpha}{\sqrt{h-\lambda_\alpha}}+\frac{K_\beta}{\sqrt{h-\lambda_\beta}}\right)+\frac{1}{8}\left(\frac{1}{n_2}-\frac{1}{n_1}\right)(K_\alpha^2-K_\beta^2) \quad (61)$$

where $\lambda_\epsilon$ is given by

| $\epsilon$ | .75 | .50 | .25 | .05 | .01 |
|---|---|---|---|---|---|
| $\lambda_\epsilon$ | .5758 | .5000 | .5758 | .9509 | 1.4020 |

Formulas (58), (59), and (60) are not changed when $n_1$ and $n_2$ are interchanged. Formulas (60) and (61) are identical when either $\alpha=\beta$ or $n_1=n_2$, or both.

TABLE 7A.[a] *Comparison of the calculated (formula 61) and tabulated values of* $\varphi$ $(\alpha, \beta, n_1, n_2)$

$\alpha=.05$, $\beta=.05$

| $n_2$ \ $n_1$ | 5 | 10 | 15 | 20 | 30 | 60 |
|---|---|---|---|---|---|---|
| 5 | 26.312 | 15.674 | 13.082 | 11.918 | 10.844 | 9.839 |
| | **25.51** | **15.75** | **13.40** | **12.36** | **11.39** | **10.49** |
| 10 | 15.674 | 8.910 | 7.240 | 6.486 | 5.787 | 5.130 |
| | **15.75** | **8.870** | **7.237** | **6.513** | **5.844** | **5.223** |
| 15 | 13.082 | 7.240 | 5.787 | 5.130 | 4.516 | 3.937 |
| | **13.40** | **7.237** | **5.777** | **5.128** | **4.527** | **3.967** |
| 20 | 11.918 | 6.486 | 5.130 | 4.516 | 3.937 | 3.390 |
| | **12.36** | **6.513** | **5.128** | **4.512** | **3.939** | **3.402** |
| 30 | 10.844 | 5.787 | 4.516 | 3.937 | 3.390 | 2.866 |
| | **11.39** | **5.844** | **4.527** | **3.939** | **3.389** | **2.869** |
| 60 | 9.839 | 5.130 | 3.937 | 3.390 | 2.866 | 2.355 |
| | **10.49** | **5.223** | **3.967** | **3.402** | **2.869** | **2.354** |

[a] Figures in bold face type are taken from [4].

TABLE 7B.[a] *Comparison of calculated (formula 61) and tabulated values of* $\varphi$ $(\alpha, \beta, n_1, n_2)$

$\alpha=.01$, $\beta=.01$

| $n_2$ \ $n_1$ | 5 | 10 | 15 | 20 | 30 | 60 |
|---|---|---|---|---|---|---|
| 5 | 135.047 | 57.720 | 43.294 | 37.428 | 32.304 | 27.816 |
| | **120.3** | **56.65** | **44.29** | **39.19** | **34.69** | **30.72** |
| 10 | 57.720 | 23.863 | 17.434 | 14.791 | 12.474 | 10.436 |
| | **56.65** | **23.51** | **17.35** | **14.84** | **12.65** | **10.74** |
| 15 | 43.294 | 17.434 | 12.474 | 10.436 | 8.650 | 7.082 |
| | **44.29** | **17.34** | **12.41** | **10.41** | **8.679** | **7.168** |
| 20 | 37.428 | 14.791 | 10.436 | 8.650 | 7.082 | 5.697 |
| | **39.19** | **14.84** | **10.41** | **8.630** | **7.082** | **5.731** |
| 30 | 32.304 | 12.474 | 8.650 | 7.082 | 5.697 | 4.471 |
| | **34.69** | **12.65** | **8.679** | **7.082** | **5.695** | **4.479** |
| 60 | 27.816 | 10.436 | 7.082 | 5.697 | 4.471 | 3.372 |
| | **30.72** | **10.74** | **7.168** | **5.731** | **4.479** | **3.372** |

[a] Figures in bold face type are taken from [4].

TABLE 7c. *Comparison of calculated (formula 61) and tabulated values of* $\varphi$ $(\alpha, \beta, n_1, n_2)$

$\alpha = .05, \beta = .25$

| $n_2$ \ $n_1$ | 5 | 10 | 15 | 20 | 30 | 60 |
|---|---|---|---|---|---|---|
| 5 | 9.742 | 7.371 | 6.674 | 6.338 | 6.012 | 5.693 |
| | **9.569** | **7.507** | **6.900** | **6.609** | **6.327** | **6.052** |
| 10 | 6.345 | 4.632 | 4.112 | 3.837 | 3.607 | 3.359 |
| | **6.285** | **4.620** | **4.123** | **3.852** | **3.646** | **3.414** |
| 15 | 5.464 | 3.892 | 3.432 | 3.195 | 2.959 | 2.722 |
| | **5.469** | **3.902** | **3.428** | **3.197** | **2.969** | **2.741** |
| 20 | 5.061 | 3.578 | 3.116 | 2.886 | 2.655 | 2.421 |
| | **5.102** | **3.577** | **3.113** | **2.885** | **2.658** | **2.429** |
| 30 | 4.682 | 3.264 | 2.815 | 2.590 | 2.361 | 2.125 |
| | **4.759** | **3.273** | **2.815** | **2.589** | **2.361** | **2.127** |
| 60 | 4.325 | 2.964 | 2.526 | 2.303 | 2.072 | 1.828 |
| | **4.439** | **2.987** | **2.533** | **2.306** | **2.073** | **1.828** |

TABLE 8. *Values of* $\varphi$ $(\alpha, \beta, n_1, n_2)$ *from* $\log \varphi = (K_\alpha + K_\beta)\sqrt{2\left(\frac{1}{n_1 - 1} + \frac{1}{n_2 - 1}\right)}$

$\alpha = .05, \beta = .05$

| $n_2$ \ $n_1$ | 5 | 10 | 15 | 20 | 30 | 60 |
|---|---|---|---|---|---|---|
| 5 | 26.83 | 16.37 | 13.98 | 12.93 | 11.96 | 11.06 |
| 10 | 16.37 | 8.963 | 7.299 | 6.570 | 5.901 | 5.284 |
| 15 | 13.98 | 7.299 | 5.803 | 5.148 | 4.545 | 3.987 |
| 20 | 12.93 | 6.570 | 5.148 | 4.524 | 3.948 | 3.412 |
| 30 | 11.96 | 5.901 | 4.545 | 3.948 | 3.393 | 2.872 |
| 60 | 11.06 | 5.284 | 3.987 | 3.393 | 2.872 | 2.355 |

$\alpha = .01, \beta = .01$

| | | | | | | |
|---|---|---|---|---|---|---|
| 5 | 104.9 | 52.15 | 41.70 | 37.33 | 33.43 | 29.95 |
| 10 | 52.15 | 22.24 | 16.63 | 14.33 | 12.31 | 10.53 |
| 15 | 41.70 | 16.63 | 12.02 | 10.15 | 8.511 | 7.072 |
| 20 | 37.33 | 14.33 | 10.15 | 8.455 | 6.973 | 5.673 |
| 30 | 33.43 | 12.31 | 8.511 | 6.973 | 5.629 | 4.447 |
| 60 | 29.95 | 10.53 | 7.072 | 5.673 | 4.447 | 3.358 |

$\alpha = .05, \beta = .25$

| | | | | | | |
|---|---|---|---|---|---|---|
| 5 | 10.17 | 7.178 | 6.421 | 6.076 | 5.752 | 5.445 |
| 10 | 7.178 | 4.694 | 4.061 | 3.771 | 3.496 | 3.234 |
| 15 | 6.421 | 4.061 | 3.455 | 3.175 | 2.908 | 2.651 |
| 20 | 6.076 | 3.771 | 3.175 | 2.898 | 2.633 | 2.376 |
| 30 | 5.752 | 3.496 | 2.908 | 2.633 | 2.366 | 2.104 |
| 60 | 5.445 | 3.234 | 2.651 | 2.376 | 2.104 | 1.829 |

It appears on the basis of several computations (not given here) that formula (58) is likely to give values of $\phi$ that are much lower than its tabulated values [4], and consequently the sample sizes given by it will fall below the minimum desired. For $\alpha = \beta$ formula (61), then equivalent to (60), gives values of $\phi$ which are much closer to its tabulated values (table 7). This is also true of (61) for $\beta > \alpha$. If in addition to $\alpha = \beta$, $n_1 = n_2 = n$, then from (60)

$$n = \lambda\alpha + \Psi\left(\frac{K_\alpha + K_\beta}{\log \phi}\right)^2. \qquad (62)$$

We have not found any formula which will give an approximately correct answer for degrees of freedom as small as, say, $n_1 = n_2 = 5$. The question of finding appropriate sample sizes for $n_1 \neq n_2$ cannot ordinarily be answered without the help of tables. In such a situation, however, the experimentalist has no choice in the determination of $n_1$ and $n_2$. If it is decided in advance to maintain a certain ratio between $n_1$ and $n_2$ (this appears to be more often the case in practice) a formula would be more practical to use than the existing tables. Since formula (61) seems to be very complicated to use, we recommend the use of (59). Values of $\phi$ as given by this formula are given in table 8. It appears that for $\alpha = \beta = .05$, formula (59) will always give sufficient sample sizes; but for $\alpha = \beta = .01$, it will give values slightly less than actually needed.

---

This paper could not have been written without the constant encouragement of Churchill Eisenhart. The author acknowledges with pleasure the help given by Lola S. Deming and Celia S. Martin for doing the enormous computations. Thanks are also due to Elizabeth Shuhany of the Statistical Laboratory, Boston University, for some computational help.

## 8. References

[1] J. Neyman and B. Tokarska, Errors of the second kind in testing "Student's" hypotheses, J. Am. Stat. Assoc. **31,** 318 (1936).
[2] Charles D. Ferris, Frank E. Grubbs, and Chalmers L. Weaver, Operating characteristics for the common statistical tests of significance, Ann. Math. Stat. **17,** 178 (1946).
[3] J. H. Curtiss, Acceptance sampling by variables, with special reference to the case in which quality is measured by average or dispersion, J. Research, NBS **39,** 271 (1947) RP 1827.
[4] Churchill Eisenhart, Millard W. Hastay, and W. Allen Wallis, Selected techniques of statistical analysis (McGraw-Hill Book Co., Inc., New York, N. Y., 1947).
[5] J. Neyman, On the problem of most efficient tests of statistical hypotheses, Phil. Trans. Roy. Soc. **231,** 289 (1932–3).
[6] "Student" (W. S. Gossett), The probable error of a mean, Biometrika **6,** 1 (1908).
[7] K. Pearson, Tables for statisticians and biometricians, Part II (University of Cambridge, England, 1931).
[8] P. C. Tang, The power function of the analysis of variance tests with tables and illustrations of their use, Statistical Research Memoirs, Vol. **2** (University of London, 1938).
[9] E. Lehmer, Inverse tables of probability of errors of the "second kind", Ann. Math. Stat. **15,** 388 (1944).
[10] Uttam Chand, Distributions related to the comparison of two means and two regression coefficients, Ann. Math. Stat. **21,** 507 (1950).
[11] M. S. Bartlett and D. G. Kendall, The statistical analysis of variance heterogeneity and the logarithmic transformation, Supp. J. Roy. Stat. Soc. **8,** 128 (1946).
[12] E. T. Whittaker and G. M. Watson, A course of modern analysis, 4th ed. (Cambridge University Press, 1935).
[13] E. A. Cornish and R. A. Fisher, Moments and cumulants in the specification of distributions, Rev. Inst. Intl. Stat. **14,** 1 (1937).
[14] J. Wishart, The cumulants of the $z$ and of the logarithmic $\chi^2$ and $t$ distributions, Biometrika **34,** 170 (1947).
[15] W. G. Cochran, Note on an approximate formula for significance levels of $z$, Ann. Math. Stat. **11,** 93 (1940).
[16] R. A. Fisher, On the dominance ratio, Proc. Roy. Soc. Edinburgh, **42,** 321 (1921–22). See also [4] chapter 16.
[17] M. S. Bartlett, Square root transformation in analysis of variance, Suppl. J. Roy. Stat. Soc. **3,** 68 (1936). See also [4] chapter 16.
[18] R. A. Fisher, Statistical methods for research workers (Oliver and Boyd, Edinburgh).

## 9. Appendix. Tabular summary of single-sampling formulas for testing hypotheses

| Section in text | Form of population | $H_1$ null hypothesis | $H_2$ alternative hypothesis | Criterion for rejecting $H_1$ | Formula for determining $N$ | Formula for determining $K_\beta$ | Notes |
|---|---|---|---|---|---|---|---|
| 4.1 | Single binomial, mean $P$<br>Sample mean $p$ | $P=P_1$ | $P=P_2$<br>$(P_2>P_1)$ | $\theta>2\,\dfrac{K_\beta \sin^{-1}\sqrt{P_1}+K_\alpha \sin^{-1}\sqrt{P_2}}{K_\alpha+K_\beta}$<br>where $\theta=2\sin^{-1}\sqrt{p}$ | $N=\frac{1}{4}\left(\dfrac{K_\alpha+K_\beta}{\sin^{-1}\sqrt{P_2}-\sin^{-1}\sqrt{P_1}}\right)^2$ | $K_\beta=2\sqrt{N}(\sin^{-1}\sqrt{P_2}-\sin^{-1}\sqrt{P_1})-K_\alpha$ | |
| 4.2 | Two binomials, means $P$ and $P^*$<br>Sample means $p$ and $p^*$ | $P=P^*$ | $P<P^*$ | $\theta'>\dfrac{K_\alpha}{\sqrt{2N}}$<br>where $\theta'=\sin^{-1}\sqrt{p^*}-\sin^{-1}\sqrt{p}$ | $N=\frac{1}{2}\left(\dfrac{K_\alpha+K_\beta}{\sin^{-1}\sqrt{P^*}-\sin^{-1}\sqrt{P}}\right)^2$ | $K_\beta=\sqrt{2N}(\sin^{-1}\sqrt{P^*}-\sin^{-1}\sqrt{P})-K_\alpha$ | |
| 5.1 | Single Poisson, mean $m$<br>Sample mean $\bar{x}$ | $m=m_1$ | $m=m_2$<br>$(m_2>m_1)$ | $\bar{x}>\dfrac{K_\alpha\sqrt{m_2}+K_\beta\sqrt{m_1}}{K_\alpha+K_\beta}$ | $N=\frac{1}{4}\left(\dfrac{K_\alpha+K_\beta}{\sqrt{m_2}-\sqrt{m_1}}\right)^2$ | $K_\beta=2\sqrt{N}(\sqrt{m_2}-\sqrt{m_1})-K_\alpha$ | |
| 5.2 | Two Poissons, means $M$ and $M^*$<br>Sample means $\bar{x}$ and $\bar{x}^*$ | $M=M^*$ | $M<M^*$ | $\sqrt{\bar{x}^*}-\sqrt{\bar{x}}>\dfrac{K_\alpha}{\sqrt{2N}}$ | $N=\frac{1}{2}\left(\dfrac{K_\alpha+K_\beta}{\sqrt{M^*}-\sqrt{M}}\right)^2$ | $K_\beta=\sqrt{2N}(\sqrt{M^*}-\sqrt{M})-K_\alpha$ | |
| 6.1 | Single normal, mean $\mu$ | $\mu=\mu_1$<br>$\sigma^2=\sigma_0^2$<br>(known) | $\mu=\mu_2$<br>$(\mu_2>\mu_1)$<br>$\sigma^2=\sigma_0^2$ (known) | $\bar{x}>\dfrac{K_\alpha\mu_2+K_\beta\mu_1}{K_\alpha+K_\beta}$ | $N=\left(\dfrac{K_\alpha+K_\beta}{\Delta}\right)^2$ | $K_\beta=\Delta\sqrt{N}-K_\alpha$ | $\Delta=\dfrac{\mu_2-\mu_1}{\sigma_0}$ |
| 6.2 | Two normals, means $\mu_1$ and $\mu_2$ | $\mu_1=\mu_2$<br>$\sigma_2^2\neq\sigma_1^2$<br>(both known) | $\mu_1<\mu_2$<br>$\sigma_2^2\neq\sigma_1^2$<br>(both known) | $\bar{x}_2-\bar{x}_1>\dfrac{K_\alpha(\mu_2-\mu_1)}{K_\alpha+K_\beta}$ | $N=\left(\dfrac{K_\alpha+K_\beta}{d}\right)^2$ | $K_\beta=\sqrt{N}d-K_\alpha$ | $d=\dfrac{\mu_2-\mu_1}{\sqrt{\sigma_1^2+\sigma_2^2}}$ |
| 6.2 | Two normals, means $\mu_1$ and $\mu_2$ | $\mu_1=\mu_2$<br>$\sigma^2=\sigma_1^2=\sigma_2^2$<br>(known) | $\mu_1<\mu_2$<br>$\sigma^2=\sigma_1^2=\sigma_2^2$<br>(known) | $\bar{x}_2-\bar{x}_1>\dfrac{K_\alpha(\mu_2-\mu_1)}{K_\alpha+K_\beta}$ | $N=2\left(\dfrac{K_\alpha+K_\beta}{\Delta}\right)^2$ | $K_\beta=\Delta\sqrt{\dfrac{N}{2}}-K_\alpha$ | $\Delta=\dfrac{\mu_2-\mu_1}{\sigma}$ |
| 6.3 | Single normal, mean $\mu$; variance $\sigma^2$<br>$s^2$=estimate of $\sigma^2$ (unknown) | $\mu=\mu_1$ | $\mu=\mu_2$<br>$(\mu_2>\mu_1)$ | $(\bar{x}-\mu_1)-k\dfrac{s}{\sqrt{N}}>0,$<br>where $k=\dfrac{K_\alpha\Delta\sqrt{N}}{K_\alpha+K_\beta}$ | $N=\dfrac{b+\sqrt{b^2-4a}}{2a}$, or<br>$N=\dfrac{a+1+\sqrt{(a-1)^2+2ab}}{2a}$ | $K_\beta=\dfrac{\Delta}{\sqrt{N-1}}\left[N^2-N\left(1+\dfrac{K_\alpha^2}{2}\right)\right]^{\frac{1}{2}}-K_\alpha$ | $a=\left(\dfrac{\Delta}{K_\alpha+K_\beta}\right)^2$<br>$b=1+a\left(1+\dfrac{K_\alpha^2}{2}\right)$ |
| 6.4 | Two normals, means $\mu_1$ and $\mu_2$ | $\mu_1=\mu_2$ | $\mu_1<\mu_2$ | $(\bar{x}_2-\bar{x}_1)-k_1\sqrt{\dfrac{2}{N}}\,s>0,$<br>where $k_1=\sqrt{\dfrac{N}{2}}\cdot\dfrac{K_\alpha\Delta}{K_\alpha+K_\beta}$ | $N=\dfrac{b_1+\sqrt{b_1^2-8a}}{2a}$, or<br>$N=\dfrac{a+2+\sqrt{(a-2)^2+2ab_1(a)}}{2a}$ | $K_\beta=\Delta\left[\dfrac{N}{2}\left(1-\dfrac{K_\alpha^2}{4(N-1)}\right)\right]^{\frac{1}{2}}-K_\alpha$ | $a=\left(\dfrac{\Delta}{K_\alpha+K_\beta}\right)^2$<br>$b_1=2+a\left(1+\dfrac{K_\alpha^2}{4}\right)$ |
| 7.1 | Single normal, variance $\sigma^2$.<br>$s^2$=estimate of $\sigma^2$ | $\sigma^2=\sigma_0^2$ | $\sigma^2=\lambda\sigma_0^2$<br>$(\lambda>1)$ | $s>\dfrac{\sqrt{\lambda}\sigma_0(K_\alpha+K_\beta)}{K_\alpha+\sqrt{\lambda}K_\alpha}$ | $n=N-1=\frac{1}{2}\left(\dfrac{K_\alpha+K_\beta\sqrt{\lambda}}{\sqrt{\lambda}-1}\right)^2$ | $\lambda(\alpha,\beta,n)=\left(\dfrac{K_\alpha+\sqrt{2n}}{\sqrt{2n}-K_\beta}\right)^2$ | $n=N-1$<br>$\lambda=\dfrac{\sigma^2}{\sigma_0^2}$ |
| 7.2 | do | do | do | $\log s>\dfrac{K_\beta\log\sigma_1+K_\alpha\log\sqrt{\lambda}\,\sigma_1}{K_\beta+K_\beta}$<br>$+\frac{1}{2}\left(\psi\left(\frac{n}{2}\right)-\log\frac{n}{2}\right)$ | $\kappa_2(n)=\left(\dfrac{\log\frac{\sigma}{\sigma_1}}{K_\alpha+K_\beta}\right)^2$ | $\lambda(\alpha,\beta,n)=e^{2\sqrt{\kappa_2(n)}\,(K_\alpha+K_\beta)}$ | |
| 7.2 | do | do | do | do | $n=1+2\left(\dfrac{K_\alpha+K_\beta}{\log\lambda}\right)^2$ | $\log\lambda=\sqrt{\dfrac{2}{n-1}}\,(K_\alpha+K_\beta)$ | |
| 7.3 | Two normals, variances $\sigma_1^2$ and $\sigma_2^2$<br>$s_1^2$ and $s_2^2$=estimates of $\sigma_1^2$ and $\sigma_2^2$ | $\sigma_1^2=\sigma_2^2$ | $\sigma_1^2>\sigma_2^2$ | $\log\dfrac{s_1^2}{s_2^2}>\dfrac{1}{n_2}-\dfrac{1}{n_1}+\dfrac{K_\alpha}{K_\alpha+K_\beta}\log\phi$ | $\log\phi=(K_\alpha+K_\beta)$<br>$\times\left[2\left(\dfrac{1}{n_1-1}+\dfrac{1}{n_2-1}\right)\right]^{\frac{1}{2}}$ | | $\phi=\dfrac{\sigma_1^2}{\sigma_2^2}$ |
| 7.3 | do | do | do | do | $\log\phi=2\left(\dfrac{K_\alpha}{\sqrt{h-\lambda_\alpha}}+\dfrac{K_\beta}{\sqrt{h-\lambda_\beta}}\right)$ | | $h=\dfrac{2n_1n_2}{n_1+n}$ |
| 7.3 | do | do | do | do | $\log\phi=2\left(\dfrac{K_\alpha}{\sqrt{h-\lambda_\alpha}}+\dfrac{K_\beta}{\sqrt{h-\lambda_\alpha}}\right)$<br>$+\frac{1}{3}\left(\frac{1}{n_2}-\frac{1}{n_1}\right)K_\alpha^2-K_\beta^2$ | | |

Journal of Research of the National Bureau of Standards Vol. 47, No. 6, December 1951 Research Paper 2278

# Asymmetries of Zeeman Patterns and g-Values for Neutral Manganese[1]

Miguel A. Catalán [2]

Spectrograms of manganese made at the Massachusetts Institute of Technology with fields in excess of 84,000 oersteds show many lines that exhibit various degrees of distortion in both the positions and the intensities of the magnetic components. The interpretation of these asymmetric patterns has been made by the approximate theory of the partial Paschen-Back effect. The $g$-values that have been derived for several energy levels of Mn I are found to conform, in most cases, with those required for $LS$-coupling. A few exceptions to this rule have been considered in some detail. General tables have been computed, which will permit explanation of the distortions in other spectra.

## 1. Introduction

Ever since the discovery of the splitting of spectral lines by a magnetic field (Zeeman effect) the observers have called attention to the fact that some of the patterns are asymmetrical, the distances between their magnetic components being not rigorously equal. These asymmetries make it difficult to compute the $g$-factors that govern the splitting. Two early examples of asymmetric patterns are given by Martinez Risco [1],[3] and by Back and Landé [2].

At that time it was impossible to determine which of these different separations between magnetic components ought to be used as coefficients in the equations for obtaining the $g$-values of the atomic levels. Back adopted an empirical procedure, which is described in his paper on manganese [3]. This procedure has since been much used because in many cases it gives values in complete agreement with the $LS$-coupling values.

In recent years some authors, who have had the opportunity of measuring the beautiful plates made at the Massachusetts Institute of Technology by Harrison and his collaborators using magnetic fields of about 85,000 oersteds, have again called attention to the fact that some of the patterns are very asymmetrical [4].

The author of this paper, who is at present working on the structure of the manganese spectrum, has measured some excellent plates made at MIT in 1939. The measurements indicate that many of the patterns are more or less asymmetrical, and that these asymmetries affect the $g$-values by as much as a few percent depending on the rules adopted to calculate the average separation between components. On these plates many of the most interesting asymmetric lines appear too weak to be measured accurately, some of the faint components being absent in many cases. It was, therefore, decided to obtain new, long-exposure spectrograms of the manganese spectrum in the magnetic field.

The large Bitter magnet of the MIT, which had not been in operation since the war, was again put to work (not, however, without considerable trouble) by J. C. van den Bosch and the writer with the help of G. R. Harrison's assistants. A beautiful set of plates in which the interesting asymmetric patterns appear strongly was then secured. The procedure employed in making the spectrograms is that described by Harrison and his collaborators [5].

The electrodes for these plates were prepared by compressing powdered manganese with silver dust. The manganese was prepared by an electrolytic process and presented to us by W. F. Meggers. It was extremely pure.

The accurate measurements of these spectrograms by the author have permitted him to ascertain the cause of the observed asymmetries and at the same time to deduce the best procedure to eliminate the distortion in the computation of $g$-values. These distortions in the magnetic patterns appear in both the positions and the intensities of the components. In the following we shall describe first the asymmetries of the positions and later we shall consider the perturbations in the intensities.

## 2. Experimental Asymmetrical Patterns

The pattern for the line $a\,^6D_{1\frac{1}{2}} - z\,^6D^\circ_{2\frac{1}{2}} = 24485.25$ $cm^{-1}$ of Mn I, at 4082.945 A, obtained experimentally shows *unequally spaced* components. Irregular intervals between adjacent components are found both in the $\pi$- and $\sigma$-components. This is an example of an *asymmetrical pattern*, which contrasts with the symmetrical ones generally described. In table 1 the theoretical values of the wave numbers of the components are compared with the observed values [6] for this line. The experimental intervals, although irregular, show curious regularities. Any cause to which the asymmetry of the pattern may reasonably be ascribed will not alter the validity of the combination principle. This means that the displacements observed in the magnetic lines will be due to displacements of the magnetic levels involved. *A perturbed level will show the same displacement in all lines that originate in it.* Double-array tables will then be suitable to represent an asymmetrical pattern, and in such tables the magnetic levels will appear with their displacements.

[1] This research was carried out during the author's visits to the United States 1948–49 and 1950–51. It was made possible by grants from the American Academy of Arts and Sciences, the American Philosophical Society, Princeton University, and Massachusetts Institute of Technology, and also through the cooperation of the National Bureau of Standards.

[2] Present address, University of Madrid, Madrid, Spain.

[3] Figures in brackets indicate the literature references at the end of this paper.

TABLE 1. *Theoretical and observed components of 24485.25 cm$^{-1}$ of* Mn I

[Lorentz Unit $a$=3.955 cm$^{-1}$]

| Polarization | Theoretical unperturbed wave number, $\nu$ | Interval, $\Delta\nu$ | Observed perturbed wave number, $\nu$ | Interval, $\Delta\nu$ |
|---|---|---|---|---|
| $\sigma$ | 24477. 45 | | 24477. 18 | |
| | | *0. 83* | | *1. 14* |
| $\sigma$ | 24478. 28 | | 24478. 32 | |
| | | *0. 83* | | *0. 89* |
| $\sigma$ | 24479. 11 | | 24479. 21 | |
| | | *0. 84* | | *0. 67* |
| $\sigma$ | 24479. 95 | | 24479. 88 | |
| $\pi$ | 24484. 00 | | 24483. 83 | |
| | | *0. 84* | | *1. 05* |
| $\pi$ | 24484. 84 | | 24484. 88 | |
| | | *0. 82* | | *0. 84* |
| $\pi$ | 24485. 66 | | 24485. 72 | |
| | | *0. 84* | | *0. 60* |
| $\pi$ | 24486. 50 | | 24486. 32 | |
| $\sigma$ | 24490. 55 | | 24490. 49 | |
| | | *0. 84* | | *1. 00* |
| $\sigma$ | 24491. 39 | | 24491. 49 | |
| | | *0. 83* | | *0. 74* |
| $\sigma$ | 24492. 22 | | 24492. 23 | |
| | | *0. 83* | | *0. 61* |
| $\sigma$ | 24493. 05 | | 24492. 84 | |

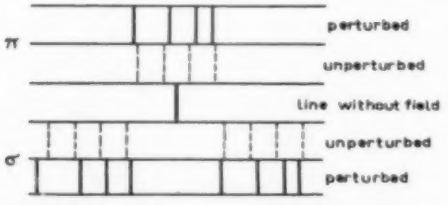


FIGURE 1. *Comparison of positions of components in a perturbed and an unperturbed pattern.*

In a perturbed pattern either the $\pi$- or the $\sigma$-components are unequally spaced, in contrast to the unperturbed pattern.

Figure 1 indicates the positions of perturbed and unperturbed components in an imaginary example.

The wave numbers in table 2 are *experimental values* that give the adopted values for the displaced levels from which the wave numbers of the components have been recalculated. The decimal parts of the resulting values are listed in table 2 under the corresponding observed value for comparison. The close agreement between calculated and observed values in table 2 proves the *validity of the combination principle* when applied to an asymmetrical pattern and hence the possibility of computing values for the displaced levels with the observed wave numbers.

The observed intervals between the consecutive magnetic levels are thus unequal, being 7.09, 7.39, and 7.67 for $a\,{}^6D_{1½}$, and 6.43, 6.50, 6.54, 6.62, and 6.67 for $z\,{}^6D^\circ_{2½}$. The differences, in both cases, cannot be ascribed to experimental errors but are clearly due to an asymmetry.

At the bottom of table 2 the pattern for another line $a\,{}^6D_{1½}-z\,{}^6D^\circ_{0½}$ is included. This Mn I line has the level $a\,{}^6D_{1½}$ in common with the other. From the observed components one may calculate the perturbed magnetic levels as before. The resulting values for the magnetic levels belonging to $a\,{}^6D_{1½}$ are exactly the same as those for the line 24485.25 and hence show the same perturbed intervals 7.09, 7.39, 7.67. Many other examples could be presented to prove the existence of asymmetrical patterns. All of them show the same singularities. The irregularities in the displacements are exactly the same for all lines having their origins in the level involved.

## 3. Asymmetrical Pattern in Theory

In 1913, while observing the Zeeman effect of the line 6708 A of lithium, Paschen and Back found that the observed pattern was in complete contradiction with the Preston rule. It is a close doublet, and there is a sort of interaction between the effects of the two lines forming it. Similar results were obtained for other close doublets and triplets, although lines that are not organically connected do not show this effect, even though their wavelengths may be very close to each other. This interaction was called the Paschen-Back effect. In some cases the observed Zeeman patterns for very close multiplets exhibit a sort of distortion due to *partial Paschen-Back effect*, the field in these cases not being strong enough for a complete interaction but only sufficient to alter the normal pattern.

The theory of the Paschen-Back effect has been developed in detail by different authors. Kiess and Shortley [7] have recently considered the distorted patterns in the oxygen and nitrogen spectra, and have found a quantitative theoretical explanation of them. The multiplets $3s\,{}^3S^\circ-3p\,{}^3P$ and $3s\,{}^5S^\circ-3p\,{}^5P$ of O I at 8446 and 7771 A with the narrow intervals 0.5, 0.7 and 2.0, 3.7 cm$^{-1}$ show a great distortion.

TABLE 2. *Observed perturbed patterns for lines 24485.25 and 24630.08 of* Mn I

[LU = 3.955 cm$^{-1}$; levels 42053.73, 42198.56, and 17568.48]

| $M$ | Level | $a^6D_{1/2}$ | | | | | | | |
|---|---|---|---|---|---|---|---|---|---|
| | | $M=-1\frac{1}{2}$ | | $M=-0\frac{1}{2}$ | | $M=0\frac{1}{2}$ | | $M=1\frac{1}{2}$ | |
| | | 17557.53 | *7.09* | 17564.62 | *7.39* | 17572.01 | *7.67* | 17579.68 | |
| $-2\frac{1}{2}$ | 42037.41 | 24479.88 | | | | | | | |
| | | .88 | | | | | | | |
| | *6.43* | | | | | | | | |
| $-1\frac{1}{2}$ | 42043.84 | 24486.32 | *7.11* | 24479.21 | | | | | |
| | | .31 | | .22 | | | | | |
| | *6.50* | | | | | | | | |
| $-0\frac{1}{2}$ | 42050.34 | 24492.84 | *7.12* | 24485.72 | *7.40* | 24478.32 | | | |
| $z\ ^6D^o_{3/2}$ | | .81 | | .72 | | .33 | | | |
| | *6.54* | | | | | | | | |
| $0\frac{1}{2}$ | 42056.88 | | | 24492.23 | *7.35* | 24484.88 | *7.70* | 24477.18 | |
| | | | | .26 | | .87 | | .20 | |
| | *6.62* | | | | | | | | |
| $1\frac{1}{2}$ | 42063.50 | | | | | 24491.49 | *7.66* | 24483.83 | |
| | | | | | | .49 | | .82 | |
| | *6.67* | | | | | | | | |
| $2\frac{1}{2}$ | 42070.17 | | | | | | | 24490.49 | |
| | | | | | | | | .49 | |
| $-0\frac{1}{2}$ | 42192.45 | 24634.93 | *7.09* | 24627.84 | *7.42* | 24620.42 | | | |
| $z\ ^6D^o_{5/2}$ | | .92 | | .83 | | .44 | | | |
| | *13.10* | | | | | | | | |
| $0\frac{1}{2}$ | 42205.55 | | | 24640.91 | *7.37* | 24633.54 | *7.67* | 24625.87 | |
| | | | | .93 | | .54 | | .87 | |

The multiplet of N I, $3s\ ^4P-3p\ ^4S^\circ$ at 7423 to 7468 A, with greater intervals, namely 46.7, 33.8, shows much smaller distortion. The results of Kiess and Shortley for N I, in a multiplet with the relatively wide separations, 46.7 and 33.8, indicate clearly that multiplets with *relatively great intervals*, in other elements, could be expected to show also measurable Paschen-Back interaction. This conclusion suggested to the writer the likelihood that the observed distortions in Mn I are due to a similar effect. In order to prove this hypothesis the structure of the levels so affected was considered in some detail.

According to the second order perturbation theory [7, p. 204] magnetic levels having the same magnetic numbers $M$, and belonging to spectroscopic levels which differ by one unit in $J$-value, and to the same term, repel each other by an amount, $\epsilon$, equal to

$$\epsilon=\frac{I^2}{\delta}, \tag{1}$$

all quantities being expressed in Lorentz units. In this formula $\delta$ is the distance between the two magnetic levels under consideration. Within the accuracy of eq 1 $\delta$ represents either the perturbed or the unperturbed distance. The factor $I$ is the interaction element; its values depend only on the particular values of $S$, $L$, $J$, and $M$ for the levels involved. Equation 2 gives the dependence of $I$ on the quantum numbers in Lorentz units, LU:

$$I=\sqrt{\frac{(J-L+S)(J+L-S)(L+S+1+J)(L+S+1-J}{4J^2(2J-1)(2J+1)}}\sqrt{J^2-M^2}. \tag{2}$$

Here the value $J$ is the larger of the two $J$-values involved. The energy perturbation is to be applied to each of the states always in the repulsive direction. If more than two states interact, the perturbations of each pair may be supposed to operate independently.

The writer has computed with formula (2) the values of $I^2$ and $I$ for the different cases. The resulting values are given in table 3 with the $I$-values above and the $I^2$-values below. In general the values of the interaction element increase when either $S$ or $L$ increases and decrease when either $J$ or $M$ increases. Hence the greatest interactions are expected in terms of high multiplicities and high $L$-values, and, within a term, the greatest interactions may be expected in the levels with smaller $J$- and $M$-values. A very important conclusion is that the sign of $M$ does not affect the $I$-values because $M$ appears in eq 2 as a square. The same $I$ factor corresponds to level $(+M)$ as to $(-M)$

Because the measured distances betweeen magnetic components and, therefore, the level-separations are expressed in wave numbers, cm$^{-1}$, it is desirable to express the values of $I$ in the same units. This is done by multiplication by the Lorentz unit (LU), which is $a=4.669\times10^{-5}\,H$ cm$^{-1}$,

TABLE 3. *Values for the interaction element, I, and its squares*

[Upper figures are *I*-values in Lorentz units; lower $I^2$-values, in $(LU)^2$]

| Even multiplicities | | | | | |
|---|---|---|---|---|---|
| Interaction between— | $M(\pm)$ | | | | |
| | $0^1/_2$ | $1^1/_2$ | $2^1/_2$ | $3^1/_2$ | $4^1/_2$ |
| $^2P_{1^1/_2}$ and $^2P_{0^1/_2}$ | 0.471<br>0.222 | ------ | ------ | ------ | ------ |
| $^2D_{2^1/_2}$ and $^2D_{1^1/_2}$ | 0.490<br>0.240 | 0.400<br>0.160 | ------ | ------ | ------ |
| $^2F_{3^1/_2}$ and $^2F_{2^1/_2}$ | 0.495<br>0.245 | 0.452<br>0.204 | 0.350<br>0.122 | ------ | ------ |
| $^4P_{1^1/_2}$ and $^4P_{0^1/_2}$ | 0.745<br>0.556 | ------ | ------ | ------ | ------ |
| $^4P_{2^1/_2}$ and $^4P_{1^1/_2}$ | 0.600<br>0.360 | 0.490<br>0.240 | ------ | ------ | ------ |
| $^4D_{1^1/_2}$ and $^4D_{0^1/_2}$ | 1.000<br>1.000 | ------ | ------ | ------ | ------ |
| $^4D_{2^1/_2}$ and $^4D_{1^1/_2}$ | 0.916<br>0.840 | 0.748<br>0.560 | ------ | ------ | ------ |
| $^4D_{3^1/_2}$ and $^4D_{2^1/_2}$ | 0.700<br>0.490 | 0.639<br>0.408 | 0.495<br>0.245 | ------ | ------ |
| $^4F_{2^1/_2}$ and $^4F_{1^1/_2}$ | 0.980<br>0.960 | 0.800<br>0.640 | ------ | ------ | ------ |
| $^4F_{3^1/_2}$ and $^4F_{2^1/_2}$ | 0.958<br>0.918 | 0.875<br>0.765 | 0.678<br>0.459 | ------ | ------ |
| $^4F_{4^1/_2}$ and $^4F_{3^1/_2}$ | 0.745<br>0.556 | 0.707<br>0.500 | 0.624<br>0.389 | 0.471<br>0.222 | ------ |
| $^4G_{3^1/_2}$ and $^4G_{2^1/_2}$ | 0.958<br>0.918 | 0.875<br>0.765 | 0.678<br>0.459 | ------ | ------ |
| $^4G_{4^1/_2}$ and $^4G_{3^1/_2}$ | 0.975<br>0.951 | 0.925<br>0.856 | 0.816<br>0.665 | 0.617<br>0.380 | ------ |
| $^4G_{5^1/_2}$ and $^4G_{4^1/_2}$ | 0.771<br>0.595 | 0.745<br>0.555 | 0.690<br>0.476 | 0.598<br>0.357 | 0.445<br>0.198 |
| $^6P_{2^1/_2}$ and $^6P_{1^1/_2}$ | 0.748<br>0.560 | 0.611<br>0.373 | ------ | ------ | ------ |
| $^6P_{3^1/_2}$ and $^6P_{2^1/_2}$ | 0.639<br>0.408 | 0.583<br>0.340 | 0.452<br>0.204 | ------ | ------ |
| $^6D_{1^1/_2}$ and $^6D_{0^1/_2}$ | 1.247<br>1.556 | ------ | ------ | ------ | ------ |
| $^6D_{2^1/_2}$ and $^6D_{1^1/_2}$ | 1.200<br>1.440 | 0.980<br>0.960 | ------ | ------ | ------ |
| $^6D_{3^1/_2}$ and $^6D_{2^1/_2}$ | 1.050<br>1.102 | 0.958<br>0.918 | 0.742<br>0.551 | ------ | ------ |
| $^6D_{4^1/_2}$ and $^6D_{3^1/_2}$ | 0.786<br>0.617 | 0.745<br>0.556 | 0.657<br>0.432 | 0.497<br>0.247 | ------ |
| $^6F_{1^1/_2}$ and $^6F_{0^1/_2}$ | 1.491<br>2.222 | ------ | ------ | ------ | ------ |
| $^6F_{2^1/_2}$ and $^6F_{1^1/_2}$ | 1.470<br>2.160 | 1.200<br>1.440 | ------ | ------ | ------ |
| $^6F_{3^1/_2}$ and $^6F_{2^1/_2}$ | 1.355<br>1.837 | 1.237<br>1.531 | 0.958<br>0.918 | ------ | ------ |

TABLE 3. *Values for the interaction element, I, and its squares*—Continued

[Upper figures are $I$-values in Lorentz units; lower $I^2$-values, in $(LU)^2$]

| Even multiplicities | | | | | |
|---|---|---|---|---|---|
| Interaction between— | $M(\pm)$ | | | | |
| | $0^1_2$ | $1^1_2$ | $2^1_2$ | $3^1_2$ | $4^1_2$ |
| $^6F_{0\frac{1}{2}}$ and $^6F_{2\frac{1}{2}}$ | 1.165<br>1.358 | 1.086<br>1.179 | 0.975<br>0.951 | 0.737<br>0.543 | ------- |
| $^6F_{1\frac{1}{2}}$ and $^6F_{0\frac{1}{2}}$ | 0.862<br>0.744 | 0.833<br>0.694 | 0.771<br>0.595 | 0.668<br>0.446 | 0.498<br>0.248 |
| $^6G_{2\frac{1}{2}}$ and $^6G_{1\frac{1}{2}}$ | 1.414<br>2.000 | 1.155<br>1.333 | ------- | ------- | ------- |
| $^6G_{1\frac{1}{2}}$ and $^6G_{2\frac{1}{2}}$ | 1.498<br>2.245 | 1.368<br>1.871 | 1.059<br>1.122 | ------- | ------- |
| $^6G_{4\frac{1}{2}}$ and $^6G_{3\frac{1}{2}}$ | 1.414<br>2.000 | 1.342<br>1.800 | 1.183<br>1.400 | 0.894<br>0.800 | ------- |
| $^6G_{3\frac{1}{2}}$ and $^6G_{4\frac{1}{2}}$ | 1.226<br>1.504 | 1.185<br>1.404 | 1.097<br>1.203 | 0.950<br>0.903 | 0.708<br>0.501 |
| $^6G_{6\frac{1}{2}}$ and $^6G_{5\frac{1}{2}}$ | 0.910<br>0.828 | 0.888<br>0.789 | 0.843<br>0.710 | 0.769<br>0.592 | 0.659<br>0.434 |

| Odd multiplicities | | | | | | |
|---|---|---|---|---|---|---|
| Interaction between— | $M(\pm)$ | | | | | |
| | 0 | 1 | 2 | 3 | 4 | 5 |
| $^3P_1$ and $^3P_0$ | 0.817<br>0.667 | ------- | ------- | ------- | ------- | ------- |
| $^3P_2$ and $^3P_1$ | 0.577<br>0.333 | 0.500<br>0.250 | ------- | ------- | ------- | ------- |
| $^3D_2$ and $^3D_1$ | 0.775<br>0.600 | 0.671<br>0.450 | ------- | ------- | ------- | ------- |
| $^3D_3$ and $^3D_2$ | 0.632<br>0.400 | 0.596<br>0.356 | 0.471<br>0.222 | ------- | ------- | ------- |
| $^3F_2$ and $^3F_2$ | 0.756<br>0.571 | 0.713<br>0.508 | 0.563<br>0.318 | ------- | ------- | ------- |
| $^3F_4$ and $^3F_3$ | 0.655<br>0.429 | 0.634<br>0.402 | 0.567<br>0.321 | 0.433<br>0.188 | ------- | ------- |
| $^3G_4$ and $^3G_3$ | 0.745<br>0.556 | 0.722<br>0.521 | 0.646<br>0.417 | 0.493<br>0.243 | ------- | ------- |
| $^3G_5$ and $^3G_4$ | 0.667<br>0.444 | 0.653<br>0.428 | 0.611<br>0.373 | 0.533<br>0.284 | 0.400<br>0.160 | ------- |
| $^5P_2$ and $^5P_1$ | 0.775<br>0.600 | 0.671<br>0.450 | ------- | ------- | ------- | ------- |
| $^5P_3$ and $^5P_2$ | 0.632<br>0.400 | 0.596<br>0.356 | 0.471<br>0.222 | ------- | ------- | ------- |
| $^5D_1$ and $^5D_0$ | 1.414<br>2.000 | ------- | ------- | ------- | ------- | ------- |
| $^5D_2$ and $^5D_1$ | 1.183<br>1.400 | 1.025<br>1.050 | ------- | ------- | ------- | ------- |
| $^5D_3$ and $^5D_2$ | 1.014<br>1.029 | 0.956<br>0.914 | 0.756<br>0.571 | ------- | ------- | ------- |
| $^5D_4$ and $^5D_3$ | 0.756<br>0.571 | 0.732<br>0.536 | 0.655<br>0.429 | 0.500<br>0.250 | ------- | ------- |

TABLE 3. *Values for the interaction element, I, and its squares*—Continued

[Upper figures are $I$-values in Lorentz units; lower $I^2$-values, in $(LU)^2$]

| Odd multiplicities | | | | | | |
|---|---|---|---|---|---|---|
| Interaction between— | $M(\pm)$ | | | | | |
| | 0 | 1 | 2 | 3 | 4 | 5 |
| $^5F_2$ and $^5F_1$ | 1.265<br>1.600 | 1.095<br>1.200 | ------<br>------ | ------<br>------ | ------<br>------ | ------<br>------ |
| $^5F_3$ and $^5F_2$ | 1.242<br>1.543 | 1.171<br>1.371 | 0.926<br>0.857 | ------<br>------ | ------<br>------ | ------<br>------ |
| $^5F_4$ and $^5F_3$ | 1.091<br>1.190 | 1.056<br>1.116 | 0.945<br>0.893 | 0.722<br>0.521 | ------<br>------ | ------<br>------ |
| $^5F_5$ and $^5F_4$ | 0.816<br>0.667 | 0.805<br>0.640 | 0.748<br>0.560 | 0.653<br>0.427 | 0.490<br>0.240 | ------<br>------ |
| $^5G_3$ and $^5G_2$ | 1.195<br>1.429 | 1.127<br>1.270 | 0.891<br>0.794 | ------<br>------ | ------<br>------ | ------<br>------ |
| $^5G_4$ and $^5G_3$ | 1.254<br>1.571 | 1.214<br>1.473 | 1.086<br>1.179 | 0.829<br>0.688 | ------<br>------ | ------<br>------ |
| $^5G_5$ and $^5G_4$ | 1.101<br>1.273 | 1.105<br>1.222 | 1.034<br>1.069 | 0.903<br>0.815 | 0.677<br>0.458 | ------<br>------ |
| $^5G_6$ and $^5G_5$ | 0.853<br>0.727 | 0.841<br>0.707 | 0.804<br>0.647 | 0.739<br>0.546 | 0.636<br>0.404 | 0.471<br>0.222 |
| $^7P_3$ and $^7P_2$ | 0.756<br>0.571 | 0.713<br>0.508 | 0.563<br>0.318 | ------<br>------ | ------<br>------ | ------<br>------ |
| $^7P_4$ and $^7P_3$ | 0.655<br>0.429 | 0.634<br>0.402 | 0.567<br>0.321 | 0.433<br>0.188 | ------<br>------ | ------<br>------ |
| $^7D_2$ and $^7D_1$ | 1.265<br>1.600 | 1.095<br>1.200 | ------<br>------ | ------<br>------ | ------<br>------ | ------<br>------ |
| $^7D_3$ and $^7D_2$ | 1.242<br>1.543 | 1.171<br>1.371 | 0.926<br>0.857 | ------<br>------ | ------<br>------ | ------<br>------ |
| $^7D_4$ and $^7D_3$ | 1.091<br>1.191 | 1.056<br>1.116 | 0.945<br>0.893 | 0.722<br>0.521 | ------<br>------ | ------<br>------ |
| $^7D_5$ and $^7D_4$ | 0.816<br>0.667 | 0.800<br>0.640 | 0.748<br>0.560 | 0.653<br>0.427 | 0.490<br>0.240 | ------<br>------ |
| $^7F_1$ and $^7F_0$ | 2.000<br>4.000 | ------<br>------ | ------<br>------ | ------<br>------ | ------<br>------ | ------<br>------ |
| $^7F_2$ and $^7F_1$ | 1.732<br>3.000 | 1.500<br>2.250 | ------<br>------ | ------<br>------ | ------<br>------ | ------<br>------ |
| $^7F_3$ and $^7F_2$ | 1.604<br>2.573 | 1.512<br>2.286 | 1.195<br>1.429 | ------<br>------ | ------<br>------ | ------<br>------ |
| $^7F_4$ and $^7F_3$ | 1.447<br>2.095 | 1.402<br>1.964 | 1.254<br>1.571 | 0.957<br>0.917 | ------<br>------ | ------<br>------ |
| $^7F_5$ and $^7F_4$ | 1.231<br>1.515 | 1.206<br>1.455 | 1.128<br>1.273 | 0.985<br>0.970 | 0.739<br>0.546 | ------<br>------ |
| $^7F_6$ and $^7F_5$ | 0.905<br>0.818 | 0.892<br>0.796 | 0.853<br>0.727 | 0.783<br>0.614 | 0.674<br>0.455 | 0.500<br>0.250 |

$H$ being the field strength in oersteds.

If the repulsion in this case is $e$, and the separation is $\Delta$, eq 1 can be written

$$e=\frac{I^2}{\Delta}a^2 \text{ cm}^{-1}, \quad (3)$$

where

$$a^2=(4.669\times10^{-5}H)^2=21.80\times10^{-10}H^2 \text{ cm}^{-2}. \quad (4)$$

Since $I^2$ is a function of $M^2$, in the following the factor $I^2/\Delta$ will be set as $f(M_J^2)$. In this notation

eq 3 will be

$$\epsilon = a^2 f(M_J^2). \tag{5}$$

The values of function $f$ being the same for $(+M)$ as for $(-M)$, we can write

$$f(M_J^2) = f[(-M)_J^2]. \tag{6}$$

Before we proceed to the computation of the effects for some Mn I lines it is of interest to estimate roughly the intervals between levels necessary to obtain measurable distortions, with a magnetic field of about 80,000 oersteds, which is close to the fields used for our spectrograms.

From eq 3 and 4 we can write

$$\Delta = \frac{I^2}{\epsilon} a^2 = \frac{I^2}{\epsilon} 21.80 \times 10^{-10} \times 80{,}000^2 = \frac{I^2}{\epsilon} \times 17 \text{ cm}^{-1}. \tag{7}$$

The accuracy of the measured wave numbers evidently depends on the region of the spectrum. At about 25,000 $\text{cm}^{-1}$ (4,000 Å) the accuracy, in the MIT spectrograms, is close to 0.05 $\text{cm}^{-1}$. This is the minimum value that $\epsilon$ can have if measurable effects are to be observed. We can then write

$$\Delta = \frac{17}{0.05} I^2 \simeq 340 I^2 \text{ cm}^{-1}. \tag{8}$$

Equation 8 is a relation between the interval $\Delta$ and the interaction factor. If we select a transition for which $I^2$ is approximately one unit (see table 3), observable effects will be possible with intervals $\Delta$ smaller than 340 $\text{cm}^{-1}$. In cases in which the $I^2$-values are greater than one unit, such as those in the $^6$D and $^6$F terms, much wider intervals will still show asymmetries. Because the term intervals in Mn I rarely exceed 200 $\text{cm}^{-1}$, it is possible to find many asymmetries in it.

The foregoing estimate shows clearly why so many asymmetries have been noted in the past by observers of the Zeeman effect. The asymmetrical patterns belong not only to the spectra of the light elements that have narrow term intervals, but also to elements of high atomic numbers whose term intervals are much wider. In these cases the $I^2$-values are sufficiently great for the intervals to show measurable asymmetries.

## 4. Positions of Magnetic Levels Affected by Partial Paschen-Back Effect

A spectroscopic level $T_J$, by influence of the magnetic field, is split up into $2J+1$ magnetic levels $T_J^M$, whose values are given by

$$T_J^M = T_J + M_J a g_J.$$

We shall consider first the simplest case in which only one other level, $T_{J-1}$, exists close to the level $T_J$ of the same term. Suppose that the relative value of $T_J$ is smaller than that of $T_{J-1}$. The magnetic levels of $T_J$ will be lowered in value by the repulsions due to the magnetic levels of $T_{J-1}$. The amounts of these displacements are given by eq 5 so that the final values of these perturbed magnetic levels $T'^M_J$ will be

$$T'^M_J = T_J + M_J a g_J - a^2 f(M_J^2). \tag{9}$$

The whole set of magnetic levels of $T_J$ is lowered in value because the repulsions are all in the same direction; the magnitudes of these displacements are different for the individual levels on account of the different values that the function $f(M_J^2)$ has for different $M_J$-values. Figure 2 illustrates the relative positions of the perturbed magnetic levels of $T_J$, compared with the unperturbed positions.

Levels with the same $M$-value have the same displacement independent of the sign of $M$; thus, all levels $M = \pm 0\frac{1}{2}$ have experienced a displacement $a$, and all with $M = \pm 1\frac{1}{2}$ have been displaced by an amount $b$. The direction of the displacements in $T_{2\frac{1}{2}}$ is contrary to that in $T_{1\frac{1}{2}}$. Levels $M = \pm 2\frac{1}{2}$ have not experienced displacement because there are no magnetic levels with such $M$-values in the level $T_{1\frac{1}{2}}$.

The intervals between consecutive magnetic levels, such as those having magnetic quantum values $M_J$ and $M_J - 1$, may be computed by eq 9. The resulting value is

$$\Delta T'^{M, M-1}_{J, J} = [M_J - (M_J - 1)] a g_J - a^2 f(M_J^2) + a^2 f[(M_J - 1)^2],$$

or

$$\Delta T'^{M, M-1}_{J, J} = a g_J - a^2 f(M_J^2) + a^2 f[(M_J - 1)^2]. \tag{10}$$

The intervals are unequal because of the influence of the quadratic terms, which have different values for the different $M$-values. Figure 2 shows clearly this inequality. The pertrubed magnetic levels appear to approach each other in the opposite direction of the perturbing level.

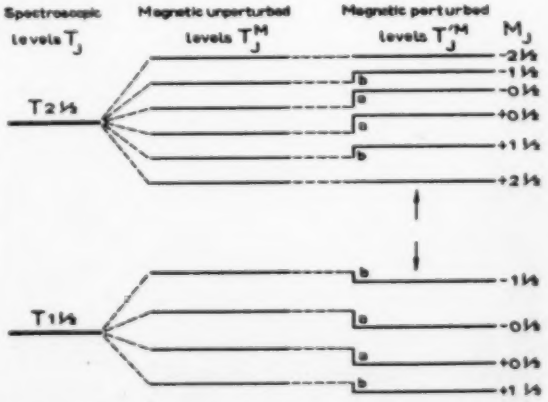


FIGURE 2. *Mutual repulsions between the magnetic levels of $T_{2\frac{1}{2}}$ and $T_{1\frac{1}{2}}$*

The magnetic levels with the same $M$-value repel each other. The magnitude of the displacements $a$ or $b$, due to the repulsion, depends on the absolute value of $M$, but is independent of the *sign* of $M$.

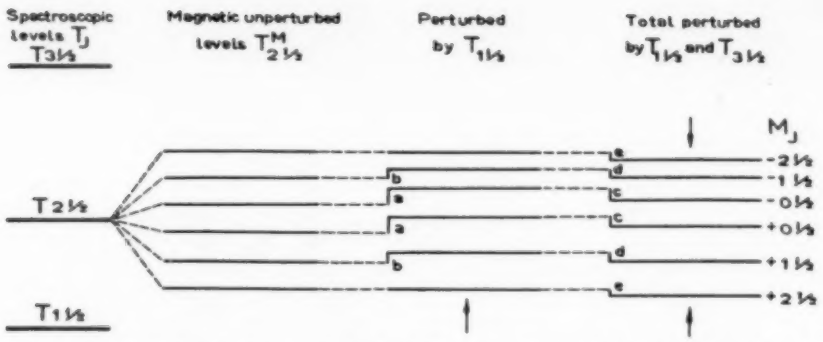


FIGURE 3. *Perturbation of magnetic levels of $T_{2\frac{1}{2}}$ due to the proximity of the magnetic levels of $T_{1\frac{1}{2}}$ and $T_{3\frac{1}{2}}$.*

The perturbations that arise from $T_{1\frac{1}{2}}$ and $T_{3\frac{1}{2}}$ may be considered to act independently. By influence of the magnetic levels of $T_{1\frac{1}{2}}$ those of $T_{2\frac{1}{2}}$ are displacedupward by amounts $a$ or $b$. These partially perturbed levels are displaced downward by amounts $c$, $d$, or $e$, by influence of magnetic levels of $T_{3\frac{1}{2}}$.

The separations between two magnetic levels having the same $M$-value but different sign are

$$\Delta T'^{+M,\,-M}_{J,\,J} = M_J a g_J - (-M)_J a g_J - a^2 f(M_J^2) + a^2 f[(-M)_J^2].$$

But the quadratic terms being equal by eq 6 cancel, and thus we have

$$\Delta T'^{+M,\,-M}_{J,\,J} = 2 M_J a g_J. \qquad (11)$$

This final equation is independent of quadratic terms, and hence we conclude that the separation between the perturbed levels is, in this particular case, independent of the perturbation and thus equal to the separation between unperturbed levels. Hence we can write

$$\Delta T'^{+M,\,-M}_{J,\,J} = \Delta T^{+M,\,-M}_{J,\,J}. \qquad (12)$$

We are now prepared to discuss the general case in which the affected level is perturbed simultaneously by two levels of the same term, one on each side of it. Figure 3 gives an illustration of this case. The level $T_{2\frac{1}{2}}$ is perturbed by the two close levels $T_{3\frac{1}{2}}$ and $T_{1\frac{1}{2}}$.

In order to obtain the final perturbed levels, it is necessary to consider independently the influences of $T_{J-1}$ and $T_{J+1}$. Each of these influences will give a quadratic term to the equation, but as they are situated on opposite sides of $T_J$, the signs will be different for the two quadratic terms. By the simple case explained before we know that the displacements are always in a contrary sense to the perturbing level. The final values of the magnetic levels will then be

$$T'^M_J = T_J + M_J a g_J - a^2 f(M_J^2) + a^2 f(M_{J+1}^2), \quad (13)$$

$a^2 f(M_J^2)$ being the perturbation due to $T_{J-1}$ and $a^2 f(M_{J+1}^2)$ that due to the level $T_{J+1}$.

The intervals between two consecutive levels with quantum numbers $M_J$ and $M_J - 1$ by eq 13 are

$$\Delta T'^{M,\,M-1}_{J,\,J} = a g_J - a^2 f(M_J^2) + a^2 f(M_{J+1}^2) + a^2 f[(M_J - 1)^2] - a^2 f[(M_{J+1} - 1)^2], \quad (14)$$

or

$$\Delta T'^{M,\,M-1}_{J,\,J} = a g_J + \text{four quadratic terms.}$$

The separations between levels with the same absolute value of $M$, but contrary sign, are

$$\Delta T'^{-M,\,+M}_{J,\,J} = M_J a g_J - (-M)_J a g_J - a^2 f(M_J^2) + a^2 f(M_{J+1}^2) + a^2 f[(-M)_J^2] - a^2 f[(-M)_{J+1}^2],$$

but this equation by eq 6 will be

$$\Delta T'^{-M,\,+M}_{J,\,J} = 2 M_J a g_J, \qquad (15)$$

a result that shows that the separations are independent of the quadratic terms and therefore equal to those of the unperturbed levels.

The magnitude of the displacements given by (3) decreases when the $J$-values increase owing to the influence of $I$ and $\Delta$. Table 3 shows that in a term $I$ decreases as $J$ increases. In spectral terms that follow Landé's interval rule, $\Delta$ increases with $J$; the function given by eq 5 will hence decrease when $J$ increases. In general this means that in a level $T_J$ the perturbations due to $T_{J-1}$ are expected to be greater than those due to $T_{J+1}$, and hence after the final perturbation the levels will appear close to each other in the direction of $T_{J+1}$ as shown in figure 3.

## 5. Positions of Components in an Asymmetric Pattern

The wave numbers of perturbed lines formed by transitions between perturbed magnetic levels $T'^M_J$ and $U''^{M'}_{J'}$ are evidently given by

$$n'^{M,\,M'}_{J,\,J'} = T'^M_J - U''^{M'}_{J'},$$

but introducing here the level values given by eq 9,

we shall have

$$n'^{M,M'}_{J,J'} = n_{J,J'} + M_J a g_J - M'_{J'} a g_{J'} - a^2 f(M_J^2) + a^2 f(M_{J'}^2). \quad (16)$$

This equation is a general formula giving all wave numbers in a perturbed pattern. In the case of parallel components $M'_J = M_J$. Equation 16 gives

$$n'^{M,M'}_{J,J'} = n_{J,J'} + M_J a \Delta g - a^2 f(M_J^2) + a^2 f(M_{J'}^2). \quad (17)$$

In the case of the normal components, with $M'_J = M_J - 1$ (or $M_J + 1$ without loss of generality)

$$n'^{M,M-1}_{J,J'} = n_{J,J'} + M_J a \Delta g + a g_{J'} - a^2 f(M_J^2) + a^2 f[(M_J - 1)^2]. \quad (18)$$

Equations 17 and 18 are closely analogous to those for unperturbed patterns except for the quadratic terms that give the perturbations.

Intervals between adjacent parallel components may be obtained by subtracting from eq 17 another equation equal to it but in which $M_J$ and $M_{J'}$ have been replaced, respectively, by $M_J - 1$ and $M_{J'} - 1$. The result is

$$a\Delta g - a^2 f(M_J^2) + a^2 f(M_{J'}^2) + a^2 f[(M_J - 1)^2] - a^2 f[(M_{J'} - 1)^2],$$

or briefly

$$a\Delta g + \text{four quadratic terms}, \quad (19)$$

which shows that the intervals between parallel components are unequal because of the quadratic terms.

The intervals between adjacent normal components may be obtained by subtracting from eq 18 another equation equal to it but in which $M_J$ and $M_J - 1$ are changed to $M_J - 1$ and $M_J - 2$ respectively. The result will be

$$a\Delta g + a g_{J'} - (-a g_{J'}) - a^2 f(M_J) + a^2 f[(M_{J'} - 1)^2] + a^2 f[(M_J - 1)^2] - a^2 f[(M_{J'} - 2)^2],$$

or briefly

$$a\Delta g + 2a g_{J'} + \text{four quadratic terms}, \quad (20)$$

which shows that here also, in the normal components, the intervals are unequal owing to the influence of the quadratic terms.

The separations between components of the same order on both sides of the line without field, and having the same $M$-value but contrary sign, are given for the parallel components by

$$M_J a\Delta g - (-M)_J a\Delta g - a^2 f(M_J^2) + a^2 f(M_{J'}^2) + a^2 f[(-M)_J^2] - a^2 f[(-M)_{J'}^2] = 2M_J a\Delta g. \quad (21)$$

The corresponding separations for the normal components are given by

$$M_J a\Delta g + a g_{J'} - (-M)_J a\Delta g - (a g_{J'}) - a^2 f(M_J^2) + a^2 f(M_{J'}^2) + a^2 f[(-M)_J^2] - a^2 f[(-M)_{J'}^2] = 2M_J a\Delta g + 2a g_{J'}. \quad (22)$$

The separations in these cases, either between parallel or normal components, are independent of the quadratic terms and hence equal to those found in patterns without distortions. This last conclusion is very important in calculating $g$-values, as we shall explain later.

## 6. Asymmetric Positions of Components in Some Zeeman Patterns of Mn I

We have predicted by theory the position of the components in an asymmetric Zeeman pattern. It is interesting now to compare the predicted positions with those found by measurement. For this purpose we have selected some lines of Mn I that are strong and thus easily observable, and for which the predicted distortions are very great (see fig. 4).

The selected lines belong to multiplets formed by combination of the low term $a\ ^6D$ with the middle terms $z\ ^6D°$ and $z\ ^6F°$. The relative values of these terms and their intervals, $\Delta$, are collected in table 4. The theoretical displacements of these terms by partial Paschen-Back interaction have been computed by means of eq 3 and 5, by using the $I^2$-values of table 3 and the value 3.955 $cm^{-1}$ for the Lorentz unit. The resulting values of the displacements are collected in table 4 under their respective $M$-values.

Table 4 shows that very great displacements are expected in levels with small $J$- and $M$-values, especially in the case of $z\ ^6F°$.

Table 5 shows the calculation of the values of the perturbed magnetic levels belonging to the spectroscopic levels of table 4. Only the levels with small $J$-values have been considered, because they show the greatest displacements. The computation has been made by use of eq 13; the values of the displacements of table 4 have been rounded to two decimals for this calculation.

In the first column of table 5 are given the spectroscopic levels, $T_J$, and their theoretical $g$-values. $LS$-coupling is supposed to be valid. The quantum numbers $M_J$ of the magnetic levels and their respective displacements $M_J a g_J$ are listed in the second and third columns. By addition of these displacements to the respective $T_J$-values the magnetic unperturbed levels $T_J^M$ are obtained as given in column 7. An LU 3.955 $cm^{-1}$ has been used in order to make the results comparable with the observed values. The values of the perturbed levels $T'^M_J$ have been computed by adding the Paschen-Back perturbations, (cols. 4 and 5) taken from table 4, to the unperturbed levels $T_J^M$. As these calculated perturbed levels do not differ much from the unperturbed ones, only their decimal parts are given (col. 8).

Table 6 shows the lines formed by combining the magnetic perturbed levels of table 5. Under the resulting calculated wave numbers are given two

groups of decimals. Those at the bottom correspond to the observed wave numbers. These observed wave numbers were derived by measuring the wavelengths of the lines of patterns on six MIT spectrograms with dispersion about 0.8 A/mm. The procedure employed in making the spectrograms was that described by Harrison and his collaborators [5].

The magnetic field for two of the spectrograms was 81,700 oersteds and for the others 84,700. All the measurements have been reduced to the field 84,700 oersteds, and accordingly values that are given in table 6 represent means of these reduced measure-

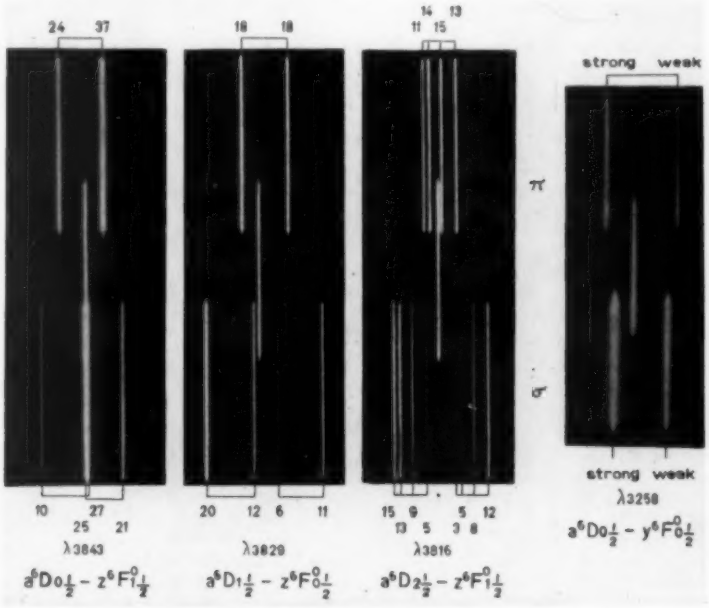


FIGURE 4. *Asymmetric Zeeman patterns of selected lines of* Mn I.

The reader may easily check the agreement between his own visual observations and the theoretical line strengths indicated in the figure close to the respective components. In the case of the line at 3258 A, the exposure times were different for the $\pi$- and the $\sigma$-components; therefore it is indicated in the figure only which component, in each type, should by theory be the stronger.

TABLE 4. *Theoretical displacements of magnetic levels in* Mn I

[in cm$^{-1}$. LU = 3.955 cm$^{-1}$]

| Spectroscopic | | | $a^{ij}f(M_j^2)$ | | | | |
|---|---|---|---|---|---|---|---|
| Designation | Level, $\nu$ | Interval, $\Delta\nu$ | $M \pm 0\frac{1}{2}$ | $1\frac{1}{2}$ | $2\frac{1}{2}$ | $3\frac{1}{2}$ | $4\frac{1}{2}$ |
| $a\ ^6D_{4\frac{1}{2}}$ | 17052. 29 | | | | | | |
| $3\frac{1}{2}$ | 17282. 00 | *229. 71* | 0. 042 | 0. 038 | 0. 029 | 0. 017 | ------ |
| $2\frac{1}{2}$ | 17451. 52 | *169. 52* | 0. 102 | 0. 085 | 0. 051 | ------ | ------ |
| $1\frac{1}{2}$ | 17568. 48 | *116. 96* | 0. 193 | 0. 128 | ------ | ------ | ------ |
| $0\frac{1}{2}$ | 17637. 15 | *68. 67* | 0. 354 | ------ | ------ | ------ | ------ |
| $z\ ^6D^o_{4\frac{1}{2}}$ | 41789. 48 | | | | | | |
| $3\frac{1}{2}$ | 41932. 64 | *143. 16* | 0. 067 | 0. 061 | 0. 047 | 0. 027 | ------ |
| $2\frac{1}{2}$ | 42053. 73 | *121. 09* | 0. 142 | 0. 119 | 0. 071 | ------ | ------ |
| $1\frac{1}{2}$ | 42143. 57 | *89. 84* | 0. 250 | 0. 167 | ------ | ------ | ------ |
| $0\frac{1}{2}$ | 42198. 56 | *54. 99* | 0. 442 | ------ | ------ | ------ | ------ |
| $z\ ^6F^o_{5\frac{1}{2}}$ | 43314. 23 | | | | | | |
| $4\frac{1}{2}$ | 43428. 58 | *114. 35* | 0. 102 | 0. 095 | 0. 081 | 0. 061 | 0. 034 |
| $3\frac{1}{2}$ | 43524. 08 | *95. 50* | 0. 223 | 0. 201 | 0. 156 | 0. 089 | ------ |
| $2\frac{1}{2}$ | 43595. 50 | *71. 42* | 0. 402 | 0. 335 | 0. 202 | ------ | ------ |
| $1\frac{1}{2}$ | 43644. 45 | *48. 95* | 0. 690 | 0. 461 | ------ | ------ | ------ |
| $0\frac{1}{2}$ | 43672. 96 | *28. 51* | 1. 219 | ------ | ------ | ------ | ------ |

TABLE 5. *Magnetic levels and g-values in* Mn I

[magnetic field 84,700 oersteds; LU = 3.955 $cm^{-1}$]

| Spectroscopic levels, $T_J$ | Magnetic quantum number, $M_J$ | Displacements $M_J a_{g_J}$ | Perturbations | | Total displacements | Magnetic levels | | | Interval, observed | g-values observed |
|---|---|---|---|---|---|---|---|---|---|---|
| | | | | | | $T^M_J$ Unperturbed | $T'^M_J$ Perturbed | | | |
| | | | | | | | Calculated | Observed | | |
| $a\ ^6D_{2½}$ | $-2½$ | −16. 38 | 0. 05 | ------ | −16. 33 | 17435. 14 | . 19 | . 18 | *6. 47* | 1. 658 |
| 17451. 52 | $-1½$ | −9. 83 | 0. 09 | −0. 13 | −9. 89 | 17441. 69 | . 63 | . 65 | *6. 50* | 1. 657 |
| $g_{2½}$ = 1. 657 | $-0½$ | −3. 28 | 0. 10 | −0. 19 | −3. 37 | 17448. 24 | . 15 | . 15 | *6. 56* | 1. 659 |
| | $0½$ | 3. 28 | 0. 10 | −0. 19 | 3. 19 | 17454. 80 | . 71 | . 71 | *6. 59* | ----- |
| | $1½$ | 9. 83 | 0. 09 | −0. 13 | 9. 77 | 17461. 35 | . 29 | . 30 | *6. 67* | ----- |
| | $2½$ | 16. 38 | 0. 05 | ------ | 16. 43 | 17467. 90 | . 95 | . 97 | | ----- |
| $a\ ^6D_{1½}$ | $-1½$ | −11. 08 | 0. 13 | ------ | −10. 95 | 17557. 40 | . 53 | . 53 | *7. 09* | 1. 867 |
| 17568. 48 | $-0½$ | −3. 69 | 0. 19 | −0. 35 | −3. 85 | 17564. 79 | . 63 | . 62 | *7. 39* | 1. 868 |
| $g_{1½}$ = 1. 867 | $0½$ | 3. 69 | 0. 19 | −0. 35 | 3. 53 | 17572. 17 | . 01 | . 01 | *7. 67* | ----- |
| | $1½$ | 11. 08 | 0. 13 | ------ | 11. 21 | 17879. 56 | . 69 | . 68 | | ----- |
| $a\ ^6D_{0½}$ | $-0½$ | −6. 59 | 0. 35 | ------ | −6. 24 | 17630. 56 | . 91 | . 94 | *13. 17* | 3. 330 |
| 17637. 15 | $0½$ | 6. 59 | 0. 35 | ------ | 6. 94 | 17643. 74 | 4. 09 | 4. 11 | | ----- |
| $g_{0½}$ = 3. 333 | | | | | | | | | | |
| $z\ ^6D^\circ_{3½}$ | $-2½$ | −16. 38 | 0. 07 | ------ | −16. 31 | 42037. 35 | . 42 | . 41 | *6. 43* | 1. 657 |
| 42053. 73 | $-1½$ | −9. 83 | 0. 12 | −0. 17 | −9. 88 | 42043. 90 | . 85 | . 84 | *6. 50* | 1. 657 |
| $g_{2½}$ = 1. 657 | $-0½$ | −3. 28 | 0. 14 | −0. 25 | −3. 39 | 42050. 45 | . 34 | . 34 | *6. 54* | 1. 654 |
| | $0½$ | 3. 28 | 0. 14 | −0. 25 | 3. 39 | 42057. 01 | 6. 90 | 6. 88 | *6. 62* | ----- |
| | $1½$ | 9. 83 | 0. 12 | −0. 17 | 9. 78 | 42063. 56 | . 51 | . 50 | *6. 67* | ----- |
| | $2½$ | 16. 38 | 0. 07 | ------ | 16. 45 | 42070. 11 | . 18 | . 17 | | ----- |
| $z\ ^6D^\circ_{1½}$ | $-1½$ | −11. 08 | 0. 17 | ------ | −10. 91 | 42132. 49 | . 66 | . 67 | *7. 03* | 1. 864 |
| 42143. 57 | $-0½$ | −3. 69 | 0. 25 | −0. 44 | −3. 88 | 42139. 89 | . 69 | . 70 | *7. 39* | 1. 868 |
| $g_{1½}$ = 1. 867 | $0½$ | 3. 69 | 0. 25 | −0. 44 | 3. 50 | 42147. 26 | . 07 | . 09 | *7. 70* | ----- |
| | $1½$ | 11. 08 | 0. 17 | ------ | 11. 25 | 42154. 65 | . 82 | . 79 | | ----- |
| $z\ ^6D^\circ_{0½}$ | $-0½$ | −6. 59 | 0. 44 | ------ | −6. 15 | 42191. 97 | 2. 41 | 2. 45 | *13. 10* | 3. 312 |
| 42198. 56 | $0½$ | 6. 59 | 0. 44 | ------ | 7. 03 | 42205. 15 | . 59 | . 55 | | ----- |
| $g_{0½}$ = 3. 333 | | | | | | | | | | |
| $z\ ^6F^\circ_{2½}$ | $-2½$ | −12. 99 | 0. 20 | ------ | −12. 79 | 43582. 51 | . 71 | . 71 | *4. 85* | 1. 313 |
| 43595. 50 | $-1½$ | −7. 80 | 0. 34 | −0. 46 | −7. 92 | 43587. 70 | . 58 | . 56 | *5. 05* | 1. 313 |
| $g_{2½}$ = 1. 314 | $-0½$ | −2. 60 | 0. 40 | −0. 69 | −2. 89 | 43592. 90 | . 61 | . 61 | *5. 18* | 1. 310 |
| | $0½$ | 2. 60 | 0. 40 | −0. 69 | 2. 31 | 43598. 10 | 7. 81 | 7. 79 | *5. 35* | ----- |
| | $1½$ | 7. 80 | 0. 34 | −0. 46 | 7. 68 | 43603. 30 | . 18 | . 14 | *5. 51* | ----- |
| | $2½$ | 12. 99 | 0. 20 | ------ | 13. 19 | 43608. 49 | . 69 | . 65 | | ----- |
| $z\ ^6F^\circ_{1½}$ | $-1½$ | −6. 33 | 0. 46 | ------ | −5. 87 | 43638. 12 | . 58 | . 59 | *3. 38* | 1. 067 |
| 43644. 45 | $-0½$ | −2. 11 | 0. 69 | −1. 22 | −2. 64 | 43642. 34 | 1. 81 | 1. 97 | *3. 98* | 1. 006 |
| $g_{1½}$ = 1. 067 | $0½$ | 2. 11 | 0. 69 | −1. 22 | 1. 58 | 43646. 56 | 6. 03 | 5. 95 | *5. 30* | ----- |
| | $1½$ | 6. 33 | 0. 46 | ------ | 6. 79 | 43650. 78 | 1. 24 | 1. 25 | | ----- |
| $z\ ^6F^\circ_{0½}$ | $-0½$ | 1. 32 | 1. 22 | ------ | 2. 54 | 43674. 28 | 5. 50 | 5. 32 | *−2. 38* | ----- |
| 43672. 96 | $0½$ | −1. 32 | 1. 22 | ------ | −0. 10 | 43671. 64 | 2. 86 | 2. 94 | | −0. 602 |
| $g_{0½}$ = 0. 667 | | | | | | | | | | |

ments. Lines marked with an asterisk (*) indicate poor measurements because of the close proximity of another line.

With the observed wave numbers a system of observed levels was derived. The values of the observed magnetic levels are listed under their respective theoretical values in table 6. To check the accuracy of the measurements, these observed values have been used to recalculate the wave numbers. The resulting values (only the decimal parts) are given between calculated and observed values in table 6. With very few exceptions the values agree to 1 or 2 units in the last decimal, thus indicating that the measurements are very consistent. The close agreement between the observed wave numbers and those derived for the observed magnetic levels is strong proof that the combination principle applies exactly to asymmetric patterns.

The observed magnetic levels thus computed have also been listed for comparison purposes in table 5, where for simplicity, only the decimal parts of their values are given in column 9. The observed intervals between consecutive levels, listed in column 10, are evidently unequal, as expected from theory. If the calculated and observed values for the perturbed levels given in table 5 are compared with each other, it will be observed that in most cases the agreement is extremely good—rarely exceeding the differences by more than 0.02 $cm^{-1}$—in spite of the

TABLE 6. *Asymmetric Zeeman patterns in multiplets* $a\,^6D - z\,^6D^\circ$ *and* $a\,^6D - z\,^6F^\circ$ *of* Mn I (*field 84,700 oersteds*)

| No field level | $M_J$ | $a\,^6D_{2\frac{1}{2}}$ = 17451.52 | | | | | | | $a\,^6D_{1\frac{1}{2}}$ = 17568.48 | | | | $a\,^6D_{\frac{1}{2}}$ = 17637.15 | |
|---|---|---|---|---|---|---|---|---|---|---|---|---|---|---|
| | | $M_J$ = | $-2\frac{1}{2}$ | $-1\frac{1}{2}$ | $-0\frac{1}{2}$ | $0\frac{1}{2}$ | $1\frac{1}{2}$ | $2\frac{1}{2}$ | $-1\frac{1}{2}$ | $-0\frac{1}{2}$ | $0\frac{1}{2}$ | $1\frac{1}{2}$ | $-0\frac{1}{2}$ | $0\frac{1}{2}$ |
| | | | 6.47 | 6.50 | 6.55 | 6.59 | 6.67 | | 7.09 | 7.39 | 7.67 | | 13.17 | |
| | | Magnetic level | 17435.19 .18 | 17441.63 .65 | 17448.15 .15 | 17454.71 .71 | 17461.29 .30 | 17467.95 .97 | 17557.53 .53 | 17564.63 .62 | 17572.01 .01 | 17559.69 .68 | 17630.91 .94 | 17644.09 .11 |
| $z\,^6D_{3\frac{1}{2}}$ 42053.73 | $-2\frac{1}{2}$ | 42037.42 | 24602.23 | 24595.79 | | | | | 24479.89 | | | | | |
| | | .41 | .23 | .76 | | | | | .88 | | | | | |
| | | *6.43* | | | | | | | .88 | | | | | |
| | $-1\frac{1}{2}$ | 42043.85 | 24608.66 | 24602.22 | 24595.70 | | | | 24486.32 | 24479.23 | | | | |
| | | .84 | .66 | .19 | .69 | | | | .31 | .22 | | | | |
| | | *6.50* | | | | | | | .32 | .21 | | | | |
| | $-0\frac{1}{2}$ | 42050.34 | | 24608.71 | 24602.19 | 24595.63 | | | 24492.81 | 24485.71 | 24478.33 | | | |
| | | .34 | | .69 | .19 | .63 | | | .81 | .72 | .33 | | | |
| | | *6.54* | | | | | | | .84 | .72 | .32 | | | |
| | $0\frac{1}{2}$ | 42056.90 | | | 24608.75 | 24602.19 | 24595.61 | | | 24492.27 | 24484.89 | 24477.21 | | |
| | | .88 | | | .73 | .17 | .58 | | | .26 | .87 | .20 | | |
| | | *6.62* | | | | | | | | .23 | .88 | .18 | | |
| | $1\frac{1}{2}$ | 42063.51 | | | | 24608.80 | 24602.22 | 24595.56 | | | 24491.50 | 24483.82 | | |
| | | .50 | | | | .79 | .20 | .53 | | | .49 | .82 | | |
| | | *6.67* | | | | | | | | | .49 | .83 | | |
| | $2\frac{1}{2}$ | 42070.18 | | | | | 24608.89 | 24602.23 | | | | 24490.49 | | |
| | | .17 | | | | | .87 | .20 | | | | .49 | | |
| $z\,^6D_{2\frac{1}{2}}$ 42143.57 | $-1\frac{1}{2}$ | 42132.66 | 24697.47 | 24691.03 | 24684.51 | | | | 24575.13 | 24568.03 | | | 24501.75 | |
| | | .67 | .49 | .02 | .52 | | | | .14 | .05 | | | .73 | |
| | | *7.03* | .44 | .02 | .54 | | | | | | | | .77 | |
| | $-0\frac{1}{2}$ | 42139.69 | | 24698.06 | 24691.54 | 2468.98 | | | 24582.16 | 24575.06 | 24567.68 | | 24508.78 | 24495.60 |
| | | .70 | | .05 | .55 | .99 | | | .17 | .08 | .69 | | .76 | .59 |
| | | *7.39* | | .04 | .55 | 5.02 | | | | | | | .75 | .58 |
| | $0\frac{1}{2}$ | 42147.07 | | | 24698.92 | 24692.36 | 24685.78 | | | 24582.44 | 24675.06 | 24567.38 | 24516.16 | 24502.98 |
| | | .09 | | | .94 | .38 | .79 | | | .47 | .08 | .41 | .15 | .98 |
| | | *7.70* | | | .92 | .39 | .79 | | | | | | .15 | 3.00 |
| | $1\frac{1}{2}$ | 42154.82 | | | | 24700.11 | 24693.53 | 24686.87 | | | 24582.81 | 24575.13 | | 24510.73 |
| | | .79 | | | | .08 | .49 | .82 | | | .78 | .11 | | .68 |
| | | | | | | .06 | .50 | .84 | | | | | | .70 |
| | | | | | | | .5 | | | | | | | |
| $z\,^6D_{0\frac{1}{2}}$ 42198.56 | $-0\frac{1}{2}$ | 42192.41 | | | | | | | 24634.88 | 24627.78 | 24620.40 | | 24561.50 | 24548.32 |
| | | .45 | | | | | | | .92 | .83 | .44 | | .51 | .34 |
| | | *13.10* | | | | | | | .93 | .84 | .42 | | .43* | .33 |
| | $0\frac{1}{2}$ | 42205.59 | | | | | | | | 24640.96 | 24633.58 | 24625.90 | 24574.68 | 24561.50 |
| | | .55 | | | | | | | | .93 | .54 | .87 | .61 | .44 |
| | | | | | | | | | | .91 | .54 | .87 | .64 | .43* |

TABLE 6. *Asymmetric Zeeman patterns in multiplets* $a\,^6D - z\,^6D^\circ$ *and* $a\,^6D - z\,^6F^\circ$ *of* Mn I (*field 84,700 oersteds*)—Continued

| No field level | $M_J$ | $a\,^6D_{3/2} = 17451.52$ | | | | | | | $a\,^6D_{1/2} = 17568.48$ | | | | $a\,^6D_{5/2} = 17637.15$ | |
|---|---|---|---|---|---|---|---|---|---|---|---|---|---|---|
| | | $M_J =$ | $-2\frac{1}{2}$ | $-1\frac{1}{2}$ | $-0\frac{1}{2}$ | $0\frac{1}{2}$ | $1\frac{1}{2}$ | $2\frac{1}{2}$ | $-1\frac{1}{2}$ | $-0\frac{1}{2}$ | $0\frac{1}{2}$ | $1\frac{1}{2}$ | $-0\frac{1}{2}$ | $0\frac{1}{2}$ |
| | | | 6.47 | 6.50 | 6.55 | 6.59 | 6.67 | | 7.09 | 7.39 | 7.67 | | 13.17 | |
| | | Magnetic level | 17435.10 | 17441.63 | 17448.15 | 17454.71 | 17461.29 | 17467.95 | 17557.52 | 17564.63 | 17572.01 | 17559.69 | 17630.91 | 17644.09 |
| | | | .18 | .65 | .15 | .71 | .30 | .97 | .53 | .62 | .01 | .68 | .94 | .11 |
| $z\,^6F_{1/2}$ 43595.50 | $-2\frac{1}{2}$ | 43582.71 | 26147.52 | 26141.08 | | | | | 26025.18 | | | | | |
| | | .71 | .53 | .06 | | | | | .18 | | | | | |
| | | *4.85* | .49* | .15* | | | | | .18 | | | | | |
| | $-1\frac{1}{2}$ | 43587.58 | 26152.39 | 26145.95 | 26139.43 | | | | 26030.05 | 26022.95 | | | | |
| | | .56 | .38 | .91 | .41 | | | | .03 | .94 | | | | |
| | | *5.05* | .49* | | .36 | | | | .05 | .93 | | | | |
| | $-0\frac{1}{2}$ | 43592.61 | | 26150.98 | 26144.46 | 26137.90 | | | 26035.09 | 26027.98 | 26020.60 | | | |
| | | .61 | | .96 | .46 | .90 | | | .08 | .99 | .60 | | | |
| | | *5.18* | | | .37* | .89 | | | .07 | .98 | .62 | | | |
| | $0\frac{1}{2}$ | 43597.81 | | | 26149.66 | 26143.10 | 26136.52 | | | 26033.18 | 26025.80 | 26018.12 | | |
| | | .79 | | | .64 | .08 | .49 | | | .17 | .78 | .11 | | |
| | | *5.35* | | | .64 | .05 | .47 | | | .15 | .75 | .10 | | |
| | $1\frac{1}{2}$ | 42603.18 | | | | 26148.47 | 26141.89 | 26135.23 | | | 26031.17 | 26023.49 | | |
| | | .14 | | | | .43 | .84 | .17 | | | .13 | .46 | | |
| | | *5.51* | | | | .45 | .80 | .17 | | | .13 | .46 | | |
| | $2\frac{1}{2}$ | 13608.69 | | | | | 26147.40 | 26140.74 | | | | 26029.00 | | |
| | | .65 | | | | | .35 | .68 | | | | 8.97 | | |
| | | | | | | | .41 | .70 | | | | 8.95 | | |
| $z\,^6F_{1/2}$ 43644.45 | $-1\frac{1}{2}$ | 43638.58 | 26203.39 | 26196.95 | 26190.43 | | | | 26081.05 | 26073.95 | | | 26007.67 | |
| | | .59 | .41 | .94 | .42 | | | | .06 | .97 | | | .65 | |
| | | *3.38* | .41 | .94 | .42 | | | | .06 | 74.00 | | | .65 | |
| | $-0\frac{1}{2}$ | 43641.81 | | 26200.18 | 26193.66 | 26187.10 | | | 26084.25 | 26077.18 | 26069.80 | | 26010.90 | 25997.72 |
| | | .97 | | .32 | .82 | .26 | | | .44 | .35 | .96 | | 11.03 | .86 |
| | | *3.98* | | .37 | .82 | .25 | | | .44 | .34 | .96* | | 11.02 | .85 |
| | $0\frac{1}{2}$ | 43646.03 | | | 26197.88 | 26191.32 | 26184.74 | | | 26081.40 | 26074.02 | 26066.34 | 26015.12 | 26001.94 |
| | | 5.95 | | | .80 | .24 | .65 | | | .33 | 3.94 | .27 | .01 | .84 |
| | | *5.30* | | | .80 | .24 | .65 | | | .28* | 3.94 | .36 | 4.97 | .82 |
| | $1\frac{1}{2}$ | 43651.24 | | | | 26196.53 | 26189.95 | 26183.29 | | | 26079.23 | 26071.55 | | 26007.15 |
| | | .25 | | | | .54 | .95 | .28 | | | .24 | .57 | | .14 |
| | | | | | | .56 | .94 | .29 | | | .26 | .57 | | .14 |
| $z\,^6F_{3/2}$ 43672.96 | $-0\frac{1}{2}$ | 43675.50 | | | | | | | 26117.97 | 26110.87 | 26103.49 | | 26044.59 | 26031.41 |
| | | .32 | | | | | | | .79 | .70 | .31 | | .38 | .21 |
| | | *−2.38* | | | | | | | .83 | .70 | .30 | | .36 | .20 |
| | $0\frac{1}{2}$ | 43672.86 | | | | | | | | 26108.23 | 26100.85 | 26093.17 | 26041.95 | 26028.77 |
| | | .94 | | | | | | | | .32 | .93 | .26 | 2.00 | .83 |
| | | | | | | | | | | .29 | .92 | .27 | 2.03 | .83 |

great differences that exist between values for perturbed and for unperturbed levels (compare cols. 7 and 8 of table 5). This proves that the approximate theory of the Paschen-Back effect applies closely to the asymmetrical patterns of the spectrum Mn I. There are, however, a few cases in which the differences between observed and calculated values, for the magnetic levels, exceed the expected errors of measurement. The most important cases are the following (see table 7).

All the components having origins in these levels show, as may be seen in table 6, very great differences between calculated and observed wave numbers. It is to be noted that all these components have origin in levels with magnetic quantum numbers $M=\pm 0\frac{1}{2}$. We shall consider this problem in the next paragraphs.

TABLE 7. *Magnetic levels with strong perturbations in* Mn I

[LU, 3.955 cm$^{-1}$]

| Designation | Level | | |
|---|---|---|---|
| | Calculated | Observed | Observed −calculated |
| $z\,^6D^{-0\frac{1}{2}}_{0\frac{1}{2}}$ | 42192. 41 | . 45 | 0. 04 |
| $z\,^6D^{0\frac{1}{2}}_{0\frac{1}{2}}$ | 42205. 59 | . 55 | −0. 04 |
| $z\,^6F^{-0\frac{1}{2}}_{1\frac{1}{2}}$ | 43641. 81 | . 97 | 0. 16 |
| $z\,^6F^{0\frac{1}{2}}_{1\frac{1}{2}}$ | 43646. 03 | 5. 95 | −0. 08 |
| $z\,^6F^{-0\frac{1}{2}}_{0\frac{1}{2}}$ | 43675. 50 | . 32 | −0. 18 |
| $z\,^6F^{0\frac{1}{2}}_{0\frac{1}{2}}$ | 43672. 86 | . 94 | 0. 08 |

## 7. Computation of *g*-Values From the Level Values

In the preceding discussion we have seen that, with few exceptions, the calculated values are closely coincident with the observed, showing that the theory is valid for these cases of manganese. It may be recalled now that eq 15 of this theory, which gives the separation between pairs of magnetic levels with the same absolute $M$-value but different sign, is independent of the quadratic terms, and hence that equal separations are obtained for perturbed and for unperturbed levels. This means that it will be possible to eliminate distortion due to weak Paschen-Back interaction by using eq 15. Solving eq 15 we have

$$g_J=\frac{\Delta T'^{-M}_{J},{}^{+M}_{J}}{2M_J a} \tag{23}$$

which gives the $g$-value corresponding to each pair of magnetic levels $T'^{-M}_{J}$ and $T'^{+M}_{J}$. This formula indicates that to obtain a $g$-value it is only necessary to divide the separation between the two levels involved by $2M_J a$. As an example the $g$-value corresponding to the observed magnetic levels 17435.18 ($M=-2\frac{1}{2}$) and 17467.97 ($M=+2\frac{1}{2}$), $a$ being equal to 3.955, may be calculated as

$$\frac{17467.97-17435.18}{2\times 2\frac{1}{2}\times 3.955}=1.658.$$

In table 5, last column, the $g$-values computed in this way for each pair $\pm M$ are listed in front of the corresponding $(-M)$-values.

## 8. Computation of *g*-Values From the Observed Components of Patterns

It is interesting now to compute $g$-values directly from the observed patterns and to compare the resulting values with those derived from levels that were given in table 5. Table 8 shows details of the calculation. In the first column are given the wavelengths and transitions of the spectroscopic lines. In the second are listed the polarizations of the magnetic components whose wave numbers are in column 3. Lines marked with (*) are poorly measured.

In order to eliminate the distortions due to partial Paschen-Back effect the separations are taken, as indicated by eq 21 and 22 between components of the same order on both sides of the line without field. These separations are written after the components of smaller wave number. Thus, the difference between the lines 24477.18 and 24492.84 is written after the former. The separations, which are given in cm$^{-1}$, are divided by $2a=2\times 3.955=7.910$ to obtain the components of the pattern in Lorentz units. These resultant components are listed in column 5. As usual, parallel components are given in parentheses.

The next step is to calculate the mean values of the intervals between adjacent components of a pattern. The intervals are given in column 6, and at the bottom of each set of intervals is written their mean value. The last interval in each set is the double value of the smallest parallel component, which itself is an interval.

In table 8 the intervals in each pattern are so closely equal that accurate mean values have been obtained. Each normal component and the mean interval provide two equations for calculating the $g$-values of the two levels involved. The resulting $g$-values are written after the respective normal component. Thus, the first component in table 8, namely 1.980, with the mean interval *0.212* gives the two $g$-values 1.874 for $a\,^6D_{1\frac{1}{2}}$ and 1.662 for $z\,^6D^{\circ}_{2\frac{1}{2}}$.

There are three lines 3843, 3833, and 3816 A whose intervals, within each pattern, are very different and hence have not been included in table 8. The line 3816 A, for example, has the following components and intervals:

| | | | | | | |
|---|---|---|---|---|---|---|
| Components | 2. 544 | 1. 987 | 1. 334 | 0. 775 | (0. 885) | (0. 326) |
| Intervals | *0. 557* | *0. 653* | *0. 559* | ..... | *0. 559* | *0. 652* |

The impossibility of deriving an accurate mean value, for the interval, with values such as 0.557 and 0.653 is evident.

Recently, Catalán and Velasco have shown, [8] and [9], that in cases such as these it is, nevertheless, possible to obtain $g$-values from the components if these are treated in separate groups, one for each

TABLE 8. *Asymmetric patterns in* Mn I

[Field 84,700 oersteds; LU 3.955 cm$^{-1}$]

| Spectroscopic transition and wavelength | Polarization | Observed pattern | Separation (cm$^{-1}$) | Component | Interval | $g$-values | |
|---|---|---|---|---|---|---|---|
| | | | | | | $a\ ^6D1\frac{1}{2}$ | $z\ ^6D_2^{1\frac{1}{2}}$ |
| | $\sigma$ | 24477. 18 | 15. 66 | 1. 980 | | 1. 874 | 1. 662 |
| | $\sigma$ | 24478. 32 | 13. 91 | 1. 759 | *0. 221* | 1. 865 | 1. 653 |
| | $\sigma$ | 24479. 21 | 12. 28 | 1. 552 | *0. 207* | 1. 870 | 1. 658 |
| | $\sigma$ | 24479. 88 | 10. 61 | 1. 339 | *0. 213* | 1. 869 | 1. 658 |
| | $\pi$ | 24483. 83 | 2. 49 | (0. 314) | | | |
| | $\pi$ | 24484. 88 | 0. 84 | (0. 106) | *0. 208* | | |
| $a\ ^6D_{1\frac{1}{2}} - z\ ^6D_{2\frac{1}{2}}^{1\frac{1}{2}}$ | | *24485. 25* | | | *0. 212* | | |
| 4082.945A | $\pi$ | 24485. 72 | -- | Mean | *0. 212* | | |
| | $\pi$ | 24486. 32 | -- | | | | |
| | $\sigma$ | 24490. 49 | -- | -- | | | |
| | $\sigma$ | 24491. 49 | -- | -- | | | |
| | $\sigma$ | 24492. 23 | -- | -- | | | |
| | $\sigma$ | 24492. 84 | -- | -- | | $a\ ^6D_{3\frac{1}{2}}$ | $z\ ^6D_{3\frac{1}{2}}^{1\frac{1}{2}}$ |
| | $\sigma$ | 24495. 58 | 20. 57 | 2. 600 | | 3. 331 | 1. 869 |
| | $\sigma$ | 24501. 77 | 8. 93 | 1. 129 | *1. 471* | 3. 322 | 1. 860 |
| | $\pi$ | 24503. 00 | 5. 75 | (0. 727) | | | |
| $a\ ^6D_{3\frac{1}{2}} - z\ ^6D_{3\frac{1}{2}}^{1\frac{1}{2}}$ | | *24506. 34* | | | *1. 454* | | |
| 4079.415A | $\pi$ | 24508. 75 | -- | Mean | *1. 463* | | |
| | $\sigma$ | 24510. 70 | -- | | | | |
| | $\sigma$ | 24516. 15 | -- | -- | | $a\ ^6D_{3\frac{1}{2}}$ | $z\ ^6D_{3\frac{1}{2}}^{3\frac{1}{2}}$ |
| | $\sigma$ | 24548. 33 | 26. 31 | 3. 325 | | 3. 325* | 3. 325* |
| $a\ ^6D_{3\frac{1}{2}} - z\ ^6D_{3\frac{1}{2}}^{3\frac{1}{2}}$ | $\pi$ | 24561. 43* | 0. 00 | (0. 000) | | | |
| 4070.280A | | *24561. 42* | | | | | |
| | $\pi$ | 24561. 43* | -- | -- | | | |
| | $\sigma$ | 24574. 64 | -- | -- | | | |
| | | | | | | $a\ ^6D_{1\frac{1}{2}}$ | $z\ ^6D_{3\frac{1}{2}}^{3\frac{1}{2}}$ |
| | $\sigma$ | 24620. 42 | 20. 49 | 2. 590 | | 1. 868 | 3. 312 |
| | $\sigma$ | 24625. 87 | 9. 06 | 1. 145 | *1. 445* | 1. 867 | 3. 311 |
| $a\ ^6D_{1\frac{1}{2}} - z\ ^6D_{3\frac{1}{2}}^{3\frac{1}{2}}$ | $\pi$ | 24627. 84 | 5. 70 | (0. 721) | | | |
| 4058.936A | | *24630. 08* | | | *1. 442* | | |
| | $\pi$ | 24633. 54 | -- | Mean | *1. 444* | | |
| | $\sigma$ | 24634. 93 | -- | | | | |
| | $\sigma$ | 24640. 91 | -- | -- | | | |
| | | | | | | $a\ ^6D_{2\frac{1}{2}}$ | $z\ ^6D_{3\frac{1}{2}}^{1\frac{1}{2}}$ |
| | $\sigma$ | 24684. 54 | 15. 52 | 1. 962 | | 1. 650 | 1. 858 |
| | $\sigma$ | 24685. 02 | 13. 90 | 1. 757 | *0. 205* | 1. 653 | 1. 861 |
| | $\sigma$ | 24685. 79 | 12. 25 | 1. 549 | *0. 208* | 1. 653 | 1. 861 |
| | $\sigma$ | 24686. 84 | 10. 60 | 1. 341 | *0. 208* | 1. 652 | 1. 860 |
| | $\pi$ | 24691. 02 | 2. 48 | (0. 314) | | | |
| $a\ ^6D_{2\frac{1}{2}} - z\ ^6D_{3\frac{1}{2}}^{1\frac{1}{2}}$ | $\pi$ | 24691. 55 | 0. 84 | (0. 106) | *0. 208* | | |
| 4048.747A | | *24692. 05* | | | *0. 212* | | |
| | $\pi$ | 24692. 39 | -- | Mean | *0. 208* | | |
| | $\pi$ | 24693. 50 | -- | | | | |
| | $\sigma$ | 24697. 44 | -- | -- | | | |
| | $\sigma$ | 24698. 04 | -- | -- | | | |
| | $\sigma$ | 24698. 92 | -- | -- | | | |
| | $\sigma$ | 24700. 06 | -- | -- | | | |
| | | | | | | $a\ ^6D_{1\frac{1}{2}}$ | $z\ ^6F_{2\frac{1}{2}}$ |
| | $\sigma$ | 26018. 10 | 16. 97 | 2. 145 | | 1. 867 | 1. 311 |
| | $\sigma$ | 26020. 62 | 12. 53 | 1. 584 | *0. 561* | 1. 862 | 1. 306 |
| | $\sigma$ | 26022. 93 | 8. 20 | 1. 037 | *0. 547* | 1. 871 | 1. 315 |
| | $\sigma$ | 26025. 18 | 3. 77 | 0. 477 | *0. 560* | 1. 867 | 1. 311 |
| | $\pi$ | 26023. 46 | 6. 59 | (0. 833) | | | |
| $a\ ^6D_{1\frac{1}{2}} - z\ ^6F_{2\frac{1}{2}}^{3\frac{1}{2}}$ | $\pi$ | 26025. 75 | 2. 23 | (0. 282) | *0. 551* | | |
| 3841. 074A | | *26027. 03* | | | *0. 564* | | |
| | $\pi$ | 26027. 98 | -- | Mean | *0. 556* | | |
| | $\pi$ | 26030. 05 | -- | | | | |
| | $\sigma$ | 26028. 95 | -- | -- | | | |
| | $\sigma$ | 26031. 13 | -- | -- | | | |
| | $\sigma$ | 26033. 15 | -- | -- | | | |
| | $\sigma$ | 26035. 07 | -- | -- | | | |

TABLE 8. *Asymmetric patterns in* Mn I—Continued

[Field 84,700 oersteds; LU 3.955 cm$^{-1}$]

| Spectroscopic transition and wavelength | Polarization | Observed pattern | Separation (cm$^{-1}$) | Component | Interval | $g$-values | |
|---|---|---|---|---|---|---|---|
| | | | | | | $a\,^6D_{0½}$ | $z\,^6F^{\circ}_{0½}$ |
| $a\,^6D_{1½} - z\,^6F^{\circ}_{0½}$ 3839.779A | $\sigma$ | 26031. 20 | 10. 83 | 1. 369 | | 3. 332 | −0. 594 |
| | $\pi$ | 26028. 83 | 15. 53 | (1. 963) | | | |
| | | *26035. 81* | | | | | |
| | $\pi$ | 26044. 36 | -- | -- | | | |
| | $\sigma$ | 26042. 03 | -- | -- | | | |
| | | | | | | $a\,^6D_{1½}$ | $z\,^6F^{\circ}_{0½}$ |
| | $\sigma$ | 26093. 27 | 24. 56 | 3. 105 | | 1. 868 | −0. 606 |
| | $\sigma$ | 26103. 30 | 4. 99 | 0. 631 | *2. 474* | 1. 867 | −0. 605 |
| $a\,^6D_{1½} - z\,^6F^{\circ}_{0½}$ 3829.679A | $\pi$ | 26100. 92 | 9. 78 | (1. 236) | | | |
| | | *26104. 47* | | | *2. 472* | | |
| | $\pi$ | 26110. 70 | -- | | | | |
| | | | | Mean | *2. 473* | | |
| | $\sigma$ | 26108. 29 | -- | | | | |
| | $\sigma$ | 26117. 83 | -- | -- | | | |
| | | | | | | $a\,^6D_{2½}$ | $z\,^6F^{\circ}_{1½}$ |
| | $\sigma$ | 26135. 17 | 17. 32* | 2. 190 | *0. 352** | 1. 671* | 1. 325* |
| | $\sigma$ | 26136. 47 | -- | -- | *0. 353** | -- | -- |
| | $\sigma$ | 26137. 89 | 11. 75 | 1. 485 | *0. 336* | 1. 658 | 1. 312 |
| | $\sigma$ | 26139. 36 | 9. 09 | 2. 149 | *0. 358* | 1. 668 | 1. 322 |
| | $\sigma$ | 26141. 15* | 6. 26* | 0. 791 | | 1. 656* | 1. 310* |
| | $\pi$ | 26140. 70 | 6. 79* | (0. 858) | *0. 345** | | |
| | $\pi$ | 26141. 80 | -- | -- | *0. 346** | | |
| $a\,^6D_{2½} - z\,^6F^{\circ}_{1½}$ 3823.891A | $\pi$ | 26143. 05 | 1. 32* | (0. 167) | | | |
| | | *26143. 98* | | | ***0. 334*** | | |
| | $\pi$ | 26144. 37* | -- | -- | | | |
| | $\pi$ | 26145. | -- | Mean | *0. 346* | | |
| | $\pi$ | 26147. 49* | -- | | | | |
| | $\sigma$ | 26147. 41 | -- | -- | | | |
| | $\sigma$ | 26148. 45 | -- | -- | | | |
| | $\sigma$ | 26149. 64 | -- | -- | | | |
| | $\sigma$ | 26150. | -- | -- | | | |
| | $\sigma$ | 26152. 49* | -- | -- | | | |

pair of magnetic levels $\pm M$. Table 9 shows the calculation of $g$-values by that method for the three lines mentioned above. The general arrangement of table 9 is similar to that of table 8, but the components have been placed in two groups. It has been possible to obtain the $g$-values for the two levels involved in all cases except one, that of the component −0.064, because in this case the interval is unknown. The $g$-value of one of the levels involved, namely 3.328 for $a\,^6D_{0½}$, has been adopted, and then the $g$-value for the other level has been derived. Table 9 shows that the $g$-values obtained for $a\,^6D_{2½}$, $a\,^6D_{1½}$, and $a\,^6D_{0½}$ are closely coincident with those obtained in table 8, thereby justifying the method of Catalán and Velasco.

It is to be noted that the $g$-values obtained for the same spectroscopic level, in different patterns, are practically identical. Very accurate mean values may be derived from the data of tables 7 and 8. The resulting values have been compiled in table 10.

The agreement between values derived from levels or from components is extremely good. This is a proof of the validity of both methods of deriving $g$-values. The method of levels, although a little more difficult to apply, is the more general, for it gives results in all cases. The method of the components is, however, much more simple and is the one usually employed by all observers of the Zeeman effect; but it must be applied with caution because in some asymmetric patterns it may give less accurate $g$-values. The method of Catalán and Velasco may serve in such cases to obtain more reliable values.

Most of the levels in table 10 have $g$-values equal to those of $LS$-coupling, but $z\,^6D^{\circ}_{0½}$, $z\,^6F^{\circ}_{1½}$, and $z\,^6F^{\circ}_{0½}$ constitute clear exceptions to the rule. These exceptions are just those derived from levels in table 7. The two magnetic levels $z\,^6D^{-0½}_{0½}$ and $z\,^6D^{+0½}_{0½}$ have been displaced unequally. The level with negative $M$-value has received a positive additional impulse of 0.04 cm$^{-1}$, and that with the positive value has received an additional negative push of 0.04 cm$^{-1}$. The distance between these two levels compared with the distance between the unperturbed levels is shortened by 0.08 cm$^{-1}$. Hence the corresponding $g$-factor is altered. The $g$-value for $LS$-coupling is 3.333, and the real value is 3.312. We cannot suggest the cause for this anomalous displacement.

The other cases are closely connected with each other, as Catalán and Velasco have shown, [9] and [7, p. 200]. The $g$-values that are obtained for the two pairs $M=\pm 1½$ and $M=\pm 0½$ for $z\,^6F_{1½}$ are quite different. The first pair gives exactly the $LS$-value, but the pair $M=\pm 0½$ gives 1.006, which is 0.061 LU smaller than the $LS$-value. The additional impulses

TABLE 9. *Zeeman patterns of level* $z\,^6F^\circ_{1/2}$ *of* Mn I

[Magnetic field 84,700 oersteds; LU 3.955 cm$^{-1}$]

| Spectroscopic transition and wavelength | Polarization | Observed pattern | Separation (cm$^{-1}$) | Component | Interval | g-values | |
|---|---|---|---|---|---|---|---|
| | | | | | | $a\,^6D_{9/2}$ | $z\,^6F^\circ_{11/2}$ |
| | $\sigma$ | 26007. 65 | −0. 51 | −0. 064 | -- | [3. 328] | 1. 067 |
| | | *26007. 30* | | | | | |
| | $\sigma$ | 26007. 14 | -- | -- | -- | -- | -- |
| | | | | | | | $z\,^6F^\circ_{9/2}$ |
| $a\,^6D_{9/2} - z\,^6F^\circ_{11/2}$ | $\sigma$ | 25997. 85 | 17. 12 | 2. 165 | -- | 3. 328 | 1. 002 |
| 3843. 988A | $\pi$ | 26001. 82 | 9. 20 | (1. 163) | -- | -- | -- |
| | | *26007. 30* | | | | | |
| | $\pi$ | 26011. 02 | -- | -- | -- | -- | -- |
| | $\sigma$ | 26014. 97 | -- | -- | -- | -- | -- |
| | | | | | | $a\,^6D_{7/2}$ | $z\,^6F^\circ_{11/2}$ |
| | $\sigma$ | 26074. 00 | 5. 26 | 0. 665 | -- | 1. 865 | 1. 065 |
| | $\pi$ | 26071. 57 | 9. 49 | (1. 200) | -- | -- | -- |
| | | *26075. 97* | | | | | |
| | $\pi$ | 26081. 06 | -- | -- | -- | -- | -- |
| | $\sigma$ | 26079. 26 | -- | -- | -- | -- | -- |
| | | | | | | | $z\,^6F^\circ_{9/2}$ |
| $a\,^6D_{7/2} - z\,^6F^\circ_{11/2}$ | $\sigma$ | 26066. 36 | 18. 08 | 2. 285 | | 1. 857 | 1. 000 |
| 3833. 865A | $\sigma$ | 26069. 96* | 11. 32* | 1. 431 | *0. 854* | 1. 860 | 1. 003 |
| | $\pi$ | 26073. 94 | 3. 40 | (0. 430) | | -- | -- |
| | | *26075. 95* | | | *0. 860* | | |
| | $\pi$ | 26077. 34 | -- | Mean | *0. 857* | | |
| | $\sigma$ | 26081. 28* | -- | -- | -- | -- | -- |
| | $\sigma$ | 26084. 44 | -- | -- | -- | -- | -- |
| | | | | | | $a\,^6D_{5/2}$ | $z\,^6F^\circ_{11/2}$ |
| | $\sigma$ | 26183. 29 | 20. 12 | 2. 544 | | 1. 659 | 1. 069 |
| | $\sigma$ | 26190. 42 | 6. 13 | 0. 775 | *1. 769* | 1. 660 | 1. 070 |
| | $\pi$ | 26189. 94 | 7. 00 | (0. 855) | | -- | -- |
| | | *26192. 93* | | | *1. 770* | -- | -- |
| | $\pi$ | 26196. 94 | -- | Mean | *1. 770* | -- | -- |
| | $\sigma$ | 26196. 55 | -- | ½ Mean | *0. 590* | -- | -- |
| | | | | | | | $z\,^6F^\circ_{9/2}$ |
| $a\,^6D_{5/2} - z\,^6F^\circ_{11/2}$ | $\sigma$ | 26203. 41 | -- | -- | -- | -- | -- |
| 3816. 746A | $\sigma$ | 26184. 65 | 15. 72 | 1. 987 | | 1. 660 | 1. 007 |
| | $\sigma$ | 26187. 25 | 10. 55 | 1. 334 | *0. 653* | 1. 660 | 1. 007 |
| | $\pi$ | 26191. 24 | 2. 58 | (0. 326) | | -- | -- |
| | | *26192. 93* | | | *0. 652* | | |
| | $\pi$ | 26193. 82 | -- | Mean | *0. 653* | -- | -- |
| | $\sigma$ | 26197. 80 | -- | -- | -- | -- | -- |
| | $\sigma$ | 26200. 37 | -- | -- | -- | -- | -- |

TABLE 10. *Mean g-values for levels of* Mn I

[Magnetic field 84,700 oersteds]

| Designation | g-values computed with the observed | | g-values for LS-coupling |
|---|---|---|---|
| | Levels | Components | |
| $a\ ^6D_{2\frac{1}{2}}$ | 1. 658 | 1. 658 | 1. 657 |
| $a\ ^6D_{1\frac{1}{2}}$ | 1. 867 | 1. 866 | 1. 867 |
| $a\ ^6D_{0\frac{1}{2}}$ | 3. 330 | 3. 328 | 3. 333 |
| $z\ ^6D^0_{2\frac{1}{2}}$ | 1. 656 | 1. 658 | 1. 657 |
| $z\ ^6D^0_{1\frac{1}{2}}$ | 1. 866 | 1. 861 | 1. 867 |
| $z\ ^6D^0_{0\frac{1}{2}}$ | 3. 312 | 3. 312 | 3. 333 |
| $z\ ^6F^0_{3\frac{1}{2}}$ | 1. 312 | 1. 314 | 1. 314 |
| $z\ ^6F^0_{1\frac{1}{2}}$, $M=\pm 1\frac{1}{2}$ | 1. 067 | 1. 068 | 1. 067 |
| $z\ ^6F^0_{1\frac{1}{2}}$, $M=\pm 0\frac{1}{2}$ | 1. 006 | 1. 004 | |
| $z\ ^6F^0_{0\frac{1}{2}}$ | −0. 602 | −0. 602 | −0. 667 |

0.16 and −0.08 $cm^{-1}$, which $z\ ^6F^{-0\frac{1}{2}}_{1\frac{1}{2}}$ and $z\ ^6F^{+0\frac{1}{2}}_{1\frac{1}{2}}$ have received, make their distance shorter by a total amount of 0.024 $cm^{-1}$, which accounts for the change of 0.061 LU in the *g*-values.

The magnetic levels $z\ ^6F^{-0\frac{1}{2}}_{0\frac{1}{2}}$ and $z\ ^6F^{+0\frac{1}{2}}_{0\frac{1}{2}}$ have received extra displacements −0.18 and 0.08 $cm^{-1}$, respectively. In this particular case of $^6F_{0\frac{1}{2}}$, on account of the fact that the *g*-value is negative, the magnetic level $M=-0\frac{1}{2}$ is smaller than $M=+0\frac{1}{2}$. Hence the distance between these magnetic levels has been shortened by a total amount of 0.26 $cm^{-1}$, and this accounts for the change of *g*-value from −0.667 (*LS*-coupling value) to −0.602.

There is a close connection between the changes in *g*-values experienced by $z\ ^6F^0_{1\frac{1}{2}}$ and $z'\ ^6F^0_{0\frac{1}{2}}$. As Catalán and Velasco have shown, the sums of the *g*-values for *LS*-coupling and for the observed levels are the same. The sum in *LS*-coupling amounts to 1.067+(−0.667)=0.400 and to 1.001+(−0.602)=0.399 for the perturbed levels. A clear explanation of this case has been given by these authors [7, p. 200].

## 9. Theoretical Computation of Line Strengths in Zeeman Patterns

The strength, ***S***, of a line is defined as a quantity that must be multiplied by the fourth power of the frequency and by the number of atoms in any one of the initial states, in order to obtain the radiated energy [7, p. 200]. There is a possibility of comparing *relative strengths* with *observed intensities* because all the lines of a Zeeman pattern have closely the same frequency and are produced by close states that have practically the same excitation.

The strength $S^M$ of a component in a Zeeman pattern depends on the strength ***S*** of the parent line through the equation

$$S^M = S \times K, \tag{24}$$

in which $K$ is a constant whose values depend on the $J$- and $M$-values of the initial levels as expressed in the following formulas:

| Spectroscopic transition | Magnetic transition | K-values |
|---|---|---|
| $J \rightarrow J-1$ | $M \rightarrow M$ | $\frac{2A(J^2-M^2)}{J(2J-1)(2J+1)}$ |
| | $M \rightarrow M \pm 1$ | $\frac{(1/2)A(J \mp M)(J \mp M-1)}{J(2J-1)(2J+1)}$ |
| $J \rightarrow J$ | $M \rightarrow M$ | $\frac{2AM^2}{J(J+1)(2J+1)}$ |
| | $M \rightarrow M \pm 1$ | $\frac{(1/2)A(J \mp M)(J \pm M-1)}{J(J+1)(2J+1)}$ |

TABLE 11. *K- and* $(K)^{1/2}$*-values for components in a Zeeman pattern*

[Upper figures are *K*-values; lower $(K)^{1/2}$-values]

| Odd multiplicities, parallel components | | | | | | | | |
|---|---|---|---|---|---|---|---|---|
| $J$ | $J-1$ | $M=-3$<br>$M=-3$ | −2<br>−2 | −1<br>−1 | 0<br>0 | +1<br>+1 | +2<br>+2 | +3<br>+3 |
| 1 | 0 | --<br>-- | --<br>-- | --<br>-- | 50. 00<br>7. 07 | --<br>-- | --<br>-- | --<br>-- |
| 2 | 1 | --<br>-- | --<br>-- | 15. 00<br>3. 87 | 20. 00<br>4. 47 | 15. 00<br>3. 87 | --<br>-- | --<br>-- |
| 3 | 2 | --<br>-- | 7. 14<br>2. 67 | 11. 43<br>3. 38 | 12. 86<br>3. 58 | 11. 43<br>3. 38 | 7. 14<br>2. 67 | --<br>-- |
| 4 | 3 | 4. 16<br>2. 04 | 7. 14<br>2. 67 | 8. 93<br>2. 99 | 9. 52<br>3. 09 | 8. 93<br>2. 99 | 7. 14<br>2. 67 | 4. 16<br>2. 04 |
| $J$ | $J$ | | | | | | | |
| 1 | 1 | --<br>-- | --<br>-- | 25. 00<br>5. 00 | 0. 00<br>0. 00 | 25. 00<br>5. 00 | --<br>-- | --<br>-- |
| 2 | 2 | --<br>-- | 20. 00<br>4. 47 | 5. 00<br>2. 24 | 0. 00<br>0. 00 | 5. 00<br>2. 24 | 20. 00<br>4. 47 | --<br>-- |
| 3 | 3 | 16. 07<br>4. 01 | 7. 14<br>2. 67 | 1. 79<br>1. 29 | 0. 00<br>0. 00 | 1. 79<br>1. 29 | 7. 14<br>2. 67 | 16. 07<br>4. 01 |

TABLE 11. *K- and $(K)^{1/2}$-values for components in a Zeeman pattern*—Continued

[Upper figures are *K*-values; lower $(K)^{1/2}$-values

| Odd multiplicities, normal components | | | | | | | | |
|---|---|---|---|---|---|---|---|---|
| $J$ | $J-1$ | $M=-2$<br>$M-1=-3$ | $-1$<br>$-2$ | 0<br>$-1$ | $+1$<br>0 | $+2$<br>$+1$ | $+3$<br>$+2$ | $+4$<br>$+3$ |
| 1 | 0 | --<br>-- | --<br>-- | --<br>-- | 25. 00<br>5. 00 | --<br>-- | --<br>-- | --<br>-- |
| 2 | 1 | --<br>-- | --<br>-- | 2. 50<br>1. 58 | 7. 50<br>2. 74 | 15. 00<br>3. 87 | --<br>-- | --<br>-- |
| 3 | 2 | --<br>-- | 0. 71<br>0. 84 | 2. 14<br>1. 46 | 4. 29<br>2. 07 | 7. 14<br>2. 67 | 10. 71<br>3. 27 | --<br>-- |
| 4 | 3 | 0. 30<br>0. 55 | 0. 90<br>0. 95 | 1. 78<br>1. 33 | 2. 98<br>1. 73 | 4. 49<br>2. 12 | 6. 25<br>2. 50 | 8. 33<br>2. 89 |
| $J$ | $J$ | | | | | | | |
| 1 | 1 | --<br>-- | --<br>-- | 12. 50<br>3. 54 | 12. 50<br>3. 54 | --<br>-- | --<br>-- | --<br>-- |
| 2 | 2 | --<br>-- | 5. 00<br>2. 24 | 7. 50<br>2. 74 | 7. 50<br>2. 74 | 5. 00<br>2. 24 | --<br>-- | --<br>-- |
| 3 | 3 | 2. 68<br>1. 64 | 4. 46<br>2. 11 | 5. 35<br>2. 31 | 5. 35<br>2. 31 | 4. 46<br>2. 11 | 2. 68<br>1. 64 | --<br>-- |

| Even multiplicities, parallel components | | | | | | | | |
|---|---|---|---|---|---|---|---|---|
| $J$ | $J-1$ | $M=-3\frac{1}{2}$<br>$M=-3\frac{1}{2}$ | $-2\frac{1}{2}$<br>$-2\frac{1}{2}$ | $-1\frac{1}{2}$<br>$-1\frac{1}{2}$ | $-0\frac{1}{2}$<br>$-0\frac{1}{2}$ | $+0\frac{1}{2}$<br>$+0\frac{1}{2}$ | $+1\frac{1}{2}$<br>$+1\frac{1}{2}$ | $+2\frac{1}{2}$<br>$+2\frac{1}{2}$ | $+3\frac{1}{2}$<br>$+3\frac{1}{2}$ |
| $1\frac{1}{2}$ | $0\frac{1}{2}$ | --<br>-- | --<br>-- | --<br>-- | 25. 00<br>5. 00 | 25. 00<br>5. 00 | --<br>-- | --<br>-- | --<br>-- |
| $2\frac{1}{2}$ | $1\frac{1}{2}$ | --<br>-- | --<br>-- | 10. 00<br>3. 16 | 15. 00<br>3. 87 | 15. 00<br>3. 87 | 10. 00<br>3. 16 | --<br>-- | --<br>-- |
| $3\frac{1}{2}$ | $2\frac{1}{2}$ | --<br>-- | 5. 36<br>2. 32 | 8. 93<br>2. 90 | 10. 71<br>3. 27 | 10. 71<br>3. 27 | 8. 93<br>2. 99 | 5. 36<br>2. 32 | --<br>-- |
| $4\frac{1}{2}$ | $3\frac{1}{2}$ | 3. 33<br>1. 82 | 5. 83<br>2. 41 | 7. 50<br>2. 74 | 8. 33<br>2. 89 | 8. 33<br>2. 89 | 7. 50<br>2. 74 | 5. 83<br>2. 41 | 3. 33<br>1. 82 |
| $J$ | $J$ | | | | | | | | |
| $0\frac{1}{2}$ | $0\frac{1}{2}$ | --<br>-- | --<br>-- | --<br>-- | 25. 00<br>5. 00 | 25. 00<br>5. 00 | --<br>-- | --<br>-- | --<br>-- |
| $1\frac{1}{2}$ | $1\frac{1}{2}$ | --<br>-- | --<br>-- | 22. 50<br>4. 74 | 2. 50<br>1. 58 | 2. 50<br>1. 58 | 22. 50<br>4. 74 | --<br>-- | --<br>-- |
| $2\frac{1}{2}$ | $2\frac{1}{2}$ | --<br>-- | 17. 85<br>4. 22 | 6. 43<br>2. 54 | 0. 71<br>0. 84 | 0. 71<br>0. 84 | 6. 43<br>2. 54 | 17. 85<br>4. 22 | --<br>-- |
| $3\frac{1}{2}$ | $3\frac{1}{2}$ | 14. 60<br>3. 82 | 7. 45<br>2. 73 | 2. 68<br>1. 61 | 0. 30<br>0. 55 | 0. 30<br>0. 55 | 2. 68<br>1. 61 | 7. 45<br>2. 73 | 14. 60<br>3. 82 |

TABLE 11. *K- and $(K)^{1/2}$-values for components in a Zeeman pattern*—Continued

[Upper figures are *K*-values; lower $(K)^{1/2}$-values]

| Even multiplicities, normal components | | | | | | | | | |
|---|---|---|---|---|---|---|---|---|---|
| $J$ | $J-1$ | $M=-2\frac{1}{2}$<br>$M=-3\frac{1}{2}$ | $-1\frac{1}{2}$<br>$-2\frac{1}{2}$ | $-0\frac{1}{2}$<br>$-1\frac{1}{2}$ | $0\frac{1}{2}$<br>$-0\frac{1}{2}$ | $1\frac{1}{2}$<br>$0\frac{1}{2}$ | $2\frac{1}{2}$<br>$1\frac{1}{2}$ | $3\frac{1}{2}$<br>$2\frac{1}{2}$ | $4\frac{1}{2}$<br>$3\frac{1}{2}$ |
| $1\frac{1}{2}$ | $0\frac{1}{2}$ | --<br>-- | --<br>-- | --<br>-- | 6. 25<br>2. 50 | 18. 75<br>4. 33 | --<br>-- | --<br>-- | --<br>-- |
| $2\frac{1}{2}$ | $1\frac{1}{2}$ | --<br>-- | --<br>-- | 1. 25<br>1. 12 | 3. 75<br>1. 94 | 7. 50<br>2. 74 | 12. 50<br>3. 54 | --<br>-- | --<br>-- |
| $3\frac{1}{2}$ | $2\frac{1}{2}$ | --<br>-- | 0. 45<br>0. 67 | 1. 34<br>1. 16 | 2. 68<br>1. 64 | 4. 46<br>2. 11 | 6. 70<br>2. 50 | 9. 37<br>3. 06 | --<br>-- |
| $4\frac{1}{2}$ | $3\frac{1}{2}$ | 0. 21<br>0. 46 | 0. 63<br>0. 79 | 1. 25<br>1. 12 | 2. 08<br>1. 44 | 3. 12<br>1. 77 | 4. 37<br>2. 09 | 5. 83<br>2. 41 | 7. 50<br>2. 74 |
| $J$ | $J$ | | | | | | | | |
| $0\frac{1}{2}$ | $0\frac{1}{2}$ | --<br>-- | --<br>-- | --<br>-- | 25. 00<br>5. 00 | --<br>-- | --<br>-- | --<br>-- | --<br>-- |
| $1\frac{1}{2}$ | $1\frac{1}{2}$ | --<br>-- | --<br>-- | 7. 50<br>2. 74 | 10. 00<br>3. 16 | 7. 50<br>2. 74 | --<br>-- | --<br>-- | --<br>-- |
| $2\frac{1}{2}$ | $2\frac{1}{2}$ | --<br>-- | 3. 57<br>1. 89 | 5. 71<br>2. 39 | 6. 43<br>2. 54 | 5. 71<br>2. 39 | 3. 57<br>1. 89 | --<br>-- | --<br>-- |
| $3\frac{1}{2}$ | $3\frac{1}{2}$ | 2. 08<br>1. 44 | 3. 57<br>1. 89 | 4. 46<br>2. 11 | 4. 76<br>2. 18 | 4. 46<br>2. 11 | 3. 57<br>1. 89 | 2. 08<br>1. 44 | --<br>-- |

The value $J$ is the larger of two $J$-values involved. For these equations it has been assumed that the observations have been made perpendicularly to the magnetic field. $K$-values have been computed by means of these equations and are given in table 11. The value 75 has been assigned to constant $A$ so that the sum of all parallel components in a pattern may be 50 and that the corresponding sum for each of the two groups of normal components may be 25. Thus the sum of all components in each pattern will be 100.

In calculations related to the strength of lines the square root $(\boldsymbol{S})^{1/2}$ of $\boldsymbol{S}$ is more convenient than the strength itself for comparison with the observed intensities. Accordingly, we have computed the square roots of the $K$-values. In table 11 the square roots are given under their respective $\boldsymbol{S}$-values. Taking the square root of both members of eq 24, we have

$$(\boldsymbol{S}^M)^{1/2}=\boldsymbol{S}^{1/2}\times K^{1/2}. \tag{25}$$

This equation means that to obtain $(\boldsymbol{S}^M)^{1/2}$-values it is only necessary to multiply the values of $K^{1/2}$ by the strengths of their respective spectroscopic lines. The quantities $(\boldsymbol{S}^M)^{1/2}$, $\boldsymbol{S}^{1/2}$, and $K^{1/2}$ are either positive or negative. The sign of $(\boldsymbol{S}^M)^{1/2}$ depends on the sign of $\boldsymbol{S}^{1/2}$ and $K^{1/2}$. The sign of $\boldsymbol{S}^{1/2}$ depends on the changes of the $L$- and $J$-values in the spectral line. The sign of $K^{1/2}$ depends on the changes in the $J$- and $M$-values for the magnetic levels of the components. Tables 12 and 13 give the signs for the different cases.

TABLE 12. *Signs of $\boldsymbol{S}^{1/2}$ (spectral lines)*

| Quantum numbers | $J\rightarrow J+1$ | $J\rightarrow J$ | $J\rightarrow J-1$ |
|---|---|---|---|
| $L\rightarrow L+1$ | + | + | − |
| $L\rightarrow L$ | − | [a] ± | − |
| $L\rightarrow L-1$ | − | + | + |

[a] Sign (+) if $S(S+1)<L(L+1)+J(J+1)$; sign (−) if $S(S+1)>L(L+1)+J(J+1)$. Here $S$ is not the strength of the line, but is the resultant spin.

TABLE 13. *Signs of $K^{1/2}$ (magnetic components)*

| Quantum numbers | $M\rightarrow M+1$ | $M\rightarrow M$ | $M\rightarrow M-1$ |
|---|---|---|---|
| $J\rightarrow J+1$ | − | + | + |
| $J\rightarrow J$ | + | [a] ± | + |
| $J\rightarrow J-1$ | + | + | − |

[a] The same sign as $M$.

## 10. Theoretical Strengths $(\boldsymbol{S}^M)^{1/2}$ of Components in Patterns of a Multiplet $^6D-{}^6F^\circ$

The strengths may be computed by formula (25). The $\boldsymbol{S}$-values for lines in a multiplet $^6D-{}^6F^\circ$ can be deduced by the classical formulas of Kronig, of Sommerfeld and Hönl, and of Russell [10]. The square roots of the values obtained are given in table 14. The signs have been computed by table 12.

In order to compute the final $(\boldsymbol{S}^M)^{1/2}$-values we have multiplied, for each pattern, the strengths of its components, given in table 11, by the strength of the line

TABLE 14. *Values of $S^{\frac{1}{2}}$ for $^6D-{}^6F^\circ$ lines*

| Levels | $^6D_{0\frac{1}{2}}$ | $^6D_{1\frac{1}{2}}$ | $^6D_{2\frac{1}{2}}$ | $^6D_{3\frac{1}{2}}$ | $^6D_{4\frac{1}{2}}$ |
|---|---|---|---|---|---|
| $^6F^\circ_{5\frac{1}{2}}$ | 18. 97 | | | | |
| $^6F^\circ_{4\frac{1}{2}}$ | 7. 45 | 15. 63 | | | |
| $^6F^\circ_{3\frac{1}{2}}$ | −2. 11 | 9. 02 | 12. 42 | | |
| $^6F^\circ_{2\frac{1}{2}}$ | | −3. 21 | 9. 13 | 9. 30 | |
| $^6F^\circ_{1\frac{1}{2}}$ | | | −3. 79 | 8. 26 | 6. 11 |
| $^6F^\circ_{0\frac{1}{2}}$ | | | | −3. 65 | 6. 83 |

without field, given in table 14. The resulting values are given in table 15.

## 11. Theoretical Computation of Line Strengths in a Zeeman Pattern Perturbed by Partial Paschen-Back Effect

The partial Paschen-Back effect, in *LS*-coupling, produces intensity distortions in the component lines of the patterns. These distortions may be calculated by the so-called second-order perturbation theory. In this theory two magnetic levels $T^M_J$ and $T^M_{J-1}$ belonging to consecutive spectroscopic levels $T_J$ and $T_{J-1}$ of a term $T$, and having the same $M$-value, interact with each other, perturbing mutually the strengths of their combinations with another third level. If we set $T^M_J < T^M_{J-1}$—the third level being inappreciably lower or higher than the other two—the perturbed strengths of the transitions are given by eq 26a and b, which we take from Kiess and Shortley [7, p. 204]

$$\text{pert.}(S^M_J)^{\frac{1}{2}} = \text{unpert.}(S^M_J)^{\frac{1}{2}} - (aI/\Delta)\ \text{unpert.}(S^M_{J-1})^{\frac{1}{2}}, \tag{26a}$$

$$\text{pert.}(S^M_{J-1})^{\frac{1}{2}} = \text{unpert.}(S^M_{J-1})^{\frac{1}{2}} + (aI/\Delta)\ \text{unpert.}(S^M_J)^{\frac{1}{2}}. \tag{26b}$$

The first members of these equations are the strengths of the perturbed transitions. The quantity $a$ is the LU in $cm^{-1}$ for the magnetic field, $I$ is the interaction factor given in table 3, and $\Delta$ the distance, in $cm^{-1}$, between the two interacting magnetic levels. The remaining factors are the strengths of

TABLE 15. *Calculated strengths in multiplet a $^6D-z\,^6F^\circ$ of* Mn I *with and without perturbation*

[Magnetic field 84,700 oersteds. Upper figures are values without perturbation. Lower are with perturbation.]

| Designation | | Designation | | | | | | | | | | | |
|---|---|---|---|---|---|---|---|---|---|---|---|---|---|
| | | a $^6D_{2\frac{1}{2}}$ | | | | | | a $^6D_{1\frac{1}{2}}$ | | | | a $^6D_{0\frac{1}{2}}$ | |
| | $M$ | $-2\frac{1}{2}$ | $-1\frac{1}{2}$ | $-0\frac{1}{2}$ | $0\frac{1}{2}$ | $1\frac{1}{2}$ | $2\frac{1}{2}$ | $-1\frac{1}{2}$ | $-0\frac{1}{2}$ | $0\frac{1}{2}$ | $1\frac{1}{2}$ | $-0\frac{1}{2}$ | $0\frac{1}{2}$ |
| $z\,^6F^\circ_{5\frac{1}{2}}$ | $-2\frac{1}{2}$ | −38. 5 | 17. 3 | -- | -- | -- | -- | 32. 9 | -- | -- | -- | -- | -- |
| | | −37. 1 | 17. 4 | -- | -- | -- | -- | 33. 5 | -- | -- | -- | -- | -- |
| | $-1\frac{1}{2}$ | 17. 3 | −23. 2 | 23. 7 | -- | -- | -- | 29. 4 | 25. 5 | -- | -- | -- | -- |
| | | 17. 8 | −20. 6 | 24. 1 | -- | -- | -- | 32. 4 | 24. 3 | -- | -- | -- | -- |
| | $-0\frac{1}{2}$ | -- | 23. 7 | −7. 7 | 23. 2 | -- | -- | −10. 4 | 36. 0 | 18. 0 | -- | -- | -- |
| | | -- | 24. 0 | −4. 6 | 23. 2 | -- | -- | −12. 3 | 37. 2 | 15. 9 | -- | -- | -- |
| | $0\frac{1}{2}$ | -- | -- | 23. 2 | 7. 7 | 23. 7 | -- | -- | −18. 0 | 36. 0 | 10. 5 | -- | -- |
| | | -- | -- | 23. 1 | 10. 7 | 23. 3 | -- | -- | −20. 2 | 34. 8 | 8. 5 | -- | -- |
| | $1\frac{1}{2}$ | -- | -- | -- | 23. 7 | 23. 2 | 17. 3 | -- | -- | −25. 5 | 29. 4 | -- | -- |
| | | -- | -- | -- | 23. 2 | 25. 8 | 16. 7 | -- | -- | −26. 7 | 26. 4 | -- | -- |
| | $2\frac{1}{2}$ | -- | -- | -- | -- | 17. 3 | 38. 5 | -- | -- | -- | −32. 9 | -- | -- |
| | | -- | -- | -- | -- | 16. 6 | 40. 0 | -- | -- | -- | −32. 4 | -- | -- |
| $z\,^6F^\circ_{4\frac{1}{2}}$ | $-1\frac{1}{2}$ | −18. 4 | −12. 0 | 4. 2 | -- | -- | -- | −39. 2 | 22. 6 | -- | -- | 26. 5 | -- |
| | | −11. 8 | −12. 9 | 5. 6 | -- | -- | -- | −36. 7 | 23. 4 | -- | -- | 27. 1 | -- |
| | $-0\frac{1}{2}$ | -- | −10. 4 | −14. 7 | 7. 4 | -- | -- | 22. 6 | −13. 1 | 26. 1 | -- | 30. 6 | 15. 3 |
| | | -- | −8. 3 | −15. 0 | 9. 0 | -- | -- | 24. 3 | −7. 8 | 25. 8 | -- | 36. 7 | 10. 1 |
| | $0\frac{1}{2}$ | -- | -- | −7. 4 | −14. 7 | 10. 4 | -- | -- | 26. 1 | 13. 0 | 22. 6 | −15. 3 | 30. 6 |
| | | -- | -- | −5. 7 | −14. 3 | 12. 4 | -- | -- | 26. 6 | 18. 3 | 20. 9 | −21. 5 | 24. 4 |
| | $1\frac{1}{2}$ | -- | -- | -- | −4. 2 | −12. 0 | 13. 4 | -- | -- | 22. 6 | 39. 2 | -- | −26. 5 |
| | | -- | -- | -- | −2. 9 | −11. 0 | 15. 1 | -- | -- | 21. 9 | 41. 6 | -- | −24. 8 |
| $z\,^6F^\circ_{3\frac{1}{2}}$ | $-0\frac{1}{2}$ | -- | -- | -- | -- | -- | -- | −15. 8 | −18. 3 | 9. 1 | -- | −34. 2 | 34. 2 |
| | | -- | -- | -- | -- | -- | -- | −11. 1 | −18. 5 | 12. 1 | -- | −29. 1 | 38. 0 |
| | $0\frac{1}{2}$ | -- | -- | -- | -- | -- | -- | -- | −9. 1 | −18. 3 | 15. 8 | 34. 2 | 34. 2 |
| | | -- | -- | -- | -- | -- | -- | -- | −6. 2 | −18. 0 | 20. 5 | 30. 3 | 39. 2 |

TABLE 16.—*Values of $aI/\Delta$ for multiplets $a\,^6D - z\,^6F^\circ$ of* Mn I

(LU = 3.955 cm$^{-1}$)

| Interacting levels | Interval | $I$-values | | | $aI/\Delta$ | | |
|---|---|---|---|---|---|---|---|
| | | $M=\pm 0\frac{1}{2}$ | $1\frac{1}{2}$ | $2\frac{1}{2}$ | $M=\pm 0\frac{1}{2}$ | $1\frac{1}{2}$ | $2\frac{1}{2}$ |
| $a\,^6D_{2\frac{1}{2}}$, $a\,^6D_{2\frac{1}{2}}$ | 169.52 | 1.050 | 0.959 | 0.742 | 0.025 | 0.022 | 0.017 |
| $a\,^6D_{2\frac{1}{2}}$, $a\,^6D_{1\frac{1}{2}}$ | 116.96 | 1.200 | 0.989 | -- | 0.041 | 0.033 | -- |
| $a\,^6D_{1\frac{1}{2}}$, $a\,^6D_{0\frac{1}{2}}$ | 68.67 | 1.247 | -- | -- | 0.072 | -- | -- |
| $z\,^6F^\circ_{3\frac{1}{2}}$, $z\,^6F^\circ_{2\frac{1}{2}}$ | 71.42 | 1.355 | 1.258 | 0.958 | 0.075 | 0.070 | 0.053 |
| $z\,^6F^\circ_{2\frac{1}{2}}$, $z\,^6F^\circ_{1\frac{1}{2}}$ | 48.95 | 1.470 | 1.200 | -- | 0.119 | 0.097 | -- |
| $z\,^6F^\circ_{1\frac{1}{2}}$, $z\,^6F^\circ_{0\frac{1}{2}}$ | 28.51 | 1.490 | -- | -- | 0.207 | -- | -- |

the unperturbed transitions. For a component perturbed by two others the changes are additive. Special care must be given in these calculations to the signs of the strengths.

## 12. Perturbations in the Strengths of the Components in Some Patterns of Mn I

We are now prepared to compare the observed intensities in some patterns of Mn I with the theoretical strengths computed by eq 26a and b. For this comparison we have selected the multiplet $a\,^6D - z\,^6F^\circ$ for two reasons. First, this multiplet has an outstanding intensity, making it easy to observe all the components of the patterns, even the faintest. Second, the $I$ factors for such terms have high values (see table 3) especially for the lower $J$-values of $z\,^6F^\circ$, and the separations $\Delta$ are relatively small, so that the magnitudes of $I/\Delta$ are very important.

First we have computed the values of $aI/\Delta$ for the different transitions in this multiplet. Only the values corresponding to small $J$-values have been considered. Within the accuracy of this calculation the separation between spectroscopic levels may be used instead of that between magnetic levels belonging to the spectroscopic levels. Values of separations have been taken from table 4 and $I$-values from table 3. For the LU, $a=3.955$ has been used. The resulting values are given in table 16.

We shall proceed now to compute independently the strength perturbations under the influence of the levels of $a\,^6D$ and $z\,^6F^\circ$. A few examples will illustrate in detail how these calculations have been made.

We select first a very simple case, that of the component $a\,^6D^{0\frac{1}{2}}_{0\frac{1}{2}} - z\,^6F^{0\frac{1}{2}}_{0\frac{1}{2}}$. Its initial state $a\,^6D^{0\frac{1}{2}}_{0\frac{1}{2}}$ is perturbed only by $a\,^6D^{0\frac{1}{2}}_{1\frac{1}{2}}$, and its final state $z\,^6F^{0\frac{1}{2}}_{0\frac{1}{2}}$ only by $z\,^6F^{0\frac{1}{2}}_{1\frac{1}{2}}$. The strengths of the unperturbed transitions involved, taken from table 15 (in the table the values are rounded) are

$$a\,^6D^{0\frac{1}{2}}_{0\frac{1}{2}} \to z\,^6F^{0\frac{1}{2}}_{1\frac{1}{2}} = 30.55$$

$$a\,^6D^{0\frac{1}{2}}_{1\frac{1}{2}} \to z\,^6F^{0\frac{1}{2}}_{0\frac{1}{2}} = -18.25 \qquad a\,^6D^{0\frac{1}{2}}_{0\frac{1}{2}} \to z\,^6F^{0\frac{1}{2}}_{0\frac{1}{2}} = 34.15$$

Factors $aI/\Delta$ taken from table 16 are: 0.207 for the influence of $z\,^6F^{0\frac{1}{2}}_{1\frac{1}{2}}$, $z\,^6F^{0\frac{1}{2}}_{0\frac{1}{2}}$, and 0.072 for that of $a\,^6D^{0\frac{1}{2}}_{1\frac{1}{2}}$, $a\,^6D^{0\frac{1}{2}}_{0\frac{1}{2}}$. The values of the perturbations will then be:

$$0.207\times 30.55 = 6.32 \text{ and } 0.072\times(-18.25) = -1.31.$$

The first is to be added (eq 26a) because it is due to the influence of level $z\,^6F_{1\frac{1}{2}}$ on another *higher* level $z\,^6F^\circ_{0\frac{1}{2}}$. The second perturbation also is to be added because it is due to the influence of level $a\,^6D_{1\frac{1}{2}}$ on another higher one, $a\,^6D_{0\frac{1}{2}}$. Hence the final value of the perturbed strength will be $34.15+6.32-1.31=39.16$.

The line $a\,^6D^{0\frac{1}{2}}_{1\frac{1}{2}} \to z\,^6F^{0\frac{1}{2}}_{1\frac{1}{2}}$ is a more complicated example. Its initial state is affected by both $a\,^6D^{0\frac{1}{2}}_{2\frac{1}{2}}$ and $a\,^6D^{0\frac{1}{2}}_{0\frac{1}{2}}$. Its final state is perturbed by $z\,^6F^{0\frac{1}{2}}_{2\frac{1}{2}}$ and $z\,^6F^{0\frac{1}{2}}_{0\frac{1}{2}}$. The strengths without perturbation of the components (see table 11) are

$$a\,^6D^{0\frac{1}{2}}_{1\frac{1}{2}} \to z\,^6F^{0\frac{1}{2}}_{2\frac{1}{2}} = 35.99$$

$$a\,^6D^{0\frac{1}{2}}_{2\frac{1}{2}} \to z\,^6F^{0\frac{1}{2}}_{1\frac{1}{2}} = -14.67 \qquad a\,^6D^{0\frac{1}{2}}_{1\frac{1}{2}} \to z\,^6F^{0\frac{1}{2}}_{1\frac{1}{2}} = 13.05 \qquad a\,^6D^{0\frac{1}{2}}_{0\frac{1}{2}} \to z\,^6F^{0\frac{1}{2}}_{1\frac{1}{2}} = 30.55$$

$$a\,^6D^{0\frac{1}{2}}_{1\frac{1}{2}} \to z\,^6F^{0\frac{1}{2}}_{0\frac{1}{2}} = -18.25$$

The values of $aI/\Delta$, as given by table 13 are 0.041 and 0.072 for the influences of $D_{2\frac{1}{2}}$, $D_{1\frac{1}{2}}$, and $D_{0\frac{1}{2}}$, $D_{1\frac{1}{2}}$, respectively; and 0.119 and 0.207 for those of $F_{2\frac{1}{2}}$, $F_{1\frac{1}{2}}$ and $F_{0\frac{1}{2}}$, $F_{1\frac{1}{2}}$, respectively.

The values of the perturbations are thus: $0.041\times(-14.67)=-0.60$, $0.072\times(30.55)=2.20$, $0.119\times(35.99)=4.28$, and $0.207\times(-18.25)=3.78$. These perturbations will be added for $D_{2\frac{1}{2}}$, $D_{1\frac{1}{2}}$ and for $F_{2\frac{1}{2}}$, $F_{1\frac{1}{2}}$; and subtracted for $D_{0\frac{1}{2}}$, $D_{1\frac{1}{2}}$ and for $F_{0\frac{1}{2}}$, $F_{1\frac{1}{2}}$ because of the relations $D_{2\frac{1}{2}}<D_{1\frac{1}{2}}<D_{0\frac{1}{2}}$ and $F_{2\frac{1}{2}}<F_{1\frac{1}{2}}<F_{0\frac{1}{2}}$. The final strength of the perturbed line will be $13.05+(-0.60)-2.20+4.38-(-3.78)=18.31$. Thus the line with strength 13.05 has been distorted, and its strength has been changed by 18.31.

With the same procedure we have computed the perturbations for some other patterns of multiplet $a\,^6D - z\,^6F^\circ$ of Mn I. The resulting values of this calculation are given in table 15. A comparison that we have made of the observed intensities with the values given in table 15 shows that in all cases the intensity perturbations are in the right direction

and of the right order of magnitude to account for the observed asymmetries. We do not intend to give here our own intensities, because they have little quantitative value, representing only visual estimates. However, it must be noted that particular care was taken in these estimates, to note in each pair of two symmetrical unperturbed components which was the stronger when perturbed. Readers of this paper may check for themselves the accuracy of these results by making visual estimates of the component intensities in figure 4 and comparing their resulting values with those given near the components, which represent the calculated perturbed strengths.

---

Many helpful suggestions were received from friends and colleagues throughout this work. During the author's long stay at the Bureau, W. F. Meggers, C. C. Kiess, and C. Moore-Sitterly constantly assisted him and kindly corrected the manuscript. While he was at Princeton University, A. G. Shenstone collaborated cordially with this work. Similarly, at the Massachusetts Institute of Technology, G. R. Harrison placed at the author's disposal instruments and spectrograms of the Zeeman effect; J. C. van den Bosch helped to prepare the magnet and took the spectrograms on which a large part of this investigation is based. To all of these cordial thanks are expressed.

In addition to the above the author is also indebted to the American Philosophical Society and to the American Academy of Arts and Sciences. The liberal support received from all of these institutions has permitted the author to carry on scientific work in America for nearly 2 years, for which he is extremely grateful.

Finally, thanks are expressed to Olga García-Riquelme, R. Velasco, M. Losada, and F. Rico, colleagues in the Institutó de Optica, Madrid, for assistance in the preparation of the manuscript and in many other ways.

## 13. References

[1] M. Martinez-Risco, Anal. Soc. Esp. de Fis. y Quim. **9,** 263 (1912); and Phys. Z. **13,** 137 (1912).
[2] E. Back und A. Landé, Zeemaneffekt und Multiplettstruktur der Spektrallinien (Julius Springer, Berlin, 1925).
[3] E. Back, Z. Phys. **13,** 205, 1923.
[4] G. R. Harrison and J. R. McNally, Jr., Phys Rev. **58,** 708 (1940); J. P. Molnar and W. J. Hitchcock, J. Opt. Soc. Am. **30,** 534 (1940); O. Laporte and J. E. Mack, Phys. Rev. **63,** 257 (1942).
[5] J. R. McNally, Jr. and G. R. Harrison, J. Opt. Soc. Am. **35,** 584 (1945).
[6] M. A. Catalán and Olga García-Riquelme, unpublished material.
[7] C. C. Kiess and G. Shortley, J. Research NBS **42,** 183 (1949) RP 1961.
[8] M. A. Catalán and R. Velasco, Proc. Phys. Soc. [A] **63,** 917 (1950).
[9] M. A. Catalán and R. Velasco, J. Opt. Soc. Am. **40,** 653 (1950); Anal. Soc. Esp. de Fis. y Quim., A, **47,** 7 (1951).
[10] H. N. Russell, Proc. Nat. Acad. Sci. **11,** 322 (1925).

Washington, July 9, 1951.

# Index to Volume 47


*A*

Page

*Abramowitz, Milton*, Tables of the functions $f_0^x \sin^{1/3} x\ dx$ and $(4/3)\sin^{-4/3}\Phi \int_0^\Phi \sin^{1/3} x\ dx$, RP2255 ..... 288
Absorption spectra of 18 methanes, RP2245 ..... 202
Acceptance sampling procedures, RP2277 ..... 491
Acetates of D-galactosylamine, RP2248 ..... 239
Acetylene, deuterated, RP2249 ..... 248
*Achhammer, Bernard G., Mary Jane Reiney, Frank W. Reinhart*, Study of degradation of polystyrene, using infrared spectrophotometry, RP2235 ..... 116
Alkalies in portland cement clinker, RP2264 ..... 349
Alumina, from clay, RP2253 ..... 269
Aluminum chloride, crystallization, RP2253 ..... 269
Annealed copper, creep of, RP2254 ..... 272
*Arnold, Robert D., Harold J. Hoge*, Vapor pressures of hydrogen deuterium and hydrogen deuteride, and dew-point pressures of their mixtures, RP2228 ..... 63
Asbestos-cement pipe, exposure to soils, RP2264 ..... 367
Ash, determination of, in synthetic rubber and latex, RP2237 ..... 135
Asymmetrical Zeeman patterns, RP2278 ..... 502

*B*

*Bailin, Louis L.*, An analysis of the effect of the discontinuity in a bifurcated circular guide upon plane longitudinal waves, RP2258 ..... 315
*Ballinger, John C., Bourdon F. Scribner*, Spectrochemical analysis of bronze by a porous electrode method, RP2246 ..... 221
Barium aluminates, heats of solution in 2.00 *N* HCl, and heats of formation, RP2269 ..... 439
Barium aluminate hydrates, heats of solution in 2.00 *N* HCl, and heats of formation, RP2269 ..... 439
Barium titanate-beryllia-titania system, dielectric constant and *Q* values, RP2222 ..... 15
*Bates, Roger G.*, First dissociation constant of phosphoric acid from 0° to 60° C; limitations of the electromotive force method for moderately strong acids, RP2236 ..... 127
—, *Vincent E. Bower, Richard G. Miller, Edgar R. Smith*, pH of solutions of potassium hydrogen *d*-tartrate from 0° to 60° C, RP2268 ..... 433
—, *Richard G. Canham*, Resolution of the dissociation constants of *d*-tartaric acid from 0° to 50° C, RP2260 ..... 343
*Bell, Rosemond K., Bruce B. Pendigo, Harry A. Bright*, Spectrophotometric determination of bismuth in lead-base and tin-base alloys, RP2250 ..... 252
Bench, electron-optical, RP2273 ..... 461
*Bendigo, Bruce B., Rosemond K. Bell, Harry A. Bright*, Spectrophotometric determination of bismuth in lead-base and tin-base alloys, RP2250 ..... 252
*Benedict, W. S., Earle K. Plyler*, Infrared spectra of eighteen halogen-substituted methanes, RP2245 ..... 202
Benzoic acid, heat capacity, enthalpy, entropy, and heat of fusion, RP2251 ..... 256
Bismuth, determination in lead-base and tin-base alloys, RP2250 ..... 252
*Bovey, Harry L., Montgomery R. Shafer, Ernest F. Fiock, Ross B. Van Lone*, Correcting for density and viscosity of incompressible fluids in float-type flowmeters, RP2247 ..... 227
*Bower, Vincent E., Roger G. Bates, Richard G. Miller, Edgar R. Smith*, pH of solutions of potassium hydrogen *d*-tartrate from 0° to 60° C, RP2268 ..... 433
*Bright, Harry A., Bruce B. Pendigo, Rosemond K. Bell*, Spectrophotometric determination of bismuth in lead-base and tin-base alloys, RP2250 ..... 252
—, *John L. Hague, Eric D. Brown*, Photometric determination of copper in iron and steel with diethyldithiocarbamate, RP2265 ..... 380
*Brode, Wallace R., George M. Wyman*, Absorption spectra of thioindigo dyes in benzene and chloroform, RP2241 ..... 170
Bronze, spectrochemical analysis of, RP2246 ..... 221
*Brown, Eric D., John L. Hague, Harry A. Bright*, Photometric determination of copper in iron and steel with diethyldithiocarbamate, RP2265 ..... 380
*Bunting, Elmer N., George R. Shelton, Ansel S. Creamer, Bernard Jaffe*, Properties of beryllium-barium titanate dielectrics, RP2222 ..... 15
*Burdick, Milton D., Benson Zweig, R. Eugene Moreland*, Linear thermal expansion of artificial graphites to 1,370° C, RP2225 ..... 35

*C*

Calcium, infrared spectrum, RP2252 ..... 262
Calorimetric properties of benzoic acid from 0° to 410° K, RP2251 ..... 256
*Canham, Richard G., Roger G. Bates*, Resolution of the dissociation constants of *d*-tartaric acid from 0° to 50° C, RP2260 ..... 343
*Carpenter, Frank G., Victor R. Deitz*, Glass spheres for the measurement of the effective opening of testing sieves, RP2238 ..... 139
*Catalan, Miguel A.*, Asymmetries of Zeeman patterns and *g*-values for neutral manganese, RP2278 ..... 502
Cathode films, hydrodynamics of, RP2240 ..... 156
Cathodic protection of steel in soils, RP2233 ..... 104
Cathode-ray oscillograph, momentary beam intensification for cold-cathode, RP2231 ..... 87
Cathodic protection, role of current distribution in, RP2220 ..... 1
*Cavallo, L., H. H. Seliger*, The absolute standardization of radioisotopes by $4\pi$ counting, RP2226 ..... 41
*Chand, Uttam*, On the derivation and accuracy of certain formulas for sample sizes and operating characteristics of nonsequential sampling procedures, RP2277 ..... 491
Characteristic numbers and vectors, RP2275 ..... 471
Characteristic roots, RP2227 ..... 45
Chromium, spark spectrum, RP2266 ..... 385
*Cis-trans* isomerism—thioindigo dyes, RP2241 ..... 170
*Clark, Lewis Jesse, Willard D. Hubbard, James I. Hoffman*, Crystallization of aluminum chloride in hydrochloric acid process for the production of alumina from clay, RP2253 ..... 269
Clay, extraction of alumina, RP2253 ..... 269
*Cohen, Ralph L., Frederic J. Linnig, Lewis T. Milliren*, Determination of ash in GR–S synthetic rubbers and latices, RP2237 ..... 135

Page

Cold-drawn copper, creep of, RP2254 ..... 272
Condensation of vapor on cylindric surfaces, RP2255 ..... 288
Convergence of Cauchy-Riemann sums to integrals, RP2243 ..... 191
Copper, determination of, in steel and iron, RP2265 ..... 380
Copper, high-purity, creep of, RP2254 ..... 272
Correcting for density and viscosity of incompressible fluids in float-type flowmeters, RP2247 ..... 227
*Corruccini, Robert J.*, Annealing of platinum for therometry, RP2232 ..... 94
Counter, $4\pi$; absolute; flow; proportional, RP2226 ..... 41
*Creamer, Ansel S., Elmer N. Bunting, George R. Shelton, Bernard Jaffe*, Properties of beryllium-barium titanate dielectrics, RP2222 ..... 15
Critical temperatures, pressures and volumes of hydrogen, deuterium, and hydrogen deuteride, RP2229 ..... 75
Crucibles, aluminum versus porcelain, in ash determination, RP2237 ..... 135
Current distribution, role in cathodic protection, RP2220 ..... 1
*Cutkosky, R. E.*, A Monte Carlo method for solving a class of integral equations, RP2234 ..... 113

*D*

*Deitz, Victor R., Frank G. Carpenter*, Glass spheres for the measurement of the effective opening of testing sieves, RP2238 ..... 139
*Denison, Irving A., Melvin Romanoff*, Effect of exposure to soils on the properties of asbestos-cement pipe, RP2264 ..... 367
Determinants, random, RP2274 ..... 465
Deuterium, hydrogen, and hydrogen deuteride, critical temperatures, pressures, and volumes, RP2229 ..... 75
Deuterium, hydrogen, and hydrogen deuteride, vapor dew-point pressures of mixtures, RP2228 ..... 63
Dew-point pressures of mixtures of hydrogen, deuterium, and hydrogen deuteride, RP2228 ..... 63
Dextrose and dextrines, determination in corn-sirup, RP2263 ..... 363
*Diamond, J. J., Donald Hubbard*, Thickness of glass electrodes, RP2270 ..... 443
*Dibeler, Vernon H., Fred L. Mohler*, Mass spectra of some organo-lead and organo-mercury compounds, RP2259 ..... 337
Dielectric constant in system beryllia-barium titanate-titania, RP2222 ..... 15
Diethyldithiocarbamate, determination of copper in iron and steel with, RP2265 ..... 380
*Digges, Thomas G., William D. Jenkins*, Creep of annealed and cold-drawn high-purity copper, RP2254 ..... 272
Dilatometric determination of linear thermal expansion to 1,370° C RP2225 ..... 35
Dissociation constant of phosphoric acid, RP2236 ..... 127
Dissociation constants of tartaric acid, RP2260 ..... 343
Distillation of hydrogen, RP2271 ..... 494

*E*

Eigenvalue, matrices, RP2256 ..... 291
Electrical deposition, RP2240 ..... 156
Electron-optical bench, RP2273 ..... 449
Emf method for dissociation constants, RP2236 ..... 127
Expansivity, photoelectric recording interferometric measurement of, RP2230 ..... 80

*F*

Filter design, conventional method of, RP2276 ..... 479
Filter method of temperature determination, RP2272 ..... 456
*Fiock, Ernest F., Montgomery R. Shafer, Harry L. Bovey, Ross B. Van Lone*, Correcting for density and viscosity of incompressible fluids in float-type flowmeters, RP2247 ..... 227
Flow-rate meters, variable-area, float or rotameter type, correcting for density and viscosity of fluids, RP2247 ..... 227
*Fookson, Abraham, Philip Pomerantz, Edwin H. Rich*, Preparation and purification of hydrogen deuteride, RP2224 ..... 31
—, —, *Simon Rothberg*, Some characteristics of Stedman packing in the distillation of hydrogen and its isotopes, RP2271 ..... 449
*Fortet, R.*, Random determinants, RP2274 ..... 465
Fourier analysis, of synchronous rectifier, RP2267 ..... 427
*Frush, Harriet L., Horace S. Isbell*, Mutarotation, hydrolysis, and structure of D-galactosylamines, RP2248 ..... 239
*Fuzukawa, George T., Robert E. McCoskey, Gerard J. King*, Calorimetric properties of benzoic acid from 0° to 410° K, RP2251 ..... 256

*G*

*g*-values, RP2278 ..... 502
*Gailar, Norman, Earle K. Plyler*, The near infrared absorption spectra of deuterated acetylene, RP2249 ..... 248
Glass electrodes, thickness of, RP2270 ..... 502
Glass spheres, for testing sieves, RP2238 ..... 139
Gradients, RP2227 ..... 45
Graphite, linear thermal expansion of, RP2225 ..... 35

*H*

*Hague, John L., Eric D. Brown, Harry A. Bright*, Photometric determination of copper in iron and steel with diethyldithiocarbamate, RP2265 ..... 380
Harmonic output, of synchronous rectifier, RP2267 ..... 427
Helmholtz's equation, RP2258 ..... 315
*Hestenes, Magnus R., William Karush*, A method of gradients for the calculation of the characteristic roots and vectors of a real symmetric matrix, RP2227 ..... 45
—, —, Solutions of $Ax=\lambda Bx$, RP2275 ..... 471
—, *J. B. Rosser, C. Lanczos, W. Karush*, Separation of close eigenvalues of a real symmetric matrix, RP2256 ..... 291

Page

*Hoffman, James I., Lewis Jesse Clark, Willard D. Hubbard,* Crystallization of aluminum chloride in hydrochloric acid process for the production of alumina from clay, RP2253 ... 269

*Hoge, Harold J., Robert D. Arnold,* Vapor pressures of hydrogen deuterium, and hydrogen deuteride, and dew-point pressures of their mixtures, RP2228 ... 63

—, *James W. Lassiter,* Critical temperatures, pressures, and volumes of hydrogen, deuterium, and hydrogen deuteride, RP2229 ... 75

*Holler, Homer D.,* The role of current distribution in cathodic protection, RP2220 ... 1

*Hubbard, Donald, J. J. Diamond,* Thickness of glass electrodes, RP2270 ... 443

*Hubbard, Willard D., Lewis Jesse Clark, James I. Hoffman,* Crystallization of aluminum chloride in hydrochloric acid process for the production of alumina from clay, RP2253 ... 269

*Humphreys, Curtis J.,* Infrared emission spectrum of calcium, RP2252 ... 202

—, *Earle K. Plyler,* Use of radiation from incandescent particles as an indication of flame temperature, RP2272 ... 456

Hydrogen and its isotopes, RP2271 ... 449

Hydrogen dueteride, preparation and purification of, RP2224 ... 31

Hydrogen, deuterium and hydrogen deuteride, critical temperatures, pressures and volumes, RP2229 ... 75

Hydrogen, deuterium and hydrogen deuteride, vapor and dew-point pressures of mixtures, RP2228 ... 63

Hydrolysis of D-galactosylamines, RP2248 ... 239

*I*

Index of refraction of lithium fluoride crystals, RP2223 ... 25

Infrared spectra of substituted methanes, RP2245 ... 202

Infrared spectrometers, calibration of, RP2223 ... 25

Infrared spectrophotometry, degradation of polystyrene as shown by, RP2235 ... 116

Integral equations, RP2234 ... 113

Interferometry, automatic photoelectric recording, RP2230 ... 80

Interferometry, multiple beam, RP2239 ... 148

Iodine 131, RP2226 ... 41

Iron, determination of copper in steel and, RP2265 ... 380

*Isbell, Horace S., Harriet L. Frush,* Mutarotation, hydrolysis, and structure of D-galactosylamines, RP2248 ... 239

Isotope abundance measurements, using organometallic compounds, RP2259 ... 343

*J*

*Jaffe, Bernard, Elmer N. Bunting, George F. Shelton, Ansel S. Creamer,* Properties of beryllium-berium titanate dielectrics, RP2222 ... 15

*Jenkins, William D., Thomas G. Digges,* Creep of annealed and cold-drawn high-purity copper, RP2254 ... 272

*K*

*Karush, W., M. P. Hestenes,* Solutions of $Ax=\lambda Bx$, RP2275 ... 471

—, —, A method of gradients for the calculation of the characteristic roots and vectors of a real symmetric matrix, RP2227 ... 45

—, *J. B. Rosser, C. Lanczos, M. P. Hestenes,* Separation of close eigenvalues of a real symmetric matrix, RP2256 ... 291

*Keulegan, Garbis H.,* Hydrodynamics of cathode films, RP2240 ... 156

*Kiess, Carl C.,* Description and analysis of the second spectrum of chromium, Cr II, RP2266 ... 285

*King, Gerard J., George T. Furukawa, Robert McCoskey,* Calorimetric properties of benzoic acid from 0° to 410° K, RP2251 ... 256

*L*

*Lalos, George T.,* A sonic-flow pyrometer for measuring gas temperatures, RP2242 ... 179

*Lanczos, C., J. B. Rosser, M. P. Hestenes, W. Karush,* Separation of close eigenvalues of a real symmetric matrix, RP2256 ... 291

*Lassiter, James W., Harold J. Hoge,* Critical temperatures, pressures, and volumes of hydrogen, deuterium, and hydrogen deuteride, RP2229 ... 75

Latex, determination of ash in, RP2237 ... 135

Lead alkalies, mass spectra of some, RP2259 ... 343

Lead-base alloys, determination of bismuth, RP2250 ... 252

*Linnig, Frederic J., Lewis T. Milliken, Ralph I. Cohen,* Determination of ash in GR-S synthetic rubbers and latices, RP2237 ... 135

Lithium fluoride, refractive index of, RP2223 ... 25

*Lukacs, Eugene,* Maximum likelihood estimates of position derived from measurements performed by hyperbolic instruments, RP2244 ... 197

*M*

Magne-gage to measure thickness of nonmagnetic envelopes, use of, RP2270 ... 443

Magnetic measurement of thickness of nonmagnetic envelopes, RP2270 ... 443

Maltose, determination in corn-sirup, RP2263 ... 363

*Marton, L., M. M. Morgan, D. C. Schubert, J. P. Shah, J. A. Simpson,* Electron-optical bench, RP2273 ... 461

Matrices, RP2227 ... 45

Matrices, eigenvalues of, RP2256 ... 291

Matrices, Hermitian, RP2275 ... 471

*McCoskey, Robert E., George T. Furukawa, Gerard J. King,* Calorimetric properties of benzoic acid from 0° to 410° K, RP2251 ... 256

*McDonald, Emma J., Roger E. Perry, Jr.,* A method for corn-sirup analysis involving selective adsorption, RP2263 ... 363

*McDorman, O. N., W. J. Schwerdtfeger,* Potential and current requirements for the cathodic protection of steel in soils, RP2233 ... 104

Measurement by hyperbolic instruments, RP2244 ... 197

*Meggers, William F.,* Multiplets and terms in technetium spectra, RP2221 ... 7

Mercury alkalies, mass spectra of some, RP2259 ... 337

*Miller, Richard C., Roger G. Bates, Vincent E. Power, Edgar R. Smith,* pH of solutions of potassium hydrogen *d*-tartrate from 0° to 60° C, RP2268 ... 433

*Milliken, Lewis T., Frederic J. Linning, Ralph I. Cohen,* Determination of ash in GR-S synthetic rubbers and latices, RP2237 ... 135

*Missimer, Joshua K., Martin J. O'Leary, Pourdon W. Scribner,* Resin bonding of offset papers containing mineral fillers, RP2262 ... 357

Page

*Mohler, Fred L., Vernon H. Dibeler,* Mass spectra of some organo-lead and organo-mercury compounds, RP2259 ... 337

Molecular structure of $C_2D_2$, RP2249 ... 248

Monte Carlo method, RP2234 ... 113

*Moreland, F. Eugene, Milton D. Purdick, Penson Zweig,* Linear thermal expansion of artificial graphites to 1,370° C, RP2225 ... 35

*Morgan, M. M., L. Marton, D. C. Schubert, J. P. Shah, J. A. Simpson,* Electron-optical bench, RP2273 ... 461

*N*

N-Acetyl-D-galactosylamines, $\alpha$ and $\beta$ forms of, RP2248 ... 239

*n*-dimensional geometry, RP2274 ... 465

*Newkirk, Terry F.,* Effect of $SO_3$ on the alkali compounds of portland cement clinker, RP2261 ... 349

*Newman, E. S., F. P. Peppler,* Heats of formation of some barium aluminates, RP 2269 ... 439

*O*

Offset papers containing mineral fillers, resin bonding of, RP2262 ... 357

*O'Leary, Martin J., Pourdon W. Scribner, Joshua K. Missimer,* Resin bonding of offset papers containing mineral fillers, RP2262 ... 357

Optical surfaces, topography of, RP2239 ... 148

Organometallic compounds, mass spectra of some, RP2259 ... 337

Oscillograph—cathode-ray—momentary beam intensification for cold-cathode, RP2231 ... 87

Oxy-acetylene flames, temperatures, RP2272 ... 456

*P*

Papers, offset, containing mineral fillers, resin bonding of, RP2262 ... 357

*Park, John N.,* A fiftyfold momentary beam intensification for a high-voltage cold-cathode oscillograph, RP 2231 ... 87

*Peppler, F. P., E. S. Newman,* Heats of formation of some barium aluminates, RP2269 ... 439

*Perry, Roger E., Jr., Emma J. McDonald,* A method for corn-sirup analysis involving selective adsorption, RP2263 ... 363

Phase equilibria, effect of $SO_3$ on alkali phases in cement clinker, RP2261 ... 349

pH of potassium hydrogen tartrate solutions, RP2268 ... 433

Phosphoric acid, dissociation constant, RP2236 ... 127

Phosphorus, 32, RP2226 ... 41

pH standards, tartrate solutions, RP2268 ... 433

Pipe, asbestos-cement in soils, RP2264 ... 367

Plastics, degradation of polystyrene, using infrared spectrophotometry, RP2235 ... 116

Platinum, annealing of, RP2232 ... 94

*Plyler, Earle K., W. S. Benedict,* Infrared spectra of eighteen halogen-substituted methanes, RP2245 ... 202

—, *Norman Gailar,* The near infrared absorption spectra of deuterated acetylene, RP2249 ... 248

—, *Curtis J. Humphreys,* Use of radiation from incandescent particles as an indication of flame temperature, RP2272 ... 456

—, *Leroy W. Tilton,* Refractivity of lithium fluoride with application to the calibration of infrared spectrometers, RP2223 ... 25

Polymers, high, RP2257 ... 298

Polystyrene, degradation of as shown by infrared spectrophotometry, RP2235 ... 116

*Pomerantz, Philip, Abraham Fookson, Edwin H. Pich,* Preparation and purification of hydrogen and its isotopes, RP2224 ... 31

—, —, *Simon Rothberg,* Some characteristics of Stedman packing in the distillation of hydrogen and its isotopes, RP2271 ... 449

Portland cement, RP2261 ... 349

Potassium hydrogen tartrate, pH of, RP2268 ... 433

Potential of steel in air-free soils, RP2233 ... 104

Protective current, cathodic protection underground, RP2233 ... 104

Pyrometer, sonic-flow for measuring gas temperatures, RP2242 ... 179

Random variables, RP2274 ... 465

Rectifier, synchronous, harmonic output, RP2267 ... 427

*R*

*Reiney, Mary Jane, Fernard G. Achhammer, Frank W. Reinhart,* Study of degradation of polystyrene, using infrared spectrophotometry, RP2235 ... 116

*Reinhart, Frank W., Fernard G. Achhammer, Mary Jane Reiney,* Study of degradation of polystyrene, using infrared spectrophotometry, RP2235 ... 116

Resin bonding offset papers containing mineral fillers, RP2262 ... 357

*Rich, Edwin H., Abraham Fookson, Philip Pomerantz,* Preparation and purification of hydrogen deuteride, RP2224 ... 31

*Romanoff, Melvin, Irving A. Denison,* Effect of exposure to soils on the properties of asbestos-cement pipe, RP2264 ... 367

*Rosser, J. P., C. Lanczos, M. P. Hestenes, W. Karush,* Separation of close eigenvalues of a real symmetric matrix, RP2256 ... 291

*Rothberg, Simon, Abraham Fookson, Philip Pomerantz,* Some characteristics of Stedman packing in the distillation of hydrogen and its isotopes, RP2273 ... 461

*Rothman, S., S. G. Weissberg, Robert Simha,* Viscosity of dilute and moderately concentrated polymer solutions, RP2257 ... 298

Rubber, synthetic, determination of ash in, RP2237 ... 135

*S*

Sampling procedures, nonsequential, RP2277 ... 491

*Saunders, James P.,* Precise topography of optical surfaces, RP2239 ... 148

*Schubert, D. C., L. Marton, M. M. Morgan, J. P. Shah, J. A. Simpson,* Electron-optical bench, RP2273 ... 461

*Schwerdtfeger, W. J., O. N. McDorman,* Potential and current requirements for the cathodic protection of steel in soils, RP2233 ... 104

*Scribner, Pourdon F., John C. Pallinger,* Spectrochemical analysis of bronze by a porous electrode method, RP2246 ... 221

—, *Martin J. O'Leary, Joshua K. Missimer,* Resin bonding of offset papers containing mineral fillers, RP2262 ... 357

*Selgin, Paul,* Harmonic output of the synchronous rectifier, RP2267 ... 427

—, Proposed revision of the conventional method of wave-filter design, RP2276 ... 479

Page

*Seliger, H. H., L. Carallo*, The absolute standardization of radioisotopes by $4\pi$ counting, RP2226 ..... 41
*Shafer, Montgomery F., Ernest F. Fiock, Harry L. Porey, Poss P. Van Loue*, Correcting for density and viscosity of incompressible fluids in float-type flowmeters, RP2247 ..... 227
*Shah, J. R., L. Marton, M. M. Morgan, D. C. Schubert, J. A. Simpson*, Electron-optical bench, RP2273 ..... 461
*Shelton, George R., Elmer N. Bunting, Ansel S. Creamer, Bernard Jaffe*, Properties of beryllium-barium titanate dielectrics, RP2222 ..... 15
Sieves, calibration of, RP2238 ..... 139
*Simha, Robert, S. G. Weissberg, S. Pothman*, Viscosity of dilute and moderately concentrated polymer solutions, RP2257 ..... 298
*Simpson, J. A., L. Marton, M. M. Morgan, D. C. Schubert, J. R. Shah*, Electron-optical bench, RP2273 ..... 461
*Smith, Edgar R., Roger G. Bates, Vincent E. Power, Richard C. Miller*, pH of solutions of potassium hydrogen *d*-tartrate from 0° to 60° C, RP2268 ..... 433
Soil tests, asbestos-cement pipe, RP2264 ..... 367
Solutions, polymer, viscosity of, RP2257 ..... 298
Spectra, atomic emission, RP2252 ..... 262
Spectra, infrared, absorption, RP2249 ..... 248
Spectra, multiplets and terms in technetium, RP2221 ..... 7
Spectra, thioindigo dyes, RP2241 ..... 170
Spectrochemical analysis of bronze, RP2246 ..... 221
Spectrometers, infrared, calibration of, RP2223 ..... 25
Spectrophotometric determination of bismuth in lead-base and tin-base alloys, RP2250 ..... 252
Spectroscopy, high resolution, RP2249 ..... 248
Spectrum of calcium, RP2252 ..... 262
Spectrum of Cr II, RP2266 ..... 385
Starch hydrolysis products, RP2263 ..... 380
Stedman packing, in the distillation of hydrogen, RP2271 ..... 449
Steel, determination of copper in iron and, RP2265 ..... 380
Sulfate phases in cement clinker, RP2261 ..... 349
*Szasz, Otto, John Todd*, Convergence of Cauchy-Riemann sums to Cauchy-Riemann integrals, RP2243 ..... 191

*T*

Tartaric acid, dissociation constants, RP2260 ..... 343
Technetium, multiplets and terms in spectra, RP2221 ..... 7
Temperature determination of flames, RP2272 ..... 456
Thermal expansion of dielectrics in system beryllia-barium titanate-titania, RP2222 ..... 15
Thermocouples, annealing of platinum for, RP2232 ..... 94
Thermodynamics of tartrate solutions, RP2260 ..... 343
Thioindigo dyes, spectra of and *cis-trans* isomerism in, RP2241 ..... 170
*Tilton, Leroy W., Earle K. Plyler*, Refractivity of lithium fluoride with application to the calibration of infrared spectrometers, RP2223 ..... 25
Tin-base alloys, determination of bismuth, RP2250 ..... 252
*Todd, John, Otto Szasz*, Convergence of Cauchy-Riemann sums to Cauchy-Riemann integrals, RP2243 ..... 191

*V*

*Van Loue, Poss P., Montgomery F. Shafer, Ernest F. Fiock, Harry L. Porey*, Correcting for density and viscosity of incompressible fluids in float-type flowmeters, RP2247 ..... 227
Vapor pressures of hydrogen, deuterium, and hydrogen deuteride, RP2228 ..... 63
Viscosity of polymer solutions, RP2257 ..... 298

*W*

Wave-filters, design of, RP2276 ..... 479
Waves, plane longitudinal, RP2258 ..... 315
*Weissberg, S. G., Robert Simha, S. Pothman*, Viscosity of dilute and moderately concentrated polymer solutions, RP2257 ..... 298
*Work, Richard N.*, A photoelectric recording interferometer for measurement of dimensional changes, RP2230 ..... 80
*Wyman, George M., Wallace R. Brode*, Absorption spectra of thioindigo dyes in benzene and chloroform, RP2241 ..... 170

*Z*

Zeeman effect of Cr II, RP2266 ..... 385
Zeeman patterns, asymmetries of, RP2278 ..... 502
*Zweig, Benson, Milton D. Burdick, P. Eugene Moreland*, Linear thermal expansion of artificial graphites to 1,370° C, RP2225 ..... 35

Engineering

RR

# Journal of Research

## of the National Bureau of Standards

US
X

DECEMBER 1951

VOLUME 47 NUMBER 6

U. S. DEPARTMENT OF COMMERCE
Charles Sawyer, Secretary
NATIONAL BUREAU OF STANDARDS
A. V. Astin, *Acting Director*

DECEMBER 1951
VOLUME • 47
NUMBER 6

# JOURNAL OF RESEARCH

## of the

## NATIONAL BUREAU OF STANDARDS

### PERIODICALS OF THE NATIONAL BUREAU OF STANDARDS

As the principal agency of the Federal Government for fundamental research in physics, chemistry, mathematics, and engineering, the National Bureau of Standards conducts projects in fourteen fields: electricity, optics, metrology, heat and power, atomic and radiation physics, chemistry, mechanics, organic and fibrous materials, metallurgy, mineral products, building technology, applied mathematics, electronics, and radio propagation. The Bureau has custody of the national standards of measurement and conducts research leading to the improvement of scientific and engineering standards and of techniques and methods of measurement. Testing methods and instruments are developed; physical constants and properties of materials are determined; and technical processes are investigated.

### JOURNAL OF RESEARCH

Internationally known as a leading scientific periodical, the Journal presents research papers by authorities in the specialized fields of physics, mathematics, chemistry, and engineering. Complete details of the work are presented, including laboratory data, experimental procedures, and theoretical and mathematical analyses. Each of the monthly issues averages 85 two-column pages; illustrated. Annual subscription: domestic, $5.50; foreign, $6.75.

### TECHNICAL NEWS BULLETIN

Summaries of current research at the National Bureau of Standards are published each month in the Technical News Bulletin. The articles are brief, with emphasis on the results of research, chosen on the basis of their scientific or technologic importance. Lists of all Bureau publications during the preceding month are given, including Research Papers, Handbooks, Applied Mathematics Series, Building Materials and Structures Reports, and Circulars. Each issue contains 12 or more two-column pages; illustrated. Annual subscription: domestic, $1.00; foreign, $1.35.

### BASIC RADIO PROPAGATION PREDICTIONS

The Predictions provide the information necessary for calculating the best frequencies for communication between any two points in the world at any time during the given month. The data are important to all users of long-range radio communications and navigation, including broadcasting, air line, steamship, and wireless services, as well as to investigators of radio propagation and ionosphere. Each issue, covering a period of one month, is released three months in advance and contains 16 large pages, including pertinent charts, drawings, and tables. Annual subscription: domestic, $1.00; foreign, $1.25.

---

Order all publications from the Superintendent of Documents,
U. S. Government Printing Office, Washington 25, D. C.

The printing of this publication has been approved by the Director of the Bureau of the Budget, April 6, 1950

Journal of Research of the National Bureau of Standards Vol. 47, No. 6 December 1951

# Contents

Page

pH of solutions of potassium hydrogen *d*-tartrate from 0° to 60° C. Roger G. Bates, Vincent E. Bower, Richard G. Miller, and Edgar R. Smith. RP2268 433

Heats of formation of some barium aluminates. R. B. Peppler and E. S. Newman. RP2269 439

Thickness of glass electrodes. J. J. Diamond and Donald Hubbard. RP2270 443

Some characteristics of Stedman packing in the distillation of hydrogen and its isotopes. Abraham Fookson, Philip Pomerantz, and Simon Rothberg. RP2271 449

Use of radiation from incandescent particles as an indication of flame temperature. Earle K. Plyler and Curtis J. Humphreys. RP2272 456

Electron-optical bench. L. Marton, M. M. Morgan, D. C. Schubert, J. R. Shah, and J. A. Simpson. RP2273 461

Random determinants. R. Fortet. RP2274 465

Solutions of $Ax=\lambda Bx$. M. R. Hestenes and W. Karush. RP2275 471

Proposed revision of the conventional method of wave-filter design. Paul J. Selgin. RP2276 479

On the derivation and accuracy of certain formulas for sample sizes and operating characteristics of nonsequential sampling procedures. Uttam Chand. RP2277 491

Asymmetries of Zeeman patterns and *g*-values for neutral manganese. Miguel A. Catalán. RP2278 502

Index to volume 47 (July to December 1951, Research Papers RP2220 to RP2278). 525

The above Research Papers may be obtained from the Superintendent of Documents, Government Printing Office, Washington 25, D. C., as follows: RP2268 .10¢; RP2269 .05¢; RP2270 .10¢; RP2271 .10¢; RP2272 .10¢; RP2273 .05¢; RP2274 .10¢; RP2275 .10¢; RP2276 .10¢; RP2277 .10¢; RP2278 20¢.

For sale by the Superintendent of Documents, U. S. Government Printing Office, Washington 25, D. C. • Price 75 cents
$5.50 per year on subscription; $6.75 foreign.
UNITED STATES GOVERNMENT PRINTING OFFICE, WASHINGTON : 1952